

R
ADIOLOGY
AND
O
NCOLOGY

vol.48 no.3

september 2014



NOVA SMER DO PODALJŠANJA CELOKUPNEGA PREŽIVETJA



Prva in edina samostojna kemoterapija, ki v primerjavi z ostalimi možnostmi zdravljenja z enim zdravilom, pri bolnicah s predhodno že večkratno zdravljenim metastatskim rakom dojke, dokazano značilno podaljša celokupno preživetje.^{1,2}



- **Halaven** (eribulin): ne-taksanski zaviralec dinamike mikrotubulov, prvo zdravilo iz nove skupine kemoterapevtikov, imenovanih *halihondrini*.
- Zdravilo HALAVEN je indicirano za zdravljenje bolnic z lokalno napredovalim ali metastatskim rakom dojke, ki je napredoval po vsaj enem režimu kemoterapije za napredovalo bolezen. Predhodna zdravljenja morajo vključevati antraciklin in taksan, bodisi kot adjuvantno zdravljenje ali za zdravljenje metastatskega raka dojke, razen če to zdravljenje za bolnice ni bilo primerno.¹
- Priporočeni odmerek 1,23 mg/m², intravensko, v obliki 2- do 5-minutne infuzije, 1. in 8. dan vsakega 21-dnevnega cikla.
- Ena 2 ml viala vsebuje 0,88 mg eribulina.
- Rastopina, pripravljena za uporabo, redčenje ni potrebno.

SKRAJŠAN POVZETEK GLAVNIH ZNAČILNOSTI ZDRAVILA

HALAVEN 0,44 mg/ml raztopina za injiciranje (eribulin)
TERAPEVTSKE INDIKACIJE: Zdravljenje lokalno napredovalega ali metastatskega raka dojke, ki je napredoval po vsaj enem režimu kemoterapije za napredovalo bolezen vključno z antraciklinom in taksanom (adjuvantno zdravljenje ali zdravljenje metastatskega raka dojke), razen če to ni bilo primerno. **ODMERJANJE IN NAČIN UPORABE:** Halaven se daje v enotah, specializiranih za dajanje citotoksične kemoterapije, in le pod nadzorom usposobljenega zdravnika z izkušnjami v uporabi citotoksičnih zdravil. **Odmerjanje:** Priporočeni odmerek eribulina v obliki raztopine je 1,23 mg/m² i.v. v obliki 2- do 5-minutne infuzije 1. in 8. dan vsakega 21-dnevnega cikla. Bolnikom je lahko slabo ali bruhanje. Treba je razmisлити o antiemetični profilaksi, vključno s kortikosteroidi. **Preložitev odmerka med zdravljenjem:** Dajanje Halavena je treba preložiti, če se pojavi kaj od naslednjih: absolutno število nevtrofilcev (ANC) < 1 x 10⁹/l, trombociti < 75 x 10⁹/l ali nehematološki neželeni učinki 3. ali 4. stopnje. **Zmanjšanje odmerka med zdravljenjem:** Za priporočila za zmanjšanje odmerka ob pojavu hematoloških ali nehematoloških neželenih učinkov glejte celoten povzetek glavnih značilnosti zdravila. **Okvara jeter zaradi zasevkov:** Priporočeni odmerek pri blagi okvari jeter (stopnje A po Child-Pughu) je 0,97 mg/m² v obliki 2- do 5-minutne i.v. infuzije 1. in 8. dan 21-dnevnega cikla. Priporočeni odmerek pri zmerni okvari jeter (stopnje B po Child-Pughu) je 0,62 mg/m² v obliki 2- do 5-minutne i.v. infuzije 1. in 8. dan 21-dnevnega cikla. Pri hudi okvari jeter (stopnje C po Child-Pughu) se pričakuje, da je treba dati še manjši odmerek eribulina. **Okvara jeter zaradi ciroze:** Zgornje odmerke se lahko uporabi za blago do zmerno okvaro, vendar se priporoča skrbno nadziranje, saj bo odmerek morda treba ponovno prilagoditi. **Okvara ledvic:** Pri hudi okvari ledvic (očistek kreatinina < 40 ml/min) bo morda treba odmerek zmanjšati. Priporočila se skrbno nadzirajo v skladu s kliničnimi podatki. **Okvara ledvic:** Pri hudi okvari ledvic (očistek kreatinina < 40 ml/min) bo morda treba odmerek zmanjšati. Priporočila se skrbno nadzirajo v skladu s kliničnimi podatki. **Način uporabe:** Odmerek se lahko razredi v do 100 ml 0,9 % raztopine natrijevega klorida (9 mg/ml) za injiciranje. Ne sme se ga redčiti v 5 % infuzijski raztopini glukoze. Pred dajanjem glejte navodila glede redčenja zdravila v celotnem povzetku glavnih značilnosti zdravila ter se prepričajte, da obstaja jeter periferne venske dostop ali prehodna centralna linija. Ni znakov, da bi eribulin povzročal mehurje ali dražlj. V primeru ekstravazacije mora biti zdravljenje simptomatsko. **KONTRAINDIKACIJE:** Preobčutljivost na zdravilno učinkovino ali katerokoli pomožno snov. Dojenje. **POSEBNA OPOZORILA IN PREDVIDNOSTNI UKREPI:** Mielosupresija je odvisna od odmerka in se kaže kot nevropatija. Pred vsakim odmerkom eribulina je treba opraviti pregled celotne krvne slike. Zdravljenje z eribulinom se lahko uvede le pri bolnikih z vrednostmi ANC $\geq 1,5 \times 10^9/l$ in s trombociti > 100 x 10⁹/l. Bolnike, pri katerih se pojavijo febrilna nevropatija, huda nevropatija ali trombotična, je treba zdravit v skladu s priporočili v celotnem povzetku glavnih značilnosti zdravila. Hudo nevropatijo se lahko zdravi z uporabo G-CSF ali enakovrednim zdravilom v skladu s smernicami. Bolnike je treba skrbno nadzirati za znake periferne motorične in senzorične nevropatije. Pri razvoju hude periferne nevrotoksičnosti je treba odmerek prestatiti ali zmanjšati. Če začnemo zdravljenje pri bolnikih s kongestivnim srčnim popuščanjem, z bradibradijami ali sočasno z zdravili, za katera je znano, da podaljšujejo interval QT, vključno z antiaritmiki razreda la in III, in z

elektrolitskimi motnjami, je priporočljivo spremljanje EKG. Pred začetkom zdravljenja s Halavenom je treba popraviti hipokallemijo in hipomagnezijo in te elektrolite je treba občasno kontrolirati med zdravljenjem. Eribulina ne smemo dajati bolnikom s prirojenim sindromom dolgega intervala QT. To zdravilo vsebuje majhne količine etanola (alkohola), manj kot 100 mg na odmerek. Eribulin je pri podganah embriotoksičen, fetotoksičen in teratogen. Halavena se ne sme uporabljati med nosečnostjo, razen kadar je to nujno potrebno. Ženske v rodni dobi naj ne zanosi v času, ko same ali njihov moški partner dobivajo Halaven, in naj med zdravljenjem in še do 3 mesece po njem uporabljajo učinkovito kontracepcijo. Moški naj se pred zdravljenjem posvetujejo o shranjevanju sperme zaradi možnosti nepopravljive neplodnosti. **INTERAKCIJE:** Eribulin se izloča do 70 % prek žolca. Sočasna uporaba učinkovin, ki zavirajo jetrne transportne beljakovine, kot so beljakovine za prenos organskih anionov in beljakovine, odporne na številna zdravila, z eribulinom se ne priporoča (npr. ciklosporin, ritonavir, sakvinavir, lopinavir in nekateri drugi zaviralci proteaze, efavirenz, emtricitabin, verapamil, klaritromicin, kinin, kinidin, dipiramidid, fenitoin, šentjanževka, lahko povzročijo znižanje koncentracij eribulina v plazmi, zato je ob sočasni uporabi indurktorjev potrebna previdnost. Eribulin je blag inhibitor encima CYP3A4. Priporočila je previdnost in spremljanje glede neželenih učinkov pri sočasni uporabi snovi, ki imajo ozko terapevtsko okno in se odstranjujejo iz telesa predvsem preko CYP3A4 (npr. alfentanil, ciklosporin, ergotamin, fentanyl, pimoizid, kinidin, sirolimus, takrolimus). **NEŽELENI UČINKI:** Povzetek varnostnega profila Neželeni učinek, o katerem najpogosteje poročajo v zvezi s Halavenom, je supresija kostnega mozga, ki se kaže kot nevropatija, levkopenija, anemija, trombocitopenija s pridruženimi okužbami. Poročali so tudi o novem začetku ali poslabšanju že obstoječe periferne nevropatije. Med neželenimi učinki, o katerih poročajo, je toksičnost za prebavila, ki se kaže kot anoreksija, navzea, bruhanje, driska, zaprtost in stomatitis. Med drugimi neželenimi učinki so utrujenost, alopecija, zvečani jetrni encimi, sepsa in mišičnoskeletni bolečinski sindrom. **Seznam neželenih učinkov, Zelo pogosti ($\geq 1/10$):** nevropatija (57,0 %) (3/4, stopnje: 49,7 %), levkopenija (29,3 %) (3/4, stopnje: 17,3 %), anemija (20,6 %) (3/4, stopnje: 2,0 %), zmanjšan apetit (21,9 %) (3/4, stopnje: 0,7 %), periferna nevropatija (35,6 %) (3/4, stopnje: 7,6 %), glavobol (17,2 %) (3/4, stopnje: 0,8 %), dispneja (13,9 %) (3/4, stopnje: 3,1 %), kašelj (13,6 %) (3/4, stopnje: 0,6 %), navzea (33,8 %) (3/4, stopnje: 1,1 %), zaprtost (19,6 %) (3/4, stopnje: 0,6 %), driska (17,9 %) (3/4, stopnje: 0,8 %), bruhanje (17,6 %) (3/4, stopnje: 0,9 %), alopecija, artralgijska in mialgijska (19,4 %) (3/4, stopnje: 1,1 %), bolečina v hrbtu (13,0 %) (3/4, stopnje: 1,5 %), bolečina v udih (10,0 %) (3/4, stopnje: 0,7 %), utrujenost/astenija (47,9 %) (3/4, stopnje: 7,8 %), pireksija (20,4 %) (3/4, stopnje: 0,6 %), zmanjšanje telesne mase (11,3 %) (3/4, stopnje: 0,3 %). **Pogosti ($\geq 1/100$ do < 1/10):** okužba sečil (8 %) (3/4, stopnje: 0,5 %), pljučnica (1,2 %) (3/4, stopnje: 0,8 %), ustna kandidiaza, ustni herpes, okužba zgornjih dihal, nazofarngitis, rinitis, limfopenija (4,9 %) (3/4, stopnje: 1,4 %), febrilna nevropatija (4,7 %) (3/4, stopnje: 4,5 %), trombotična (4,3 %) (3/4, stopnje: 0,7 %), hipokallemija (6,1 %) (3/4, stopnje:

1,7 %), hipomagnezija (2,9 %) (3/4, stopnje: 0,2 %), dehidracija (2,8 %) (3/4, stopnje: 0,5 %), hiperglikemija, hipofosfatemija, nespečnost, depresija, disgezija, omotičnost (7,9 %) (3/4, stopnje: 0,5 %), hipoestezija, letargija, nevrotoksičnost, obilnejše solzenje (6,0 %) (3/4, stopnje: 0,1 %), konjunktivitis, vrtoglavica, tahikardija, vročinski valovi, orofaringealna bolečina, epistaksa, rinoreja, bolečina v trebuhu, stomatitis (9,3 %) (3/4, stopnje: 0,8 %), suha usta, dispneja (5,9 %) (3/4, stopnje: 0,2 %), gastroezofagealna refluksna bolezen, razjede v ustih, distenzija trebuha, zvišanje alanin-aminotransferaze (7,6 %) (3/4, stopnje: 2,1 %), zvišanje aspartat-aminotransferaze (7,4 %) (3/4, stopnje: 1,5 %), zvišanje gama-glutamyltransferaze (1,8 %) (3/4, stopnje: 0,9 %), hiperbilirubinemija (1,5 %) (3/4, stopnje: 0,3 %), izpuščaji, pruritus (3,9 %) (3/4, stopnje: 0,1 %), boleznin nohtov, nočno potenje, suha koža, eritem, hiperhidroza, bolečina v kosteh (9,6 %) (3/4, stopnje: 1,7 %), mišični spazmi (5,1 %) (3/4, stopnje: 0,1 %), mišično-skeletna bolečina in mišično-skeletna bolečina v prsih, mišična oslabelost, disurija, vnetje sluznice (8,3 %) (3/4, stopnje: 1,1 %), periferni edem, bolečina, mrzlica, bolečina v prsih, gripi podobna bolezen. **Občasni ($\geq 1/1.000$ do < 1/100):** sepsa (0,5 %) (3/4, stopnje: 0,2 %), nevropenična sepsa (0,1 %) (3/4, stopnje: 0,1 %), herpes zoster, tinitus, globoka venska tromboza, pljučna embolija, hepatotoksičnost (1,0 %) (3/4, stopnje: 0,6 %), palmarno-plantarna eritrodisezija, hematurnija, proteinurija, odpoved ledvic. **Redki ($\geq 1/10.000$ do < 1/1.000):** diseminirana intravaskularna koagulacija, intersticijska pljučna bolezen, pankreatitis, angioedem. **Za popoln opis neželenih učinkov glejte celoten povzetek glavnih značilnosti zdravila.** Vrsta ovjnine in vsebina: viala z 2 ml raztopine. **Režim izdaje:** H Imetnik dovoljenja za promet: Eisai Europe Ltd, European Knowledge Centre, Mosquito Way, Hatfield, Hertfordshire, AL10 9SN, Velika Britanija HAL-270614, julij 2014

Pred predpisovanjem in uporabo zdravila prosimo preberite celoten povzetek glavnih značilnosti zdravila!

Viri: (1) Povzetek glavnih značilnosti zdravila Halaven, junij 2014; (2) Cortes J et al. *Lancet* 2011; 377: 914–23.

 **PharmaSwiss**
Choose More Life

Odgovoren za trženje v Sloveniji:
PharmaSwiss d.o.o., Brodišče 32, 1236 Trzin
telefon: +386 1 236 47 00, faks: +386 1 283 38 10

HAL-0714-01, julij 2014



Publisher

Association of Radiology and Oncology

Affiliated with

Slovenian Medical Association – Slovenian Association of Radiology, Nuclear Medicine Society,
Slovenian Society for Radiotherapy and Oncology, and Slovenian Cancer Society
Croatian Medical Association – Croatian Society of Radiology
Societas Radiologorum Hungarorum
Friuli-Venezia Giulia regional groups of S.I.R.M.
Italian Society of Medical Radiology

Aims and scope

Radiology and Oncology is a journal devoted to publication of original contributions in diagnostic and interventional radiology, computerized tomography, ultrasound, magnetic resonance, nuclear medicine, radiotherapy, clinical and experimental oncology, radiobiology, radiophysics and radiation protection.

Editor-in-Chief

Gregor Serša Ljubljana, Slovenia

Executive Editor

Viljem Kovač Ljubljana, Slovenia

Deputy Editors

Andrej Čör Izola, Slovenia

Maja Čemažar Ljubljana, Slovenia

Igor Kocijančič Ljubljana, Slovenia

Karmen Stanič Ljubljana, Slovenia

Primož Strojjan Ljubljana, Slovenia

Editorial Board

Karl H. Bohuslavizki Hamburg, Germany

Christian Dittrich Vienna, Austria

Metka Filipič Ljubljana, Slovenia

Tullio Giraldi Trieste, Italy

Maria Gódey Budapest, Hungary

Vassil Hadjidekov Sofia, Bulgaria

Håkan Nyström Uppsala, Sweden

Marko Hočevar Ljubljana, Slovenia

Miklós Kásler Budapest, Hungary

Michael Kirschfink Heidelberg, Germany

Janko Kos Ljubljana, Slovenia

Tamara Lah Turnšek Ljubljana, Slovenia

Damijan Miklavčič Ljubljana, Slovenia

Luka Milas Houston, USA

Damir Miletić Rijeka, Croatia

Maja Osmak Zagreb, Croatia

Branko Palčič Vancouver, Canada

Dušan Pavčnik Portland, USA

Geoffrey J. Pilkington Portsmouth, UK

Ervin B. Podgoršak Montreal, Canada

Mirjana Rajer Ljubljana, Slovenia

Borut Štabuc Ljubljana, Slovenia

Ranka Štern-Padovan Zagreb, Croatia

Justin Teissié Toulouse, France

Gillian M. Tozer Sheffield, UK

Andrea Veronesi Aviano, Italy

Branko Zakotnik Ljubljana, Slovenia

Advisory Committee

Marija Auersperg Ljubljana, Slovenia

Tomaž Benulič Ljubljana, Slovenia

Božo Casar Ljubljana, Slovenia

Jure Fettich Ljubljana, Slovenia

Valentin Fidler Ljubljana, Slovenia

Berta Jereb Ljubljana, Slovenia

Vladimir Jevtič Ljubljana, Slovenia

Maksimilijan Kadivec Ljubljana, Slovenia

Stojan Plesničar Ljubljana, Slovenia

Uroš Smrdel Ljubljana, Slovenia

Živa Zupančič Ljubljana, Slovenia

Editorial office

Radiology and Oncology

Zaloška cesta 2

P. O. Box 2217

SI-1000 Ljubljana

Slovenia

Phone: +386 1 5879 369

Phone/Fax: +386 1 5879 434

E-mail: gserta@onko-i.si

Copyright © Radiology and Oncology. All rights reserved.

Reader for English

Vida Kološa

Secretary

Mira Klemenčič

Zvezdana Vukmirović

Design

Monika Fink-Serša, Samo Rován, Ivana Ljubanović

Layout

Matjaž Lužar

Printed by

Tiskarna Ozimek, Slovenia

Published quarterly in 400 copies

Beneficiary name: DRUŠTVO RADIOLOGIJE IN ONKOLOGIJE

Zaloška cesta 2

1000 Ljubljana

Slovenia

Beneficiary bank account number: SI56 02010-0090006751

IBAN: SI56 0201 0009 0006 751

Our bank name: Nova Ljubljanska banka, d.d.,

Ljubljana, Trg republike 2,

1520 Ljubljana; Slovenia

SWIFT: LJBAS12X

Subscription fee for institutions EUR 100, individuals EUR 50

The publication of this journal is subsidized by the Slovenian Research Agency.

Indexed and abstracted by:

Science Citation Index Expanded (SciSearch®)

Journal Citation Reports/Science Edition

Scopus

PubMed

PubMed Central

EMBASE/Excerpta Medica

DOAJ

Open J-gate

Chemical Abstracts

Biomedicina Slovenica

Summon by Serial Solutions (ProQuest)

This journal is printed on acid-free paper

On the web: ISSN 1581-3207

<http://www.degruyter.com/view/j/raon>

<http://www.radioloncol.com>

contents

review

- 219 **The role of fluorine-18-fluorodeoxyglucose positron emission tomography in evaluating the response to tyrosine-kinase inhibitors in patients with metastatic primary renal cell carcinoma**
Carmelo Caldarella, Barbara Muoio, Maria Antonietta Isgrò, Emilio Porfiri, Giorgio Treglia, Luca Giovannella

nuclear medicine

- 228 **Incidental uptake of 18F-fluorocholine (FCH) in the head or in the neck of patients with prostate cancer**
Marina Hodolic, Virginie Huchet, Sona Balogova, Laure Michaud, Khaldoun Kerrou, Valérie Nataf, Marino Cimitan, Jure Fettich, Jean-Noël Talbot

radiology

- 235 **Clinical and radiologic features of extraskeletal myxoid chondrosarcoma including initial presentation, local recurrence, and metastases**
Neena Kapoor, Aul B. Shinagare, Jyothi P. Jagannathan, Shaan H. Shah, Katherine M. Krajewski, Jason L. Hornick, Nikhil H. Ramaiya
- 243 **Osteoblastic bone metastases from renal cell carcinoma**
Vladka Salapura, Irena Zupan, Bostjan Seruga, Gordana Gasljevic, Pavel Kavcic

experimental oncology

- 247 **The effect of radiation dose on mouse skeletal muscle remodeling**
Justin P. Hardee, Melissa J. Puppa, Dennis K. Fix, Song Gao, Kimbell L. Hetzler, Ted A. Bateman, James A. Carson
- 257 **Identification of plasma biomarker candidates in glioblastoma using an antibody-array-based proteomic approach**
Klemen Zupancic, Andrej Blejec, Ana Herman, Matija Veber, Urska Verbovsek, Marjan Korsic, Miomir Knezevic, Primož Rozman, Tamara Lah Turnsek, Kristina Gruden, Helena Motaln
- 267 **Segmentation of hepatic vessels from MRI images for planning of electroporation based treatments in the liver**
Marija Marcan, Denis Pavliha, Maja Marolt Music, Igor Fuckan, Ratko Magjarevic, Damijan Miklavcic

clinical oncology

- 282 **Microinvasive cervical squamous cell carcinoma in Slovenia during the period 2001-2007**
Helena Gutnik, Jasenka P. Matic, Maja Primic Zakelj, Margareta Strojan Flezar
- 289 **The influence of folate pathway polymorphisms on high-dose methotrexate-related toxicity and survival in children with non-Hodgkin malignant lymphoma**
Nina Erculj, Barbara Faganel Kotnik, Marusa Debeljak, Janez Jazbec, Vita Dolzan
- 293 **MRI-assisted cervix cancer brachytherapy pre-planning, based on application in paracervical anaesthesia: final report**
Primož Petric, Robert Hudej, Omar Hanuna, Primož Marolt, Noora Mohammed A. A. Al-Hammadi, Mohamed P. Riyas, Barbara Segedin
- 301 **Olfaction and gustation abilities after a total laryngectomy**
Gordana Mumovic, Irena Hocevar-Boltezar
- 307 **Circulating serum sVCAM-1 concentration in advanced ovarian cancer patients: correlation with concentration in ascites**
Marina Jakimovska, Katarina Cerne, Ivan Verdenik, Borut Kobal
- 314 **Post-mastectomy radiotherapy benefits subgroups of breast cancer patients with T1-2 tumor and 1-3 axillary lymph node(s) metastasis**
Yu-Li Su, Shan-Hsuan Li, Yen-Yang Chen, Hui-Chun Chen, Yen Tang, Cheng-Hua Huang, Fong-Fu Chou, Shih-Chung Wu, Kun-Ming Rau
- 323 **MRI to delineate the gross tumor volume of nasopharyngeal cancers: which sequences and planes should be used?**
Aron Popovtzer, Mohannad Ibrahim, Daniel Tatro, Felix Y. Feng, Randall K. Ten Haken, Avraham Eisbruch

I *slovenian abstracts*

The role of fluorine-18-fluorodeoxyglucose positron emission tomography in evaluating the response to tyrosine-kinase inhibitors in patients with metastatic primary renal cell carcinoma

Carmelo Caldarella¹, Barbara Muoio², Maria Antonietta Isgrò³, Emilio Porfiri⁴, Giorgio Treglia⁵, Luca Giovanella⁵

¹ Institute of Nuclear Medicine, PET/CT Center, Catholic University, Rome, Italy

² School of Medicine, Catholic University, Rome, Italy

³ Institute of Biochemistry and Clinical Biochemistry, Catholic University, Rome, Italy

⁴ School of Cancer Sciences, University of Birmingham, Birmingham, United Kingdom

⁵ Department of Nuclear Medicine and PET/CT Center, Oncology Institute of Southern Switzerland, Bellinzona, Switzerland

Radiol Oncol 2014; 48(3): 219-227.

Received 8 February 2013

Accepted 21 August 2013

Correspondence to: Dr. Carmelo Caldarella, M.D., Institute of Nuclear Medicine, PET/CT Center, Department of Bioimaging and Radiological Sciences, Catholic University, Largo Gemelli 8, 00168 Rome, Italy. Phone: +390630156200; Fax: +39063013745; E-mail: carmelocaldarella@yahoo.it

Disclosure: No potential conflicts of interest were disclosed.

Background. Positron emission tomography-computed tomography (PET-CT) using fluorodeoxyglucose (FDG) is increasingly used in the evaluation of patients with advanced renal cell carcinoma (RCC), primarily for staging purposes. The aim of this paper is to perform a systematic review about the usefulness of PET-CT using FDG in response assessment after treatment with tyrosine-kinase inhibitors (TKIs) in patients with advanced RCC.

Materials and methods. The scientific literature about the role of PET-CT using FDG in the assessment of response to treatment with TKIs in patients affected by advanced RCC was systematically reviewed.

Results. Seven studies about the role of PET-CT using FDG in the response assessment after treatment with TKIs (essentially sunitinib and sorafenib) in advanced RCC were retrieved in full-text and analysed, to determine the predictive role of this morpho-functional imaging method on patient outcome.

Conclusions. To date, the role of PET-CT using FDG in evaluating the response to TKIs in metastatic RCC patients is still not well defined, partly due to heterogeneity of available studies; however, PET-CT reveals potential role for the selection of patients undergoing therapy with TKIs. The use of contrast-enhanced PET-CT appears to be promising for a "multi-dimensional" evaluation of treatment response in these patients.

Key words: fluorodeoxyglucose; positron emission tomography; advanced renal cell carcinoma; tyrosine-kinase inhibitors; response to treatment

Introduction

Primary renal malignancies are relatively uncommon tumours which can arise from either renal cortex or transitional epithelium of intra-renal urinary tract and pelvis. Renal cell carcinoma (RCC)

accounts for about 3% of all adult malignant neoplasms in the United States (the 14th most common malignancy worldwide in 2002), with an estimated incidence rate of 0.7–1.5 cases per 100 000 persons per year; renal pelvis malignancies are less common, with an estimated incidence rate of about 0.5

cases per 100 000 persons per year.^{1,2} Several risk factors, such as cigarette smoking, obesity, hypertension, diabetes mellitus and reproductive factors, besides genetic predisposition (von Hippel-Lindau disease), have been identified for RCC, which may explain the high variability of incidence rates worldwide.^{3,4} Clear cell carcinoma is the most common histological subtype of RCC (82%), followed by papillary carcinoma (11%); chromophobe, collecting duct carcinoma and unclassified RCC are far less common.⁵

Early detection of the primary tumour is desired, but disease-related symptoms (like haematuria, flank pain, fever and weight loss) are non-specific, therefore about 20–30% of patients have metastatic disease at diagnosis, with an expected 5-year survival of approximately 10%. Microscopic metastatic disease may also be apparent several years after curative nephrectomy.^{6–8} Patients with metastatic RCC are usually resistant to conventional cytotoxic chemotherapy agents and radiation therapy; efficacy of interleukin-2 and interferon alpha is limited, with an important toxicity burden. However, in a single centre experience, Motzer *et al.* have reported a significant rise in 2-year-survival rate from 3% (without therapy) to 20% (after interleukin-2, interferon alpha or both) in 670 patients with metastatic RCC.⁹ Selective multi target receptor tyrosine-kinase inhibitors (TKIs), like sunitinib and sorafenib, have been recently approved as novel therapeutic antiangiogenic agents for treatment of advanced RCC, with reported satisfactory results on progression-free survival and quality of life.^{10–13}

Positron emission tomography – computed tomography (PET-CT) is a combined functional and morphological nuclear medicine imaging technique which uses radio-labelled substances (radiopharmaceuticals) to visualize particular metabolic characteristics of either normal or pathological tissues. Fluorine-18-fluorodeoxyglucose (FDG) is a radioactive analogue of glucose, which is intravenously injected to detect increased glycolytic activity in tumour tissues. Unlike most cancers which show intense accumulation of FDG, due to their high glucose metabolism, RCC shows variable intensity of FDG uptake; besides, physiological urinary excretion of FDG makes it difficult to assess the metabolic activity of the primary tumour.¹⁴ However, PET-CT using FDG performs better in the detection of distant metastases, with sensitivity and specificity values of 79% and 90%, respectively, as reported on a recent meta-analysis, but with poorer performance on the detection of the primary neoplasm.^{15,16}

More recently, PET-CT using FDG has been used more and more extensively to assess the treatment response to TKIs in patients with metastatic RCC; however, to date, a systematic evaluation of these studies does not exist in the literature. Therefore, the aim of our paper is to systematically and critically review the published data on this setting to assess the role of PET-CT using FDG in evaluating the treatment response to TKIs in patients with metastatic RCC.

Materials and methods

Search strategy

A comprehensive computer literature search of PubMed/MEDLINE, Scopus, and Embase databases was carried out to find relevant published articles concerning the evaluation of treatment response in patients with metastatic RCC undergoing therapy with TKIs. We used a search algorithm based on a combination of the terms: (“PET” OR “positron emission tomography”) AND (“kidney” OR “renal”). No language restriction was used. The search was performed from inception to October 17th, 2012. To expand our search, references of the retrieved articles were also screened for additional studies.

Study selection

Studies or subsets in studies investigating the role of PET-CT using FDG in patients with metastatic RCC undergoing therapy with TKIs were eligible for inclusion. Case reports, small case series, review articles, letters, editorials and conference proceedings were excluded. The following inclusion criteria were applied to select studies for this systematic review:

PET-CT using FDG performed in patients undergoing therapy with TKIs for metastatic RCC,

A sample size of at least 5 patients with metastatic RCC who underwent PET-CT using FDG after treatment with TKIs, with available data about baseline pre-treatment PET-CT,

Available follow-up data about patient outcome, like progression-free survival (PFS) and/or overall survival (OS),

No data overlap (when possible duplicate studies were found; only the most complete article was included).

Two researchers (CC and GT) independently reviewed the title and abstract of the retrieved articles, applying the above-mentioned selection cri-

TABLE 1. Basic study characteristics

Authors	Journal/year	Country	Study design	Patients performing PET-CT	Mean age	%Male
Vercellino <i>et al.</i> ²²	Cancer Biother Rad 2009	France	Prospective	12	59	83
Lyrdal <i>et al.</i> ¹⁹	Nucl Med Commun 2009	Sweden	Prospective	10	61	80
Minamimoto <i>et al.</i> ²⁴	Clin Nucl Med 2010	Japan	Prospective	12	61.5	67
Revheim <i>et al.</i> ²⁵	Clin Oncol 2011	Norway	Prospective	14	60	NR
Kayani <i>et al.</i> ²³	Clin Cancer Res 2011	UK	Prospective	44	61	75
Ueno <i>et al.</i> ²⁰	BMC Cancer 2012	Japan	Prospective	30	64	83
Khandani <i>et al.</i> ¹⁸	Nucl Med Commun 2012	USA	Prospective	26	59.5	73

NR = Not reported

teria. Articles were rejected if clearly ineligible. The same two researchers then independently evaluated the full-text version of the included articles to determine their eligibility for inclusion.

Data extraction

Information about basic study data (authors, journal, year of publication, country of origin), study design (prospective or retrospective), patient characteristics (number of patients with metastatic RCC with PET-CT evaluation after therapy) and outcome data (PFS, OS) were collected. Only studies providing such complete information were included.

Quality assessment

Two independent reviewers evaluated the methodology of the selected studies using the Quality Assessment Tool for Diagnostic Accuracy Studies (QUADAS).¹⁷ This 14-items tool is composed by five items related to verification bias, three items related to review bias, two items relating to generalizability and context and spectrum bias, and four to reporting. Reviewers, who were blinded to the purposes of the meta-analysis, recorded a score of "1" for "yes" and "0" for "no" for each of the 14 items; all disagreements were resolved by means of consensus. Inter-rater reliability was also evaluated.

Results

Literature search

The comprehensive computer literature search from PubMed/MEDLINE, Embase and Scopus da-

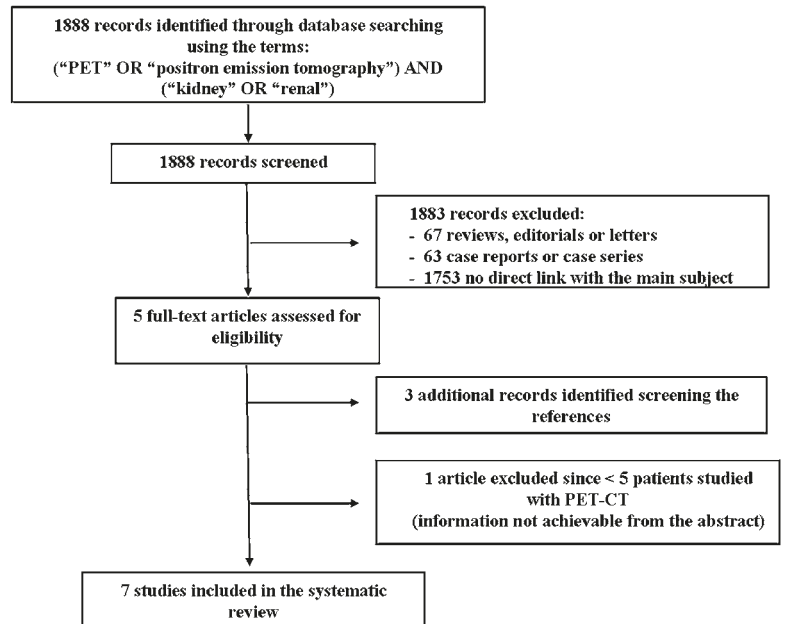


FIGURE 1. Literature search.

tabases revealed 1888 articles (Figure 1). Reviewing titles and abstracts, 5 articles were potentially eligible for inclusion applying the selection criteria mentioned above and were retrieved in full-text version.¹⁸⁻²² Three additional studies were retrieved screening the references.²³⁻²⁵ One study was ultimately rejected since the full-text version analysis revealed that only one patient underwent PET-CT for evaluation of response to therapy, while baseline study was performed in all subjects.²¹ Most papers were excluded because they were not related to the main subject of this review.

Seven studies, comprising a total sample size of 137 patients with metastatic RCC, met all inclusion criteria and were included in this systematic re-

TABLE 2. Treatment and post-therapy PET/CT evaluation

Authors	Therapy (n)	Prior nephrectomy (%)	Patients performing post-therapy PET-CT scan	Post-therapy PET scan timing
Vercellino <i>et al.</i> ²²	Sunitinib (12)	10 (83)	12	1 cycle
Lyrdal <i>et al.</i> ¹⁹	Sorafenib (10)	9 (90)	10	1 cycle
Minamimoto <i>et al.</i> ²⁴	Sunitinib (5) Sorafenib (7)	10 (83)	12	1 cycle
Revheim <i>et al.</i> ²⁵	Sunitinib (14)	13 (93)	13*	2 cycles
Kayani <i>et al.</i> ²³	Sunitinib (44)	No	43**	1 cycle (43 pts) 3 cycles (39 pts)
Ueno <i>et al.</i> ²⁰	Sunitinib (16) Sorafenib (14)	22 (73)	30	1 cycle
Khandani <i>et al.</i> ¹⁸	Sorafenib (26)	No	17	1 cycle

* Not performed in 1 patient because of rapid status deterioration

** Not performed in 1 patient because of negative baseline scan

view. The characteristics of these studies are summarized in Tables 1–3.

Quality assessment

Overall, the seven studies included in this systematic review have shown moderate methodological quality according to QUADAS. Studies scored between 7/14 and 11/14 with a median score of 9/14. The index test and the reference standard were often interpreted without blinding, and this represents the most critical issue about the methodological quality of the included studies.

Literature analysis

A preliminary prospective study about the usefulness of PET-CT using FDG in evaluating the early metabolic response to therapy with TKIs in patients with metastatic RCC was conducted by Vercellino *et al.*²² Twelve patients (overall 29 metastatic sites) were assessed with PET-CT at baseline and after the first cycle of sunitinib therapy was completed (at day 42): the metabolic response was assessed using European Organization for Research and Treatment of Cancer (EORTC) criteria, while CT (performed at day 84) was used to evaluate the morphological response according to Response Evaluation Criteria in Solid Tumors (RECIST).^{26,27} Maximum Standardized Uptake Value (SUVmax) and percentage variation in SUVmax (%SUVmax) were considered on a lesion-based analysis to assess the entity of response to the treatment. Patients with metabolic partial response on post-therapy PET-CT showed long PFS, but metabolic status was not predictive of clinical status at last follow-up: as the authors themselves stated, re-

sults were not statistically significant because of the small sample size. Increase of lesion size on CT was not predictive of progression: despite overall %SUVmax of -17%, the sum of lesion size remained unchanged. Particularly, in 2 patients with non-significant SUVmax decrease, a slight (non-significant) increase in lesion size, associated to reduction in tumour density, was associated to long PFS, presumably due to intralesional necrosis.

Lyrdal *et al.* studied 10 patients with histologically proven metastatic RCC (overall 52 lesions) and evidence of disease progression despite previous cytokine treatment, who underwent PET-CT using FDG at baseline and 1–2 months after sorafenib therapy.¹⁹ Post-therapy glycolytic activity and percentage decrease in glycolytic activity were measured on both soft tissue and skeletal lesions; lesion diameter was assessed by using diagnostic CT. In all lesions, mean FDG uptake significantly decreased to 75% compared to the initial values (71% in 39 soft tissue lesions and 82% in 13 skeletal ones). Best responders, with a percentage decrease greater than 20%, had significantly better mean OS than patients with least response (18.1 vs. 12.9 months); however, no significant correlation was observed between decrease in FDG uptake and PFS. A significant 20% decrease in soft tissue lesions diameter was observed on diagnostic CT. The authors demonstrate that PET-CT using FDG is a promising modality to evaluate response to sorafenib in both soft tissue and skeletal metastases of RCC; a clear advantage in comparison with RECIST evaluation was observed, since RECIST is limited to soft tissue lesions.

Minamimoto *et al.* analysed a prospective series of 12 patients with a total of 42 metastatic RCC lesions undergoing either sorafenib (7 patients) or

TABLE 3. FDG uptake quantification indexes and response

Authors	Quantification indexes	Partial response	Stable disease	Disease progression
Vercellino <i>et al.</i> ²²	SUVmax %SUVmax	4	7	1
Lyrdal <i>et al.</i> ¹⁹	SUVmax SUVmean	NR	1	8
Minamimoto <i>et al.</i> ²⁴	SUVmax %SUVmax	12	6	3
Revheim <i>et al.</i> ²⁵	SUVmax	6	3	4
Kayani <i>et al.</i> ²³	SUVmax %SUVmax	24	14	4
Ueno <i>et al.</i> ²⁰	SUVmax	12	10	8
Khandani <i>et al.</i> ¹⁸	SUVmax %SUVmax	NR	NR	NR

NR = Not reported

sunitinib (5 patients) treatment; PET co-registered with contrast-enhanced CT (ceCT) was performed at baseline and after one cycle of therapy in all patients, to evaluate the early response and to predict PFS.²⁴ According to EORTC 1999 criteria, patients were distinguished into metabolic partial response (SUVmax decreased > 25%), stable disease (SUVmax change less than 25%) and progressive disease (SUVmax increased > 25%).²⁸ PET and CT were consistent in defining disease status in 8 patients, mostly with stable disease. Only a moderate reduction in mean SUVmax was noticeable in both sunitinib- and sorafenib-treated patients, with no statistically significant differences in PFS between the two therapy subsets. However, significant differences in PFS were confirmed between partial response and stable disease patients, as well as between partial response and progressive disease patients; besides, patients with PET-defined metabolic response showed longer PFS than patients with metabolic progressive disease.

Fourteen patients with metastatic RCC on-going first-line or second-line sunitinib treatment after cytokine and/or vascular endothelial growth factor (VEGF)-capture therapy failure were reviewed by Revheim *et al.*²⁵ PET-CT using FDG was performed before and after two treatment periods in all but one patient with highly metabolic lung and nodal lesions, who showed rapid deterioration and poor prognosis before post-therapy PET-CT examination could be obtained. The authors have found that patients with relatively low baseline FDG uptake in targeted lesions (SUVmax < 5) had significantly longer PFS than patients with relatively high baseline FDG uptake (SUVmax > 5); moreover, patients with SUVmax < 5 showed improved outcome after 3 months of follow-up, compared with patients with SUVmax > 5. Partial

metabolic response according to EORTC criteria well correlated with longer PFS; Motzer scoring system (poor *vs.* intermediate) did not significantly correlate with either PFS or baseline FDG uptake.

The relevance of sequential PET-CT using FDG, performed at various intervals after therapy with sunitinib in patients with newly diagnosed metastatic RCC, as a surrogate marker of response to therapy was investigated by Kayani *et al.*, as a part of a prospective phase II multicentre trial.²³ Forty-four patients underwent PET-CT at baseline; 43 of them repeated this examination after the first cycle (at 4 weeks) and 39 had a third PET-CT scan after the third cycle of sunitinib (at 16 weeks). Changes in SUVmax between the baseline and 4-weeks, as well as between the baseline and 16-weeks, were calculated and compared with outcome (PFS and OS) data. The authors have demonstrated that both a SUVmax higher than 7.1 and a higher number of active lesions (more than 8) at baseline were predictive of shorter OS. Furthermore, despite evidence of metabolic response in 24/43 patients after one cycle of therapy and a median 22% reduction in SUVmax at the site of the previously most active lesion, there was no significant correlation between median reduction in SUVmax and PFS or OS, irrespective of the SUVmax at baseline. Similar results were obtained in 16/39 patients who showed metabolic response after the third cycle of therapy (16% reduction in SUVmax); however, a negative correlation was observed between disease progression and OS. Finally, a higher baseline SUVmax was negatively associated with metabolic response at both 4-weeks and 16-weeks scans (7.1 in metabolic non-responders; 4.4 in metabolic responders), whilst 10/12 patients with disease progression on 16-weeks PET-CT had been metabolic responders

after one cycle of therapy (that is, 4-weeks scan had no prognostic significance).

A prospectively conducted study protocol by Ueno *et al.* on 30 histologically confirmed metastatic RCC patients undergoing sunitinib or sorafenib treatment was evaluated by using PET-CT before treatment and after 1 month of therapy.²⁰ SUVmax of all lesions was calculated to obtain the mean SUVmax of the individual patient on both baseline and post-therapy examination; the mean ratio of SUVmax change and mean ratio in lesion diameter change on CT were obtained to classify patients as good, intermediate or poor responders, and compared with mean PFS and OS for each response group. Despite no complete response was obtained, an average reduction in mean SUVmax from baseline to post-therapy examination was observed (-18%; range -55 to 65%), and a slight reduction in mean lesion diameter (-6%; range -30 to 30%), with no significant differences across subtypes of tumour (clear cell *vs* papillary carcinoma). The Cox-analysis survival of good (lesion diameter sum not increased and SUVmax reduced > 20%), intermediate (lesion diameter sum not increased and SUVmax reduced < 20%) and poor responders (lesion diameter sum increased or appearance of new lesions) showed statistically significant difference in PFS as well as in OS. By using classical EORTC criteria for patient classification, instead, no association was observed between PFS and degree of response. Authors demonstrate that using a combination of PET (metabolic response) and CT (tumour size response) criteria in spite of classical EORTC criteria could predict PFS and OS in these patients.

Lastly, Khandani *et al.* have prospectively investigated eventual differences in the intensity of FDG uptake at baseline in clear cell and non-clear cell RCC, and whether changes in metabolic burden in targeted lesions could predict response to sorafenib in 17 patients.¹⁸ Therefore, PET-CT images were acquired at baseline and at completion of therapy, before nephrectomy was performed; baseline SUVmax and relative changes in SUVmax at post-therapy scan were calculated for each patient and tumour subtype. Clear cell RCC patients showed lower SUVmax at baseline than non-clear cell RCC (3.9 *vs.* 7.9); an inverse correlation was found between the metabolic activity of clear cell RCC primary tumour at baseline and the degree of size response to sorafenib on CT (correlation not found for non-clear cell RCC). Due to the limited sample size (13 clear cell and 4 non-clear cell RCC), only a weak inverse correlation was detected between relative

change in SUVmax and tumour size response, suggesting a limited relationship between metabolic effects of sorafenib and morphological changes on CT. Finally, no significant differences in the rate of recurrence and outcome measures were found between patients with high baseline SUVmax (> 4) and low baseline SUVmax (< 4).

Discussion

It is well known that FDG is physiologically excreted by the urinary system, therefore hampering the accurate assessment of the primary renal lesion in terms of metabolic burden and aggressiveness, as well as interfering with the evaluation of response after targeted therapy. However, in recent years, PET-CT using FDG has played an increasingly important role in the management of patients affected by primary renal cell malignancies, specifically for the evaluation of metastatic lesions. In fact, as reported by Wang *et al.* in a recently published meta-analysis on fourteen studies, PET-CT using FDG is a reliable diagnostic tool for the detection of extrarenal lesions of RCC, with pooled sensitivity and specificity values of 79% and 90%, respectively (in the same studies, the authors report a pooled sensitivity and specificity of 62% and 88%, respectively, for renal lesions).¹⁶

Traditional therapeutic regimens with cytotoxic agents and/or radiation therapy fail in most patients with advanced RCC, with a significant toxicity burden; neither interleukin-2 nor interferon alpha, alone or in association with cytotoxic drugs, show evidence of long-term efficacy in this setting, with no significant benefit on the survival and recurrence rate.²⁹⁻³² Therapy with TKIs, alone or in combination with immune-chemotherapeutic agents is currently performed in patients with metastatic RCC, with satisfactory results.¹⁰⁻¹³ A recent Swedish register-based study has demonstrated a significant impact of the duration of first-line treatment when sorafenib is used in sequential therapy with sunitinib in patients with RCC.³³ Eichelberg *et al.* have shown that 50% patients with metastatic RCC, previously undergoing sorafenib with unsatisfactory results, benefit from a secondary use of sunitinib, with a significant increase in progression-free survival from 8-10 to 17 months.³⁴

As demonstrated by our review, in the last three years PET-CT using FDG has been increasingly performed to assess the therapeutic efficacy of TKIs (notably, sunitinib and sorafenib) in patients with metastatic RCC, irrespective of previ-

ous treatments or nephrectomy. Reduction in FDG uptake from pre-therapy to post-therapy evaluation is used by all selected studies as an estimate of treatment response: therefore, a baseline PET-CT examination showing significant metabolic activity within lesions is mandatory to correctly assess the response to therapy at the post-treatment scan. Within a prospective cohort of patients by Kayani *et al.*, 43 patients from a total of 44 have undergone PET-CT after 1 cycle of sunitinib (4 weeks), since the remaining patient had a negative baseline scan.²³ Likewise, in the same study, 39 patients were re-evaluated after 3 cycles of sunitinib (16 weeks): however, the lesion-based analysis of response had to exclude previous pathologic sites which showed a complete/near complete normalization of FDG uptake after 1 cycle of therapy.

In all the selected studies outcome measures such as PFS and OS were included: authors compared them among groups of patients derived in accordance to the disease status as assessed by post-treatment PET-CT. A slight-to-moderate reduction in FDG uptake from baseline to post-therapy scan was observed in most patients, while only a minority of patients showed disease progression; a complete metabolic response (*i.e.* complete normalization of FDG uptake in all lesions in a single patient) was never achievable. Actually, in many studies, a good correlation was found between partial metabolic response and PFS or OS, with the highest survival rates in patients showing the greatest reduction in SUVmax.^{19,20,24,25} Thus, PET-CT appears to show a high predictive value in the evaluation of response to therapy in both skeletal and soft tissue metastases of RCC. However, contradictory results arise from our literature analysis. In their pilot study, Vercellino *et al.* also have observed a longer PFS in patients with partial metabolic response rather than in patients with stable disease or progression; however, a statistical significance was not reached, presumably due to their small sample size (12 patients).²² Similarly, Khandani *et al.* detected only a weak inverse correlation between relative change in SUVmax and tumour size response, and no correlation with PFS or OS, in 13 patients with metastatic clear cell RCC.¹⁸ On a larger population, Kayani *et al.* have found no correlation between median reduction in SUVmax and PFS or OS, especially when PET-CT was performed after 1 cycle of therapy; as authors themselves state, the exclusion of patients with clinical or radiological progression from the sequential PET-CT analysis could have influenced these results somehow.²³ Conversely, they found that higher SUVmax at baseline and higher

number of lesions were predictors of shorter OS, as observed in other studies.^{18,25}

Increase in FDG uptake (*i.e.* a metabolic progression of disease) was associated with lower OS, though not always with a less favourable PFS.²³

Some studies have compared the predictive value of post-therapy PET-CT using FDG and clinical/morphological criteria and scores.^{19,20,24,25} In these settings, post-therapy PET-CT performed better than clinical scores (Motzer score) or morphological criteria (RECIST) in predicting PFS and OS, therefore resulting in a stronger prediction of response to treatment. As observed by Lyrdal *et al.*, post-therapy PET-CT is more useful than RECIST criteria, particularly for the evaluation of skeletal lesions, as RECIST is limited to soft tissue lesions.¹⁹ RECIST criteria exhibit significant limitations when response to cytostatic (like TKIs), rather than cytotoxic therapies (traditional chemotherapeutic agents, interferon), has to be evaluated, therefore emphasizing the role of metabolic changes on post-treatment PET-CT in this setting. Furthermore, using a combination of metabolic activity assessment (lowering in FDG uptake) and morphological changes (reduction in tumour size) better contributes to predict PFS and OS, rather than metabolic assessment alone.²⁰ Reduction in lesion size is not an accurate predictor of good response, by itself: responding lesions sometimes showed an increase in size, despite extensive necrosis, evidence of low FDG uptake and high PFS.²²

Most authors have used SUVmax, which is an indirect estimate of the glycolytic activity in the most active pixel within the lesion, as an index to detect eventual changes in metabolic activity from baseline to post-treatment scan. The absolute (SUVdiff) or relative (SUVrel) variation in SUVmax have been used as they reflect the changes in the amount of vital tumour cells induced by therapy. However, active inflammation in sites of responding lesions could also accumulate FDG; this could partly explain the apparent low correlation with PFS and OS observed in some studies.

Some studies showed a negative correlation between baseline SUVmax in the most active lesion and outcome.^{18,23,25} Higher baseline SUVmax and higher number of metabolically active lesions were significantly associated with greater risk of disease progression and poorer PFS or OS. Moreover, patients with higher baseline SUVmax showed a lower response rate than patients with lower baseline SUVmax, even after one cycle of therapy.²³

Interestingly, the efficacy of PET-CT in the prediction of response to treatment and patient out-

come was not affected neither by the therapeutic drug used (sorafenib *vs.* sunitinib), nor by the histological subtype of tumour; only a slight difference in baseline SUVmax was observed, with lower mean values in clear cell RCC. Khandani *et al.* have found that changes in SUVmax weakly correlated with tumour size response only in clear cell RCC patients, while non-clear cell RCC did not; however, only 4 non-clear cell RCC patients were included, therefore limiting the statistical relevance of the results.¹⁸

Conclusions

The role of PET-CT using FDG in assessing the response to TKIs in metastatic RCC patients is still not well defined, partly due to heterogeneity of available studies. However, PET-CT reveals potential role for the selection of patients undergoing therapy with TKIs. The use of contrast-enhanced PET-CT appears to be promising for a “multi-dimensional” evaluation of treatment response in these patients.

References

1. Chow WH, Devesa SS, Warren JL, Fraumeni JF Jr. Rising incidence of renal cell cancer in the United States. *JAMA* 1999; **281**: 1628-31.
2. Ferlay J, Bray F, Pisani P, Parkin DM. GLOBOCAN 2002: cancer incidence, mortality, and prevalence worldwide. Lyon: IARC Press. <http://www.dep.iarc.fr/>. Accessed 10 October 2012.
3. Chow WH, Dong LM, Devesa SS. Epidemiology and risk factors for kidney cancer. *Nat Rev Urol* 2010; **7**: 245-57.
4. Weikert S, Ljungberg B. Contemporary epidemiology of renal cell carcinoma: perspectives of primary prevention. *World J Urol* 2010; **28**: 247-52.
5. Klatt T, Pantuck AJ, Kleid MD, Beldegrun AS. Understanding the natural biology of kidney cancer: implications for targeted cancer therapy. *Rev Urol* 2007; **9**: 47-56.
6. Bukowski RM. Prognostic factors for survival in metastatic renal cell carcinoma: update 2008. *Cancer* 2009; **115**: 2273-81.
7. Cruz A, Ramírez LM, Sánchez E, Ruiz M, Moreno I, López J, et al. Gastric metastasis from renal cancer six years after nephrectomy. *Rev Esp Enferm Dig* 2011; **103**: 660-1.
8. Motzer RJ, Bander NH, Nanus DM. Renal-cell carcinoma. *N Engl J Med* 1996; **335**: 865-75.
9. Motzer RJ, Mazumdar M, Bacik J, Berg W, Amsterdam A, Ferrara J. Survival and prognostic stratification of 670 patients with advanced renal cell carcinoma. *J Clin Oncol* 1999; **17**: 2530-40.
10. Castellano D, del Muro XG, Pérez-Gracia JL, González-Larriba JL, Abrio MV, Ruiz MA, et al. Patient-reported outcomes in a phase III, randomized study of sunitinib versus interferon- α as first-line systemic therapy for patients with metastatic renal cell carcinoma in a European population. *Ann Oncol* 2009; **20**: 1803-12.
11. Cella D, Michaelson MD, Bushmakina AG, Cappelleri JC, Charbonneau C, Kim ST, et al. Health-related quality of life in patients with metastatic renal cell carcinoma treated with sunitinib vs interferon- α in a phase III trial: final results and geographical analysis. *Br J Cancer* 2010; **102**: 658-64.
12. Jonasch E, Corn P, Pagliaro LC, Warneke CL, Johnson MM, Tamboli P, et al. Upfront, randomized, phase 2 trial of sorafenib versus sorafenib and low-dose interferon α in patients with advanced renal cell carcinoma: clinical and biomarker analysis. *Cancer* 2010; **116**: 57-65.
13. Procopio G, Verzoni E, Bracarda S, Ricci S, Sacco C, Ridolfi L, et al. Sorafenib with interleukin-2 vs sorafenib alone in metastatic renal cell carcinoma: the ROSORC trial. *Br J Cancer* 2011; **104**: 1256-61.
14. Jadvar H, Kherbache HM, Pinski JK, Conti PS. Diagnostic role of [F-18]-FDG positron emission tomography in restaging renal cell carcinoma. *Clin Nephrol* 2003; **60**: 395-400.
15. Powles T, Murray I, Brock C, Oliver T, Avril N. Molecular positron emission tomography and PET/CT imaging in urological malignancies. *Eur Urol* 2007; **51**: 1511-20.
16. Wang HY, Ding HJ, Chen JH, Chao CH, Lu YY, Lin WY, et al. Meta-analysis of the diagnostic performance of [18F]FDG-PET and PET/CT in renal cell carcinoma. *Cancer Imaging* 2012; **12**: 464-74.
17. Whiting PF, Weswood ME, Rutjes AW, Reitsma JB, Bossuyt PN, Kleijnen J. Evaluation of QUADAS, a tool for the quality assessment of diagnostic accuracy studies. *BMC Med Res Methodol* 2006; **6**: 9.
18. Khandani AH, Cowey CL, Moore DT, Gohil H, Rathmell WK. Primary renal cell carcinoma: relationship between 18F-FDG uptake and response to neoadjuvant sorafenib. *Nucl Med Commun* 2012; **33**: 967-73.
19. Lyrdal D, Bojisen M, Suurkula M, Lundstam S, Stierner U. Evaluation of sorafenib treatment in metastatic renal cell carcinoma with 2-fluoro-2-deoxyglucose positron emission tomography and computed tomography. *Nucl Med Commun* 2009; **30**: 519-24.
20. Ueno D, Yao M, Tateishi U, Minamimoto R, Makiyama K, Hayashi N, et al. Early assessment by FDG-PET/CT of patients with advanced renal cell carcinoma treated with tyrosine kinase inhibitors is predictive of disease course. *BMC Cancer* 2012; **12**: 162.
21. Vaishampayan UN, Heilbrun LK, Shields AF, Lawhorn-Crews J, Baranowski K, Smith D, et al. Phase II trial of interferon and thalidomide in metastatic renal cell carcinoma. *Invest New Drugs* 2007; **25**: 69-75.
22. Vercellino L, Bousquet G, Baillet G, Barré E, Mathieu O, Just PA, et al. 18F-FDG PET/CT imaging for an early assessment of response to sunitinib in metastatic renal cell carcinoma: preliminary study. *Cancer Biother Radiopharm* 2009; **24**: 137-44.
23. Kayani I, Avril N, Bomanji J, Chowdhury S, Rockall A, Sahdev A, et al. Sequential FDG-PET/CT as a biomarker of response to Sunitinib in metastatic clear cell renal cancer. *Clin Cancer Res* 2011; **17**: 6021-8.
24. Minamimoto R, Nakaigawa N, Tateishi U, Suzuki A, Shizukuishi K, Kishida T, et al. Evaluation of response to multikinase inhibitor in metastatic renal cell carcinoma by FDG PET/contrast-enhanced CT. *Clin Nucl Med* 2010; **35**: 918-23.
25. Revheim ME, Winge-Main AK, Hagen G, Fjeld JG, Fosså SD, Lilleby W. Combined positron emission tomography/computed tomography in sunitinib therapy assessment of patients with metastatic renal cell carcinoma. *Clin Oncol (R Coll Radiol)* 2011; **23**: 339-43.
26. Young H, Baum R, Cremerius U, Herholz K, Hoekstra O, Lammertsma AA, et al. Measurement of clinical and subclinical tumour response using [18F]-fluorodeoxyglucose and positron emission tomography: review and 1999 EORTC recommendations. European Organization for Research and Treatment of Cancer (EORTC) PET Study Group. *Eur J Cancer* 1999; **35**: 1773-82.
27. Therasse P, Arbuick SG, Eisenhauer EA, Wanders J, Kaplan RS, Rubinstein L, et al. New guidelines to evaluate the response to treatment in solid tumors. European Organization for Research and Treatment of Cancer, National Cancer Institute of the United States, National Cancer Institute of Canada. *J Natl Cancer Inst* 2000; **92**: 205-16.
28. Stroobants S, Goeminne J, Seegers M, Dimitrijevic S, Dupont P, Nuyts J, et al. 18FDG-Positron emission tomography for the early prediction of response in advanced soft tissue sarcoma treated with imatinib mesylate (Glivec). *Eur J Cancer* 2003; **39**: 2012-20.
29. Atzpodiens J, Schmitt E, Gertenbach U, Fornara P, Heynemann H, Maskow A, et al. Adjuvant treatment with interleukin-2- and interferon- α 2a-based chemioimmunotherapy in renal cell carcinoma post tumour nephrectomy: results of a prospectively randomised trial of the German Cooperative Renal Carcinoma Chemioimmunotherapy Group (DGCIN). *Br J Cancer* 2005; **92**: 843-6.

30. Bex A, Mallo H, Kerst M, Haanen J, Horenblas S, de Gast GC. A phase-II study of pegylated interferon alfa-2b for patients with metastatic renal cell carcinoma and removal of the primary tumor. *Cancer Immunol Immunother* 2005; **54**: 713-9.
31. Hudes G, Carducci M, Tomczak P, Dutcher J, Figlin R, Kapoor A, et al. Temsirolimus, interferon alfa, or both for advanced renal-cell carcinoma. *N Engl J Med* 2007; **356**: 2271-81.
32. Segota E, Mekhail T, Olencki T, Hutson TE, Dreicer R, Wacker B, et al. Phase II trial of capecitabine and rHu-interferon-alpha-2a in patients with metastatic renal cell carcinoma, limited efficacy, and moderate toxicity. *Urol Oncol* 2007; **25**: 46-52.
33. Ambring A, Björholt I, Lesén E, Stiernér U, Odén A. Treatment with sorafenib and sunitinib in renal cell cancer: a Swedish register-based study. *Med Oncol* 2013; **30**: 331.
34. Eichelberg C, Heuer R, Chun FK, Hinrichs K, Zacharias M, Huland H, et al. Sequential use of the tyrosine kinase inhibitors sorafenib and sunitinib in metastatic renal cell carcinoma: a retrospective outcome analysis. *Eur Urol* 2008; **54**: 1373-8.

Incidental uptake of ^{18}F -fluorocholine (FCH) in the head or in the neck of patients with prostate cancer

Marina Hodolic¹, Virginie Huchet², Sona Balogova^{2,3}, Laure Michaud^{2,4}, Khaldoun Kerrou², Valérie Nataf^{2,5}, Marino Cimitan⁶, Jure Fettich¹, Jean-Noël Talbot^{2,4}

¹ Department for nuclear medicine, University Medical Centre, Ljubljana, Slovenia

² Médecine nucléaire, Hôpital Tenon, AP-HP, Paris, France

³ Comenius University, Bratislava, Slovakia

⁴ Université Pierre et Marie Curie, Paris, France

⁵ Radiopharmacie, Hôpital Tenon, AP-HP, Paris, France

⁶ Nuclear Medicine Unit, National Cancer Institute CRO IRCCS, Aviano, Italy

Radiol Oncol 2014; 48(3): 228-234.

Received 13 August 2013

Accepted 11 October 2013

Correspondence to: DR. Marina Hodolič, Department for Nuclear Medicine, University Medical Centre, Zaloška 2, SI-1000 Ljubljana, Slovenia. Phone: +386 1 522 35 48; Fax: +386 1 522 22 37; E-mail: marina.hodolic@gmail.com

Disclosure: No potential conflicts of interest were disclosed.

Background. Positron emission tomography-computed tomography (PET/CT) with ^{18}F -fluorocholine (FCH) is routinely performed in patients with prostate cancer. In this clinical context, foci of FCH uptake in the head or in the neck were considered as incidentalomas, except for those suggestive of multiple bone metastases.

Results. In 8 patients the incidental focus corresponded to a benign tumour. The standard of truth was histology in two cases, correlative imaging with MRI in four cases, $^{99\text{m}}\text{Tc}$ -SestaMIBI scintigraphy, ultrasonography and biochemistry in one case and biochemistry including PTH assay in one case. The final diagnosis of benign tumours consisted in 3 pituitary adenomas, 2 meningiomas, 2 hyperfunctioning parathyroid glands and 1 thyroid adenoma.

Malignancy was proven histologically in 2 other patients: 1 papillary carcinoma of the thyroid and 1 cerebellar metastasis.

Conclusions. To the best of our knowledge, FCH uptake by pituitary adenomas or hyperfunctioning parathyroid glands has never been described previously. We thus discuss whether there might be a future indication for FCH PET/CT when one such tumour is already known or suspected: to detect a residual or recurrent pituitary adenoma after surgery, to guide surgery or radiotherapy of a meningioma or to localise a hyperfunctioning parathyroid gland. In these potential indications, comparative studies with reference PET tracers or with $^{99\text{m}}\text{Tc}$ -sestaMIBI in case of hyperparathyroidism could be undertaken.

Key words: FCH, PET/CT; incidentaloma; meningioma; pituitary adenoma; hyperparathyroidism; thyroid adenoma

Introduction

Positron emission tomography-computed tomography (PET/CT) with radiolabeled choline is becoming the first line nuclear medicine examination in patients with prostate cancer¹, especially where there is evidence of biochemical recurrence.² ^{11}C -choline has low urinary excretion, which is favourable for detecting pelvic foci, but its routine

use is not possible in centres lacking an on-site cyclotron. ^{18}F -fluorocholine (FCH), which can be delivered as easily as ^{18}F -fluorodeoxyglucose (FDG), has proven clinical utility for PET imaging of cancers with slow growth and low aggressiveness, frequently missed with FDG.³

FCH is currently registered in several EU countries for the detection of bone metastasis in prostate cancer, which is currently its most frequent indica-

TABLE 1. Patients with incidentaloma in the head or in the neck on FCH PET/CT performed for prostate cancer staging or restaging benign tumours

No.	Age	Prostate cancer setting for FCH PET/CT	Incidental FCH uptake in head and neck region	Diagnostic modality(ies) for characterisation
1.	78	Biochemical recurrence under HT	Pituitary	MRI: Macroadenoma of pituitary gland
2.	64	Biochemical recurrence after HT	Pituitary	MRI: Residual pituitary adenoma in the right side of sella turcica
3.	81	Biochemical recurrence after prostatectomy, under HT	Pituitary	Post-surgical histology: non-functioning pituitary adenoma
4.	72	Initial staging	Frontal lobe	MRI: Meningioma in the anterior cranial fossa
5.	70	Biochemical recurrence, under HT	Between cerebellum and medulla	MRI: Meningioma at the level of foramen magnum on the right side
6.	56	Initial staging	Behind the left thyroid lobe	Serum PTH: 160 ng/L, ultrasonography and 99mTc-SestaMIBI/123I scintigraphy: recurrent parathyroid adenoma at the same location
7.	75	Biochemical recurrence after high intensity focused ultrasound, no HT	Behind the left thyroid lobe	Serum PTH: 134 ng/L, calcemia: 2.6 mmol/L, normal serum calcidiol
8.	52	Biochemical recurrence after prostatectomy, under HT	Left thyroid lobe	Ultrasonography: multinodular thyroid gland. Cytology of the target nodule: thyroid adenoma

HT = hormonal treatment; PTH = parathyroid hormone; MRI = magnetic resonance imaging

tion for use. FCH foci can reveal secondary lesions of prostate cancer not only in the skeleton but also in soft tissue, and may be found in unexpected locations such as penis.⁴ But FCH foci may also correspond to other primary cancers³ or inflammatory lesions.⁵

Foci in the head or in the neck are unexpected in patients referred for prostate cancer.⁶ We reviewed the reports of FCH PET/CTs performed in our centres in patients with prostate cancer, to select those in which such foci have been reported. We then searched whether the origin and the nature of each focus has been characterised during follow-up. As FCH PET/CT is developing rapidly, we consider it is useful to share experience about the frequency of incidental FCH foci in the head or in the neck, about their possible benign non-inflammatory aetiology and to speculate on a potential indication of FCH PET/CT in the management of those tumours, in comparison with other PET tracers according to a review of literature.

Patients and methods

The patients, referred for prostate cancer staging or restaging, were fasting for 6-10 hours prior to FCH PET/CT. PET/CT was performed after intravenous injection of 200-300 MBq of FCH (IASOcholine®, Graz, Austria, or Advanced Accelerator Applications, Saint Genis-Pouilly, France), according to the body weight of the patient. Whole body acquisition was performed during two minutes for each of 9-10 bed positions, from midthigh to skull, using Siemens Biograph mCT or Philips TF16 PET/CT

scanners. Whole body images were presented in the usual transaxial, coronal and saggital slices, for PET, CT and PET/CT fusion.

In University Medical Centre Ljubljana, the reports of FCH PET/CTs performed in prostate cancer patients were reviewed from 29th February 2012 until 11th November 2012. FCH PET/CTs were performed in compliance with Slovenian marketing authorisation granted to Iasocholine in April 2011.

In Hospital Tenon, in Paris, the reports of FCH PET/CTs performed in prostate cancer patients were reviewed from 12th November 2004 until 11th November 2012. FCH PET/CTs were performed as part of two successive clinical studies (CH02 Eudra CT number: 2004-003019-21 and then Ichorpro EudraCT number 2007-004419-69) until November 2009 and then in compliance with the French marketing authorisation granted to Iasocholine in April 2010.

We searched for solitary or multiple lesion(s) in the head (including brain) or in the neck, excluding only images evocative of bone metastatic spread or non-focal uptake such as diffuse intense uptake by the thyroid gland or the physiologic FCH uptake by the salivary or the lachrymal glands. When such foci were visible in the head or in the neck, we requested further data in order to try to characterise the lesions.

Results

In 8 patients referred to FCH PET/CT for prostate cancer, an incidental focus was found in the head

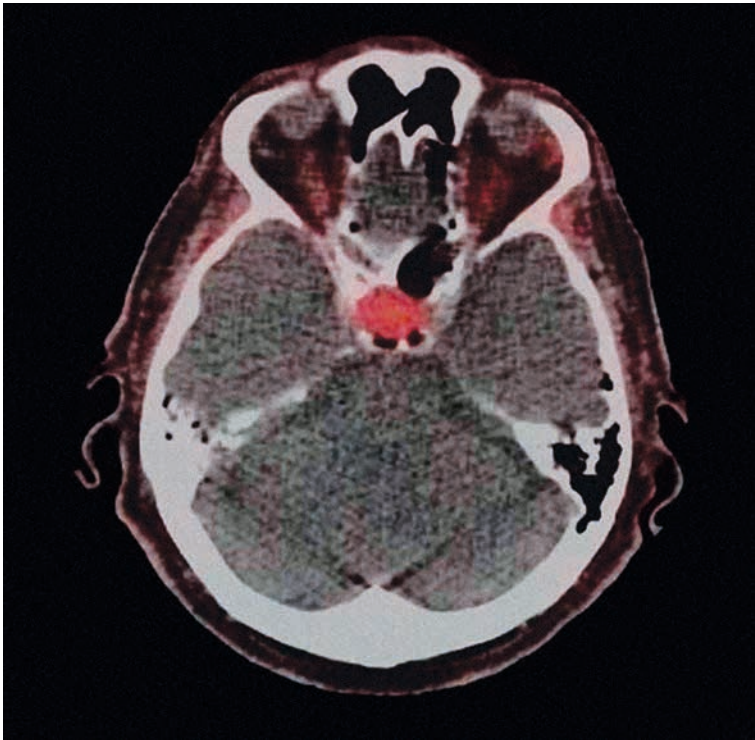


FIGURE 1. Positron emission tomography-computed tomography axial slice: Macroadenoma of pituitary gland that incidentally took-up ^{18}F -fluorocholine (SUVmax 3.7).

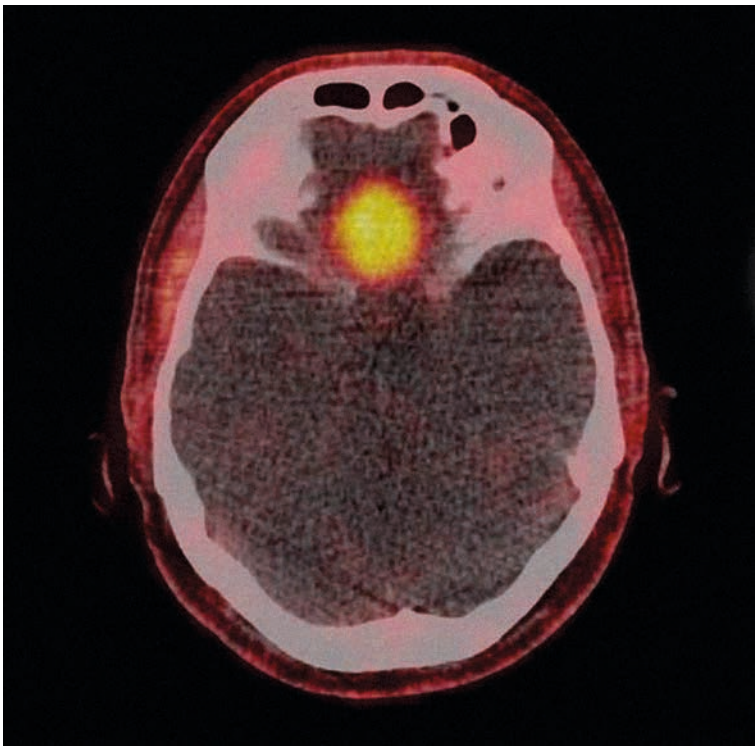


FIGURE 2. Positron emission tomography-computed tomography axial slice: Meningioma in the anterior cranial fossa that incidentally took-up ^{18}F -fluorocholine (SUVmax 3.7).

and neck region, which was finally diagnosed as corresponding to a benign tumour (Table 1). The standard of truth was histology in 2 cases, correlative imaging with MRI in 4 cases, $^{99\text{m}}\text{Tc}$ -sestaMIBI scintigraphy, ultrasonography and biology in one case, biology including PTH assay in one case. There were 3 pituitary adenomas (Figure 1), 2 meningiomas (Figure 2), 2 hyperfunctioning parathyroid glands (Figure 3) and 1 thyroid adenoma (Figure 4).

In 2 patients, the incidental focus corresponded histologically to a malignant lesion: 1 papillary carcinoma of the thyroid 45 mm in size and 1 cerebellar metastasis of a second primary cancer in the lung.

Discussion

To the best of our knowledge, the frequency of incidentalomas discovered on FCH PET/CT in head or in the neck has never been published. It was estimated to be 1.9% in our series, a thyroid nodule being the most frequent cause of incidentaloma (41%). Actually, our survey showed that the mention in the report of an incidental FCH uptake in the head or the neck led to further investigations in only 52% of cases. The variable impact of this discovery on patient management is probably due to the fact that, in patients with known prostate cancer, the characterisation of a brain lesion was considered more important than that of thyroid nodule or a focus in the thyroid bed. Overall the final diagnosis of those incidental foci which were further explored corresponded to a non-malignant lesion in 80% of cases (8/10).

The main limitation of this study is the fact that not all incidentalomas have been explored and that the final diagnosis of benign tumour is based on histology in only two cases (Table 1): one pituitary adenoma (patient #3) and one thyroid adenoma (patient #8). In the other cases, it has been set by a multidisciplinary medical team on follow-up data which were independent from FCH PET/CT.

Providing that those preliminary findings would be confirmed in larger series, we will briefly discuss if deliberately performing FCH PET/CT in patients presenting with or suspected of a benign tumour in the head or in the neck could be justified.

Pituitary adenomas

The pituitary gland has a moderately intense physiologic uptake of FCH, as shown on PET/MRI⁷, although it has been neglected in some previous

articles using PET/CT.⁵ In the 3 cases of pituitary adenoma of our series, an intense tumour uptake was observed.

To the best of our knowledge, this is the first mention of this incidental finding on FCH PET/CT. In one case, unexpected recurrence of a resected adenoma, suspected on FCH PET/CT, was confirmed by MRI. An inflammatory reaction after the surgical resection cannot be ruled out but seems improbable after three years. In another case, a non-functioning pituitary adenoma was confirmed at surgery; the patient also had another incidental FCH focus in the left vocal cord which was demonstrated to correspond to a calcified granuloma, confirming that inflammatory head and neck lesions can also show FCH uptake.⁵

The FDG uptake by functioning and non-functioning pituitary adenomas had been documented by several case reports and one series of such cases.⁸ FDG pituitary focus corresponded in most cases to macroadenoma and only rarely to microadenoma or malignancy.⁹ However, in case of adrenocorticotrophic hormone (ACTH) or growth hormone (GH) producing microadenomas, FDG PET, as a complement to MRI, resulted in 12 positive readings of 20 surgically verified pituitary microadenomas.¹⁰ The potential superiority of aminoacid PET tracers ^{11}C -tyrosine and ^{11}C -methionine over FDG in the visualisation and therapy follow-up of pituitary adenomas, in particular ACTH-secreting adenomas has been demonstrated.¹¹⁻¹³ PET imaging of prolactinomas and GH-secreting adenomas with ^{11}C -raclopride, a D2 radioligand, was proposed in the differential diagnosis with meningiomas and skull base neuromas and in treatment monitoring.¹⁴ Somatostatin receptors (SSR) can also be over-expressed in functioning pituitary adenomas, in particular those which are ACTH-secreting. On the other hand, no incidental uptake by a pituitary adenoma on SSR PET/CT has been reported until now, probably due to the physiologic pituitary uptake of the somatostatin analogue labelled with ^{68}Ga . In contrast SSR-PET/CT performed in a deliberate search for the source of inappropriate ACTH serum levels may lead in rare cases to detecting a pituitary adenoma in an unexpected location.¹⁵⁻¹⁶

We conclude from our observations that a definite FCH uptake in the pituitary should lead to characterisation of a probable lesion, at least with MRI. If recurrence or persistence of a known pituitary adenoma is suspected, it is doubtful whether FCH PET/CT will have any indication, or whether FDG should be preferred if PET/CT is indicated and ^{11}C -labeled tracers not available. Similarly to

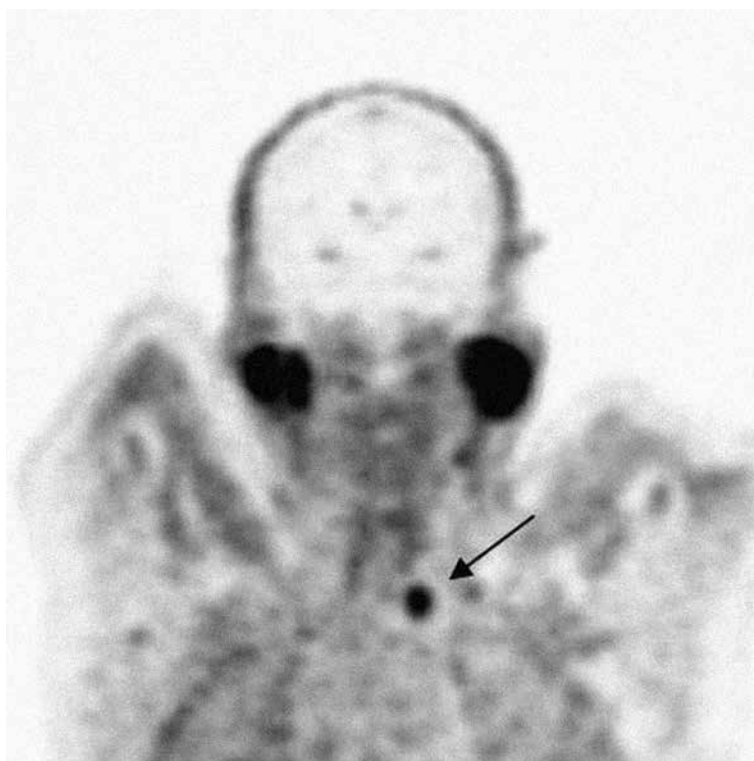


FIGURE 3. Positron emission tomography-computed tomography coronal slice: Adenoma of the parathyroid that incidentally took-up ^{18}F -fluorocholine (SUVmax 3.4).



FIGURE 4. Positron emission tomography-computed tomography axial slice: Thyroid adenoma that incidentally took-up ^{18}F -fluorocholine (SUVmax 3.3).

^{11}C -methionine and in contrast with FDG, FCH has the advantage of a low background activity in the brain cortex.

Meningiomas

FCH uptake is faint in the normal brain parenchyma, which permits PET/CT detection of gliomas,

even in some low grade tumours, and also of meningiomas⁵, as illustrated in the present study. It has been suggested that dynamic FCH PET acquisition can differentiate between those tumours.¹⁷ PET/MRI may also be useful to distinguish between glioblastoma and meningioma that both showed moderately intense FCH uptake while it was faint in brain tumours of a lower grade.⁷

Detection of meningiomas with ¹¹C-choline PET/CT was also reported.¹⁸ Relative to the contralateral side, ¹¹C-choline uptake was increased in all 7 meningiomas, whereas FDG uptake was decreased in 6 patients and increased in 1 of the 2 patients with grade II meningiomas. ¹¹C-acetate, another lipid PET tracer, showed high uptake in all 20 meningiomas, in contrast to the low uptake in surrounding normal brain tissue¹⁹, whereas with FDG 17 foci appeared photopenic and 3 hyperintense. ¹³N-ammonia also had relatively greater uptake in 10 meningiomas when compared with FDG.²⁰ Aminoacid PET tracers are also capable of demonstrating meningiomas: for delineation of gross tumour volume in stereotactic radiotherapy using ¹¹C-methionine²¹, or in recurrent cases using ¹⁸F-fluoroethyltyrosine²², or in one patient referred to FDOPA PET for Parkinson's disease.²³ Furthermore, imaging meningioma with SSR scintigraphy has been reported for more than two decades and, more recently, a potential role for SSR PET/CT has been assessed, the detection rate being better than that of MRI.²⁴

In conclusion, an intense incidental FCH uptake may lead to discovery of a meningioma; in prostate cancer patients, this can have a major impact on their management since anti-androgen therapy would favour tumour development and put them at risk for neurological symptoms. It is clear that the field of view of the "whole-body" FCH PET/CT acquisition should include the brain⁶ in case of prostate cancer. In case of a known meningioma, determination of metabolic volume prior to radiotherapy or for surgery guidance is a valid indication for PET imaging. However many tracers can be used; for the moment, FCH may be seen as a newcomer.

Hyperfunctioning parathyroid glands

To the best of our knowledge, FCH uptake by hyperfunctioning parathyroid glands has never been described before. In one recent case report, a parathyroid adenoma was discovered on ¹¹C-choline PET/CT.²⁵ The discovery of an incidental hyperfunctioning parathyroid gland on FDG PET has

been reported.²⁶⁻²⁷ FDG has been proposed to stage parathyroid carcinoma, being more aggressive than adenoma or hyperplasia.²⁸ Discrepant results have been reported with FDG in the detection of adenoma or hyperplasia, a very low sensitivity in two short series^{29,30} or, in comparison with ^{99m}Tc-SestaMIBI, a better sensitivity (86% *vs.* 43%) but a lower specificity (78% *vs.* 90%)³¹; no recent series have been published. ¹¹C-methionine is currently the PET competitor for the detection of parathyroid adenomas, with a patient-based sensitivity of 81% and specificity of 70% according to a recent meta-analysis.³²

In conclusion, in the case of patient #6, unexpected parathyroid tumours can be localised on FCH PET/CT, on basis of the anatomical location on CT of a cervical FCH focus. Such an incidental image should prompt biochemical work-up, including serum PTH assay (patient #7), as prolonged hyperparathyroidism will be detrimental in those elderly patients and requires medical or surgical treatment.

Whether localising hyperfunctioning parathyroid glands could become an indication for FCH PET/CT requires comparative studies *vs.* the reference functional imaging ^{99m}Tc-SestaMIBI/¹²³I scintigraphy and/or *vs.* ¹¹C-methionine, the PET competitor. FCH PET imaging will benefit from a better resolution than SPECT, and delivery will be easier than for ¹¹C-methionine. But differential diagnosis with thyroid nodules taking-up FCH, as illustrated in our series, will be difficult, in particular in case of multinodular goitre, since dual isotope acquisition is not possible and subtraction technique will be very difficult.

Thyroid adenomas

Concerning FCH uptake by a benign thyroid nodule, two cases similar to that of patient #8 have been reported recently.^{33,34} Numerous articles addressed the diagnostic value of incidental FDG uptake by a thyroid nodule. It actually corresponds to a non-malignant origin in a majority of cases, 70%, 59% or 65% as derived from two recent large series and a meta-analysis.³⁵⁻³⁷

The FCH foci in the thyroid gland previously reported in literature corresponded to benign adenomas.^{33,34} However, in the present series 1 of the 2 incidental thyroid foci of FCH uptake which could be characterised corresponded to a papillary carcinoma. ¹¹C-choline has even been proposed in the detection of thyroid carcinoma and its metastases, performing better than FDG in a preliminary

series of 4 patients.³⁸ Therefore, it seems prudent that FCH uptake by a thyroid nodule prompts an adequate work-up to rule-out thyroid cancer.

In contrast it is unlikely that FCH may be helpful in characterising a thyroid nodule as malignant or benign. Even FDG lacks specificity for the detection of cancer in a thyroid nodule and, since FCH usually detects less-aggressive tumours, it may be expected non-malignant nodules would take-up FCH even more frequently.

Cost and cost-effectiveness

In the present study, the detection of those incidental lesions per se implied no extra-cost since FCH PET/CT was indicated because of prostate cancer. In the above discussion, we then speculated that the present finding of FCH uptake in some of those incidentalomas could lead to a deliberate indication of FCH PET/CT in patients with a diagnosed or suspected benign tumour. In this case, the cost-effectiveness of FCH PET/CT should be re-evaluated for each type of benign tumour, bearing in mind the cost of FCH PET/CT and of the alternative nuclear medicine examinations.³⁹ Briefly, PET/CT with FCH is more expensive than with FDG, and PET/CT is usually more expensive than SPECT/CT due to the higher price of the machine, but this is not always true e.g. 111In-pentretotide, somatostatin receptor ligand for SPECT, one of the alternatives for meningioma detection, is more expensive than FDG or FCH.

Conclusions

We described incidental FCH uptake in the head or in the neck, in 1.9% of the PET/CTs performed for staging or restaging prostate cancer. Some of those incidental FCH foci corresponded to malignancies, but more frequently (80%) to various benign tumours. In particular, for the first time, we observed FCH uptake in pituitary adenomas and in hyperfunctioning parathyroid glands. Such foci should be mentioned in the report, as meningioma or hyperparathyroidism may directly impact on management of a patient with prostate cancer. Since FCH is taken-up by slow-growing malignancies it could be expected that FCH PET/CT can detect benign tumours even more frequently than FDG PET/CT.

Furthermore, there might be a future indication for FCH PET/CT when one such tumour is already known or suspected: for post-operative control of

a resected pituitary adenoma, to guide surgery or radiotherapy of a meningioma or to localise hyperfunctioning parathyroid glands. In those indications, comparative studies with reference PET tracers could be undertaken, on basis of published case reports and the present preliminary series.

Acknowledgment

Authors acknowledge the motivation of team of our Nuclear Medicine centres for performing FCH PET/CT. They are grateful to Dr John Frank for English editing of their manuscript.

References

- Balogova S, Kobetz A, Huchet V, Michaud L, Kerrou K, Paycha F, et al. Evolution of the prescription of nuclear medicine examinations in prostate cancer since the registration of fluorocholine (18F): a two-year survey at hospital Tenon. *Med Nucl* 2012; **36**: 363-70.
- Cimitan M, Bortolus R, Morassut S, Canzonieri V, Garbeglio A, Baresic T, et al. [18F] fluorocholine PET/CT imaging for the detection of recurrent prostate cancer at PSA relapse: experience in 100 consecutive patients. *Eur J Nucl Med Mol Imaging* 2006; **33**: 1387-98.
- Treglia G, Giovannini E, Di Franco D, Calcagni ML, Rufini V, Picchio M, et al. The role of positron emission tomography using carbon-11 and fluorine-18 choline in tumors other than prostate cancer: a systematic review. *Ann Nucl Med* 2012; **26**: 451-61.
- Hodolič M, Fettich J, Cimitan M, Kragelj B, Goldsmith SJ. Unusual F-18 choline uptake in penile metastasis from prostate cancer. *Clin Nucl Med* 2012; **37**: e89-90.
- Schillaci O, Calabria F, Tavolozza M, Ciccio C, Carlini M, Caracciolo CR, et al. 18F-choline PET/CT physiological distribution and pitfalls in image interpretation: experience in 80 patients with prostate cancer. *Nucl Med Commun* 2010; **31**: 39-45.
- Balogova S, Nataf V, Gutman F, Huchet V, Kerrou K, Pascal O, et al. Biological recurrence of prostate cancer: Interest of whole-body fluorocholine (18F) PET/CT. *Med Nucl* 2010; **34**: 540-5.
- Mertens K, Ham H, Deblaere K, Kalala JP, Van den Broecke C, Slaets D, et al. Distribution patterns of 18F-labelled fluoromethylcholine in normal structures and tumors of the head: a PET/MRI evaluation. *Clin Nucl Med* 2012; **37**: e196-203.
- Jeong SY, Lee SW, Lee HJ, Kang S, Seo JH, Chun KA, et al. Incidental pituitary uptake on whole-body 18F-FDG PET/CT: a multicentre study. *Eur J Nucl Med Mol Imaging* 2010; **37**: 2334-43.
- Hyun SH, Choi JY, Lee KH, Choe YS, Kim BT. Incidental focal 18F-FDG uptake in the pituitary gland: clinical significance and differential diagnostic criteria. *J Nucl Med* 2011; **52**: 547-50.
- De Souza B, Brunetti A, Fulham MJ, Brooks RA, DeMichele D, Cook P et al. Pituitary microadenomas: a PET study. *Radiology* 1990; **177**: 39-44.
- Daemen BJ, Zwertbroek R, Elsinga PH, Paans AM, Doorenbos H, Vaalburg W. PET studies with L-[1-11C]tyrosine, L-[methyl-11C]methionine and 18F-fluorodeoxyglucose in prolactinomas in relation to bromocryptine treatment. *Eur J Nucl Med* 1991; **18**: 453-60.
- Bergström M, Muhr C, Lundberg PO, Långström B. PET as a tool in the clinical evaluation of pituitary adenomas. *J Nucl Med* 1991; **32**: 10-5.
- Tang BN, Levivier M, Heureux M, Wikler D, Massager N, Devriendt D et al. 11C-methionine PET for the diagnosis and management of recurrent pituitary adenomas. *Eur J Nucl Med Mol Imaging* 2006; **33**: 169-78.
- Muhr C. Positron emission tomography in acromegaly and other pituitary adenoma patients. *Neuroendocrinology* 2006; **83**: 205-10.

15. Naswa N, Das CJ, Sharma P, Karunanithi S, Bal C, Kumar R. Ectopic pituitary adenoma with empty sella in the setting of MEN-1 syndrome detection with 68Ga-DOTANOC PET/CT. *Jpn J Radiol* 2012; **30**: 783-6.
16. Veit JA, Boehm B, Luster M, Scheuerle A, Rotter N, Rettinger G, et al. Detection of paranasal ectopic adrenocorticotrophic hormone-secreting pituitary adenoma by Ga-68-DOTANOC positron-emission tomography-computed tomography. *Laryngoscope* 2013; **123**: 1132-5.
17. Mertens K, Bolcaen J, Ham H, Deblaere K, Van den Broecke C, Boterberg T, et al. The optimal timing for imaging brain tumours and other brain lesions with 18F-labelled fluoromethylcholine: a dynamic positron emission tomography study. *Nucl Med Commun* 2012; **33**: 954-9.
18. Giovacchini G, Fallanca F, Landoni C, Gianolli L, Picozzi P, Attuati L, et al. C-11 choline versus F-18 fluorodeoxyglucose for imaging meningiomas: an initial experience. *Clin Nucl Med* 2009; **34**: 7-10.
19. Liu RS, Chang CP, Guo WY, Pan DH, Ho DM, Chang CW, et al. 1-11C-acetate versus 18F-FDG PET in detection of meningioma and monitoring the effect of gamma-knife radiosurgery. *J Nucl Med* 2010; **51**: 883-91.
20. Xiangsong Z, Xingchong S, Chang Y, Xiaoyan W, Zhifeng C. 13N-NH3 versus F-18 FDG in detection of intracranial meningioma: initial report. *Clin Nucl Med* 2011; **36**: 1003-6.
21. Astner ST, Dobrei-Ciuchendea M, Essler M, Bundschuh RA, Sai H, Schwaiger M, et al. Effect of 11C-methionine-positron emission tomography on gross tumor volume delineation in stereotactic radiotherapy of skull base meningiomas. *Int J Radiat Oncol Biol Phys* 2008; **72**: 1161-7.
22. Rutten I, Cabay JE, Withofs N, Lemaire C, Aerts J, Baart V, et al. PET/CT of skull base meningiomas using 2-18F-fluoro-L-tyrosine: initial report. *J Nucl Med* 2007; **48**: 720-5.
23. González-Forero M, Prieto E, Domínguez I, Vigil C, Peñuelas I, Arbizu J. Dual time point 18F-FDOPA PET as a tool for characterizing brain tumors. *Rev Esp Med Nucl* 2011; **30**: 88-93.
24. Afshar-Oromieh A, Giesel FL, Linhart HG, Haberkorn U, Haufe S, Combs SE, et al. Detection of cranial meningiomas: comparison of 68Ga-DOTATOC PET/CT and contrast-enhanced MRI. *Eur J Nucl Med Mol Imaging* 2012; **39**: 1409-15.
25. Mapelli P, Busnardo E, Magnani P, Freschi M, Picchio M, Gianolli L, et al. Incidental finding of parathyroid adenoma with 11C-choline PET/CT. *Clin Nucl Med* 2012; **37**: 593-5.
26. Mendoza PL, Ongkeko EE, Santiago JF. Silent parathyroid adenoma mistakenly interpreted on FDG-PET as thyroid cancer metastasis in a patient with elevated thyroglobulin and negative I-131 whole body scan and removed by radioguided minimally invasive surgery. *Clin Nucl Med* 2008; **33**: 23-5.
27. Kim MK, Kim GS, Kim SY, Baek KH, Kang MI, Lee KW, et al. F-18 FDG-avid intrathyroidal parathyroid adenoma mimicking follicular neoplasm. *Clin Nucl Med* 2009; **34**: 178-9.
28. Evangelista L, Sorgato N, Torresan F, Boschin IM, Pennelli G, Saladini G, et al. FDG-PET/CT and parathyroid carcinoma: Review of literature and illustrative case series. *World J Clin Oncol* 2011; **2**: 348-54.
29. Sisson JC, Thompson NW, Ackerman RJ, Wahl RL. Use of 2-[F-18]-fluoro-2-deoxy-D-glucose PET to locate parathyroid adenomas in primary hyperparathyroidism. *Radiology* 1994; **192**: 280.
30. Melon P, Luxen A, Hamoir E, Meurisse M. Fluorine-18-fluorodeoxyglucose positron emission tomography for preoperative parathyroid imaging in primary hyperparathyroidism. *Eur J Nucl Med* 1995; **22**: 556-8.
31. Neumann DR, Esselstyn CB, MacIntyre WJ, Go RT, Obuchowski NA, Chen EQ, Licata AA. Comparison of FDG-PET and sestamibi-SPECT in primary hyperparathyroidism. *J Nucl Med* 1996; **37**: 1809-15.
32. Caldarella C, Treglia G, Isgrò MA, Giordano A. Diagnostic performance of positron emission tomography using 11C-methionine in patients with suspected parathyroid adenoma: a meta-analysis. *Endocrine* 2013; **43**: 78-83.
33. García Vicente AM, Núñez García A, Soriano Castrejón AM, Jiménez Londoño GA, Cordero García JM, Palomar Muñoz A. Pitfalls with 18F-choline PET/CT in patients with prostate cancer. *Rev Esp Med Nucl Imagen Mol* 2013; **32**: 37-9.
34. Treglia G, Giovannini E, Mirk P, Di Franco D, Oragano L, Bertagna F. A thyroid incidentaloma detected by 18F-Choline PET/CT. *Clin Nucl Med* 2014; **39**(4): e267-9.
35. Yang Z, Shi W, Zhu B, Hu S, Zhang Y, Wang M, et al. Prevalence and risk of cancer of thyroid incidentaloma identified by fluorine-18 fluorodeoxyglucose positron emission tomography/computed tomography. *J Otolaryngol Head Neck Surg* 2012; **41**: 327-33.
36. Bertagna F, Treglia G, Piccardo A, Giovannini E, Bosio G, Biasiotto G, et al. F18-FDG-PET/CT thyroid incidentalomas: a wide retrospective analysis in three Italian centres on the significance of focal uptake and SUV value. *Endocrine* 2013; **43**: 678-85.
37. Soelberg KK, Bonnema SJ, Brix TH, Hegedüs L. Risk of malignancy in thyroid incidentalomas detected by 18F-fluorodeoxyglucose positron emission tomography: a systematic review. *Thyroid* 2012; **22**: 918-25.
38. Wu HB, Wang QS, Wang MF, Li HS. Utility of ¹¹C-choline imaging as a supplement to F-18 FDG PET imaging for detection of thyroid carcinoma. *Clin Nucl Med* 2011; **36**: 91-5.
39. Hodolic M, Michaud L, Huchet V, Balogova S, Nataf V, Kerrou K, et al. Consequence of the introduction of routine FCH PET/CT imaging in patients with prostate cancer: a dual centre survey. *Radiol Oncol* 2014; **48**: 20-8.

Clinical and radiologic features of extraskeletal myxoid chondrosarcoma including initial presentation, local recurrence, and metastases

Neena Kapoor, Atul B. Shinagare, Jyothi P. Jagannathan, Shaan H. Shah, Katherine M. Krajewski, Jason L. Hornick, Nikhil H. Ramaiya

Department of Imaging, Dana-Farber Cancer Institute/ Brigham and Women's Hospital, Harvard Medical School, Boston, MA 02115, USA

Radiol Oncol 2014; 48(3): 235-242.

Received 17 October 2013
Accepted 23 October 2013

Correspondence to: Neena Kapoor, M.D., Department of Imaging, Department of Radiology, Brigham and Women's Hospital, Harvard Medical School, 450 Brookline Ave, Boston, MA 02115, USA. Phone: +1 617 650 7465; Fax: +1 617 582 8574 ; Email: nkapoor@partners.org

Disclosure: No potential conflicts of interest were disclosed.

Background. The aim of the study was to evaluate the clinical and imaging features of extraskeletal myxoid chondrosarcoma (EMC) including initial presentation, recurrence, and metastases.

Patients and methods. In this institutional review board-approved retrospective study, imaging features of 13 patients with pathologically proven EMC seen from August 1995 to December 2011 were analyzed. The group included 3 women and 10 men and the mean age was 54 years (range 29-73 years). Imaging studies were evaluated by two radiologists in consensus. Location, size, and imaging features of primary tumors were recorded as well as the presence of recurrent disease and location of metastases.

Results. Among 13 patients, 3 died during the timeframe of this study. Nine patients had primary tumor in the lower extremity, and average tumor size was 9.3 cm (range 3.3-18 cm). On MRI, primary tumors were hyperintense on T2, isointense to muscle on T1, and demonstrated peripheral/septal enhancement. Three patients had local recurrence and 12 had metastatic disease, with lung involvement being the most common. Tumor density on contrast enhanced CT ranged from 8.2 to 82.9 Hounsfield unit (HU). FDG-PET/CT imaging was performed in 3 patients. One patient had no FDG avid disease and 2 patients had metastatic disease with standard uptake values (SUV) of 2.8 and 7.4. The patient with intense FDG uptake demonstrated more solid appearing tumor burden and had the shortest survival.

Conclusions. EMC is a rare tumor that often occurs in the lower extremities and frequently metastasizes to the lungs. Increased tumor density and increased FDG uptake may be related to more aggressive disease.

Key words: extraskeletal myxoid chondrosarcoma; CT; MRI; FDG-PET/CT

Introduction

Extraskeletal myxoid chondrosarcoma (EMC) is a rare soft tissue tumor characterized by uniform spindle cells arranged in a reticular growth pattern in abundant myxoid stroma.^{1,2} Considered to be slow growing, it generally arises in the deep soft tissues of the proximal limbs but several unusual sites such as the scrotum and finger have been documented.³⁻⁵ The typical appearance is of a lobulated mass composed of gelatinous nodules with internal fibrous septa.⁶ Although originally

believed to be a variant of chondrosarcoma, the World Health organization has classified it as a tumor of uncertain differentiation due to its lack of cartilaginous differentiation.³ Additionally, cytogenetic studies have shown that EMC is a unique entity with a reciprocal translocation, t(9;22) (q22;q12), not seen in conventional skeletal chondrosarcoma.⁷⁻¹² Despite being considered a low grade sarcoma with a prolonged clinical course, extraskeletal myxoid chondrosarcoma has been shown to have a high rate of local recurrence and metastasis.¹³

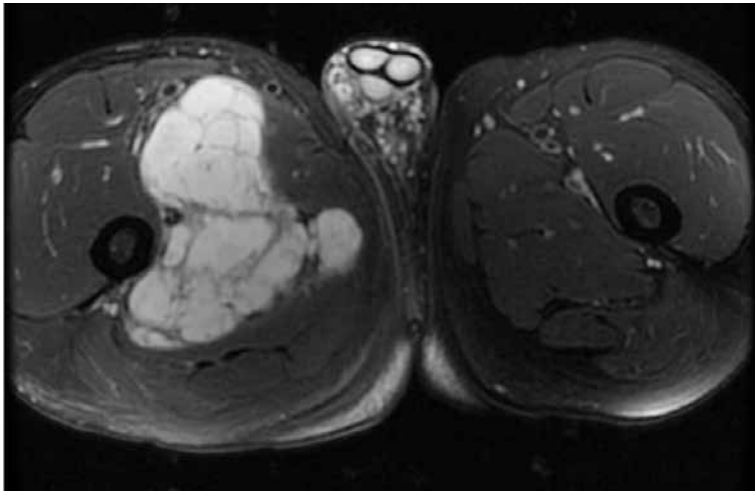


FIGURE 1A. 64 year old male with slow growing extraskelletal myxoid chondrosarcoma. Axial T2 fat-saturated (FS) MRI demonstrates a large lobulated T2 hyperintense mass with T2 hypointense internal fibrous septa.

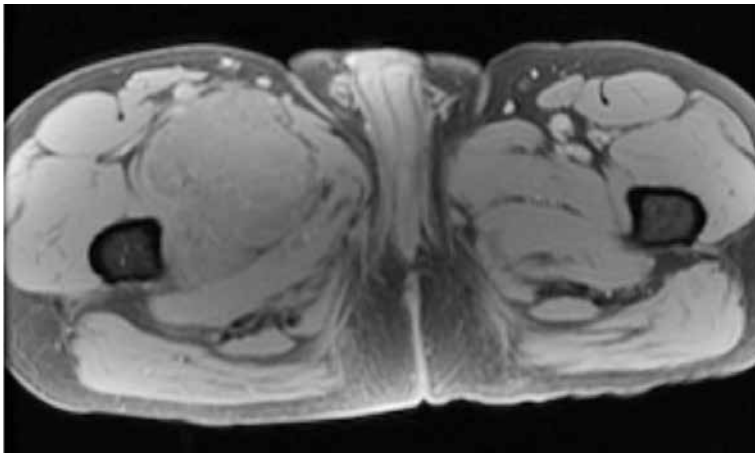


FIGURE 1B. Axial T1 fast spoiled gradient-echo (FSPGR) FS pre-contrast MRI shows that this tumor is isointense to muscle on T1 weighted images.

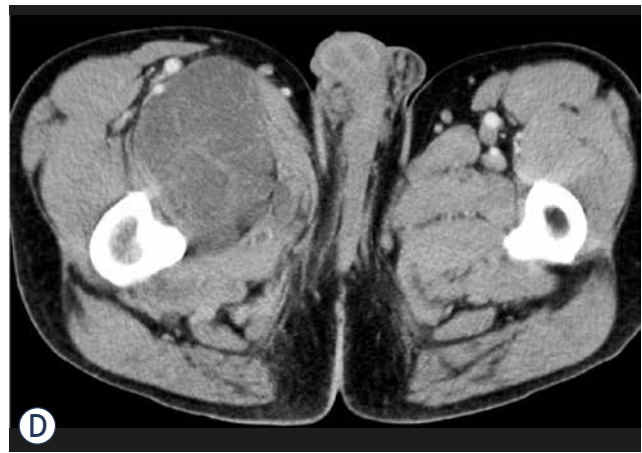
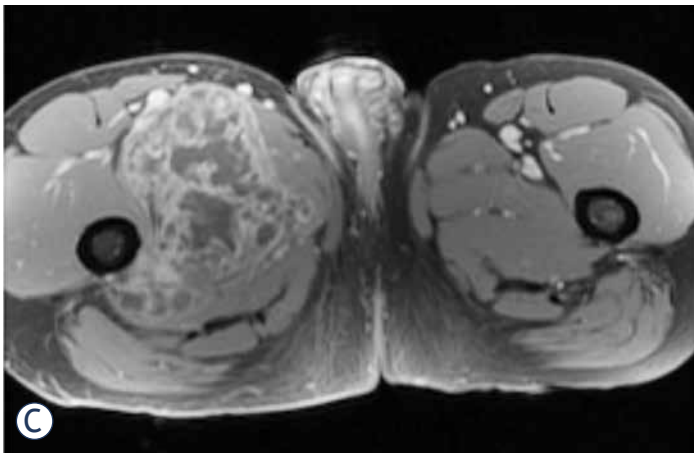


FIGURE 1C. Axial T1 FSPGR FS post-contrast MRI demonstrates peripheral/septal contrast enhancement. **(D).** Axial contrast enhanced CT shows that this mass is slightly hypodense to muscle.

The literature documenting the imaging features of extraskelletal myxoid chondrosarcoma is limited. With rare exception, most of the radiology literature has consisted of case reports or has been based on a single imaging modality with little evaluation of the imaging spectrum.³⁻⁶ The purpose of this study was to evaluate the imaging features of primary extraskelletal myxoid chondrosarcoma, as well as the imaging characteristics of local recurrence and metastatic disease.

Patients and methods

Patients

In this institutional review board-approved retrospective study, the electronic medical records of 13 patients with pathologically proven extraskelletal myxoid chondrosarcoma who were evaluated at our institution from August 1995 to December 2011 were reviewed. No patients with pathologically proved EMC were excluded from the study.

Image analysis

A systematic review of all imaging studies, including baseline and follow-up studies, was performed by two radiologists with 8 and 13 years of experience in consensus. A total of 7 MRIs, 26 CTs, and 3 FDG-PET/CT studies were analyzed. Four of the 13 patients had MR imaging of their primary tumor at our institution. For these patients the location and size (largest dimension in two orthogonal planes) was documented. The T1, T2, and enhancement characteristics were noted. T2 images with and without fat saturation and STIR images were in-

cluded when evaluating T2 characteristics of the tumors. The same features were also evaluated in the 3 patients with histologically proven local recurrence.

Twelve patients had metastatic disease, with all undergoing contrast enhanced CT. Two radiologists reviewed the sites and imaging features of metastases in consensus. The Hounsfield unit (HU) of the center of each primary, recurrent, and metastatic site was measured to determine if CT attenuation correlated with the classic pathologic description of abundant myxoid stroma. Density measurements were performed on lung metastases only if tumor opacity on mediastinal window images was greater than half the size of that seen on lung window images. This technique has been used in other studies to correlate CT attenuation of lung nodules with prognosis.^{14,15} FDG-PET/CT imaging was performed on three patients with metastatic disease who demonstrated progressive disease on diagnostic restaging CT scans and were enrolled in experimental clinical trials. On FDG-PET/CT, the FDG avidity (standard uptake value [SUV]_{max}) of the largest tumor was recorded.

Histopathologic and clinical correlation

The histology was reviewed by a single pathologist from our institution with expertise in sarcoma. The following pathologic features were recorded: mitotic rate, necrosis, and tumor margin. It is impractical and unnecessary in clinical practice to histologically confirm each metastatic site. However, at least one metastatic site in each of these patients was confirmed by biopsy. The remaining sites of disease were presumed to be metastatic if they showed unequivocal progression on imaging or if they showed treatment response consistent with the overall clinical picture. Other clinical features including primary presentation, treatment offered, recurrence or metastasis-free interval and outcome were also noted.

Statistical analysis

In order to study the effect of size of the primary tumor on behavior of EMC, we correlated the tumor size (largest dimension in two orthogonal planes) with metastasis-free interval using Spearman correlation. Since in our experience, the majority of EMCs occurred in the extremities, the extremity EMCs were compared with EMC in the torso for differences in size and metastasis-free interval (Mann-Whitney test). Non-parametric tests were used in order to minimize the effect of a few outly-

ing values. We originally intended to analyze the effect of size and location on recurrence-free interval and survival; however, given the small number of patients with local recurrence and patients deceased, we did not perform that analysis.

Results

Patients

The patient population consisted of 3 women and 10 men, with a mean age of 54 years (range 29–73 years) (Table 1). Nine patients had their primary tumor in the lower extremity. The site of primary tumor was in the pelvis for 2 patients and in the spine for 2 patients (Table 2). The average follow up interval was 40.5 months (range 7–194 months). One patient was lost to follow up. Three patients had locally recurrent disease and 12 patients had metastases. Three patients died during the time-frame of the study, 1 was lost to follow up, and 9 are still alive.

Imaging features of primary disease

The average tumor size was 9.3 cm (range 3.3–18 cm). All tumors were large and lobular, with no internal calcification. Four patients had MRI of the primary tumor. Tumors were isointense to muscle on T1, hyperintense to muscle on T2, and contained T2 hypointense internal septa. Primary tumors also demonstrated peripheral/septal enhancement (Figure 1). Contrast enhanced CT imaging was

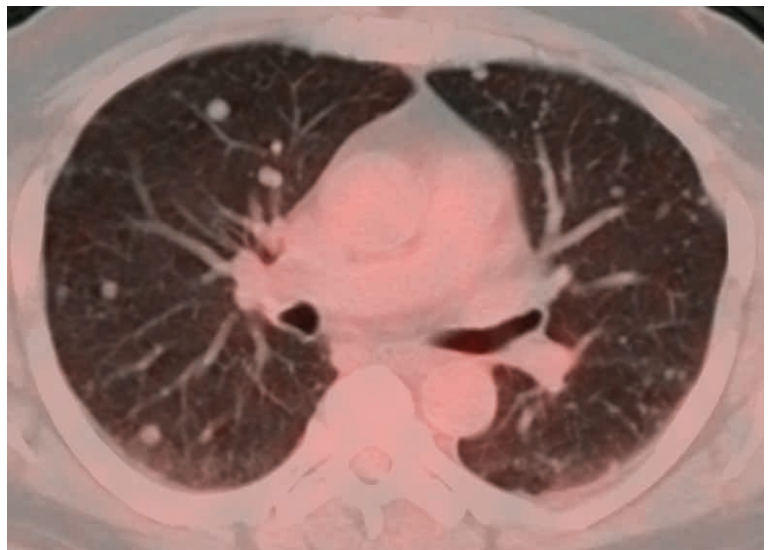


FIGURE 1E. FDG-PET/CT images show no significant FDG uptake in numerous lung metastases.

TABLE 1. Clinical features of patients with extraskelletal myxoid chondrosarcoma

Case	Age	Gender	Primary site	Tumor size (cm)	Time to recurrence (months)	Time from diagnosis to metastases (months)	Survival after diagnosis (months)
1	68	M	Thigh	3.3		25	
2	67	M	Foot	4.2		40	
3	53	M	Thigh	7		50	
4	43	M	Thigh	9.5		0	
5	29	M	Calf	12		10	18
6	68	F	Thigh	13		0	
7	64	M	Thigh	14		0	81
8	44	F	Thigh	15		0	
9	73	M	Thigh	18	81	93	143
10	32	M	Spine	4.3			
11	59	F	Spine	6.6		0	
12	54	M	Pelvis	8	4	4	
13	62	M	Pelvis	10	72	50	

F = female; M = male



FIGURE 2. 54 year old male with extraskelletal myxoid chondrosarcoma. FDG-PET/CT imaging shows mild peripheral FDG uptake with an standard uptake value (SUV)_{max} of 2.8 in a patient with mildly dense tumor burden.

available for 2 primary tumors which were slightly hypodense to muscle with HU measuring 23.4 and 30.2 (Table 3).

Local recurrence

Three patients had locally recurrent disease. The average time to recurrence was 52.3 months (range 4–81 months). Surveillance imaging varied among patients but generally consisted of CT imaging

every 3–6 months. Of the three patients with local recurrence, one patient had routine MRI surveillance every year while the other two patients had MRI based on their clinical situation. One patient had clinical symptoms that lead to an MRI while the other patient has local recurrence that was detected on surveillance CT. Of note, MRI in this case revealed more extensive tumor burden which was underestimated on CT. In all cases, there was no statistically significant correlation between the size of the original tumor and recurrent disease.

The appearance of recurrent disease was similar to that of primary disease. Masses were lobular, extremely T2 hyperintense, isointense on T1, and usually demonstrated T2 hypointense internal septa and peripheral/septal enhancement. The three patients also had contrast enhanced CT imaging of their local recurrence. Two patients had recurrent tumor that was isodense to muscle. The HU of the other patient's recurrent tumor was 72.4. However, this tumor was immediately adjacent to a femoral prosthesis and measurement was compromised by substantial streak artifact. The density of this tumor was likely closer to that of the patient's metastatic disease which measured 32.4 to 39.7 HU.

Metastatic disease

Twelve patients developed metastases. The average time between initial presentation and development of metastatic disease was 7 months (range 0–93 months). Imaging follow up for patients var-

TABLE 2. Location of metastatic disease

Site	Total number of patients
Lung Pleura/parenchyma	12
Bone	3
Abdominal/pelvic nodes	2
Soft tissues	2
Mediastinal nodes	1
Peritoneum	1
Abdominal/pelvic viscera	0

ied but generally consisted of CT staging every 3 to 6 months. There was no correlation between size of the primary tumor and metastasis free interval. All twelve patients had lung metastases, making it the most frequent site of tumor metastasis regardless of original tumor site (Table 2). Bone was the next most common site, though far less likely with only 3 patients developing osseous metastases. Osseous metastases were lytic in all three, and in 2 of the 3 patients were associated with a soft tissue component. Abdominal or pelvic viscera, such as liver, spleen, pancreas, and kidneys, were not involved. Metastatic lesions demonstrated HU ranging from 8.2 to 82.9, with median of 31.2 HU. No correlation was seen between tumor size and metastasis-free interval. No significant difference was seen in tumor size or metastasis-free interval between EMC in the extremity or torso.

FDG-PET/CT imaging was performed on three patients with metastases who demonstrated progressive disease on diagnostic restaging CT scans and were enrolled in experimental clinical trials. One patient had non-FDG avid disease and another patient had mild peripheral tumor uptake with an SUV_{max} 2.8 (Figure 1 and 2). The third patient had intense FDG avid disease with an SUV_{max} of 7.4 (Figure 3). During the time period of this study, 2 of these 3 patients died. The patient with intense FDG uptake was also the patient with solid appearing metastatic disease (82.9 HU). This patient died within 18 months of diagnosis. The patient with no significant FDG uptake had low density metastases on contrast enhanced CT (33.6 HU), which is more typical of myxoid tumors, and died 81 months after diagnosis. The patient with mildly FDG avid disease had metastatic tumor measuring 41.0 HU. This patient is still a live, approximately 43 months after diagnosis. Table 4 summarizes the SUV_{max} , CT density, and survival after diagnosis for the three patients who obtained FDG-PET/CT imaging.



FIGURE 3A. 29 year old male with unusually aggressive extraskelatal myxoid chondrosarcoma presenting in the calf. Axial FDG-PET/CT demonstrating significant FDG uptake (SUV_{max} 7.4) in bone metastasis in a patient with high density tumor burden.

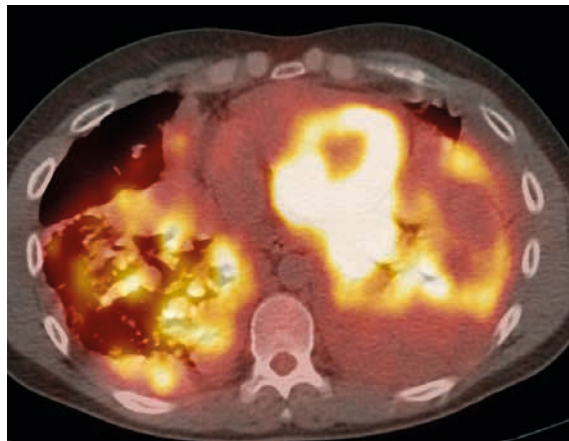


FIGURE 3B. Axial FDG-PET/CT also showing significant FDG uptake in pulmonary and pleural metastases.

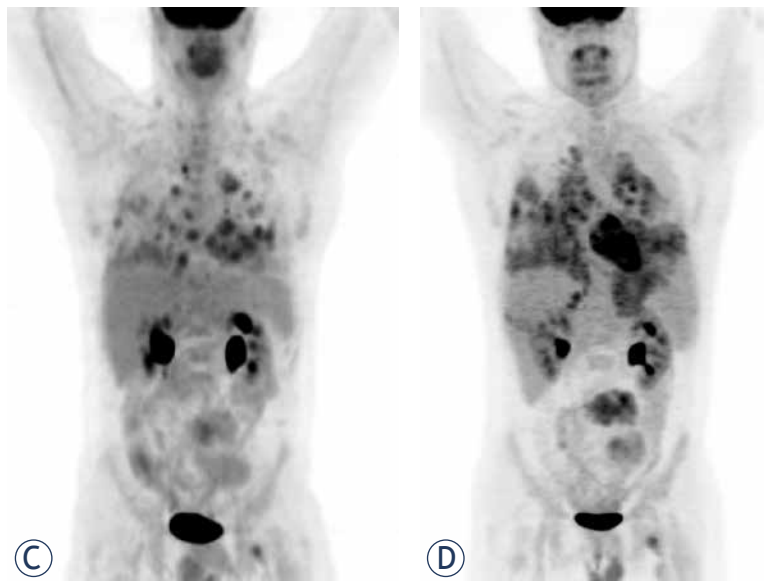


FIGURE 3C. FDG PET study on October 2008 demonstrating tumor burden. (D). FDG PET study on December 2008 shows rapid evolution of tumor burden from October 2008.

TABLE 3. Hounsfield units of primary, recurrent, and metastatic tumor burden

Case	Primary	Recurrence	Mediastinal nodes	Abdominal nodes	Retroperitoneum	Lung	Soft tissue	Bone
1				29.4		25.7		
2						11.0		
3						20.3		
4						14.0		
5			61.1			82.9		56.4
6						8.2		
7	23.4		21.2		33.6	21.4	26.8	
9		72.4			39.7	34.8		32.4
11	30.2		38.1			20.0	53.2	
12		41.0				37.3		
13		32.2				16.9		

Hounsfield units were measured in the center of the lesion on contrast enhanced CTs. If patients had multiple studies, the study with the largest tumor burden was used. For patients with multiple lung or nodal metastases, the average Hounsfield unit is provided. One patient had lung metastases that were too small to accurately measure.

TABLE 4. Density and standard uptake value (SUV)_{max} of patients with PET imaging

	Survival after diagnosis	SUV _{max}	HU
Case 7	81	0	33.6
Case 12		2.8	41.0
Case 5	18	7.4	82.9

Highest Hounsfield unit (HU) measured including primary, recurrent, or metastatic tumor burden on contrast enhanced CT.

Histopathologic correlation

Eleven of the thirteen patients had wide local excision as part of their treatment. The two patients who were not treated surgically had pulmonary metastases at the time of presentation. Three tumors demonstrated necrosis. Mitotic rate was generally low, ranging from 1–4 per 10 high-power fields. Of note, the patient with intense FDG uptake showed high grade tumor. Histologically, tumor cells were arranged in a reticular architecture with abundant myxoid stroma. Tumors were composed of bland and uniform spindle cells with hyperchromatic nuclei and delicate eosinophilic cytoplasm. Fluorescence in situ hybridization (FISH) using break-apart probes showed EWSR1 rearrangement at 22q12 in one case (Figure 4).

Clinical correlation

Three patients died during the course of this study. All but 2 of the 13 patients were initially treated

with surgical resection. The 2 patients who did not receive surgery had pulmonary metastases at the time of presentation. Five patients received chemotherapy and radiation as additional treatment at some point during their illness. Two received only additional radiation therapy after surgery and 1 received only additional chemotherapy. As mentioned, 1 patient demonstrated particularly aggressive tumor. This patient had a wide local resection of his primary tumor and later went on to receive radiation and chemotherapy.

Discussion

Extraskelatal myxoid chondrosarcoma is a rare neoplasm. The radiology literature about this entity is sparse, and to our knowledge this is one of the first studies to report the entire imaging spectrum of primary, recurrent, and metastatic disease of patients from a single institution.

Extraskelatal myxoid chondrosarcoma predominantly occurs in the soft tissues of the lower extremities and has a prolonged clinical course.¹³ The mean age of the cohort was 54 years (range 29–73 years), similar to other studies.^{2,13} Approximately 54% of patients in this cohort had primary disease in the thigh, which is consistent with prior reported studies. The average tumor size was 9.3 cm with a range of 3.3 to 18 cm (Table 1).

On MRI, all primary tumors were hyperintense on T2, isointense to muscle on T1, and demonstrated peripheral/septal enhancement. These results



FIGURE 4A. 62 year old male with extraskelatal myxoid chondrosarcoma in the pelvis. Axial contrast enhanced CT showing locally recurrent tumor in the left perineum that is isointense to muscle.

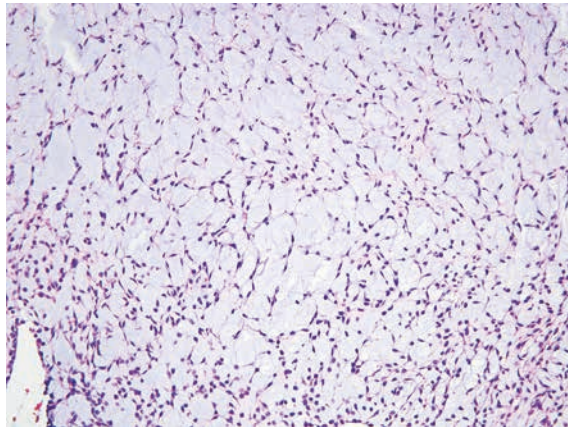


FIGURE 4D. The tumor cells are arranged in a reticular architecture with abundant myxoid stroma.

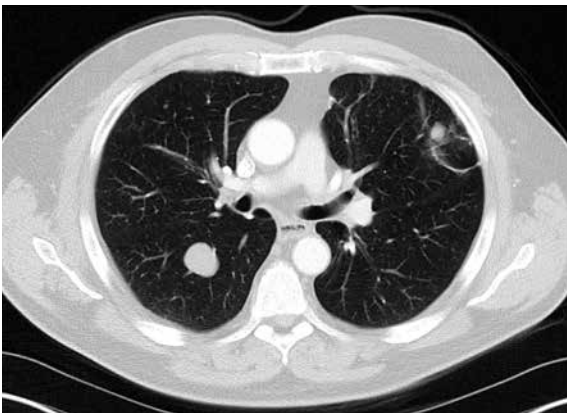


FIGURE 4B. Numerous, large lung metastases.

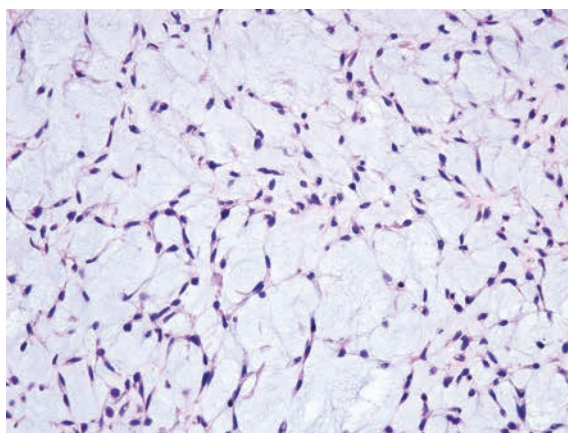


FIGURE 4E. The tumor is composed of bland and uniform spindle cells with hyperchromatic nuclei and delicate eosinophilic cytoplasm.

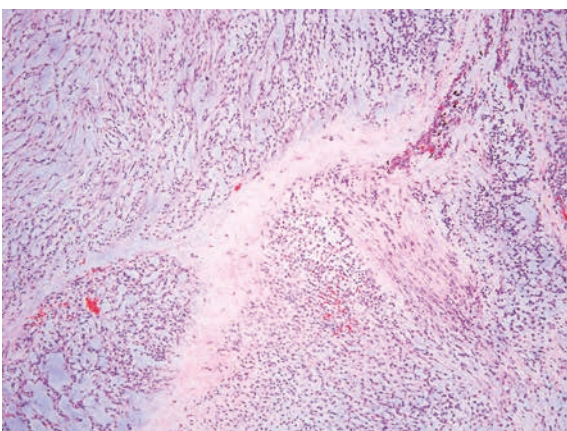


FIGURE 4C. The tumor shows a lobulated appearance.

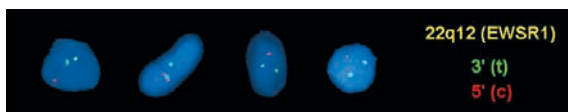


FIGURE 4F. Fluorescence in situ hybridization (FISH) using break-apart probes shows EWSR1 rearrangement at 22q12. Note the separation of the red (centromeric) and green (telomeric) probes

differ from another study in which the T1 characteristics were predominantly intermediate or high relative to muscle.⁶ This could reflect some degree of variability in the T1 appearance of the tumor.

High T2 signal and heterogeneous enhancement are similar findings to previously reported MRI characteristics of primary tumor.⁶ On contrast enhanced CT, primary tumors were isodense to slightly hypodense to muscle with no internal calcification. Local recurrence occurred in three patients with similar imaging features to the primary tumor. Given that EMC can have a similar density to muscle on CT while appearing extremely hyper-

intense on T2 weighted MRI, MRI seems to be the best modality for detecting primary disease and local recurrence.

Twelve patients had metastatic disease, with all 12 having at least lung metastases. Bone and nodal involvement was present in several patients. Interestingly, abdominal visceral involvement was not seen. These findings are similar to a prior study which showed that lung metastases were the most common site of metastatic disease.² The total number of patients in our study with metastases was higher than a previous study which reported 13 out of 42 patients either presenting with or developing metastases during an average follow up period of 7.4 years.¹³ The higher level of metastases in our cohort could be due to the fact that our institution is a tertiary care hospital that is a referral center for complicated cases.

Three out of 13 patients died in this study population. This corresponds to the low grade nature of EMC and previous reports of an overall survival of 100% at 5 years and 88% at 10 years.¹³ One of the patients who died had a particularly aggressive form of the disease. This patient was the youngest at 29 years and only lived 18 months after diagnosis. Imaging findings in this patient were somewhat different than the other patients. On CT, the patient's tumor was more solid appearing (82.9 HU) than that of other patients. It was also FDG avid with an SUV_{max} of 7.4. Two other patients had FDG-PET/CT imaging. Their tumors were either not FDG avid or only mildly so. Their disease burden demonstrated lower Hounsfield unit values and a more protracted clinical course which is typical of EMC. This raises the possibility that tumor density on contrast enhanced CT and FDG-PET could provide useful prognostic information. FDG-PET uptake has already been shown to have prognostic significance in other types of conventional chondrosarcoma.¹⁶ This is not to suggest that FDG-PET/CT imaging should be done in all cases of EMC, but rather that it may be useful in patients where there is concern about tumor aggressiveness and in patients with tumor burden that is hyperdense to muscle on contrast enhanced CT.

Our study has several limitations. First, the sample size was small due to the rarity of the disease, particularly in a single institution. Second, some patients presented to our institution after initial imaging and treatment were performed at an outside hospital. Imaging of the primary tumor was therefore not available for some of these cases. Despite the limitations of this study, our findings raise the hypothesis that tumor density on contrast

enhanced CT and FDG-PET uptake may correlate with clinical behavior. This requires further exploration. Furthermore, although it is a rare tumor, EMC should be included in one's differential for extraskelatal soft tissues masses which display little to no internal calcification, peripheral/septal enhancement, and increased T2 prolongation. Imaging of the chest is also crucial given the frequency of lung metastases in patients with this tumor.

References

- Saleh G, Evans HL, Ro JY, Ayala AG. Extraskelatal myxoid chondrosarcoma. A clinicopathologic study of ten patients with long-term follow up. *Cancer* 1992; **70**: 2827-30.
- Meis-Kindblom JM, Bergh P, Gunterberg B, Kindblom LG. Extraskelatal myxoid chondrosarcoma: a reappraisal of its morphologic spectrum and prognostic factors based on 117 cases. *Am J Surg Pathol* 1999; **23**: 636-50.
- Mendez-Probst CE, Erdeljan P, Castonguay M, Gabril M, Wehrli B, Razvi H. Myxoid chondrosarcoma of the scrotum: a case report and review of literature. *Can Urol Assoc J* 2010; **4**: (E)109-11.
- Gebhardt MC, Parekh SG, Rosenberg AE, Rosenthal DI. Extraskelatal myxoid chondrosarcoma of the knee. *Skeletal Radiol* 1999; **28**: 354-8.
- Okamoto S, Hara K, Sumita S, Sato K, Hisaoka M, Aoki T, et al. Extraskelatal myxoid chondrosarcoma arising in the finger. *Skeletal Radiol* 2002; **31**: 296-300.
- Tateishi U, Hasegawa T, Nojima T, Takegami T, Arai Y. MRI features of extraskelatal myxoid chondrosarcoma. *Skeletal Radiol* 2006; **35**: 27-33.
- Hirabayashi Y, Ishida T, Yoshida MA, Kojima T, Ebihara Y, Machinami R, et al. Translocation (9;22)(q22;q12). Recurrent chromosome abnormality in extraskelatal myxoid chondrosarcoma. *Cancer Genet Cytogenet* 1995; **81**: 33-7.
- Orndal C, Carlen B, Akerman M, Willén H, Mandahl N, Heim S, et al. Chromosomal abnormality t(9;22)(q22;q12) in an extraskelatal myxoid chondrosarcoma characterized by fine needle aspiration cytology, electron microscopy, immunohistochemistry and DNA flow cytometry. *Cytopathology* 1991; **2**: 261-70.
- Sciot R, Dal Cin P, Fletcher C, Samson I, Smith M, De Vos R, et al. t(9;22)(q22-31;q11-12) is a consistent marker of extraskelatal myxoid chondrosarcoma: evaluation of three cases. *Mod Pathol* 1995; **8**: 765-8.
- Stenman G, Andersson H, Mandahl N, Meis-Kindblom JM, Kindblom LG. Translocation t(9;22)(q22;q12) is a primary cytogenetic abnormality in extraskelatal myxoid chondrosarcoma. *Int J Cancer* 1995; **62**: 398-402.
- Turc-Carel C, Dal Cin P, Rao U, Karakousis C, Sandberg AA. Recurrent breakpoints at 9q31 and 22q12.2 in extraskelatal myxoid chondrosarcoma. *Cancer Genet Cytogenet* 1988; **30**: 145-50.
- Rubin BP, Fletcher JA. Skeletal and extraskelatal myxoid chondrosarcoma: related or distinct tumors? *Adv Anat Pathol* 1999; **6**: 204-12.
- Kawaguchi S, Wada T, Nagoya S, Ikeda T, Isu K, Yamashiro K, et al. Extraskelatal myxoid chondrosarcoma: a multi-institute study of 42 cases in Japan. *Cancer* 2003; **97**: 1285-92.
- Kondo T, Yamada K, Noda K, Nakayama H, Kameda Y. Radiologic-prognostic correlation in patients with small pulmonary adenocarcinoma. *Lung Cancer* 2002; **36**: 49-57.
- Saito H, Kameda Y, Masui K, Murakami S, Kondo T, Ito H, et al. Correlation between thin-section findings, histopathological and clinical findings of small pulmonary adenocarcinomas. *Lung Cancer* 2011; **71**: 137-43.
- Brenner W, Conrad EU, Eary JF. FDG PET imaging for grading and prediction of outcome in chondrosarcoma patients. *Eur J Nucl Med Mol Imaging* 2004; **31**: 189-95.

case report

Osteoblastic bone metastases from renal cell carcinoma

Vladka Salapura¹, Irena Zupan², Bostjan Seruga³, Gorana Gasljevic⁴, Pavel Kavcic¹

¹ Clinical Radiology Institute, UMC Ljubljana, Ljubljana, Slovenia

² Clinical Department of Haematology, UMC Ljubljana, Ljubljana, Slovenia

³ Sector of Medical Oncology, Institute of Oncology Ljubljana, Ljubljana, Slovenia

⁴ Department of Pathology, Institute of Oncology Ljubljana, Ljubljana, Slovenia

Radiol Oncol 2014; 48(3): 243-246.

Received 7. March 2013

Accepted 12 May 2013

Correspondence to: Vladka Salapura, M.D., Ph.D., Clinical Radiology Institute, UMC Ljubljana, Zaloška 7, 1000 Ljubljana, Slovenia.
Phone: +386 41 33 66 97; E-mail: salapura@siol.net

Disclosure: No potential conflicts of interest were disclosed.

Background. RCC accounts for only 2–3% of all cancers. Due to its' non-specific symptoms disease is often diagnosed in advanced stage. Disseminated RCC frequently produces bone metastases that are almost always highly destructive, hyper vascularized and purely osteolytic.

Case report. In this article we describe a case of a 71-year old male patient with disseminated osteoblastic bone metastases from renal cell carcinoma (RCC), and present a short review of published literature reporting cases of osteoblastic bone metastases from RCC. Our patient presented with thoracic pain aggravated by movement. He was diagnosed with predominantly osteoblastic bone metastases in the skeleton of thoracic and lumbar vertebra along with metastases in iliac bones, ribs, humerus and clavicles. Initially, origin of bone metastases was unknown, but later a small tumor in patient's right kidney was identified. Microscopic evaluation of the open bone biopsy showed clear cell RCC with sarcomatoid differentiation.

Conclusions. Although, due to its' rarity, RCC is not included in the primary differential diagnosis in patients with osteoblastic metastases, such rare cases suggest that RCC may be considered in the diagnosis when there no other primary tumor is found.

Key words: renal cell carcinoma; osteoblastic bone metastases

Introduction

Renal cell carcinoma (RCC) accounts for 2–3% of all cancers.¹ Due to non-specific symptoms disease is often diagnosed relatively late. Approximately one third of patients with newly diagnosed RCC already have metastatic disease.² Metastases to the bones are frequent and occur in 35% to 40% of cases with advanced RCCs.³ Usually, these metastases are highly destructive, hypervascular and osteolytic.³ In a series of 1668 patients with RCC all detected bone metastases were exclusively osteolytic prior to the initiation of therapy.⁴ It is well known that specific therapies, such as radiotherapy may induce sclerotic changes in osteolytic bone lesions.

To our knowledge there are only six cases of patients with osteoblastic metastases from RCC reported in the literature: two involving well differentiated RCC^{5,6}; two involving RCC with sarcomatoid differentiation^{7,8}; one mixed clear cell with oncocytic features⁸ and one unclassified type.⁸ In this article we represent a case of osteoblastic bone metastases from clear cell RCC with sarcomatoid differentiation.

Case report

71-year old male was admitted to emergency department due to a chest pain that was aggravated

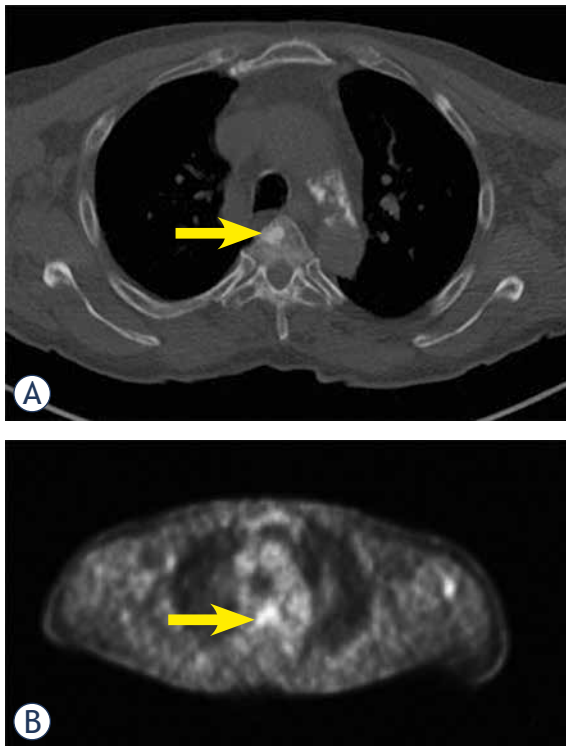


FIGURE 1. A. CT scan shows osteoblastic metastasis in the anterior part of thoracic vertebral body (arrow); B. PET-scan shows that the lesion is metabolically active (arrow).

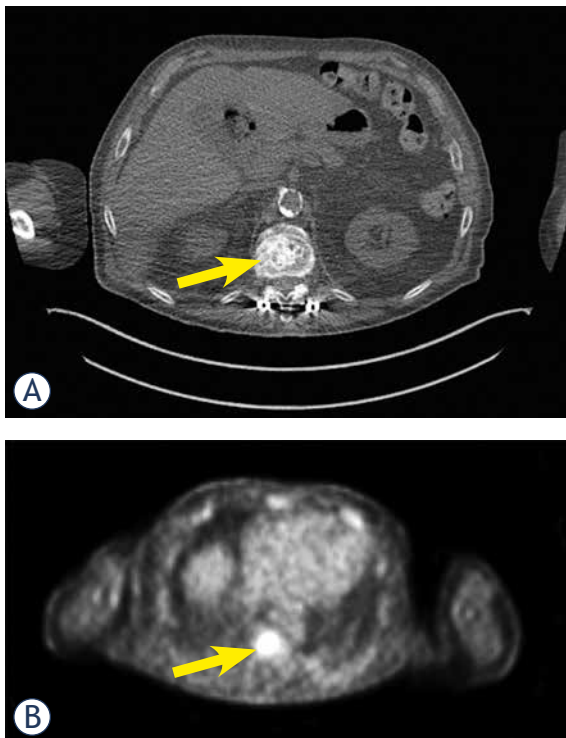
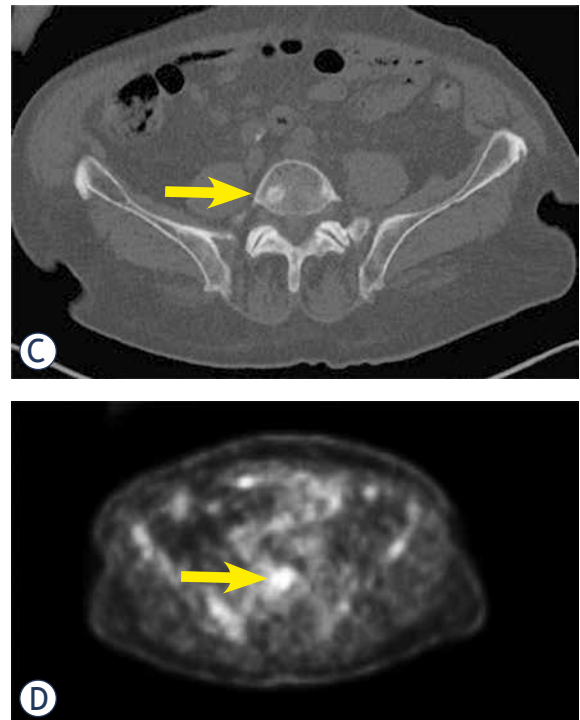


FIGURE 2. A and C. CT scan shows osteoblastic metastases in lumbar vertebral bodies (arrows); B and D. the same lesions show metabolic activity on PET-scan (arrows).

by moving or breathing. Patient also had unexplained weight loss of 22 kg in the last 3 months. Medical history included arterial hypertension, diabetes and chronic kidney disease. Laboratory data showed normocytic anemia, elevated inflammatory parameters, elevated alkaline phosphatase and creatinine. Chest X-ray did not show any abnormalities. Initially, pulmonary embolisms were suspected, but chest computer tomography angiography (CTA) did not show any abnormalities in the lungs. Abdominal ultrasound examination found already known adrenal adenoma with no other abnormalities. As attending physician was suspicious of malignant disease patient was hospitalized. During hospitalization ^{18}F -fluorodeoxyglucose PET/CT imaging was done which revealed disseminated predominantly osteoblastic metastatic lesions in thoracic (Figure 1) and lumbar spine (Figure 2), iliac bones (Figure 3), ribs, humerus and clavicles. However, primary tumor was not identified initially. For further characterization magnetic resonance imaging (MRI) was planned, but unfortunately it was contraindicated due to more than 20 years old osteosynthetic material present in the lumbar vertebra. A CT guided biopsy of small osteoblastic lesion in the iliac crest was ordered. Unfortunately, biopsy was inconclusive, since it showed only a fatty bone marrow without any malignant cells. Finally, patient underwent an open bone biopsy of large osteoblastic lesion in the eleventh thoracic



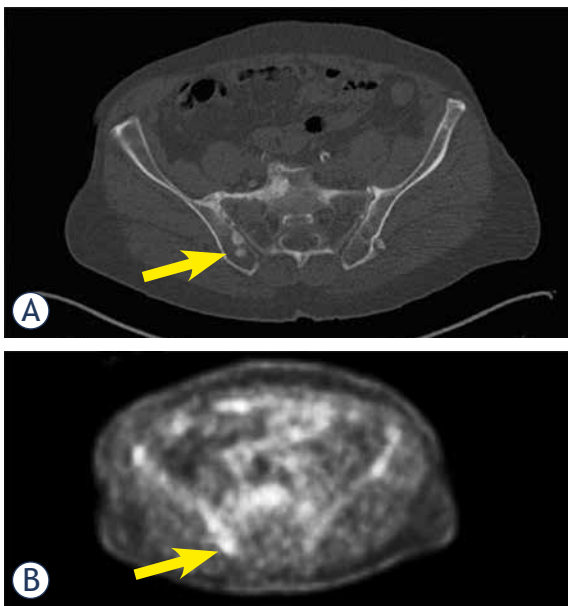


FIGURE 3. A. CT scan shows multiple osteoblastic metastases in the right iliac bone (arrow); B. PET-scan confirms these lesions to be metabolically active metastatic lesions (arrow).

vertebra. Microscopic evaluation of the open biopsy showed clear cell RCC with sarcomatoid differentiation (Figure 4).

Afterwards patient was presented to medical oncologist. Control CT scan confirmed a small carcinoma in the right kidney (Figure 5) with diffuse bone metastases, which were predominantly osteoblastic. Additionally, numerous new tiny lung metastases were found leaving no suspicion that primary tumor was not in the lungs. His prostate specific antigen was 0.3 ng/ml and therefore it was very unlikely that osteoblastic metastases were from prostate cancer. At presentation patient had several poor-prognosis risk factors (WHO performance status 2-3, anemia and time from initial diagnosis to the start of treatment less than 1 year), which indicated short life expectancy. He was offered treatment with mammalian target of rapamycin (mTOR) inhibitor temsirolimus. Unfortunately, despite treatment with temsirolimus patient gradually deteriorated and after two months of treatment CT scan showed progression of disease in his lungs. Few weeks later patient died.

Discussion

The most common cancer types that metastasize to the bones are prostate, breast, lung cancer and RCC.⁹ When osteoblastic bone metastases are found

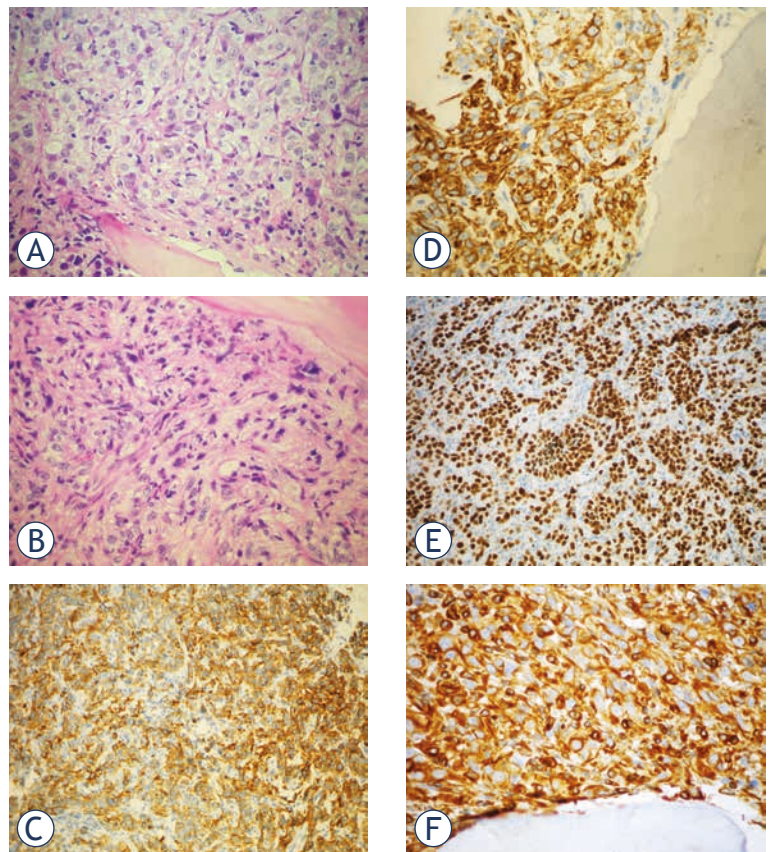


FIGURE 4. A. Metastasis of the RCC in the bone: cells with copious clear cytoplasm and nuclei with prominent, eosinophilic nucleoli; bone trabecule is in the bottom part of the field; H&E 40x; B. More spindled tumor cells, «sarcomatoid» differentiation; H&E, 40x; C. Positivity for CAM5.2; IHC CAM5.2, 20x; D. Positivity for RCC; IHC RCC, 40x; E. Positivity for PAX8, IHC PAX8, 20x; F. Positivity for Vimentin; IHC Vimentin, 40x.

in an adult male patient the most likely origin of malignancy is prostate cancer. However, when osteoblastic bone metastases are found in conjunction with an enhancing renal mass, the more likely pathology is urothelial carcinoma. Urothelial carcinoma such as transitional cell carcinoma commonly metastasizes to bones and can produce both osteolytic and osteoblastic metastases.¹⁰ RCC almost always produces osteolytic metastases and is therefore usually not considered in the differential diagnosis of osteoblastic metastases. However, advanced RCC can present with osteoblastic metastases as was also found in our case.

RCC is made up of a number of different histological subtypes and each is caused by alterations of different genes. The common sites of metastases are lung, liver, bones, adrenals and lymph nodes.¹¹ Some RCCs are associated with unfavorable histological features such as sarcomatoid differentiation, which indicate aggressive behavior. Our and two previously published case reports^{8,9} of patients

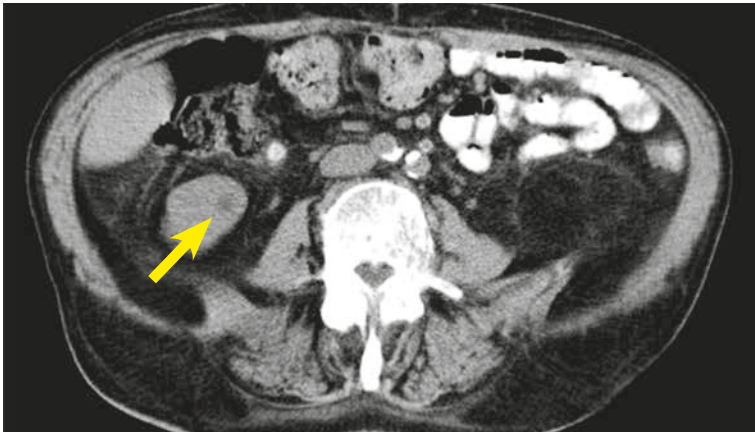


FIGURE 5. Abdominal CT scan shows small primary renal tumor in the the right kidney (contrast enhanced CT was not performed due to patient's poor renal function with glomerular filtration less then 30 mL/min/1.73 m²).

with osteoblastic bone metastases from RCC reported sarcomatoid differentiation in bone metastases. This shows that sarcomatoid differentiation in bone metastases from RCC can be associated with osteoblastic metastases.

Patients with metastatic RCC of bone have expected median survival of around 12 months; survival of those with sarcomatoid differentiation can be even worse.^{12,13} Now, the outlook is changing thanks to the advancements in targeted molecular therapy and cytoreductive nephrectomy.¹¹ RCC is an immunogenic tumor that has ability to manipulate and suppress the natural immune system. The primary tumor might suppress the antitumor effect of the host defense mechanism and divert the immune cells away from the distant metastases.¹⁴ Hence, removal of primary tumor (cytoreductive nephrectomy) together with additional immunotherapy can augment the host immune system thereby producing better survival and quality of life.¹¹

New imaging techniques are also being developed. A recent study presented the first clinical validation of a molecular imaging biomarker for malignancy. It was shown that highly malignant clear cell RCC can be identified using (124)I-girentuximab PET/CT imaging with high sensitivity and specificity.¹⁵

With the progression in diagnostics, surgery, new radiotherapy techniques and the discovery of the new biological therapies which are more effective and less toxic, major changes of the therapeutic results are expected. In spite of this, RCC still remains a big challenge for the future research.¹⁶

Conclusions

In this article we presented a rare case of RCC with predominantly osteoblastic metastases. Although, due to its' rarity, RCC is not included in the primary differential diagnosis in patients with osteoblastic metastases, such rare cases suggest that RCC may be considered in the diagnosis when there no other primary tumor is found. Especially, as survival of patients with metastatic RCC continues to increase due to new therapies, we may begin to see unusual radiologic characteristics of metastases, (such as osteoblastic metastases) more often. Ongoing research in treatment and imaging will help to optimize management of metastatic RCC in the future.

References

- McLaughlin JK, Lipworth L. Epidemiologic aspects of renal cell cancer. *Semin Oncol* 2000; **27**: 115-23.
- Patard JJ, Kim HL, Lam JS, Dorey FJ, Pantuck AJ, Zisman A, et al. Use of the University of California Los Angeles integrated staging system to predict survival in renal cell carcinoma: an international multicenter study. *J Clin Oncol* 2004; **22**: 3316-22.
- Lin PP, Mirza AN, Lewis VO, Cannon CP, Tu SM, Tannir NM, et al. Patient survival after surgery for osseous metastases from renal cell carcinoma. *J Bone Joint Surg Am* 2007; **89**: 1794-1801.
- Forbes GS, McLeod RA, Hattery RR. Radiographic manifestations of bone metastases from renal carcinoma. *AJR Am J Roentgenol* 1977; **129**: 61-6.
- Reidy JF. Osteoblastic metastases from a hypernephroma. *Br J Radiol* 1975; **48**: 225-7.
- Neugut AI, Casper ES, Godwin TA, Smith J. Osteoblastic metastases in renal cell carcinoma. *Br J Radiol* 1981; **54**: 1002-4.
- Liu PT, Conley CR, Callstrom MR. Sclerotic bone metastases from sarcomatoid renal cell carcinoma. *Skeletal Radiol* 1999; **28**: 590.
- Sneag DB, Krajewski KM, Howard S, Jagannathan JP, Star KV, Ramaiya N. Sclerotic osseous metastases from renal cell carcinoma. *Skeletal Radiol* 2012; **41**: 1169-75.
- Coleman RE. Metastatic bone disease: clinical features, pathophysiology and treatment strategies. *Cancer Treat Rev* 2001; **27**: 165-76.
- Shinagare AB, Fennessy FM, Ramaiya NH, Jagannathan JP, Taplin ME, van den Abbeele AD. Urothelial cancers of the upper urinary tract: metastatic pattern and its correlation with tumor histopathology and location. *J Comput Assist Tomogr* 2011; **35**: 217-22.
- Bhat S. Role of surgery in advanced/metastatic renal cell carcinoma. *Indian J Urol* 2010; **26**: 167-76.
- Toyoda Y, Shinohara N, Harabayashi T, Abe T, Akino T, Sazawa A et al. Survival and prognostic classification of patients with metastatic renal cell carcinoma of bone. *Eur Urol* 2007; **52**: 163-8.
- Keegan KA, Schupp CW, Chamie K, Helleenthal NJ, Evans CP, Koppie TM. Histopathology of surgically treated renal cell carcinoma: survival differences by subtype and stage. *J Urol* 2012; **188**: 391-7.
- Rosenberg SA, Yang JC, White DE. Durability of complete response in patients with metastatic cancer treatment with high dose IL2 identification of the antigen mediating response. *Ann Surg* 1998; **229**: 307-19.
- Divgi CR, Uzzo RG, Gatsonis C, Bartz R, Treutner S, Yu JQ, et al. Positron emission tomography/computed tomography identification of clear cell renal cell carcinoma: results from the REDECT trial. *J Clin Oncol* 2013; **31**: 187-94.
- Rajer M. Kidney cancer. *Radiol Oncol* 2007; **41**: 64-71.

The effect of radiation dose on mouse skeletal muscle remodeling

Justin P. Hardee¹, Melissa J. Puppa¹, Dennis K. Fix¹, Song Gao¹, Kimbell L. Hetzler¹, Ted A. Bateman², James A. Carson¹

¹ Department of Exercise Science, University of South Carolina, Columbia, SC, USA

² Departments of Biomedical Engineering and Radiation Oncology, University of North Carolina - Chapel Hill, Chapel Hill, NC, USA

Radiol Oncol 2014; 48(3): 247-256.

Received 28 February 2014

Accepted 11 April 2014

Correspondence to: James A. Carson, Ph.D, University of South Carolina, Department of Exercise Science, Public Health Research Center, 921 Assembly Street, Room 301, Columbia, SC 29208, USA. E-mail: carsonj@mailbox.sc.edu

Disclosure: No potential conflicts of interest were disclosed.

Background. The purpose of this study was to determine the effect of two clinically relevant radiation doses on the susceptibility of mouse skeletal muscle to remodeling.

Materials and methods. Alterations in muscle morphology and regulatory signaling were examined in tibialis anterior and gastrocnemius muscles after radiation doses that differed in total biological effective dose (BED). Female C57BL/6 (8-wk) mice were randomly assigned to non-irradiated control, four fractionated doses of 4 Gy (4x4 Gy; BED 37 Gy), or a single 16 Gy dose (16 Gy; BED 100 Gy). Mice were sacrificed 2 weeks after the initial radiation exposure.

Results. The 16 Gy, but not 4x4 Gy, decreased total muscle protein and RNA content. Related to muscle regeneration, both 16 Gy and 4x4 Gy increased the incidence of central nuclei containing myofibers, but only 16 Gy increased the extracellular matrix volume. However, only 4x4 Gy increased muscle 4-hydroxynonenal expression. While both 16 Gy and 4x4 Gy decreased IIB myofiber mean cross-sectional area (CSA), only 16 Gy decreased IIA myofiber CSA. 16 Gy increased the incidence of small diameter IIA and IIB myofibers, while 4x4 Gy only increased the incidence of small diameter IIB myofibers. Both treatments decreased the frequency and CSA of low succinate dehydrogenase activity (SDH) fibers. Only 16 Gy increased the incidence of small diameter myofibers having high SDH activity. Neither treatment altered muscle signaling related to protein turnover or oxidative metabolism.

Conclusions. Collectively, these results demonstrate that radiation dose differentially affects muscle remodeling, and these effects appear to be related to fiber type and oxidative metabolism.

Key words: extracellular matrix; irradiation; oxidative metabolism; regeneration; skeletal muscle

Introduction

The maintenance of skeletal muscle mass and metabolic function are critical for health.¹ Skeletal muscle is a highly heterogeneous, plastic tissue that possesses varying metabolic and contractile properties. Muscle morphology, fiber type, and oxidative capacity can be influenced by many factors including its microenvironment, nutrient supply, and contractile activity.¹ The application of radiation to skeletal muscle can alter the response to overload and impair regenerative processes.²⁻⁵ Radiation therapy is a common therapeutic mo-

dality for cancer⁶, and may contribute to muscular fatigue and weakness seen during treatment.⁷⁻⁹ Many of the biological effects of radiation therapy are tissue specific¹⁰, but the molecular mechanisms underlying tissue damage have not been clearly defined. Due to the post-mitotic state of skeletal muscle myofibers, basal muscle function has been commonly considered highly resistant to radiation.^{11,12} However, muscle contains many cell types that can influence the myofiber microenvironment to disrupt homeostasis. Therefore, understanding the adverse effects of radiation on skeletal muscle metabolism is needed to improve

patient treatments and outcomes during radiation therapy.

Skeletal muscle mitochondria play an important role in metabolic health and myofiber function.¹³ Acute alterations to mitochondrial oxidative metabolism have been reported following therapeutic doses of radiation¹⁴, and can persist for up to 40 weeks following irradiation.¹⁵ Recent work suggests mitochondria may be susceptible to radiation, and may be a source of radiation-induced oxidative stress.¹⁴⁻¹⁶ Radiation increases the production of reactive oxygen and nitrogen species, which can result in oxidative damage to various cellular components. Specifically, radiation-induced free radical formation can result in protein oxidation, lipid peroxidation, and DNA damage.¹⁷ Skeletal myofibers vary in metabolic function and susceptibility to oxidative stress^{18,19}, which may influence the muscles response to radiation. However, despite increased oxidative damage and impaired mitochondrial function following radiation^{14,15}, the susceptibility of skeletal muscle to radiation-induced oxidative stress is poorly understood.

In addition to myofiber metabolic properties, the total radiation dose applied may be a significant variable in the disruption of muscle homeostasis. Higher radiation doses impair muscle regeneration², attenuate overload-induced hypertrophy^{3-5,20,21}, and alter the structure and function of skeletal muscle.^{11,12,22-24} However, fractionating radiation into smaller doses attenuates skeletal muscle amino acid release when compared to a single larger dose.²⁵ Despite the potential benefits of fractionation, lower radiation doses that are more clinically relevant can also impair skeletal muscle development²⁶ and increase indices of muscle remodeling.²⁷ Altered muscle plasticity following radiation exposure has been attributed to impaired satellite cell activity.^{26,28,29} Satellite cell and myoblast proliferation are reduced with as little as 2 Gy radiation exposure.²⁸⁻³⁰ These changes are accompanied by the induction of oxidative stress and apoptosis.^{26,28,30,31} Although there is evidence to suggest radiation dose can influence skeletal muscle remodeling, the role of skeletal muscle fiber type and metabolic capacity have not been determined.

The purpose of this study was to determine the effect of two clinically relevant radiation doses on the susceptibility of mouse skeletal muscle to remodeling. We hypothesized radiation would induce muscle remodeling in a dose dependent manner and that glycolytic type IIB muscle fibers would be more susceptible to radiation-induced changes in size and distribution, when compared to

more oxidative type IIA muscle fibers. Alterations in muscle morphology and regulatory signaling were examined in female C57BL/6 mouse tibialis anterior and gastrocnemius muscles after radiation doses that differed in total biological effective dose (BED). Mice were exposed to radiation with a single (16 Gy; BED 100 Gy) or fractionated (4x4 Gy; BED 37 Gy) doses over a period of 2 weeks.

Materials and methods

Animals

Twenty-four female C57BL/6 mice were purchased from Jackson Laboratory (Bar Harbor, ME) and housed at the animal resource facility at the University of North Carolina-Chapel Hill. Mice were grouped housed, given access to food and water *ad libitum*, and kept on a 12-hour light-dark cycle. The study was approved by the Institutional Animal Care and Use Committee at the University of North Carolina-Chapel Hill and was carried out in compliance with the Guide for the Care and Use of Laboratory Animals (National Institutes of Health, Bethesda, MD).

Experimental design

At 8 weeks of age, mice were randomly assigned (n=8/group) to non-irradiated control, four fractionated doses of 4 Gray (4x4 Gy; BED 37 Gy), or a single 16 Gy dose (16 Gy; BED 100 Gy) based on the total biological effective dose (BED). Mice in the 16 Gy treatment received a single radiation dose on day 1. Mice in the 4x4 Gy treatment were exposed to fractionated radiation doses every other day over a period of two weeks (Figure 1). This dosing strategy was designed to model normal tissue radiation exposure during the treatment of pelvic malignancies such as cervical cancer when treated with external beam radiotherapy, where muscles in each hip would be exposed to approximately half (up to 0.9 Gy per fraction) of the total dose that the tumor receives (54 Gy in 30x1.8 Gy fractions). Specifically, the BED was calculated using the Fowler equation, accounting for dose-per-fraction and relative tissue sensitivity ($\alpha/\beta = 3$). The calculated BED for the fractionated and single dosing strategies of mouse-limb exposures are 37 Gy and 100 Gy, respectively. By comparison, the BED exposure to each human-hip during treatment (30x0.9 Gy) is 35 Gy.³² Mice were sacrificed 2-weeks following the first radiation exposure. This time-point was chosen to examine the acute effects that may develop following radiation exposure.³³

Hindlimb irradiation

Radiation to the hindlimbs was performed as previously described, with slight modifications.²⁷ Animals were anesthetized with 4% isoflurane and placed in an irradiator device (X-RAD 320, North Branford, CT). Sedation was maintained with constant 2.5% isoflurane administration throughout the procedure. The collimator was adjusted so the radiation field included only the region distal to the pelvis. Irradiation was performed with 320 kV X-rays at a dose rate of 0.5 Gy/min for a total BED of 37 and 100 Gy. Control mice underwent the same procedure without radiation exposure.

Hindlimb grip strength

Prior to sacrifice, hindlimb grip strength was measured with the Grip Tester (Model 1027CSM; Columbus Instruments, Columbus, OH) with slight modifications as previously described.³⁴ Mice were held with hindlimbs positioned on a horizontal grid connected to a force transducer. Mice were then pulled away from the grid until they could no longer maintain grip. Each mouse underwent two sets of five repetitions of force measurements with two minutes rest between each set. The highest and lowest force measurements from each set were removed and an average force measurement for each mouse was calculated.

Tissue collection

At the time of sacrifice, mice were euthanized by cervical dislocation. Hindlimb skeletal muscles were excised, snap-frozen in liquid nitrogen, and stored at -80°C until analysis. The tibia and femur were removed, cleaned of all soft tissue, and stored in ethanol until analysis.

Total muscle protein and RNA content

Total muscle protein and RNA content of the gastrocnemius muscle was determined according to Fleck and Munro as previously described.^{35,36} Briefly, frozen muscle samples (~20 mg) were homogenized in 0.2M HClO₄ and centrifuged (4°C at 12,000 × g for 10 minutes). Following two washes in 0.2M HClO₄, the remaining pellet was air dried, suspended in 0.3M KOH and incubated at 37°C overnight. An aliquot was removed and total protein concentration was determined by the Bradford method.³⁷ To the remaining sample, 1.2M HClO₄ was added and centrifuged for 10 minutes at 4°C

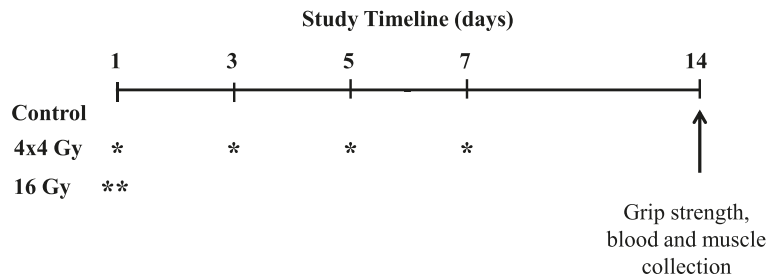


FIGURE 1. Experimental Design. At 8-weeks of age twenty-four female C57BL/6 mice were randomly assigned to non-irradiated control, four fractionated doses of 4 Gray (4x4 Gy; BED 37 Gy), or a single 16 Gy dose (16 Gy; BED 100 Gy) based on the total biological effective dose (BED). Mice were sacrificed 2-weeks after the first radiation exposure. All mice underwent sham or radiation exposure starting on day 1. Mice receiving fractionated doses (4x4 Gy) were irradiated every other day over a period of 2 weeks. Mice receiving a single radiation (16 Gy) were only irradiated on day 1. Grip strength was performed in the morning prior to sacrifice. * = 4 Gy radiation exposure; ** = 16 Gy radiation exposure.

(12,000 × g). After centrifugation, the supernatant was removed and the pellet was washed twice with 0.2M HClO₄, with subsequent supernatants removed and pooled with previous washes. Absorbance was read at 260 nm to determine total RNA concentration.

Tibialis anterior morphology

Transverse muscle sections (~10 μm) were cut from the mid-belly of the tibialis anterior (TA) on a cryostat at -20°C and stored at -80°C until further analysis. Hematoxylin and eosin (H&E) staining was performed on cross-sections to determine myofiber morphology as described previously.^{27,36} H&E stained muscle sections were digitized at 400X magnification and analyzed using a computer with ImageJ imaging software (NIH, Bethesda, MD). Centralized nuclei, defined as a nuclei found equidistant from a well-defined sarcolemma, were quantified from these images, and were expressed as the percent of centralized nuclei per total muscle fibers. The extracellular matrix area was quantified as previously described.³⁸ Images containing well-defined sarcolemma were traced and the extracellular matrix is expressed as the percentage of whole muscle.

Immunohistochemistry for myosin heavy chain type IIA and IIB

Immunohistochemistry for myosin heavy chain type IIA and IIB was performed as previously described.³⁹ Transverse sections of the TA were air dried for 10 minutes, fixed in cold acetone for 1

TABLE 1. Body weight, hindlimb grip strength, and tibialis anterior muscle mass at sacrifice in control and irradiated mice

Treatment	n	Body weight (g, AM ± SE)*	Grip strength (N, AM ± SE)	TA mass (mg, AM ± SE)	TA:BW (AM ± SE)
Control	8	21.9 ± 0.3	0.70 ± 0.03	37 ± 1.4	1.7 ± 0.06
4x4 Gy	8	22.0 ± 0.3	0.67 ± 0.03	37 ± 1.0	1.7 ± 0.04
16 Gy	8	22.2 ± 0.2	0.67 ± 0.03	35 ± 0.6	1.6 ± 0.04

n = number of animals; *AM ± SE = means ± standard error; N = newtons; TA = tibialis anterior; TA:BW = TA normalized to body weight; g = grams; mg = milligrams; Gy = Gray

minute, and washed in PBS for 5 minutes. Sections were quenched in 0.3% H₂O₂-methanol solution for 20 minutes and rinsed in PBS for 5 minutes three times. Sections were blocked in 10% normal goat serum (Vectastain ABC kit, Vector Laboratories, Burlingame, CA) in PBS for 1 h at room temperature and then incubated overnight at 4°C with primary antibodies (SC-71 for type IIA; BF-F3 for type IIB; Iowa Hybridoma Bank). Sections were then washed three times for 5 minutes in PBS. Secondary antibodies (Vector Laboratories) were applied to the sections for 1 h at 37 °C and sections were washed again three times for 5 minutes in PBS. Avidin-biotin complex system (ABC; Vector Laboratories) was used to detect the biotinylated secondary antibody by incubating sections in ABC solution at room temperature for 30 min. Sections were washed three times for 5 minutes in PBS and visualized by incubating in DAB solution for 6 minutes (Vectastain DAB kit, Vector Laboratories, Burlingame, CA). The sections were rinsed in dH₂O, dried, and mounted by cover glasses with a mounting media. Muscle sections were digitized and analyzed ImageJ imaging software. The percentage of type IIA and IIB was quantified and is expressed as the percent per total muscle fibers. Fiber-type specific cross-sectional area (CSA) was quantified by an investigator blinded to each group.

Succinate dehydrogenase activity

Succinate dehydrogenase (SDH) enzyme activity was performed as previously described to determine muscle oxidative capacity.³⁹ Briefly, frozen cross-sections were air dried for 10 minutes, followed by incubation in a solution containing 0.2M phosphate buffer (pH 7.4), 0.1M MgCl₂, 2.4 mM nitroblue tetrazolium (NBT), and 0.2M succinate acid for 45 minutes at 37°C. Sections were then washed in dH₂O for 3 minutes, dehydrated in 50% ethanol for 2 minutes, and mounted for viewing with mounting media. Digital photographs were

taken from each section at 200X magnification with a Nikon spot camera, and fibers were traced with ImageJ imaging software (~150 per animal). The intensity of SDH staining activity was determined by subtracting the background from each slide to create an integrated optical density for each myofiber. Based on the optical density fibers were classified as light or dark stained. The percentage of each stain was quantified and was expressed as a percent per total muscle fibers. Myofiber CSA was quantified in dark and light stained fibers.

Western blot analysis

Western blot analysis was performed as previously described.^{36,39} Briefly, frozen gastrocnemius muscle was homogenized, and protein concentration was determined by the Bradford method.³⁷ Crude muscle homogenates (15-40 µg) were fractionated on 8-15% polyacrylamide gels. Gels were transferred to polyvinylidene difluoride membranes overnight at 4°C. Equal protein loading of the gels was assessed by Ponceau staining. Membranes were then blocked in 5% milk-TBST for one hour at room temperature. Primary antibodies for 4-hydroxynonenal (4-HNE; Alpha Diagnostics), ubiquitin, phosphorylated (T202/Y204) and total ERK1/2, phosphorylated (T180/Y182) and total p38, phosphorylated (S473 and T308) and total Akt, phosphorylated (S253) and total FOXO3A, Atrogin-1, LC3B, PGC-1α (Santa Cruz Biotechnology), mitochondria transcription factor A (TFAM), NADH-ubiquinone oxidoreductase 75 kDa subunit (NDUFS1), cytochrome c, glyceraldehyde 3-phosphate dehydrogenase (GAPDH) were incubated at 1:2000 to 1:10,000 dilutions in 5% milk-TBST overnight at 4°C. Secondary anti-rabbit and anti-mouse IgG conjugated antibodies were incubated with membranes at a 1:2000 dilution in 5% milk-TBST for 2 hours at room temperature. All antibodies were purchased from Cell Signaling unless otherwise stated. Enhanced chemiluminescence was used to visualize the antibody-antigen interaction and developed by autoradiography (Kodak, Biomax). Immunoblots were digitally scanned and analyzed by measuring the integrated optical density of each band using ImageJ imaging software.

Slot blot analysis

The slot blot technique was performed to detect lipid peroxidation and protein ubiquitination in muscle as previously described.³⁹ Briefly, graded

quantities (10, 20, and 30 μ g) of crude muscle homogenates were transferred to a PVDF membrane using the Bio-Dot SF microfiltration apparatus (Bio-Rad, Hercules, CA) following the manufacturer's instructions. The membrane was then probed and analyzed as described above (Western blot analysis).

Statistical Analysis

Results are reported as means \pm standard error of the mean. Comparisons between treatment groups were assessed by one-way analysis of variance (ANOVA). Post hoc analyses were performed with the Tukey's multiple comparison test when appropriate. Frequency histograms and the percentage of small and large myofibers were compared by Chi-square analysis. Significance was set at $P < .05$. Statistical analysis was performed using SigmaStat version 3.5 (Systat Software Inc., Richmond, CA).

Results

Body weight, hindlimb grip strength, muscle mass & total muscle protein and RNA content

At 8 weeks of age twenty-four female C57BL/6 mice were subjected to radiation or sham procedures and were sacrificed 2 weeks following the first exposure (Figure 1). Neither radiation treatment altered overall body weight, hindlimb grip strength, and tibialis anterior muscle mass (Table 1). There was also no radiation effect on gastrocnemius muscle mass (Table 2). However, the 16 Gy treatment decreased total gastrocnemius protein 35% and RNA content 20% when compared to control muscle (Table 2). In contrast, gastrocnemius total protein and RNA content was not altered by the 4x4 Gy treatment.

Tibialis anterior morphology

The percentage of centralized nuclei and extracellular matrix (ECM) area was quantified to examine characteristics of muscle remodeling. Both radiation treatments increased the percentage of myofibers containing centralized nuclei (Figure 2A). Only the 16 Gy treatment increased the percentage of ECM when compared to control muscle (Figure 2B). No changes were observed with 4x4 Gy treatment (Figure 2B). Neither treatment altered muscle signaling related to remodeling and growth (Figure 2C).

TABLE 2. Gastrocnemius muscle mass, total protein and RNA content in control and irradiated mice.

Treatment	n	Gastroc mass (mg, AM \pm SE)	Protein (mg/muscle, AM \pm SE)	RNA (mg/muscle, AM \pm SE)	Protein/RNA (AM \pm SE)
Control	6	101 \pm 1.3	13.9 \pm 1.6	126 \pm 3	0.11 \pm 0.01
4x4 Gy	7	102 \pm 2.5	10.3 \pm 1.6	116 \pm 9	0.09 \pm 0.02
16 Gy	6	98 \pm 1.4	9.1 \pm 0.5*	101 \pm 10*	0.09 \pm 0.01

n = number of animals; AM \pm SE = means \pm standard error; Gastroc = gastrocnemius; mg = milligram; Gy = Gray; * = statistically different from Control

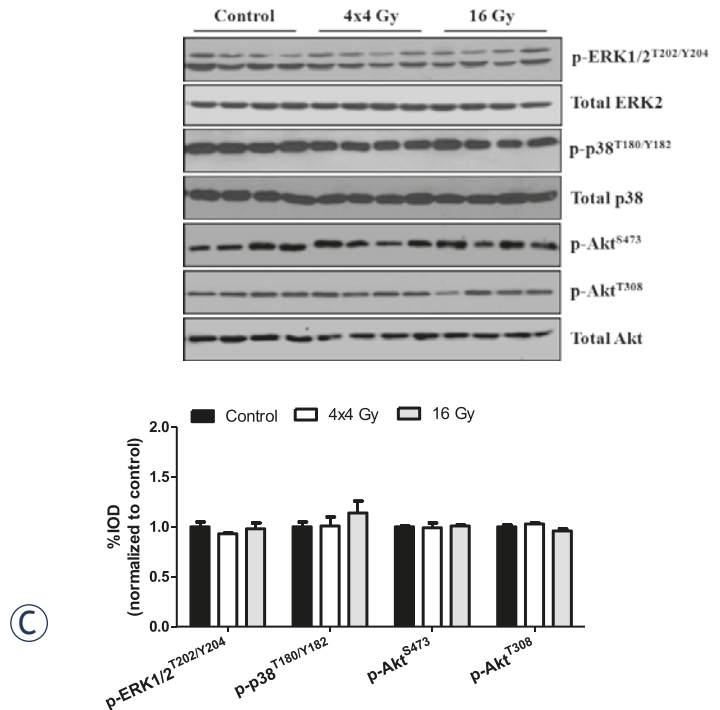
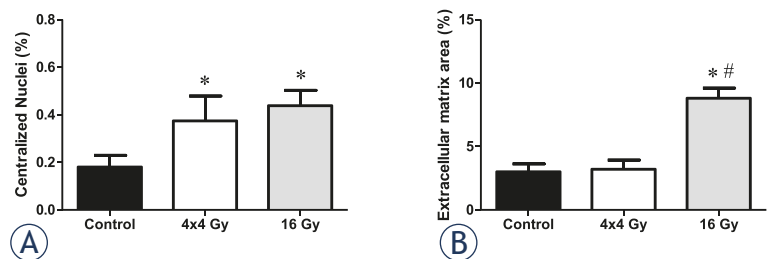


FIGURE 2. Effects of hindlimb irradiation on muscle regeneration and remodeling. A The percentage of myofibers containing centralized nuclei in the tibialis anterior muscle. Centralized nuclei were defined as nuclei found at equidistance from a well-defined sarcolemma and are expressed as the percent of centralized nuclei per total muscle fibers. B The percentage of extracellular matrix area in the tibialis anterior muscle. Extracellular matrix is expressed as the percent of extracellular matrix per total muscle area. C Upper. Representative immunoblot of phosphorylated and total forms of ERK1/2, p38, and Akt proteins in the gastrocnemius muscle. Lower. Quantification of phospho protein activation (ERK1/2, p38, and Akt) is shown as the ratio of phosphorylated to total protein expression. Values are means \pm standard error. Statistical significance was set at $P < .05$. * = statistically different from control; # = statistically different from 4x4 Gy.

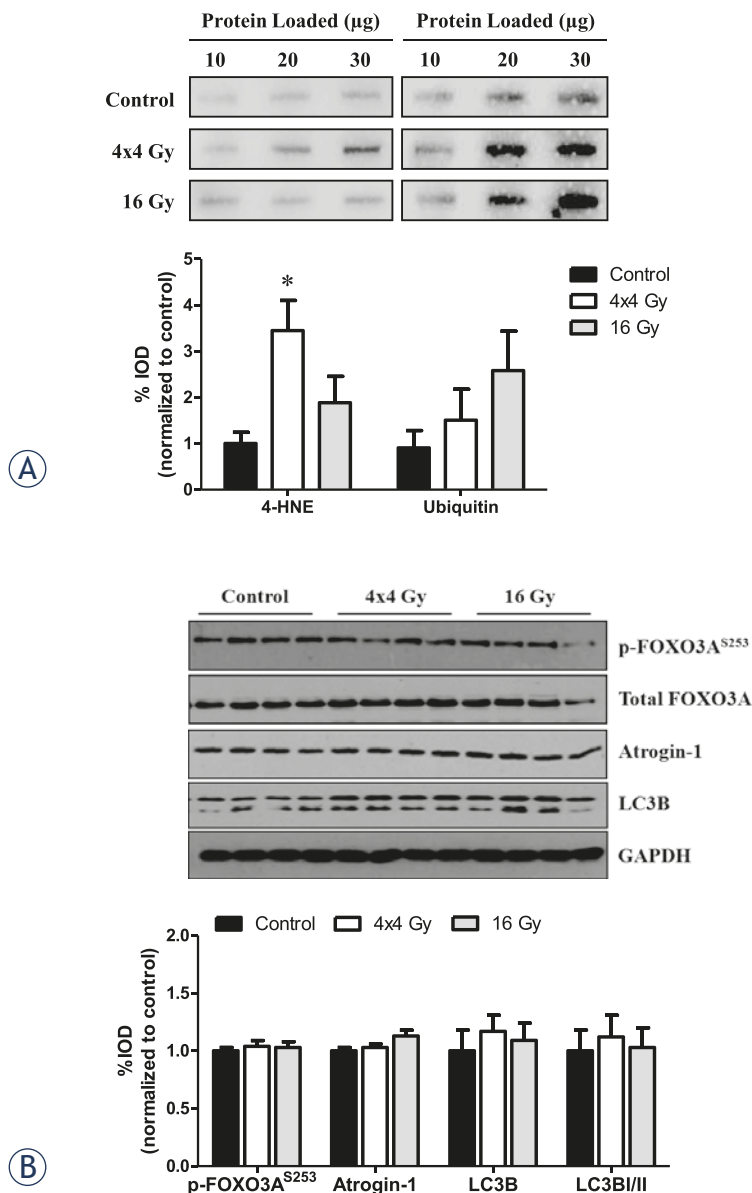


FIGURE 3. Effects of hindlimb irradiation on gastrocnemius muscle oxidative stress and protein turnover. **A Upper left.** Representative immunoblot of 4HNE protein expression. **Lower left.** Quantification of 4HNE protein expression. **Upper right.** Representative immunoblot of ubiquitin protein expression. **Lower right.** Quantification of ubiquitin protein expression. **B Upper.** Representative immunoblot of phosphorylated and total FOXO3A, and total Atrogin-1, LC3B and GAPDH protein expression. **Lower.** Quantification of phosphorylated and total FOXO3A, and total Atrogin-1, LC3B and GAPDH proteins. Values are normalized to control and are presented as means \pm standard error. Statistical significance was set at $P < .05$. * = statistically different from control; 4-HNE = 4-hydroxynonenal; μg = microgram; Gy = gray.

Skeletal muscle oxidative stress and protein turnover

We examined the effects of radiation dose on muscle oxidative stress and protein turnover in the gastrocnemius muscle. The 4x4 Gy treatment increased

the expression of 4-hydroxynonenal (4-HNE) protein, a marker of oxidative stress, while no change was found with the 16 Gy treatment (Figure 3A). Ubiquitination of proteins was not significantly altered by either radiation treatment. However, the 16 Gy treatment demonstrated a highly variable response ($P = .10$; Figure 3A). Neither treatment altered muscle signaling related to protein turnover and autophagy (Figure 3B).

Tibialis anterior type IIA and IIB fiber-type

Type IIA and IIB fiber incidence and size distribution were examined in the tibialis anterior (TA) muscle of control and irradiated mice. Neither radiation treatment altered the overall percentage of type IIA and IIB fibers in the muscle (Figure 4A). Only the 16 Gy treatment decreased type IIA myofiber cross-sectional area (CSA) (Figure 4B) and increased the incidence of small diameter IIA myofibers when compared to the control and 4x4 Gy treatments (Figure 4C). In contrast, both radiation treatments decreased type IIB myofiber mean CSA (Figure 4B), which was accompanied by an increased incidence of small diameter myofibers (Figure 4D).

Skeletal muscle oxidative capacity

Succinate dehydrogenase activity (SDH) in myofibers was examined as an indicator of myofiber oxidative metabolic capacity.³⁹ Neither radiation treatment altered the percentage of high SDH activity fibers found in the muscle ($P = .07$; Figure 5A). In contrast, both radiation treatments decreased the percentage of low SDH activity fibers (Figure 5A). Neither radiation treatment altered muscle protein expression related to mitochondrial biogenesis and oxidative metabolism (Figure 5B). Only the 16 Gy treatment increased the incidence of small myofibers with high SDH activity (Figure 5C), while both radiation treatments increased the incidence of small myofibers exhibiting low SDH activity (Figure 5D).

Discussion

Despite recent advances in radiation treatment to minimize exposure to surrounding normal tissues, treated patients still display muscular fatigue and weakness.⁸ Additionally, radiation exposure can directly alter the response of rodent skeletal mus-

cle to overload and injury.^{11,12,22,23} While radiation is thought to be detrimental to skeletal muscle function, the biological basis of these radiation-induced responses has not been clearly delineated. Furthermore, the ability of radiation dose alone to induce skeletal muscle remodeling has not been clearly defined. We report the novel finding that radiation dose can differentially affect muscle morphology and oxidative damage. Our results demonstrate that both radiation treatments increase muscle remodeling as indicated by the prevalence on central nuclei containing fibers, but only the 16 Gy treatment increased the muscle's extracellular matrix volume. Conversely, only the 4x4 Gy treatment increased muscle oxidative damage. Additionally, radiation-induced alterations to myofiber size were affected by fiber type and fiber oxidative capacity. None of these changes were associated with altered protein expression related to mitochondrial biogenesis, oxidative metabolism or signaling involved in the regulation of skeletal muscle mass. Collectively, these results demonstrate that radiation dose differentially affects muscle remodeling, and these affects are impacted by fiber type and oxidative metabolism.

We provide morphological evidence that radiation dose is a critical element for the induction of skeletal muscle remodeling. High and low radiation doses have been shown to attenuate overload and normal maturation induced muscle growth.^{3-5,20,26} Regardless of the BED there was an increase in myofibers exhibiting centralized nuclei, an indicator of muscle regeneration. Similar findings have also been reported in response to lower radiation doses.²⁷ In this study, a larger BED resulted in an expansion of the extracellular matrix area and was accompanied by a decrease in total protein and RNA content. The decrease in total protein content may therefore be related to muscle remodeling. The release of skeletal muscle amino acids that occurs as a result of muscle proteolysis is thought to occur in several muscle wasting conditions.^{1,40} Altman and Schwenen⁷ demonstrated increased release of amino acids 4-6 hours following high dose radiation, and was this response was attenuated by fractionating into smaller doses.²⁵ However, muscle morphology was not examined in these studies. We report that neither radiation dose was able to alter muscle mass or volitional grip strength. Thus, it appears that neither radiation treatment influenced normal muscle growth over the 2-week experimental period. In support of this, we found no radiation-induced changes in muscle signaling related to muscle growth, in-

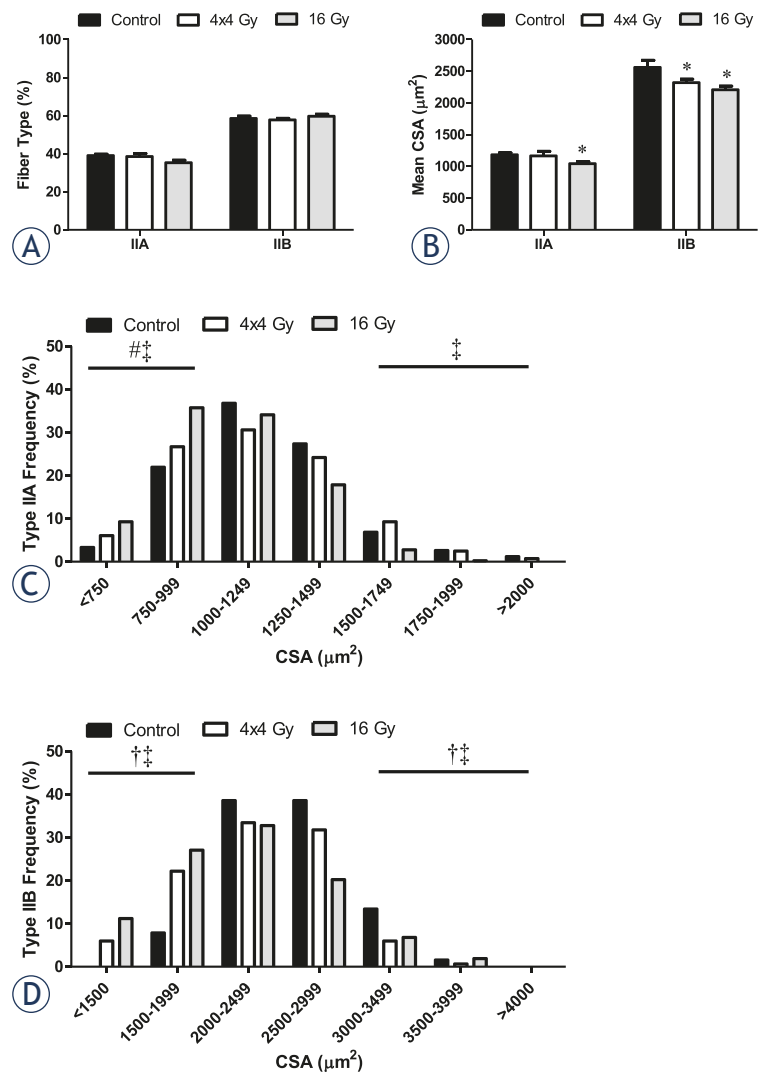


FIGURE 4. Effects of hindlimb irradiation on tibialis anterior myosin heavy chain IIA and IIB expression and size. A The percentage of type IIA and IIB myofibers. B Mean cross-sectional area (CSA) of type IIA and IIB myofibers. C Mean CSA distribution of type IIA myofibers. D Mean CSA distribution of type IIB myofibers. The frequencies of small and large myofibers ($\pm 2SD$ of mean) were compared by Chi-square analysis. Values are means \pm standard error. Statistical significance was set at $P < .05$. Black box, Control. White box, 4x4 Gy. Grey box, 16 Gy. μm = micrometer; Gy = gray. * = statistically different from control; † = statistical difference between control and 4x4 Gy; ‡ = statistical difference between control and 16 Gy; # = statistical difference between 4x4 Gy and 16 Gy.

cluding Akt and FOXO signaling pathways. Future work is needed to understand the associations between altered protein content and muscle remodeling in response to radiation.

Our results demonstrate radiation can induce fiber-type specific alterations in size and distribution that are related to the total BED. Regardless of the dose applied, decreased type IIB myofiber CSA was accompanied by an increase in small fib-

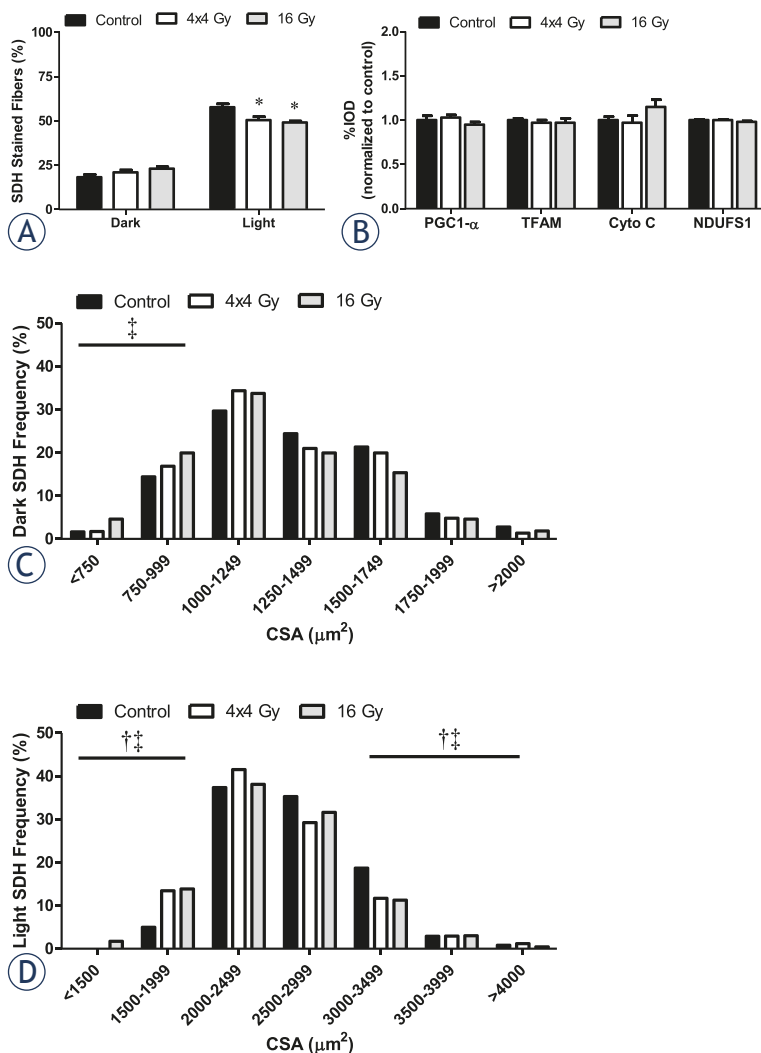


FIGURE 5. Effects of hindlimb irradiation on muscle oxidative capacity. A The percentage of dark and light SDH stained myofibers in the tibialis anterior muscle. B Quantification of total forms of PGC-1 α , TFAM, cytochrome C, and NDUFS1 proteins in the gastrocnemius muscle. C Mean cross-sectional area (CSA) distribution of dark SDH stained myofibers in the tibialis anterior muscle. D Mean CSA distribution of light SDH stained myofibers in the tibialis anterior muscle. The frequencies of small and large myofibers (± 2 SD of mean) were compared by Chi-square analysis. Values are means \pm standard error. Statistical significance was set at $P < .05$. Black box, Control. White box, 4x4 Gy. Grey box, 16 Gy. μm = micrometer; Gy = gray; * = statistically different from control; † = statistical difference between control and 4x4 Gy; ‡ = statistical difference between control and 16 Gy.

er incidence. Similar findings have been reported in the extensor digitorum longus of mice and rats exposed to a single radiation dose.^{3,4} Intermediate (type IIA/IIX) and glycolytic fiber (type IIB) size was decreased in mice³, and in all rat fiber types (type I, IIA, IIX, and IIB).⁴ In addition, myofibrillar degeneration and myofiber atrophy in type II fibers occurred following x-ray irradiation in rabbit pectoralis major muscle, but specific isoforms

were not quantified.¹¹ Type IIB myofibers are more susceptible to free radical formation and oxidative stress^{18,19}, which may account for the radiation-induced disruption of muscle homeostasis. Interestingly, we found the increase in small type IIA myofiber incidence was attenuated by the use of a lower dose. Further, changes in small fiber incidence were independent of an overall fiber type shift, which is consistent with previous reports.^{3,4} It has been suggested that a minimal radiation dose is needed to induce skeletal muscle proteolysis^{7,25}; however, specific myofiber alterations were not examined in these studies. Our findings provide evidence that fiber type can interact with radiation in a dose-dependent manner, and this relationship has a significant impact on radiation-induced muscle remodeling. Further research is needed to determine the cellular signals underlying this relationship.

There is currently a limited understanding of how radiation affects myofiber metabolic properties. Mitochondria are a likely target of radiation for the induction of cellular dysfunction that leads to tissue damage.¹⁶ Since oxidative capacity and mitochondrial content can vary by muscle fiber phenotype, these properties may influence the radiation sensitivity of myofibers. Similar to our fiber type analysis, both radiation doses in our study decreased the size of myofibers with low oxidative capacity, but only the 16 Gy dose decreased the size of myofibers with high oxidative capacity. Thus, there were differential responses related to the muscle fiber's metabolic properties and the radiation dose applied. Skeletal muscle irradiation increases acute oxidative stress and alter proteins related to contractile function and energy metabolism.⁴¹ Our results support differential responses to radiation-induced oxidative stress which may be dependent on the muscles oxidative capacity. We found evidence of oxidative stress, as indicated by increased 4-HNE protein expression, which persisted for a week after the last radiation exposure. Interestingly, the 4x4 Gy dose had greater 4-HNE protein expression, indicating that this may be more dependent on the timing of the last radiation exposure rather than the total dose applied. Cardiac muscle cells have demonstrated radiation-induced alterations to mitochondrial function.^{14,15} A clinically relevant dose (2 Gy) was sufficient to increase cardiac myocyte mitochondrial protein oxidation, and resulted in decreased mitochondrial respiration and protein expression four weeks after radiation exposure.¹⁴ Similar mitochondrial impairments were also observed 40 weeks follow-

ing acute radiation.¹⁵ These results demonstrate the potential for acute radiation to induce long-term mitochondrial dysfunction.^{14,15} Future research is needed to determine if these responses occur in skeletal muscle.

In summary, we demonstrate dose dependent radiation-induced muscle remodeling related to expansion of the extracellular matrix and oxidative stress. The effect of radiation dose on myofiber size was affected by fiber type and oxidative metabolism. Our results demonstrate that type IIB, glycolytic myofibers were susceptible to radiation-induced changes in myofiber size regardless of the total dose. However, type IIA oxidative myofiber size was not affected by the lower radiation dose. The current findings provide rationale for further examination of how radiation dose interacts with muscle fiber type and oxidative capacity to alter the remodeling response. The presence of differential responses to various radiation doses may have important clinical ramifications for the maintenance of muscle mass and function in individuals undergoing radiation treatment. Future research is needed to determine long-term functional outcomes following radiation to skeletal muscle.

Acknowledgment

We thank Dr. Jeffrey Willey for a critical review of the manuscript.

References

1. Wolfe RR. The underappreciated role of muscle in health and disease. *Am J Clin Nutr* 2006; **84**: 475-82.
2. Gulati AK. The effect of X-irradiation on skeletal muscle regeneration in the adult rat. *J Neurol Sci* 1987; **78**: 111-120.
3. Rosenblatt JD, Parry DJ. Gamma irradiation prevents compensatory hypertrophy of overloaded mouse extensor digitorum longus muscle. *J Appl Physiol* 1992; **73**: 2538-43.
4. Rosenblatt JD, Parry DJ. Adaptation of rat extensor digitorum longus muscle to gamma irradiation and overload. *Pflugers Arch* 1993; **423**: 255-64.
5. Rosenblatt JD, Yong D, Parry DJ. Satellite cell activity is required for hypertrophy of overloaded adult rat muscle. *Muscle Nerve* 1994; **17**: 608-13.
6. Zachariah B, Balducci L, Venkattaramanabalaaji GV, Casey L, Greenberg HM, DellRegato JA. Radiotherapy for cancer patients aged 80 and older: a study of effectiveness and side effects. *Int J Radiat Oncol Biol Phys* 1997; **39**: 1125-9.
7. Altman KI, Schwenen M. Increased catabolism of muscle proteins as a manifestation of radiation myopathy. *Radiat Environ Biophys* 1987; **26**: 171-80.
8. Giacalone A, Quitadamo D, Zanet E, Berretta M, Spina M, Tirelli U. Cancer-related fatigue in the elderly. *Support Care Cancer* 2013; **21**: 2899-911.
9. Kurohara SS, Rubin P, Hempelmann LH. Creatinuria and fatigue in patients undergoing radiation therapy. *Radiology* 1961; **77**: 804-12.
10. Denekamp J, Rojas A. Cell kinetics and radiation pathology. *Experientia* 1989; **45**: 33-41.
11. Khan MY. Radiation-induced changes in skeletal muscle. An electron microscopic study. *J Neuropathol Exp Neurol* 1974; **33**: 42-57.
12. Lewis RB. Changes in striated muscle following single intense doses of x-rays. *Lab Invest* 1954; **3**: 48-55.
13. Nunnari J, Suomalainen A. Mitochondria: in sickness and in health. *Cell* 2012; **148**: 1145-59.
14. Barjaktarovic Z, Schmaltz D, Shyla A, Azimzadeh O, Schulz S, Haagen J, et al. Radiation-induced signaling results in mitochondrial impairment in mouse heart at 4 weeks after exposure to X-rays. *PLoS One* 2011; **6**: e27811.
15. Barjaktarovic Z, Shyla A, Azimzadeh O, Schulz S, Haagen J, Dorr W, et al. Ionising radiation induces persistent alterations in the cardiac mitochondrial function of C57BL/6 mice 40 weeks after local heart exposure. *Radiother Oncol* 2013; **106**: 404-10.
16. Kam WW, Banati RB. Effects of ionizing radiation on mitochondria. *Free Radic Biol Med* 2013; **65C**: 607-19.
17. Azimzadeh O, Scherthan H, Sarioglu H, Barjaktarovic Z, Conrad M, Vogt A, et al. Rapid proteomic remodeling of cardiac tissue caused by total body ionizing radiation. *Proteomics* 2011; **11**: 3299-311.
18. Anderson EJ, Neuffer PD. Type II skeletal myofibers possess unique properties that potentiate mitochondrial H(2)O(2) generation. *Am J Physiol Cell Physiol* 2006; **290**: C844-51.
19. Feng J, Xie H, Meany DL, Thompson LV, Arriaga EA, Griffin TJ. Quantitative proteomic profiling of muscle type-dependent and age-dependent protein carbonylation in rat skeletal muscle mitochondria. *J Gerontol A Biol Sci Med Sci* 2008; **63**: 1137-1152.
20. Adams GR, Caiozzo VJ, Haddad F, Baldwin KM. Cellular and molecular responses to increased skeletal muscle loading after irradiation. *Am J Physiol Cell Physiol* 2002; **283**: C1182-95.
21. Phelan JN, Gonyea WJ. Effect of radiation on satellite cell activity and protein expression in overloaded mammalian skeletal muscle. *Anat Rec* 1997; **247**: 179-88.
22. Bergstrom RM, Salmi A. Radiation-induced damage in the ultrastructure of striated muscle. *Exp Cell Res* 1962; **26**: 226-8.
23. Darden EB, Jr. Changes in membrane potentials, K content, and fiber structure in irradiated frog sartorius muscle. *Am J Physiol* 1960; **198**: 709-14.
24. Wernig A, Zwyer M, Irintchev A. Function of skeletal muscle tissue formed after myoblast transplantation into irradiated mouse muscles. *J Physiol* 2000; **522 Pt 2**: 333-45.
25. Schwenen M, Altman KI, Schroder W. Radiation-induced increase in the release of amino acids by isolated, perfused skeletal muscle. *Int J Radiat Biol* 1989; **55**: 257-69.
26. Olive M, Blanco R, Rivera R, Cinos C, Ferrer I. Cell death induced by gamma irradiation of developing skeletal muscle. *J Anat* 1995; **187 (Pt 1)**: 127-32.
27. Bandstra ER, Thompson RW, Nelson GA, Willey JS, Judex S, Cairns MA, et al. Musculoskeletal changes in mice from 20-50 cGy of simulated galactic cosmic rays. *Radiat Res* 2009; **172**: 21-9.
28. Caiozzo VJ, Giedzinski E, Baker M, Suarez T, Izadi A, Lan M, et al. The radiosensitivity of satellite cells: cell cycle regulation, apoptosis and oxidative stress. *Radiat Res* 2010; **174**: 582-9.
29. Cho-Lim JJ, Caiozzo VJ, Tseng BP, Giedzinski E, Baker MJ, Limoli CL. Satellite cells say NO to radiation. *Radiat Res* 2011; **175**: 561-8.
30. Jurdana M, Cemazar M, Pegan K, Mars T. Effect of ionizing radiation on human skeletal muscle precursor cells. *Radiol Oncol* 2013; **47**: 376-81.
31. Latella L, Lukas J, Simone C, Puri PL, Bartek J. Differentiation-induced radioresistance in muscle cells. *Mol Cell Biol* 2004; **24**: 6350-61.
32. Fowler JF. 21 years of biologically effective dose. *Br J Radiol* 2010; **83**: 554-68.
33. Nagler RM. Extended-term effects of head and neck irradiation in a rodent. *Eur J Cancer* 2001; **37**: 1938-45.
34. Puppa MJ, White JP, Velazquez KT, Baltgalvis KA, Sato S, Baynes JW, et al. The effect of exercise on IL-6-induced cachexia in the Apc (Min/+) mouse. *J Cachexia Sarcopenia Muscle* 2012; **3**: 117-37.

35. Fleck A, Munro HN. The precision of ultraviolet absorption measurements in the Schmidt-Thannhauser procedure for nucleic acid estimation. *Biochim Biophys Acta* 1962; **55**: 571-83.
36. Mehl KA, Davis JM, Berger FG, Carson JA. Myofiber degeneration/regeneration is induced in the cachectic ApcMin/+ mouse. *J Appl Physiol* 2005; **99**: 2379-87.
37. Bradford MM. A rapid and sensitive method for the quantitation of microgram quantities of protein utilizing the principle of protein-dye binding. *Anal Biochem* 1976; **72**: 248-54.
38. Huang Y, de Boer WB, Adams LA, Macquillan G, Rossi E, Rigby P, et al. Image analysis of liver collagen using sirius red is more accurate and correlates better with serum fibrosis markers than trichrome. *Liver Int* 2013; **33**: 1249-56.
39. White JP, Baltgalvis KA, Puppa MJ, Sato S, Baynes JW, Carson JA. Muscle oxidative capacity during IL-6-dependent cancer cachexia. *Am J Physiol Regul Integr Comp Physiol* 2010; **300**: R201-11.
40. Tisdale MJ. Cachexia in cancer patients. *Nat Rev Cancer* 2002; **2**: 862-71.
41. Fedorova M, Kuleva N, Hoffmann R. Reversible and irreversible modifications of skeletal muscle proteins in a rat model of acute oxidative stress. *Biochim Biophys Acta* 2009; **1792**: 1185-93.

Identification of plasma biomarker candidates in glioblastoma using an antibody-array-based proteomic approach

Klemen Zupancic¹, Andrej Blejec², Ana Herman³, Matija Veber⁴, Urska Verbovsek⁵, Marjan Korsic⁶, Miomir Knezevic⁴, Primoz Rozman³, Tamara Lah Turnsek^{5,7}, Kristina Gruden¹, Helena Motaln⁵

¹ Department of Biotechnology and Systems Biology, National Institute of Biology, Ljubljana, Slovenia

² Department of Entomology, National Institute of Biology, Ljubljana, Slovenia

³ Blood Transfusion Centre, Immunohaematology Department Ljubljana, Slovenia

⁴ Educell Ltd., Trzin, Slovenia

⁵ Department of Genetic Toxicology and Cancer Biology, National Institute of Biology, Ljubljana, Slovenia

⁶ Department of Neurosurgery, University Medical Centre Ljubljana, University of Ljubljana, Ljubljana, Slovenia

⁷ Faculty of Chemistry and Chemical Engineering, University of Ljubljana, Ljubljana, Slovenia

Radiol Oncol 2014; 48(3): 257-266.

Received 13 January 2014

Accepted 10 March 2014

Correspondence to: Dr. Helena Motaln, Department of Genetic Toxicology and Cancer Biology, National Institute of Biology, Večna pot 111, SI-1000 Ljubljana, Slovenia. E-mail: helena.motaln@nib.si

Disclosure: No potential conflicts of interest were disclosed.

Background. Glioblastoma multiforme (GBM) is a brain tumour with a very high patient mortality rate, with a median survival of 47 weeks. This might be improved by the identification of novel diagnostic, prognostic and predictive therapy-response biomarkers, preferentially through the monitoring of the patient blood. The aim of this study was to define the impact of GBM in terms of alterations of the plasma protein levels in these patients.

Materials and methods. We used a commercially available antibody array that includes 656 antibodies to analyse blood plasma samples from 17 healthy volunteers in comparison with 17 blood plasma samples from patients with GBM.

Results. We identified 11 plasma proteins that are statistically most strongly associated with the presence of GBM. These proteins belong to three functional signalling pathways: T-cell signalling and immune responses; cell adhesion and migration; and cell-cycle control and apoptosis. Thus, we can consider this identified set of proteins as potential diagnostic biomarker candidates for GBM. In addition, a set of 16 plasma proteins were significantly associated with the overall survival of these patients with GBM. Guanine nucleotide binding protein alpha (GNAO1) was associated with both GBM presence and survival of patients with GBM.

Conclusions. Antibody array analysis represents a useful tool for the screening of plasma samples for potential cancer biomarker candidates in small-scale exploratory experiments; however, clinical validation of these candidates requires their further evaluation in a larger study on an independent cohort of patients.

Key words: glioblastoma; proteomics; biomarker; antibody array; plasma

Introduction

Glioblastoma multiforme (GBM) is the most aggressive primary brain tumour, and following surgical resection, it is conventionally treated with ionising radiation and chemotherapy. The high mortality of

patients with GBM is seen by the median survival of 47 weeks, with patients with GBM only rarely surviving more than 3 years.¹ This is partially due to infiltrative invasion of the single tumour cells into the surrounding parenchyma, where these cells are missed by the treatment strategies that

target the bulk tumour mass. Thus, when deciding among adjuvant treatment protocols, there is the need to consider the tumour cellular and genetic heterogeneity, and the development of tumour resistance to such therapies², which are mostly due to the presence of variable numbers of GBM stem-like cells. In the light of this, novel predictive biomarkers of responses to GBM therapy are urgently needed to improve the outcome of GBM therapy, such that these can be monitored pre-operatively and post-operatively in the biological fluids of the patients using a robust and non-invasive method.

Until recently, the search for biomarkers in the body fluids of patients with GBM has not been very extensive³, as GBM only rarely shows metastases.⁴ However, recent plasma and serum analyses in glioma patients have been promising, with the identification of some new circulating biomarkers.^{5,6} The origin of such secreted molecular biomarkers might be the GBM cells, as these secrete a variety of substances when cultured *in vitro*.⁷ Using proteomic immunological analyses, it has been shown that as well as proteins, cell cultures of brain tumours also secrete protein-loaded microvesicles that can be found in the patient sera.⁸ These biomarkers might also be secreted into the body fluids of patients with GBM by the stromal cells that are a part of the GBM microenvironment. A plethora of cytokines is secreted by the immune cells and mesenchymal stem cells that infiltrate the tumour, which have been reported by us and others to affect GBM aggressiveness, and might thus also be considered as useful biomarkers.⁹ This indicates the importance of the contributions of the tumour micro-environment to the origin of such plasma protein biomarkers. Finally, the systemic host response might result in the release of inflammatory biomarkers, which might also be relevant as biomarkers of glioma progression.^{6,10}

Different, non-targeted, proteomics approaches have been developed for the identification of molecular biomarkers of glioma progression in patient body fluids, such as in cerebrospinal fluid^{11,12,13} and in peripheral blood plasma^{14,15} and serum.^{16,17} Recently, in the search for novel protein biomarkers, the plasma of patients with GBM was analysed by liquid chromatography/ tandem mass spectrometry and compared to healthy volunteers.¹⁵ Although mass spectrometry is being widely used for cancer biomarker discovery, its use with plasma and serum samples has serious limitations, because of its low sensitivity due to the presence of high-abundance proteins.¹⁸ Depletion of the most abundant proteins from such samples

to allow the detection of putative low-abundance biomarkers might introduce artefacts and bias the quantification.¹⁹ Therefore, here we propose the use of arrays that are comprised of a broad spectrum of antibodies. In this way, we have quantified the plasma levels of 656 proteins in 17 non-depleted blood-plasma samples from patients with GBM, and compared these with the same protein levels in 17 plasma samples from healthy volunteers. In this study, we identified several plasma biomarker candidate proteins with diagnostic and prognostic potential, which we propose to validate in a larger cohort of patients with GBM.

Materials and methods

Ethics statement

This study was approved by the National Ethics Committee and is registered at ClinicalTrials.gov (healthy volunteers: document No. 149/05/08; GBM patients: No. 90/01/11; ClinicalTrials.gov ID: NCT01525459). All of the healthy volunteers and patients with GBM involved signed the informed consent form. Patients were treated in University Clinical Centre Ljubljana, Slovenia.

Healthy volunteers, glioblastoma patients and plasma sample collection

Seventeen healthy volunteers (HVs) were selected to represent a population distribution considering age, gender (9 female, 8 male) and body mass index, and were analysed in detail in our previous study.²⁰ The inclusion criterion for the HVs was age of 20-60 years, and the exclusion criteria were prior record of acute or chronic diseases and pregnancy. None of the HVs had ever been diagnosed with neoplastic disease. All of the HVs were in good health at the time of sampling.

The inclusion criteria for the 17 patients (6 female, 11 male) with GBM (GPs) were: first diagnosis with primary malignant glioma (World Health Organisation WHO grade IV) and age of 20-80 years. The diagnosis was made after surgery, according to standard clinical and histopathological analyses of the tumour tissue at the Neurosurgery Department of the University Clinical Centre in Ljubljana, and the Institute of Pathology of the Medical Faculty. The exclusion criteria for the GPs were pregnancy and brain metastasis.

All of the participants in the study were Caucasians. The HVs and GPs were non-smokers and were not taking oral contraceptives or other

drugs for at least 1 month prior to sampling. The morning fasting blood samples were collected between 07:00 and 09:00 hours (on the morning of the surgery for the GPs) from the 17 HVs and 17 GPs. The relevant clinical characteristics of the HVs and GPs are given in the Supplemental Information Table 1.

Blood sample processing

Eight millilitres of whole blood were drawn from each participant and transferred to preparation tubes containing 1.0 mL 0.1 M sodium citrate (362782, Beckton, Dickinson and Company); these were immediately centrifuged at $1800\times g$ for 20 min at room temperature. The plasma was then aliquoted to separate tubes and stored at -80°C until analysis. All of the blood samples were processed within 1 h of being drawn.

Antibody arrays

All of the 34 plasma samples from the HVs and GPs were analysed using the Explorer antibody array (Full Moon BioSystems), which has 656 different antibodies spotted on each array, as two replicates.

To clear the plasma samples, 800 μL of each was thawed by centrifugation ($20817\times g$ at 4°C for 10 min), as suggested by the manufacturer. Then, 400 μL of the middle clear liquid was transferred into a new tube and analysed using the NanoDrop microvolume spectroscopic technique (Thermo Scientific), to confirm sample clarity and to estimate total protein concentration.

Each sample was analysed on one antibody array slide in five batches, according to the manufacturer specifications. To eliminate any batch effects, each batch was set to consist of an equal number of random HV and GP samples. First, 20 μL of each plasma sample were biotinylated (3 μL of biotin in dimethyl formamide solution, 10 $\mu\text{g}/\mu\text{L}$, supplied with the antibody arrays), while the antibody array slides were blocked using 3% (w/v) dry milk solution. The coupling step was performed for 2 h, after which the slides were washed intensively 10 times, before being submerged into 60 mL of detection buffer (supplied with the antibody arrays) with 60 μL of Cy3-streptavidin solution, 0.5 mg/mL (GE Healthcare; as suggested by FullMoon BioSystems) for 20 min in the dark; the washing step was then repeated (10 times). After the last wash, the slides were dried by centrifugation ($142\times g$ at room temperature for 2 min) and scanned within 12 h using an LS200 microarray scanner (TECAN), with a

single-channel laser at 543 nm and the filter at 590 nm, and with 10- μm resolution.

The raw images from the microarray scanner were analysed using ImaGene software (BioDiscovery). Spots of poor quality (*e.g.*, unequal signal, artefacts, comet tails) were automatically flagged as poor-quality spots (using the software default settings). The images were also inspected manually, and all of the poor-quality spots were excluded from further analysis (with an "NA" value assigned to them). If the mean signal of the spot did not reach the value of two standard deviations of the background, the spot was flagged as an empty spot. The array values were normalised by quantile normalisation²¹ to correct for any technical, chip-to-chip, or day-to-day variations. As there were two technical replicates of each spot on each microarray, the geometric means between the replicates were calculated. If one of the replicates was flagged as an empty spot or a poor-quality spot, only the other replicate was considered. If the absolute difference between two replicate spots was greater than their geometric mean, the spots were substituted with the "NA" value. All "NA" values were excluded from further statistical analysis. Then all of the spots flagged as empty were substituted by half of the global (over all of the microarrays), minimal, non-empty spot value. This data is available in the Supplemental Information Table 2.

Statistical analysis of the differences in the plasma protein levels between the healthy volunteers and GBM patients

We used Wilcoxon, Mann-Whitney non-parametric statistical tests with the critical alpha p value of 0.05. When all of the GP samples were compared to all of the HV samples, we identified 42 proteins with altered plasma levels.

As there was a significant difference in the mean ages between the HVs and GPs (HV mean age, 39 years; GP mean age, 60 years), we speculated that this difference might account for some of the differences in the levels of these 42 identified proteins. We therefore performed the analysis, where the HVs were separated into the groups of younger HVs (HV_Y; age, <40 years; $n = 8$) and older HVs (HV_O; age, ≥ 40 years; $n = 9$), these two HV age groups were compared separately against the GPs (all >40 years; $n = 17$). We again used Wilcoxon, Mann-Whitney non-parametric statistical tests with the critical alpha p value of 0.05, in combination with an absolute $\log_2\text{FC} > 0.5$ cut-off, to identify the proteins with altered levels in the plasma sam-

ples. We then further analysed only the proteins with significantly altered plasma levels in both the HVs vs. GPs and the HV_O vs. GPs comparisons that had absolute log₂ fold changes >0.5 in both of these comparisons (n = 11).

The list of these 11 biomarker candidates was annotated according to the official gene symbol, UniProt accession ID, tissue expression, molecular class and primary localisation. This annotation was performed using the Human Protein Reference Database (<http://www.hprd.org/>). We also examined each protein in the Human Proteome Atlas Database (<http://www.proteinatlas.org>) for the grade of tissue expression in normal tissue and in glial tumours. All of these data are summarised in Table 2. The main functional categories that these proteins correspond to were determined using DAVID Bioinformatics Resources 6.7²², to better understand the origins of the differences between the GPs and the HVs.

Survival analysis of the patients with GBM

The GPs were grouped according to their survival after their diagnosis, to short-term survivors (GP_S) and long-term survivors (GP_L). The cut-off for survival was chosen in previous studies as from 6 months²³ up to 36 months.²⁴ To choose a biologically relevant cut-off, we performed Wilcoxon, Mann-Whitney non-parametric statistical tests, using only the cut-offs of 6 months and 12 months survival after diagnosis, as only one of the GPs in the present study survived for more than 24 months. We chose the cut-off of 12 months, as the statistical test revealed more proteins with altered levels in plasma between the GP_S and GP_L survival groups at this cut-off.

We also determined how well the proteins associated with survival separated between the GPs with different survivals after diagnosis, and determined the antibody array signal value (cut-off value) that provided the most significant separation of the samples. We separated all of the GP samples into two groups according to the cut-off of the antibody array signal. The cut-offs were selected to group samples into two groups (lower and higher signals) in six predetermined ratios: 0.25:0.75, 0.35:0.65, 0.45:0.55, 0.55:0.45, 0.65:0.35 and 0.75:0.25. The significances of the differences (*p* values) between the groups (for all of the cut-offs) were determined with log-rank analyses. The Kaplan-Meier curves were constructed (R version 2.15.1, libraries KMSurv 0.1-5, knitr 1.2.10, patchD-

VI 1.9, survival 2.37-4) to visualise the groups with the most significant differences for each protein.

Western blotting

The concentrations of the total proteins in the samples were determined using the Bradford assay²⁵ 50 µL of 1000×-diluted samples were mixed with 200-µL Roti®-Quant universal reagent (Carl Roth, Karlsruhe, Germany), which was diluted in milli-Q water (1:5) prior to the reaction. The optimal dilution of the samples was calculated to have a final concentration of total protein between 3 mg/ml and 6 mg/ml.

The plasma samples were pooled to have 7 pools for the GPs (4 pools GP_S, 3 pools GP_L) and 7 pools for the HVs (3 pools HV_V, 4 pools HV_O) for joint analysis on one transfer membrane. Prior to the loading of each protein sample onto the electrophoresis gel (15 µl), they were diluted 1:50 in phosphate-buffered saline. The electrophoresis of the precast Mini-PROTEAN TGX gradient (4% to 15% acrilamide) gels (#456-1086, BioRad) was performed for 3 h at room temperature and under constant current (25 mA). The separated proteins were transferred from the gel to the immunoblot PVDF membrane (#162-0174, BioRad) at 4°C for 18 h under constant current (45 mA). Two membranes were prepared; one for incubation with the primary anti-GNAO1 rabbit polyclonal antibody (ABIN406520, Antibodies Online; 1:50 dilution), and the other with the primary anti-CDKN1B mouse monoclonal antibody (E6764, Spring Bioscience; 1:100 dilution), at 4°C for 18 h. After washing the membranes with phosphate-buffered saline with 0.1% Tween, they were incubated with the secondary antibodies conjugated with horseradish peroxidase and diluted 1:2500, for 3 h at room temperature. An anti-rabbit IgG antibody was used for GNAO1 (W4011, Promega), and an anti-mouse IgG antibody was used for CDKN1B (W4021, Promega). After this, the membranes were incubated with Amersham ECL Prime Western Blotting Detection Reagent (RPN2232, Amersham) and exposed to Amersham Hyperfilm MP (#28-9068-42, GE Healthcare), for 5 s. The membranes were washed for 18 h at 4°C, and incubated with a goat anti-human IgM antibody with conjugated horseradish peroxidase (ABIN102628, Antibodies Online) at a dilution of 1:20,000 for the loading control. The detection proceeded in the same manner as described above.

The Western blotting images were scanned using a standard office scanner at 600 dpi (see

Supplemental Information Figure 1 for raw images). The bands were quantified with ImageJ, using the default settings. The data were then normalised according to the IgM levels.²⁶ Basic, two-sided, unpaired t-tests were used to determine the *p* values when comparing the different groups; *p* < 0.05 was considered as statistically significant.

Results

Identification of proteins showing altered plasma levels in GPs compared to HVs, using antibody arrays

To reveal the plasma protein biomarker candidates, we screened blood plasma samples collected from two types of subjects, healthy volunteers (HV) and GBM patients (GPs), using commercial explorer antibody arrays. To provide a broader overview of the differences in the levels of plasma proteins be-

tween the HVs and GPs, Wilcoxon, Mann-Whitney non-parametric statistical tests were performed, comparing the GP samples against the HV samples, with an applied stringency for *p* < 0.05. Forty-two proteins with significantly altered plasma levels in the GPs were identified, of which five were increased and 37 were decreased in the GPs (see Supplemental Information Table 3).

In our previous study on HVs²⁰, we reported that age did not affect the gene expression in blood cells or the plasma metabolites. In contrast, in the present study, we found that age has a significant impact on the various plasma proteins analysed in the HVs. In addition, fewer low-abundant proteins were detected in the plasma of the older subjects (Figure 1, HV₀).

To identify the biomarker candidates that were independent of age, we further analysed only the proteins with significantly altered plasma levels in both the HV *versus* GP and the HV₀ *versus* GP com-

TABLE 1. Potential plasma protein biomarker candidates for GBM, as identified by the antibody array screening approach used in the present study

Protein name	Gene name	Difference in protein abundance *	Molecular class	Expression	CL	ExN	ExG	Published deregulation
Increased in GBM patients								
Ferritin light chain	FTL	1.65	Storage protein	PL, BC, BR	C	3	1.4	Increased in plasma (MS, ELISA) and in CSF (RIHC) of GPs ^{11,15}
Guanine nucleotide binding protein, alpha	GNAO1	1.65	G protein	BC, BR	M	0	0.4	Decreased in high-grade glioma brain tissue of GPs (IB, IHC) ²⁷
S100 calcium binding protein A9	S100A9	1.66	Calcium binding protein	PL, BC, BR	C	0	0.3	Increased in plasma of GPs (MS, ELISA) ¹⁵
Decreased in GBM patients								
Cyclin dependent kinase inhibitor 1B	CDKN1B	0.62	Cell cycle protein	BC, BR	N	2	2.0	Decreased in brain tissue in GPs with poor prognosis (IHS) ²⁸
FAS-associated death domain protein	FADD	0.52	Adapter molecule	BR	C	0	1.1	Up-regulation of TNFR1 through FADD induces apoptosis in GBM cells (RT-PCR, IHS, IB) ²⁹
Intercellular adhesion molecule 1	ICAM1	0.66	Adhesion molecule	PL, BC, BR	M	0	0.9	Increased in tumour tissue of GPs (RT-PCR) ³⁰
DNA mismatch repair protein Mlh1	MLH1	0.57	DNA repair protein	PL	N	2	2.4	Decreased in recurrent tumour tissue of GPs (IHS) ³¹
Matrix metalloproteinase 11	MMP11	0.62	Metalloprotease	BC, BR	E	0	0.4	Increased in tumour tissue of GPs (RT-PCR, IHS, IB) ³²
DNA polymerase, gamma	POLG	0.54	DNA polymerase	BC	M	2	0.7	/
S phase kinase associated protein 1A (p19A)	SKP1	0.60	Ubiquitin proteasome protein	BR	N	3	2.7	/
Sialyltransferase 8	ST8SIA1	0.59	Sialyltransferase	PL, BC	G	1	1.5	/

* Fold-change in GBM patients when compared to healthy volunteers;

Protein expression: PL = plasma; BC = blood cells; BR = brain;

CL = Cellular localisation; M = plasma membrane; C = cytoplasm; E = extracellular; N = nucleus; G = Golgi apparatus;

ExN; ExG = average grade of protein tissue expression in normal (ExN) and glioma tumour (ExG) tissue, according to the Human Protein Atlas Database (<http://www.proteinatlas.org>); 0, none; 1, low; 2, medium; 3, high)

MS = mass spectrometry; ELISA = enzyme-linked immunosorbent assay; (R)IHC = (radio) immunohistochemistry; IB = immune-blotting; RT-PCR = real-time polymerase chain reaction

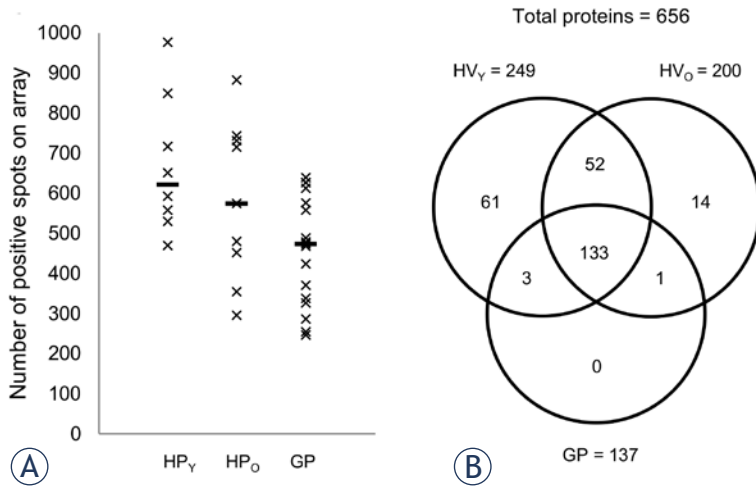


FIGURE 1. Differences in the detectable levels of the plasma proteins in healthy volunteers and patients with GBM. (A) Comparison of the positive spots (of 1312 spots on each array) in the younger HVs (<40 years; n = 8), the older HVs (≥40 years; n = 9) and all of the GPs (>40 years; n = 17). Horizontal bars: median for each group. (B) Venn diagram showing the overlap of the detectable proteins in the different patient groups. A protein was considered detectable when it was flagged as positive in ≥75% of the samples in the same group.

parisons. These were considered to be the potential protein biomarker candidates (Table 1), of which ferritin (FTL), guanine nucleotide binding protein alpha (GNAO1) and the S100 calcium-binding protein A9 (S100A9) levels were increased; all of the others (FADD, CDKN1B, ICAM1, MLH1, MMP11, POLG, SKP1, ST8SIA1) were decreased.

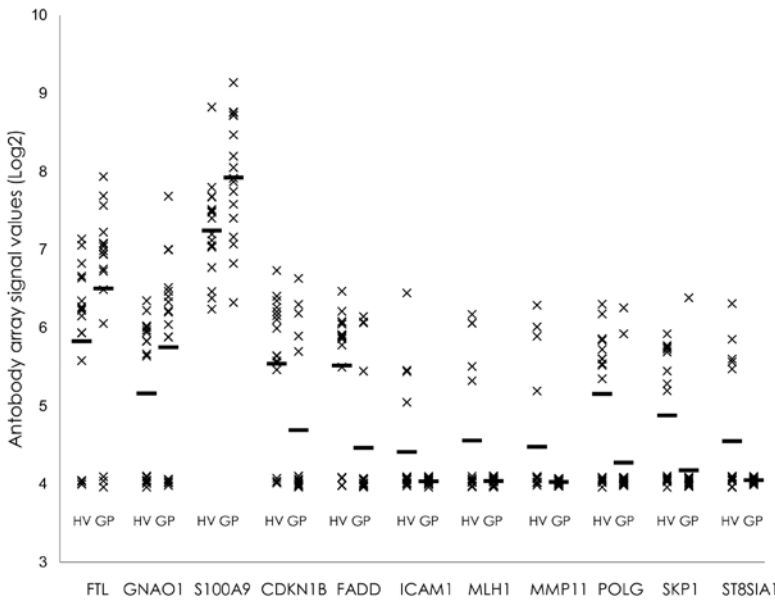


FIGURE 2. Relative abundances of the putative GBM protein biomarkers in the individual plasma samples analysed. Horizontal bars: mean for each group. A relative protein abundance of 4 represents the background for non-detected proteins.

The distributions of the protein abundance in study participants are presented in Figure 2. ICAM1, MLH1, MMP11 and ST8SIA1 were not detected in any of the GP plasma samples, and were detected in only a limited number of the HV plasma samples. Interestingly, MMP11 (in 4 out of 9 female subjects) and ST8SIA1 (in 5 out of 9 female subjects) were detected only in the HV women (see Supplemental Information Table 2). The biomarker potential of these proteins should be investigated further in a large scale (i.e., with higher sample numbers) clinical trial with a more sensitive assay.

All of the 11 proteins identified as having altered plasma levels were further analysed with the DAVID database to see if they are part of the same processes; three processes were found to be most represented: (1) T-cell signalling and immune responses; (2) cell adhesion and migration; and (3) cell-cycle control and apoptosis. As the group 1 plasma proteins with assigned roles in numerous T-cell signalling and immune response processes were strongly represented, this suggests that at least some of these might have derived from immune cells that responded to the tumour with chemokine paracrine signalling *in vivo*.

Altered levels of plasma proteins in the GP samples are associated with patients survival

To determine whether the survival of the GPs after diagnosis is related to the levels of any plasma proteins, the GP samples were grouped according to the short-term survivors (GP_S; t <356 days; n = 12) and the long-term survivors (GP_L; t >365 days; n = 5). As gender had no significant effects on survival (p = 0.77), all of the GP samples were analysed as one group. Twenty-three proteins that showed different plasma levels across these groups of patients were identified, using Wilcoxon, Mann-Whitney non-parametric statistical tests, with an applied stringency of p <0.05. These 23 proteins were further analysed using log-rank analysis, to determine the antibody array signal values that discriminate best between the patients with short-term and long-term survivals. After this analysis, only 16 proteins remained significantly associated with survival (Table 2), of which five were increased in the plasma of the GP_L patients (MYOG, CD8A, GNAO1, ALPL, GHGA), and 11 were decreased (DFFA, MAPR2K1, E2F5, PARP1, CD27, CDC37, TFDP2, STAT1, EIF4EBP1, PDGFA, COL18A1). Kaplan-Meier graphs were constructed for each of these 16 proteins (Supplemental Information

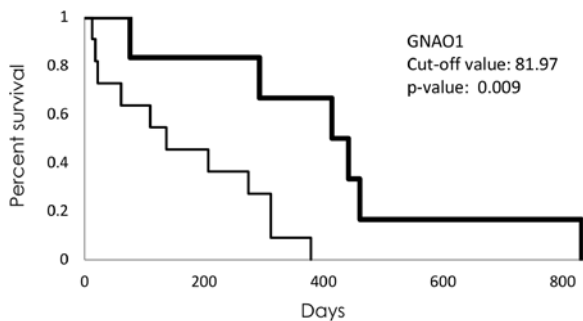


FIGURE 3. Kaplan-Meier graph of survival of the patients with GBM according to GNAO1 signal intensity. Thick line represents patients with higher signal intensity than cut-off value (81.97); thin line represents patients with lower signal intensity.

Figure 2), of which GNAO1 was the most interesting (Figure 3), as it was associated with GBM presence and survival of GBM patients.

Western blotting confirmation of CDKN1B and GNAO1

To confirm the technical validity of the antibody array method, Western blotting was performed with the pooled plasma protein samples of the HVs ($n = 6$) and the GPs ($n = 6$) for the two chosen proteins: guanine nucleotide binding protein alpha (GNAO1) and cyclin-dependent kinase inhibitor 1B (CDKN1B). After quantification of the bands on the raw images (Supplemental Information Figure 1) and normalisation according to the IgM levels, the individual values were plotted according to their relative Western blotting signals (Figure 4). The plasma levels of GNAO1 showed up-regulation of 3.7-fold ($p = 5.9 \times 10^{-5}$) in the GPs compared to the HVs, while CDKN1B showed down-regulation of plasma levels in the GPs, by 5.9-fold ($p = 8.5 \times 10^{-8}$). The plasma levels of GNAO1 were also increased 1.56-fold in the sample pools from the GPs with longer survival compared to sample pools of the GPs with shorter survival ($p = 0.11$). As these data are consistent with the antibody array data, this Western blotting suggests that the antibody arrays provide accurate data as a first step in biomarker identification.

Discussion

About 90% of human plasma is comprised of the 10 most-abundant soluble proteins.³³ Although techniques for plasma depletion of these abundant proteins^{34,35} have increased the sensitivity of conventional mass spectroscopy methods for proteomic analyses of low-abundance proteins, this depletion

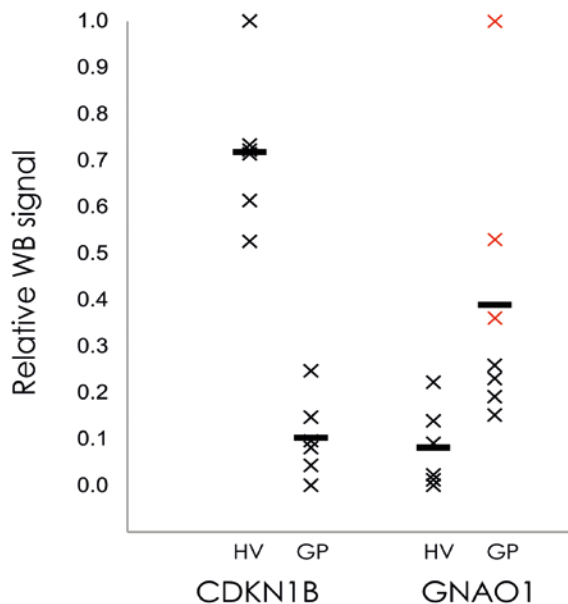


FIGURE 4. Quantification of Western blotting signals for the two putative plasma biomarkers for patients with GBM: CDKN1B and GNAO1. Plasma samples were pooled for the HVs and GPs, and following Western blotting they were quantified and normalized using image densitometry, as described in Material and Methods. Horizontal bars: mean for each group. Red crosses: GNAO1 of three pools of samples from patients who survived longer than 1 year.

is never complete.³⁴ Moreover, it has been reported that this procedure for the removal of the abundant proteins might affect the quantitative analysis of low-abundance proteins.¹⁹ We therefore performed the analyses on the non-depleted plasma samples derived from the HVs and GPs using antibody arrays, through which we have identified novel protein biomarker candidates for diagnosis and prognosis of patients with GBM.

We identified a set of 11 proteins that showed significantly altered plasma levels in the GPs, as compared to the HVs. Using DAVID bioinformatics analyses, we identified three plasma protein clusters that correspond to the following pathways: (1) T-cell signalling and immune responses; (2) cell adhesion and migration; and (3) cell cycle control and apoptosis. These same pathways were reported in one GBM plasma protein study¹⁵, whereas only the second and the third pathways were identified in a GBM tissue study.¹³ This would imply that the second and the third pathways are involved the intra-tumour cellular cross-talk, whereas the proteins of the first pathway might be involved in host immune system responses to GBM.

Three of the 11 deregulated proteins (FTL, GNAO1, S100A9) were increased in the patients

TABLE 2. Identification of the 16 proteins that correlate with longer survival of patients with GBM

Protein name	Gene name	p value	Cut-off *	Regulation in longer survivors
DNA fragmentation factor 45	DFFA	0.002	97.85	Decreased
MEK1	MAP2K1	0.002	64.91	Decreased
E2F transcription factor 5	E2F5	0.003	75.43	Decreased
ADP ribosyltransferase	PARP1	0.006	52.44	Decreased
Myogenic factor 4	MYOG	0.007	108.67	Increased
CD8 Antigen, alpha polypeptide	CD8A	0.009	86.3	Increased
Guanine nucleotide binding protein, alpha	GNAO1	0.009	81.97	Increased
CD27	CD27	0.014	170.66	Decreased
CDC37	CDC37	0.016	312.01	Decreased
Transcription factor DP2	TFDP2	0.018	16.36	Decreased
STAT1	STAT1	0.02	95.77	Decreased
Eukaryotic translation initiation factor 4E binding protein 1	EIF4EBP1	0.023	79.95	Decreased
Platelet-derived growth factor alpha polypeptide	PDGFA	0.03	65.67	Decreased
Alkaline phosphatase, liver	ALPL	0.032	200.13	Increased
Collagen type XVIII alpha 1	COL18A1	0.033	54.68	Decreased
Chromogranin A	CHGA	0.049	80.82	Increased

*Cut-off of microarray signal (intensity), to discriminate patients with shorter versus longer survival, as identified for each protein.

with GBM, where the others were either decreased (CDKN1B, FADD, POLG, SKP1) or were not detected (ICAM1, MLH1, MMP11, ST8SIA1). ST8SIA1 and MMP11 were detected only in the HV women. As ST8SIA1 is involved in breast cancer growth³⁶ and MMP11 is mostly expressed in placenta³⁷, this would argue for their gender-specific association. Increased FTL and S100A9 have been reported previously for cerebrospinal fluid¹¹ and plasma of patients with GP using iTRAQ-based liquid chromatography/ tandem mass spectrometry and enzyme-linked immunosorbent assays¹⁵, thus justifying our methodological approach. Both, FTL and S100A9 are increased in serum under inflammatory conditions, and they might thus represent tumour-related inflammatory responses. The relevance of increased inflammation parameters in the blood of glioma patients, such as erythrocyte sedimentation rate and C-reactive protein levels, has recently been reported¹⁰, and these parameters might collectively have a strong prognostic significance, as should be tested in further clinical studies, based on the criteria by Gautam *et al.*¹⁵

Among the proteins CDKN1B (p27/Kip1), ICAM1, MLH1, MMP11 and ST8SIA1, which we found were significantly decreased in the plasma from the patients with GP, only the CDKN1B decrease has been

previously reported for plasma by others; the mutation and deregulation of this tumour suppressor protein that is involved in the regulation of cell-cycle progression is a common feature of many cancers³⁸, including glioma, where it has been significantly associated with short survival^{39,40} and glioma grading⁴⁰ in larger population studies. For POLG and SKP1, which we detected only in the plasma from the HVs, both have been studied previously in GBM tissue^{41,42}, where POLG expression was associated with mtDNA replication regulator genes, and was interpreted as a prognostic factor.⁴¹

With respect to prognosis, we found 16 plasma proteins that were significantly associated with GP survival. It is significant that a set of the most strongly associated proteins ($p < 0.01$), DFFA, MAP2K1, E2F5, PARP1, predict for longer survival when decreased, which is as would be expected, as these proteins have tumour-promoting characteristics. However, with three proteins, MYOG, CD8A and GNAO1 ($p < 0.01$), when these are increased, this predicts for longer survival. In the present study, only GNAO1 - a subunit of heterotrimeric G protein complex was identified as having both diagnostic and prognostic potential. Contrary to our results, in GBM tissue lower levels of GNAO1 as compared to low grade glioma and normal brain

tissue have been detected and indicated to affect physical properties of the cell membrane²⁷, which may be implying on its secretion from the GBM into the bloodstream. Consistently, we found plasma level of GNAO1 increased 2.9-fold in the GBM patients who showed longer survival, whereas in the GBM patients with shorter survival, it was increased by only 1.2-fold, when compared to the HVs. Although GNAO1 was identified as part of human plasma proteome⁴³, it is normally located in the plasma membrane of different cell types. However, mutations in GNAO1 gene can cause abnormal excretion of GNAO1 protein, which was associated with epileptic encephalopathy and disturbed calcium flow in the neuronal cells.⁴⁴ As calcium flow is important for proliferation of neuronal cells⁴⁵, disturbed calcium flow induces apoptosis in GBM cells⁴⁶, which might explain the elevated levels of GNAO1 in GP with longer survival. Although increased plasma levels of GNAO1 have not been associated with GBM to date, this increase has been correlated to poor prognosis in patients with gastric cancer, where high abundance of the GNAO1 protein was suggested to promote cancer-cell viability via pro-apoptotic protein interference.⁴⁷ As we detected lower levels of GNAO1 in the GP_S compared to the GP_L, this coincides with the observation that GNAO1 down-regulation increases proliferation by senescence suppression in hepatocellular carcinoma cells.⁴⁸ Here, we therefore propose that deregulation of this tumour suppressor gene, as reflected by the higher levels of GNAO1 in the plasma of the GPs, might also be associated with prolonged survival of GBM patients.

In conclusion, we have identified novel plasma biomarker candidates that have potential for diagnostic application development. Out of all of the differentially altered plasma proteins in the plasma samples from the patients with GBM, only GNAO1 is predictive for longer patient survival. To our knowledge, this is also a first association of GNAO1 plasma levels with GBM. We have thus provided evidence that plasma screening using antibody arrays can allow for the identification of novel GBM plasma diagnostic and prognostic biomarker candidates. However, clinical validation of these candidates requires their further evaluation in a larger study on an independent cohort of patients.

Acknowledgements

This work was supported by the SYSTHER/INREMOS project on Systems Biology Tools

Development for Cell Therapy and Drug Development (Con. No.: 3211-06-000539 2006-2011), Slovenian Research Agency (Programme P1-0245) and by Spirit Slovenia Public Agency (MR-09/27). The funders had no role in study design, data collection and analysis, decision to publish, or preparation of the manuscript.

The authors acknowledge the contributions of Petra Konečnik and Mojca Jež in the sample preparation, Andrej Porčnik for help with retrieving the relevant clinical data, and Živa Ramšak and Ana Rotter for assistance with the data analysis.

Abbreviations

HV, healthy volunteer; HV_{<40}, HV <40 years old; HV_{≥40}, HV ≥40 years old; GP, glioblastoma patient; GBM, glioblastoma multiforme; WHO, World Health Organisation

Author contributions

Conceived and designed the experiments: KZ, KG, HM, TTL, MKn. Performed the experiments: KZ, AH, MV, UV. Analysed the data: KZ, AB. Contributed reagents/ materials/ analysis tools: MKo, PR. Wrote the manuscript: KZ, HM, KG, TTL.

References

- 1 Van Meir EG, Hadjipanayis CG, Norden AD, Shu H-K, Wen PY, Olson JJ. Exciting new advances in neuro-oncology: the avenue to a cure for malignant glioma. *CA Cancer J Clin* 2010; **60**: 166-93.
- 2 Ardebili SY, Zajc I, Gole B, Campos B, Herold-Mende C, Drmota S, et al. CD133/prominin1 is prognostic for GBM patient's survival, but inversely correlated with cysteine cathepsins' expression in glioblastoma derived spheroids. *Radiol Oncol* 2011; **45**: 102-15.
- 3 Kalinina J, Peng J, Ritchie JC, Van Meir EG. Proteomics of gliomas: initial biomarker discovery and evolution of technology. *Neuro Oncol* 2011; **13**: 926-42.
- 4 Martens T, Matschke J, Müller C, Riethdorf S, Balabanov S, Westphal M, et al. Skeletal spread of an anaplastic astrocytoma (WHO grade III) and preservation of histopathological properties within metastases. *Clin Neurol Neurosurg* 2013; **115**: 323-8.
- 5 Xu BJ, An Q a, Srinivasa Gowda S, Yan W, Pierce L a, Abel TW, et al. Identification of blood protein biomarkers that aid in the clinical assessment of patients with malignant glioma. *Int J Oncol* 2012; **40**: 1995-2003.
- 6 Reynés G, Vila V, Martín M, Parada A, Fleitas T, Reganon E, et al. Circulating markers of angiogenesis, inflammation, and coagulation in patients with glioblastoma. *J Neurooncol* 2011; **102**: 35-41.
- 7 Gupta MK, Polisetty R V, Ramamoorthy K, Tiwary S, Kaur N, Uppin MS, et al. Secretome analysis of Glioblastoma cell line - HNGC-2. *Mol Biosyst* 2013; **9**: 1390-400.
- 8 Graner MW, Alzate O, Dechkovskaia AM, Keene JD, Sampson JH, Mitchell DA, et al. Proteomic and immunologic analyses of brain tumor exosomes. *FASEB J* 2009; **23**: 1541-57.

- 9 Motal H, Gruden K, Hren M, Schichor C, Primon M, Rotter A, et al. Human mesenchymal stem cells exploit the immune response mediating chemokines to impact the phenotype of glioblastoma. *Cell Transplant* 2012; **21**: 1529-45.
- 10 Strojnik T, Šmigoc T, Lah T. Neurosurgery Prognostic values of erythrocyte sedimentation rate and C-reactive protein in the blood of glioma patients. *Anticancer Res* 2014; **34**: 339-47.
- 11 Sato Y, Honda Y, Asoh T, Ozumi K, Ohshima Y, Honda E. Cerebrospinal fluid ferritin in glioblastoma: evidence for tumor synthesis. *J Neurooncol* 1998; **40**: 47-50.
- 12 Com E, Clavreul A, Lagarrigue M, Michalak S, Menei P, Pineau C. Quantitative proteomic Isotope-Coded Protein Label (ICPL) analysis reveals alteration of several functional processes in the glioblastoma. *J Proteomics* 2012; **75**: 3898-913.
- 13 Fang X, Wang C, Balgley BM, Zhao K, Wang W, He F, et al. Targeted Tissue Proteomic Analysis of Human Astrocytomas. *J Proteome Res* 2012; **11**: 3937-46.
- 14 Carlsson A, Persson O, Ingvarsson J, Widegren B, Salford L, Borrebaeck CAK, et al. Plasma proteome profiling reveals biomarker patterns associated with prognosis and therapy selection in glioblastoma multiforme patients. *Proteomics Clin Appl* 2010; **4**: 591-602.
- 15 Gautam P, Nair SC, Gupta MK, Sharma R, Polisetty RV, Uppin MS, et al. Proteins with altered levels in plasma from glioblastoma patients as revealed by iTRAQ-based quantitative proteomic analysis. *PLoS One* 2012; **7**: e46153.
- 16 Elstner A, Stockhammer F, Nguyen-Dobinsky T-N, Nguyen QL, Pilgermann I, Gill A, et al. Identification of diagnostic serum protein profiles of glioblastoma patients. *J Neurooncology* 2011; **102**: 71-80.
- 17 Gollapalli K, Ray S, Srivastava R, Renu D, Singh P, Dhali S, et al. Investigation of serum proteome alterations in human glioblastoma multiforme. *Proteomics* 2012; **12**: 2378-90.
- 18 Diamandis EP. Mass spectrometry as a diagnostic and a cancer biomarker discovery tool: opportunities and potential limitations. *Mol Cell Proteomics* 2004; **3**: 367-78.
- 19 Liu T, Qian W-J, Mottaz HM, Gritsenko MA, Norbeck AD, Moore RJ, et al. Evaluation of multiprotein immunoaffinity subtraction for plasma proteomics and candidate biomarker discovery using mass spectrometry. *Mol Cell Proteomics* 2006; **5**: 2167-74.
- 20 Gruden K, Hren M, Herman A, Blejec A, Albrecht T, Selbig J, et al. A "crossomics" study analysing variability of different components in peripheral blood of healthy caucasoid individuals. *PLoS One* 2012; **7**: e28761.
- 21 Bolstad BM, Irizarry R, Åstrand M, Speed TP, Astrand M. A comparison of normalization methods for high density oligonucleotide array data based on variance and bias. *Bioinformatics* 2003; **19**: 185-93.
- 22 Huang DW, Sherman BT, Lempicki RA. Bioinformatics enrichment tools: paths toward the comprehensive functional analysis of large gene lists. *Nucleic Acids Res* 2009; **37**: 1-13.
- 23 Kraus JA, Felsberg J, Tonn JC, Reifenberger G, Pietsch T. Molecular genetic analysis of the TP53, PTEN, CDKN2A, EGFR, CDK4 and MDM2 tumour-associated genes in supratentorial primitive neuroectodermal tumours and glioblastomas of childhood. *Neuropathol Appl Neurobiol* 2002; **28**: 325-33.
- 24 Sonoda Y, Kumabe T, Watanabe M, Nakazato Y, Inoue T, Kanamori M, et al. Long-term survivors of glioblastoma: clinical features and molecular analysis. *Acta Neurochir (Wien)* 2009; **151**: 1349-58.
- 25 Bradford MM. A rapid and sensitive method for the quantitation of microgram quantities of protein utilizing the principle of protein-dye binding. *Anal Biochem* 1976; **72**: 248-54.
- 26 Hamelincx D, Zhou H, Li L, Verweij C, Dillon D, Feng Z, et al. Optimized normalization for antibody microarrays and application to serum-protein profiling. *Mol Cell Proteomics MCP* 2005; **4**: 773-84.
- 27 Takenaka K, Kanaho Y, Hara A, Zhang W, Ando T, Sakai N, et al. A guanine nucleotide-binding protein in human astrocytoma. *Neuro Res* 1990; **12**: 223-5.
- 28 Kirla RM, Haapasalo HK, Kalimo H, Salminen EK. Low expression of p27 indicates a poor prognosis in patients with high-grade astrocytomas. *Cancer* 2003; **97**: 644-8.
- 29 Huang P, Rani MRS, Ahluwalia MS, Bae E, Prayson RA, Weil RJ, et al. Endothelial expression of TNF receptor-1 generates a proapoptotic signal inhibited by integrin $\alpha 6 \beta 1$ in glioblastoma. *Cancer Res* 2012; **72**: 1428-37.
- 30 Berindan-Neagoe I, Chiorean R, Braicu C, Florian IS, Leucuta D, Crisan D, et al. Quantitative mRNA expression of genes involved in angiogenesis, coagulation and inflammation in multiforme glioblastoma tumoral tissue versus peritumoral brain tissue: lack of correlation with clinical data. *Eur Cytokine Netw* 2012; **23**: 45-55.
- 31 Stark AM, Doukas A, Hugo H-H, Mehdorn HM. The expression of mismatch repair proteins MLH1, MSH2 and MSH6 correlates with the Ki67 proliferation index and survival in patients with recurrent glioblastoma. *Neuro Res* 2010; **32**: 816-20.
- 32 Stojic J, Hagemann C, Haas S, Herbold C, Kühnel S, Gerngras S, et al. Expression of matrix metalloproteinases MMP-1, MMP-11 and MMP-19 is correlated with the WHO-grading of human malignant gliomas. *Neurosci Res* 2008; **60**: 40-9.
- 33 Liumbruno G, D'Alessandro A, Grazzini G, Zolla L. Blood-related proteomics. *J Proteomics* 2010; **73**: 483-507.
- 34 Tu C, Rudnick PA, Martinez MY, Cheek KL, Stein SE, Slebos RJC, et al. Depletion of abundant plasma proteins and limitations of plasma proteomics. *J Proteome Res* 2010; **9**: 4982-91.
- 35 Echan LA, Tang H-Y, Ali-Khan N, Lee K, Speicher DW. Depletion of multiple high-abundance proteins improves protein profiling capacities of human serum and plasma. *Proteomics* 2005; **5**: 3292-303.
- 36 Cazet A, Lefebvre J, Adriaenssens E, Julien S, Bobowski M, Grigoriadis A, et al. GD₃ synthase expression enhances proliferation and tumor growth of MDA-MB-231 breast cancer cells through c-Met activation. *Mol Cancer Res* 2010; **8**: 1526-35.
- 37 Su AI, Wiltshire T, Batalov S, Lapp H, Ching KA, Block D, et al. A gene atlas of the mouse and human protein-encoding transcriptomes. *Proc Natl Acad Sci U S A* 2004; **101**: 6062-7.
- 38 Hanahan D, Weinberg RA. Hallmarks of cancer: the next generation. *Cell* 2011; **144**: 646-74.
- 39 Nabika S, Kiya K, Satoh H, Mizoue T, Kondo H, Katagiri M, et al. Prognostic significance of expression patterns of EGFR family, p21 and p27 in high-grade astrocytoma. *Hiroshima J Med Sci* 2010; **59**: 65-70.
- 40 Shen A, Wang Y, Zhao Y, Zou L, Sun L, Cheng C. Expression of CRM1 in human gliomas and its significance in p27 expression and clinical prognosis. *Neurosurgery* 2009; **65**: 153-9; discussion 159-60.
- 41 Correia RL, Oba-Shinjo SM, Uno M, Huang N, Marie SKN. Mitochondrial DNA depletion and its correlation with TFAM, TFB1M, TFB2M and POLG in human diffusely infiltrating astrocytomas. *Mitochondrion* 2011; **11**: 48-53.
- 42 Hagedorn M, Delugin M, Abraldes I, Allain N, Belaud-Rotureau M-A, Turmo M, et al. FBXW7/hCDC4 controls glioma cell proliferation in vitro and is a prognostic marker for survival in glioblastoma patients. *Cell Div* 2007; **2**: 9.
- 43 Liu X, Valentine SJ, Plasencia MD, Trimpin S, Naylor S, Clemmer DE. Mapping the human plasma proteome by SCX-LC-IMS-MS. *J Am Soc Mass Spectrom* 2007; **18**: 1249-64.
- 44 Nakamura K, Kodera H, Akita T, Shiina M, Kato M, Hoshino H, et al. De Novo mutations in GNAO1, encoding a Gao subunit of heterotrimeric G proteins, cause epileptic encephalopathy. *Am J Hum Genet* 2013; **93**: 496-505.
- 45 Galli C, Meucci O, Scorziello A, Werge TM, Calissano P, Schettini G. Apoptosis in cerebellar granule cells is blocked by high KCl, forskolin, and IGF-1 through distinct mechanisms of action: the involvement of intracellular calcium and RNA synthesis. *J Neurosci* 1995; **15**: 1172-9.
- 46 Valeriy NCK, Dziegielewska B, Hosing AS, Augustin E, Gray LS, Brautigan DL, et al. Inhibition of T-type calcium channels disrupts Akt signaling and promotes apoptosis in glioblastoma cells. *Biochem Pharmacol* 2013; **85**: 888-97.
- 47 Liu Z, Zhang J, Wu L, Liu J, Zhang M. Overexpression of GNAO1 correlates with poor prognosis in patients with gastric cancer and plays a role in gastric cancer cell proliferation and apoptosis. *Int J Mol Med* 2014; **33**: 589-96.
- 48 Pei X, Zhang J, Wu L, Lü B, Zhang X, Yang D, et al. The down-regulation of GNAO1 and its promoting role in hepatocellular carcinoma. *Biosci Rep* 2013; **33**: e00069.

Segmentation of hepatic vessels from MRI images for planning of electroporation-based treatments in the liver

Marija Marcan¹, Denis Pavliha¹, Maja Marolt Music², Igor Fuckan³, Ratko Magjarevic⁴, Damijan Miklavcic¹

¹ University of Ljubljana, Faculty of Electrical Engineering, Ljubljana, Slovenia

² Institute of Oncology Ljubljana, Ljubljana, Slovenia

³ Clinical Department for Diagnostic and Interventional Radiology, Clinical Hospital "Dubrava", Zagreb, Croatia

⁴ University of Zagreb, Faculty of Electrical Engineering and Computing, Zagreb, Croatia

Radiol Oncol 2014; 48(3): 267-281.

Received 9 January 2014

Accepted 10 April 2014

Correspondence to: Prof. Damijan Miklavcic, Ph.D., Faculty of Electrical Engineering, University of Ljubljana, Tržaška 25, 1000 Ljubljana, Slovenia. E-mail: damijan.miklavcic@fe.uni-lj.si

Disclosure: No potential conflicts of interest were disclosed.

Introduction. Electroporation-based treatments rely on increasing the permeability of the cell membrane by high voltage electric pulses delivered to tissue via electrodes. To ensure that the whole tumor is covered by the sufficiently high electric field, accurate numerical models are built based on individual patient geometry. For the purpose of reconstruction of hepatic vessels from MRI images we searched for an optimal segmentation method that would meet the following initial criteria: identify major hepatic vessels, be robust and work with minimal user input.

Materials and methods. We tested the approaches based on vessel enhancement filtering, thresholding, and their combination in local thresholding. The methods were evaluated on a phantom and clinical data.

Results. Results show that thresholding based on variance minimization provides less error than the one based on entropy maximization. Best results were achieved by performing local thresholding of the original de-biased image in the regions of interest which were determined through previous vessel-enhancement filtering. In evaluation on clinical cases the proposed method scored in average *sensitivity* of 93.68%, *average symmetric surface distance* of 0.89 mm and *Hausdorff distance* of 4.04 mm.

Conclusions. The proposed method to segment hepatic vessels from MRI images based on local thresholding meets all the initial criteria set at the beginning of the study and necessary to be used in treatment planning of electroporation-based treatments: it identifies the major vessels, provides results with consistent accuracy and works completely automatically. Whether the achieved accuracy is acceptable or not for treatment planning models remains to be verified through numerical modeling of effects of the segmentation error on the distribution of the electric field.

Key words: electrochemotherapy; non-thermal irreversible electroporation; treatment planning; hepatic vessel segmentation; non-invasive tumor treatments; MRI of liver

Introduction

Exposing a biological cell to a sufficiently high electric field causes increased permeability of the cell membrane. This increased permeability of the membrane allows transfer of molecules which normally lack membrane transport mechanism into the cell. The described effect of the electric field on

the cell is called *electroporation*.^{1,2} Electroporation can be classified as either reversible or irreversible. The reversible/irreversible nature of electroporation is in strong correlation with pulse amplitude, duration and number of pulses. In reversible electroporation, the cell membrane eventually returns to its normal state. Irreversible electroporation however leads to cell death because the cell

membrane is permanently disrupted or due to the extensive loss of the intracellular components. Combination of reversible electroporation with traditional methods of chemotherapy has resulted in a new method for tumor treatment named *electrochemotherapy* (ECT).³⁻⁵ Irreversible electroporation (IRE) has found its application in tumor treatment as a tissue ablation procedure, its main advantage being the fact that, if controlled properly, it does not thermally damage the tissue.⁶⁻⁸

Tumor treatments based on electroporation like ECT and IRE include placement of the electrodes in the tissue and delivery of the electric pulses. In order for the treatment to be successful the whole tumor must be covered by a sufficiently high electric field. The magnitude and distribution of the electric field depends on the number and the position of the electrodes, the amplitudes of pulses applied per electrode pair and the electric properties of the tissue, especially conductivity.^{9,10}

Prediction of parameters needed for successful treatment is easier for surface tumors which is why the ECT was first performed on skin tumors.⁴ Ensuring the complete tumor coverage with a sufficiently high electric field is however more challenging in the case of deep-seated solid tumors as well as large tumors.¹¹ This was well demonstrated in a case where a patient with a deep-seated tumor in the thigh was treated with ECT.¹² The post-treatment evaluation showed that 6% of the tumor volume was not covered by a sufficiently high electric field, which caused the tumor to regrow. The reasons which reduce predictability of the electric field distribution in deep-seated tumors are the tumor position, high diversity in tumor size and shape, and presence of the surrounding tissues with different electric conductivities. Predictability of an adequate distribution of the electric field can be best achieved by calculating a patient-specific treatment plan as a part of an electroporation-based treatment procedure.¹³ A patient-specific treatment plan for electroporation-based treatment of deep-seated solid tumors takes into account patient geometry and tissue properties to generate an optimal set of treatment parameters.^{14,15}

Correctness of a treatment plan is ensured by an accurate model of the patient which includes the tumor with critical surrounding tissues and structures. The patient model is built by segmenting the medical images and then used to perform numerical calculations of the electric field distribution. A proof-of-concept was provided in a clinical study in which colorectal metastases in the liver were treated by means of ECT.¹⁶ For the purpose

of the mentioned clinical study, an algorithm for automatic segmentation of the liver from MRI images was developed.¹⁷ Similar treatment planning process is well-established in radiotherapy where it has been in use for decades.¹⁸ Generation of models from medical images for subsequent numerical calculations has also been used as a part of treatment planning for radiofrequency ablation (RFA) of liver tumors.^{19,20}

Other than liver and tumor tissue, critical structures that need to be included in the model for both RFA and electroporation-based treatments of the liver are hepatic vessels. For the purpose of radiofrequency ablation, vessels which measure more than 3 mm in diameter size have been described as critical because of their influence on heat propagation.²¹ In case of electroporation-based treatment of the liver the hepatic vessels are important for other reasons. Firstly, the electric conductivity of the vessels is different than that of the liver tissue and tumors, which can have an impact on the electric field distribution, especially in cases when a tumor is situated close to large vessels.²² Secondly, during an electroporation-based treatment the surgeons insert needle electrodes into the liver tissue and these should not damage larger hepatic vessels. The hepatic vessels which were identified by surgeons as critical are vena cava and vena porta with branches up to second order, left, middle and right hepatic vein, and larger hepatic arteries. These vessels will thus be the ones we will most certainly want to include in our model. Lastly, the model of vessels built from medical images can be used for intra-operative visualization to help surgeons navigate during the insertion of the electrodes.

The problem of segmentation of vessels in general²³ and hepatic vessels in particular has been an area of interest for several decades. The interest in segmentation of hepatic vessels resulted in exploring several different approaches. First attempts were based solely on thresholding²⁴ and region growing.^{25,26} The evolution of highly popular methods for enhancement of tubular structures²⁷⁻²⁹ resulted in their combinations with thresholding³⁰ and region growing.^{20,31-33} Other than tube-enhancing filtering the traditional methods of segmentation were enhanced through use of Gaussian mixture models^{34,35} and by utilizing morphology of the vascular tree through centerline extraction.^{20,31} More advanced methods for segmentation of hepatic vessels include those based on graph-cuts^{36,37}, active contours³⁸ and morphological properties embedded in context-based voting system.³⁹

All these methods for vessel segmentation have however been designed for and applied to CT images. To our knowledge, no method so far was tested on MRI images. Although CT images have been considered superior for hepatic vessels, the vessels are also visible in MRI images, especially when a contrast agent is applied. With respect to the colorectal metastases of the liver, multiple studies have shown that MRI is superior to CT in sensitivity and accuracy of detecting tumor lesions.⁴⁰⁻⁴⁵ If MRI is a modality of choice for detecting the tumors, using the same modality to segment the hepatic vessels would avoid the need for registration and errors that inevitably come with it. Another reason why MRI is a method of choice for planning of electroporation-based treatments is possibility to directly observe the distribution of the electric field using the magnetic resonance electric impedance tomography (MREIT), which was described in the work of Kranjc *et al.*^{46,47} and is being actively explored.

Given all of the mentioned advantages of MRI over CT in treatment of colorectal metastases in the liver with electroporation-based treatments, we directed our research towards segmentation and validation of segmentation of hepatic vessels from MRI images. The segmentation method used for hepatic vessels has to be robust and include minimal or no user interaction. These prerequisites are necessary for using the procedure for hepatic vessel segmentation as a module in the process of treatment planning.⁴⁸ Having this in mind, the segmentation methods we tested were built upon already established and robust approaches based on filtering, vessel enhancement, automatic thresholding and region growing. Data used in validation consisted of two sources: a phantom and clinical cases. The phantom was used to optimize the segmentation parameters and analyze the performance of methods in detail. Images of clinical cases were then used to validate the performance of segmentation methods under realistic conditions.

Materials and methods

Segmentation of hepatic vessels

In order to segment the hepatic vessels from MRI images we tested several simple approaches, alone and their combinations. The main approaches include vessel enhancement filtering, thresholding, region growing, connected component analysis and morphological operations.

To determine the optimal method for our purpose we tested two different thresholding methods

on different input: on original de-biased images and on the results of vessel enhancement filtering. The thresholding of that input was performed on the slice level and is referred to as *global* thresholding. The thresholding method that performed best on phantoms was also tested *locally* on smaller regions of original de-biased images determined by vessel enhancement filtering.

Pre-processing phase

Prior to running any of the methods on the original images we performed de-biasing in order to remove the inhomogeneity of image intensity. The intensity inhomogeneity is a product of the magnetic field inhomogeneity in the MRI device.⁴⁹ The applied de-biasing method is publicly available and based on the work of Zheng *et al.*⁵⁰ After de-biasing the images were masked with the results of liver segmentation.¹⁷

Vessel enhancement filtering

The filter we used is based on the work of Frangi *et al.*²⁸ The filter differentiates line-like from blob-like and plate-like structures by observing the relationships between eigenvalues of the Hessian matrix in each voxel of the image. Before applying the filter, the image is scaled by filtering with Gaussian kernels of different size σ . The value of σ is set to a value that equals the size of the diameter of the vessels we wish to enhance.

For each scale σ the probability of a voxel belonging to a line, i.e. *vesselness* is calculated as:

$$v(\sigma) = \begin{cases} 0 & \text{if } \lambda_2 > 0 \parallel \lambda_3 > 0 \\ (1 - \exp(-\frac{R_a^2}{2\alpha^2})) \exp(-\frac{R_b^2}{2\beta^2}) (1 - \exp(-\frac{S^2}{c})) & \text{else} \end{cases} \quad (1)$$

where $|\lambda_1| \leq |\lambda_2| \leq |\lambda_3|$ are eigenvalues of the Hessian matrix in three dimensions, $R_a = \frac{|\lambda_2|}{|\lambda_3|}$ and $R_b = \frac{|\lambda_1|}{\sqrt{|\lambda_2 \lambda_3|}}$

are parameters which discriminate line-like structures from plate-like and blob-like structures, and

$S = \|H_\sigma\|_F = \sqrt{\sum_j \lambda_j^2}$ is the Frobenius norm of the

Hessian matrix. Values of parameters α and β were chosen through optimization on phantoms and were selected as 0.3 and 0.7, respectively. Value of parameter c is calculated for each case and for each value of scale σ according to the following equation:

$$c = \frac{1}{2} \|H_{\sigma}\|_F = \frac{1}{2} \sqrt{\sum_j \lambda_j^2} \quad (2)$$

The parameter c is used in the expression for vesselness as is, without squaring and multiplying by 2 as it is done in the original work of Frangi *et al.*²⁸ The reason for this is better enhancement of vessel structures. The final vesselness filtered image is obtained by calculating the maximum of vesselness values at different scales for each voxel of the image.

Thresholding

Out of many thresholding methods developed until today we chose to implement two of the most successful as reported by Sankur *et al.*⁵¹ The first method is based on minimizing intra-class variance.⁵² The second method is based on maximization of image entropy.⁵³ Both methods are completely automatic and were implemented to determine the threshold on slice level on an image histogram with values in the 16-bit range.

We assessed the performance of the two thresholding methods globally on de-biased original images and vesselness filtered images of both phantoms and clinical cases. Additionally we assessed the method that performed better globally on smaller regions of interest. The details of local thresholding are described in the section *Proposed method*.

Proposed method

Through analysis of the results of previously described methods applied on both phantom and clinical data, we derived a method comprised of the best aspects of vessel enhancement filtering and thresholding. Vessel enhancement filtering is excellent for locating the position of the vessels but unable to determine their exact borders. Thresholding of the de-biased original image can detect vessel borders but not with consistent accuracy throughout the whole image. The proposed method is therefore based on *local* thresholding of smaller regions of interest (ROI), rather than deriving a single threshold for the whole slice. The ROIs for local thresholding are determined based on the output of vessel enhancement filtering. Detailed steps of the proposed method with all the input, output, parameters and dimension in which the step is performed are provided in Table 1.

First, we performed sinc interpolation to obtain isotropic voxels (O2) so that we could perform vesselness filtering.⁵⁴ After that we applied the vesselness filtering on the interpolated, de-biased, masked original images (O3). The filtered image (O4) was interpolated once again to obtain the orig-

inal voxel size (O5). In the end of the filtering section the result of vesselness filtering has to be once again masked with the original liver mask to suppress the high response which appears in the area where background borders with the liver (O6).

The output of the vesselness filtering has high values for voxels with high probability of belonging to a vessel and is very low for very small vessels. The voxels with small vesselness values might also be a result of image noise. For this reason we have chosen a small threshold of 0.05 of the maximum vesselness value. All of the voxels with a vesselness value higher than this threshold are isolated into a basic vessel model (O7). A basic vessel model thus consists of voxels with high certainty of belonging to a vessel. The same small threshold for output of Frangi's vessel enhancing filter was already successfully used in the work of Dongen *et al.* to prevent false positives in the algorithm for extraction of pulmonary vasculature.⁵⁵

To eliminate the smallest vessels which are not of interest for electroporation-based treatments we morphologically open the results to remove all objects with a diameter smaller than 3 mm. We need to keep only larger objects (O8) because the smallest hepatic vessels from the list of those that should not be damaged during the electrode insertion are the main hepatic arteries, and they measure around 3 mm in diameter and more.⁵⁶

After we have extracted and morphologically opened the basic vessel model (O8) we proceed with local thresholding to determine the exact vessel borders. To extract the ROIs we first perform the connected component analysis on the slice level to break the basic vessel model into smaller 2D objects (O9). These objects are then morphologically dilated with a structuring element in the shape of a disc with a radius of 5 pixel. The dilation gives us the ROIs (O10) within which we perform the local thresholding (O12). The threshold for each ROI is calculated based on variance minimization.

The final steps in the proposed method are meant to refine the results by adding possibly missed nearby voxels and removing small objects. For this purpose we perform region growing with results of local thresholding (O12) as seed points. Region growing is performed on de-biased original images in 3D by searching the 27-neighborhood of each seed voxel. A threshold for adding new voxels is determined on a slice level as a median value of intensities of voxels already marked as vessels. The thresholds are re-calculated after each series of newly found voxels. The region growing stops once there are no new voxels that could be added.

TABLE 1. Sequential list of all the steps performed within the proposed optimal method, along with inputs, outputs and parameters of each step and the dimension (2D or 3D) in which the step is performed. (Ox) denotes an output from a previous step where x is the step number

No	Step	Input	Output	Parameters	Dimension
1	Bias removal	Original unmasked image	De-biased image (O1)	/	2D
2	Sinc interpolation to obtain isotropic voxels	De-biased image (O1) Liver mask	Interpolated de-biased image (O2') Interpolated liver mask (O2'')	/	3D
3	Masking	Interpolated de-biased image (O2') Interpolated liver mask (O2'')	Interpolated masked de-biased image (O3)	/	2D
4	Frangi filtering	Interpolated masked de-biased image (O3)	Interpolated vesselness filtered image (O4)	Gaussian kernel $\sigma=[1,1,2]$ with a step of 0.5 $\alpha=0.3$ $\beta=0.7$ $c=$ half of Frobenius norm	3D
5	Interpolation to original voxel size	Interpolated vesselness filtered image (O4)	Vesselness filtered image (O5)	/	3D
6	Masking	Vesselness filtered image (O5) Liver mask	Masked vesselness filtered image (O6)	/	2D
7	Thresholding with a low threshold	Masked vesselness filtered image (O6)	Basic vessel model (O7)	Threshold = $0.05 * \max(\text{vesselness})$	3D
8	Removal of small objects	Basic vessel model (O7)	Basic vessel model with objects with diameter > 3 mm (O8)	Size of small object = number of pixel of a circle with 3 mm diameter	2D
9	Connected component analysis	Basic vessel model with objects with diameter > 3 mm (O8)	Basic objects (O9)	/	2D
10	Dilation	Basic object (O9)	ROI of object (O10)	Structuring element: disc with radius = 5	2D, per object
11	Masking	De-biased image (O1) Liver mask	Masked de-biased image (O11)	/	2D
12	Local thresholding	ROI of object (O10) Masked de-biased image (O11)	Locally thresholded image (O12)	Threshold determined for each ROI through variance minimization	2D, per object
13	Region growing	Locally thresholded image (O12) Masked de-biased image (O11)	Region grown image (O13)	Threshold = median of locally thresholded image, per slice 27-neighborhood	2D/3D
14	Erosion	Liver mask	Eroded mask (O14)	Structuring element: disc with radius = 6	2D
15	Masking	Region grown image (O13) Eroded mask (O14)	Segmented image (O15)	/	2D
16	Removal of small objects	Segmented image (O15)	Segmented image with objects with diameter > 3 mm (O16)	Size of small object = number of pixel of a circle with 3 mm diameter	2D

After region growing we mask the results (O13) with an eroded liver mask (O14) to eliminate boundary outliers. This step is in general unnecessary if the provided liver masks are completely accurate and contain only liver voxels. Otherwise the results of the vessel segmentation will also include a small strip around the liver which in original images is of similar intensity as vessels. The final step in the proposed method includes once again mor-

phologically opening the results (O15) to remove all objects with a diameter smaller than 3 mm.

In order to give better insight into the proposed method we provide output of all the relevant steps in Figure 1. The outputs are the result of applying the proposed method on a clinical case. For all of the presented steps we provide a one slice output and for some steps also the complete 3D model, if relevant.

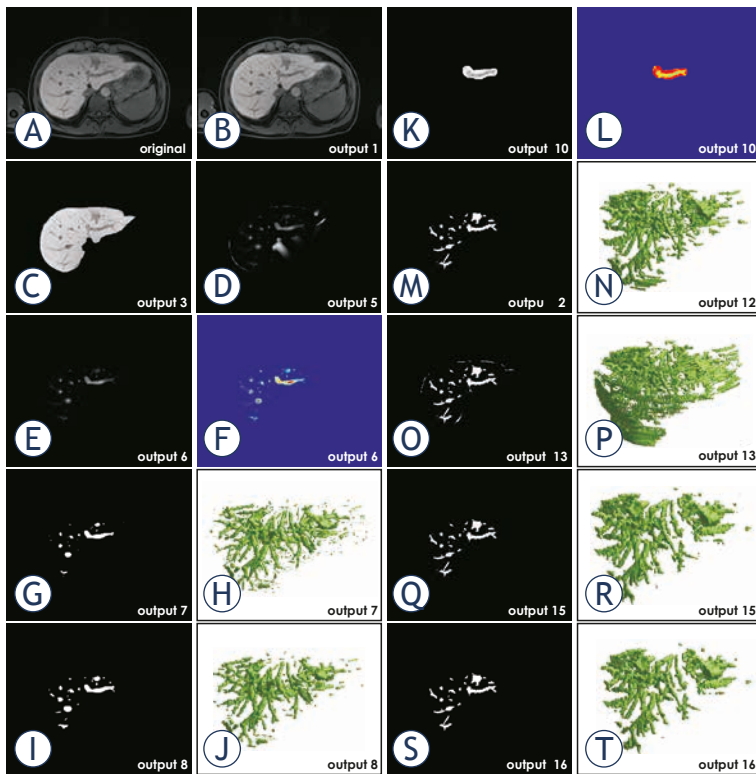


FIGURE 1. Output of the proposed method applied on a clinical case. (A) Original image. (B) De-biased original image. (C) Masked de-biased original image. (D) Vesselness filtered image. (E) Masked vesselness filtered image. (F) The same output as in E, presented in colored scale. (G) Basic vessel model with small objects. (H) Basic vessel model with small objects shown in 3D. (I) Basic vessel model without small objects. (J) Basic vessel model without small objects shown in 3D. (K) Basic object with ROI. (L) Basic object with ROI in colored scale. (M) Result of local thresholding. (N) Result of local thresholding shown in 3D. (O) Result of region growing. (P) Result of region growing shown in 3D. (Q) Result of masking with an eroded mask. (R) Result of masking with an eroded mask shown in 3D. (S) Final result after the removal of small objects. (T) Final result after the removal of small objects shown in 3D.

Most of the parameters that are used in the proposed method are calculated automatically based on the image. These parameters include the two most critical parameters: the value of c used in the vessel enhancing filter that influences the filter output most⁵⁷ and thresholds in the local thresholding step. Values of two of the remaining parameters of the vessel enhancing filter, α and β , were chosen based on validation on phantoms. The rest of the parameters that had to be set do not directly influence the accuracy of the results but rather determine the region of interest in which the main parameters operate. These less-sensitive parameters are namely a threshold in step 7 and a structuring element in step 9 (Table 1). We would, however, not suggest setting these parameters to more than $\pm 25\%$ of the values used in this paper. There is one parameter remaining that strongly influences the

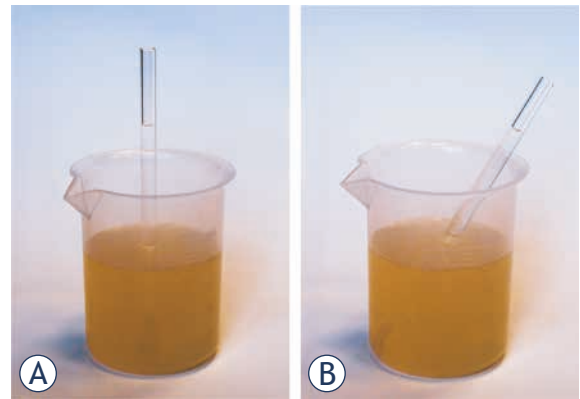


FIGURE 2. A simple phantom constructed for validation of hepatic vessel segmentation from MRI images. The phantom is made of agarose gel and a glass tube filled with physiological solution inserted in: (A) perpendicular position. (B) tilted position.

output of the vessel enhancement filter, and that is the value of σ in the Gaussian kernel. This parameter needs to be set only once and according to the size of the vessels one wishes to extract, as is stated in the work of Frangi *et al.*²⁸

Phantom design

Our primary concern in hepatic vessel segmentation was the accuracy of segmentation rather than the segmentation sensitivity to the depth of the vessel tree. For this reason we created a phantom which enabled detailed observation of whether a certain method over- or undersegments. The phantom was composed of a cup filled with agarose gel and a tube filled with physiological solution inserted into that gel, similar to the work of Merkx *et al.*⁵⁸ and Jiang *et al.*⁵⁹ The gel was prepared as a 0.5% solution of agarose in 100 ml distilled water, doped with 0.17 mM $MnCl_2$ to enhance MRI signal properties.⁶⁰ Three glass tubes with outer diameters of 4, 6 and 8 mm were filled with physiological solution in order to model the vessels. Each tube was inserted into its own cup filled with agarose gel perpendicularly to the cup bottom. Another set of tubes, also with 4, 6 and 8 mm outer diameters were inserted into another three cups filled with agarose gel, but this time in a tilted position. In total, we had six cups containing tubes. An example demonstrating different positions of the tube inside the cup is shown in Figure 2. All six cups were placed in a Siemens Avanto 1.5T MRI device and imaged at the same time in order to ensure the same imaging conditions for all six phantoms. Imaging parameters were set as in the standard protocol for imaging of the abdomen: T1-weighted, VIBE breath-hold, coronal plane with body coil. We im-

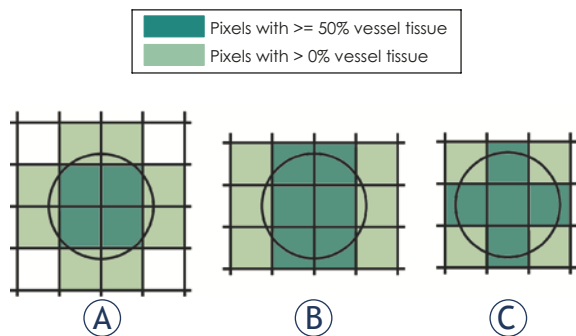


FIGURE 3. Theoretical model of reference vessel area with all possible positions of the object relative to the sampling grid. An example for the 2.56 pixel/diameter resolution. **(A)** vessel with a center in the pixel point, **(B)** vessel with the center on the middle of one of the pixels' edges, **(C)** vessel with a center position right in the middle of one of the pixels. The pixels with $\geq 50\%$ vessel tissue are a subset of pixels with $>0\%$ vessel tissue.

aged in two intra-slice resolutions: 1.56 mm by 1.56 mm and 1.04 mm by 1.04 mm. The slice thickness in both cases was 2 mm.

In order to be able to directly compare different vessel diameters imaged with different resolutions, we expressed the vessel diameters in *number of pixel/diameter* instead of in mm. The same approach was already used in papers which also evaluated accuracy of determining vessel area from MR angiography data.^{58,59} When expressed in pixel/diameter, the value of different resolutions we observed were 2.56 pix, 3.84 pix, 5.12 pix, 5.76 pix and 7.69 pix per diameter.

Clinical data

For validation on clinical data we obtained MRI images of six patients that were a part of Phase I/II clinical study "Treatment of Liver Metastases with Electrochemotherapy (ECTJ)" (EudraCT number 2008-008290-54; ClinicalTrials.gov (NCT01264952)).¹⁶ The study was conducted at the Institute of Oncology Ljubljana, Ljubljana, Slovenia. Regulatory approvals from the Institutional board, as well as from the National Medical Ethics Committee were obtained. Written consents of the patients were obtained. The series on which we performed the segmentation were the ones on which the colorectal metastases are most visible. The segmentation of the liver was also performed on the same image series by a method described by Pavliha *et al.*¹⁷ The reason for choosing the series where the liver, hepatic vessels and colorectal metastases are all visible was to avoid the need for subsequent registration. The chosen series were T1-weighted, VIBE breath-hold, transversal plane,

with body coil and imaged 20 minutes after injection of the Primovist® (Bayer Group, Germany) contrast agent. Images were acquired with a Siemens AVANTO 1.5T MRI device at the Institute of Oncology in Ljubljana. In three cases the inter-slice resolution was 0.684 mm by 0.684 mm with a slice thickness of 2.75 mm. In the other three cases the inter-slice resolution was 1.188 mm by 1.188 mm with a slice thickness of 3 mm.

Accuracy assessment metrics

Phantom data

Once the images have been segmented, we counted the number of pixel characterized as 'vessel' in each slice, thus obtaining the *segmented vessel area*. For *reference vessel area* we created a theoretical model which observes different ways in which a perfect circle can be positioned relative to the sampling grid of certain size, depending on the circle size and the grid size. The illustration of our theoretical model for the case of 2.56 pixel/diameter is presented in Figure 3.

The need for such theoretical model is caused by *partial volume effect*, i.e. an artifact in medical imaging where the value of a border pixel between different tissue types is influenced by the amount of tissues it is composed of. After segmentation, the pixel can be characterized as belonging to only one tissue type. Which type will it be depends on the amount in which a certain type is present in the pixel, but also on the segmentation method. Some segmentation methods, for instance, would characterize every pixel that contains any amount of vessel as a vessel pixel.⁵⁹ We have therefore defined three reference area values in our theoretical considerations. The first value, the *optimal vessel area* is the number of all pixels which contain at least half of the vessel tissue (pixels marked darker in Figure 3). The second reference value, the *maximum vessel area* is the number of all pixels that contain any amount of the vessel tissue (all colored pixels in Figure 3). The third reference value is *calculated vessel area* which is the mathematically calculated area of the perfect circle, expressed in number of pixels. The three reference area values (optimal, maximum and calculated) are calculated for each resolution and each of the three positions of object illustrated in Figure 3. The final *optimal vessel area* for a certain resolution is the smallest of the optimal vessel area calculated for three positions (in Figure 3 that would be 4 pixels in case A). The final *maximum vessel area* for a certain resolution is the largest of the maximum vessel area calculated for

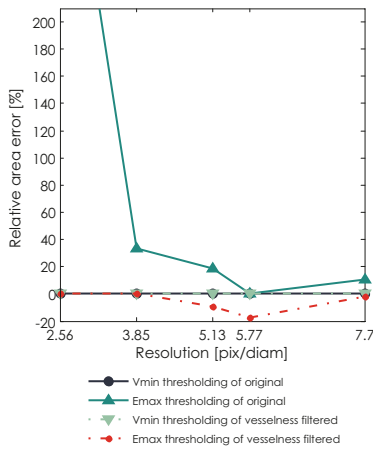


FIGURE 4. Median accuracy of segmented area of phantom in perpendicular position as a function of resolution for different segmentation methods: variance minimization thresholding of the original image, entropy maximization thresholding of the original image, vesselness filtered image thresholded by variance minimization thresholding, and vesselness filtered image thresholded by entropy maximization thresholding.

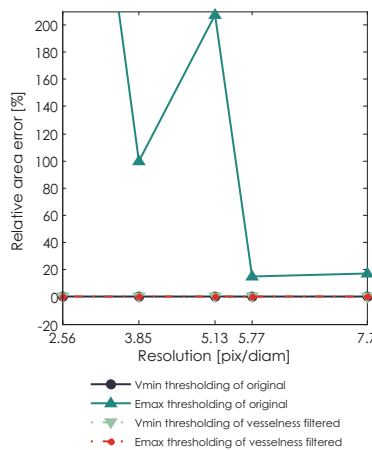


FIGURE 5. Median accuracy of segmented area of phantom in filtered position as a function of resolution for different segmentation methods: variance minimization thresholding of the original image, entropy maximization thresholding of the original image, vesselness filtered image thresholded by variance minimization thresholding, and vesselness filtered image thresholded by entropy maximization thresholding.

three positions (in Figure 3 that would be 12 pixels in cases A and B).

If the number of pixel contained in segmented vessel area falls in the range between *optimal vessel area* and *maximum vessel area*, we consider the segmentation valid. Otherwise, we count the number of pixels outside this range as *pixels missed*. The segmentation error is expressed as *relative area error*, in percent:

$$\text{relative area error } [\%] = \frac{\text{number of pixels missed}}{\text{calculated vessel area}} * 100\% \quad (3)$$

Clinical data

The gold standard for the evaluation of segmentation of clinical data is a segmentation performed by manually determining an optimal threshold for each slice and manually drawing possibly missed contours. The segmentation result was additionally validated by one of the authors (MMM) who is an experienced radiologist and who manually adjusted the segmentation where necessary. The evaluation of the segmentation of clinical data was performed on the level of objects detected in individual slices.

Metrics used for validation included a hit rate, i.e. a ratio of the number of detected objects against the number of all objects in the image, sensitivity (SEN = true positives / (true positives + false negatives)), average symmetric surface distance

(ASSD)^{34,61} and Hausdorff distance. ASSD provides a measure of the average mutual distance between edges of the two surfaces, while Hausdorff distance is in fact the maximum symmetric surface distance. ASSD and Hausdorff distance were calculated according to equations (4) and (5), respectively:

$$ASSD = \frac{\sum_{a \in A} \min_{b \in B} \|a - b\| + \sum_{b \in B} \min_{a \in A} \|a - b\|}{N_A + N_B} \quad (4)$$

$$H(A, B) = \max \left\{ \max_{a \in A} (\min_{b \in B} \|a - b\|), \max_{b \in B} (\min_{a \in A} \|a - b\|) \right\} \quad (5)$$

where A and B denote the borders of segmented and reference objects, a and b are points on A and B respectively. $\|a - b\|$ denotes the distance between a and b. N_A and N_B are the number of points on A and B.

We have chosen to use ASSD and Hausdorff distance to describe the segmentation specificity rather than a measure of specificity itself (SPEC=true negatives / (false positives + true negatives)) since a high number of true negatives (background) would always yield a high value of specificity. The values of sensitivity, ASSD and Hausdorff distance for the whole image were obtained by calculating a median of those values for all objects. We calculated the median instead of the mean since the data did not conform to Normal distribution.

Additional to previously described metrics we also used the receiver operating characteristics (ROC) curve analysis to objectively compare results of image filtering with original and de-biased images.⁶²⁻⁶⁴ The ROC curves used were constructed with threshold as a parameter.

Results

The first part of this section shows the results of segmenting phantom images. There we assess the performance of thresholding algorithms based on variance minimization and entropy maximization on original and vesselness filtered images. The second part shows the results of segmenting images obtained from clinical cases. In this part we present the comparison of methods that performed best on phantoms and the method based on local thresholding, i.e. the proposed method.

Images of phantoms

For the validation on phantom data, Figure 4 shows relative area error of different segmentation meth-

ods for segmentation of tube phantom in perpendicular position under different image resolutions. The thresholding method based on variance minimization produces 0% error on both original images and vesselness filtered images. The thresholding method based on entropy maximization undersegments the vesselness filtered images and highly oversegments the original images. As could be expected, an absolute value of error drops with increasing resolution.

Figure 5 also shows the same error as Figure 4, only for the phantom in tilted position. The thresholding method based on variance minimization again produces 0% error on both original images and vesselness filtered images. The thresholding method based on entropy maximization produces an error only in the case of original images, which as expected drops with increasing resolution. Notably, an absolute error of the method based on entropy maximization applied on original images is higher for the phantom with tube in tilted position than for the phantom in perpendicular position. An error for the same thresholding method applied on vesselness filtered images in the case of tilted phantom is 0%.

In conclusion, thresholding based on variance minimization outperformed the thresholding based on entropy maximization on both original and vesselness filtered images.

Images of clinical cases

In this section the thresholding method that performed best on images of phantoms, which is thresholding based on variance minimization, was also applied to images of clinical cases. The thresholding was first applied globally on de-biased original images and on vesselness filtered images. After that we applied our proposed method which is based on local thresholding.

Based on visual inspection only it was possible to determine that direct global slice-by-slice thresholding of vesselness filtered images results in large undersegmentation of the vessels. The segmentation inaccuracy is shown in Figure 6, where Figure A shows one slice of the original data while Figure B shows the result of the segmentation of the same slice using thresholding of the result of the vesselness filter. Figure 6.C shows the result of global thresholding of the de-biased original slice based on minimization of variance. Although more accurate than thresholding of the vesselness filtered image, this approach detects many false positives on the liver border. In Figure 6.D we can observe that false positives from Figure 6.C can

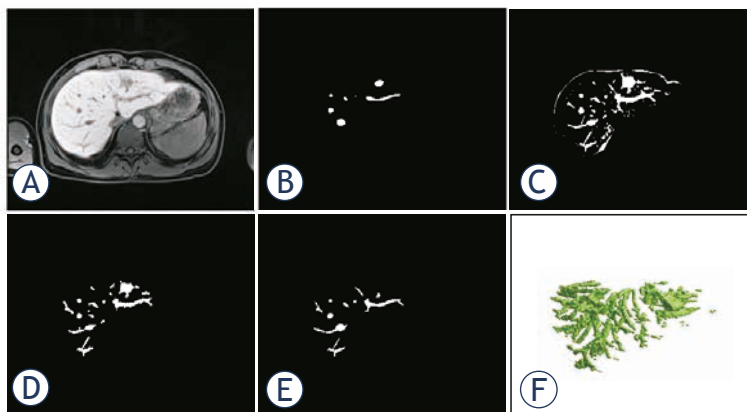


FIGURE 6. Visual comparison of performance of global thresholding and our proposed method. (A) Original image slice. (B) Results of variance minimization based global thresholding of the vesselness filtered image. (C) Results of variance minimization based global thresholding of the de-biased original image. (D) Results of our proposed method. (E) Gold standard – a radiologist segmentation. (F) 3D result of the segmentation by the method in (D).

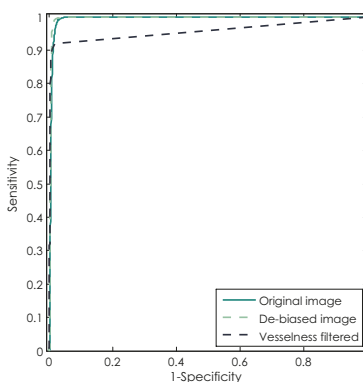


FIGURE 7. Demonstration of performance of simple binary classifier (thresholding) on original image, original image with removed bias and vesselness filtered image using ROC curves.

be avoided by our proposed method which also provides the highest level of accuracy. Figure 6.E shows the gold standard – the radiologist segmentation. Figure 6.F is a 3D representation of the segmentation by the proposed method.

To additionally explore the potential of differently filtered images at providing an accurate segmentation, we observed the ROC curves of original images, de-biased images and vesselness filtered images. As shown in Figure 7, optimal thresholding of the de-biased images can provide highly accurate segmentations, while slightly outperforming thresholding of the original images and more significantly of the vesselness filtered images. Regardless of the choice of the threshold, direct thresholding of vesselness filtered images can barely reach the sensitivity above 90%.

Final comparison of methods that performed best on phantoms (global thresholding of original de-biased images and vesselness filtered images

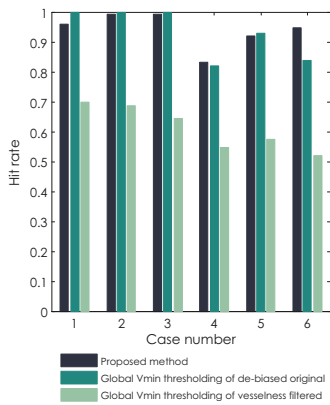


FIGURE 8. Comparison of hit rates for all six clinical cases segmented with three methods: the proposed method, global variance minimization thresholding of the original de-biased image and global variance minimization thresholding of the vesselness filtered image.

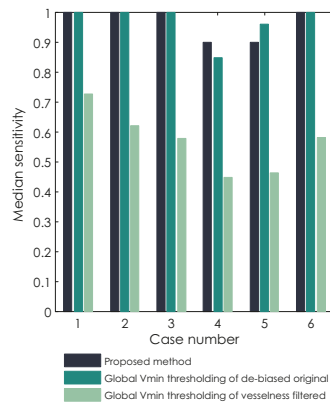


FIGURE 9. Comparison of median sensitivity for all six clinical cases segmented with three methods: the proposed method, global variance minimization thresholding of the original de-biased image and global variance minimization thresholding of the vesselness filtered image.

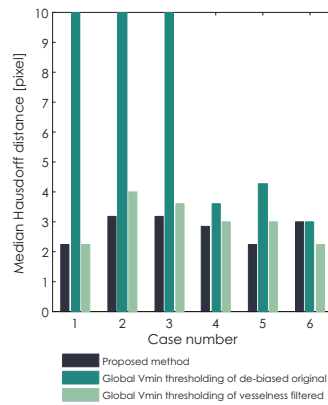


FIGURE 10. Comparison of median Hausdorff distance for all six clinical cases segmented with three methods: the proposed method, global variance minimization thresholding of the original de-biased image and global variance minimization thresholding of the vesselness filtered image.

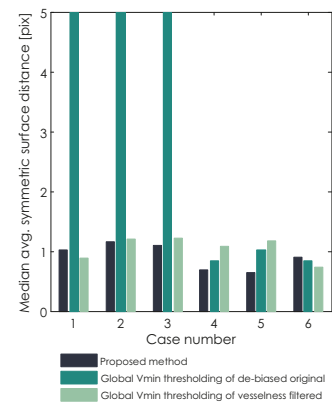


FIGURE 11. Comparison of median average symmetric surface distance (ASSD) for all six clinical cases segmented with three methods: the proposed method, global variance minimization thresholding of the original de-biased image and global variance minimization thresholding of the vesselness filtered image.

based on variance minimization) and the proposed method based on local thresholding is given by observing hit rate, median sensitivity, median Hausdorff distance and median average symmetric surface distance (ASSD) per clinical case. In Figure 8 we can observe that methods based on global thresholding of the original de-biased images have a hit rate around or above 90%, while results of global thresholding of vesselness filtered images identify less than 70% of all objects. Similar results are observed for median sensitivity in Figure 9. The values of median sensitivity are again around or above 90% for global thresholding of original de-biased images and below 70% for global thresholding of vesselness filtered images.

The differences between the proposed method and methods based on global thresholding can be observed through median Hausdorff distance and median ASSD in Figures 10 and 11, respectively. Values of median Hausdorff distance for the proposed method are for all cases in the range of around 2.2 pixels to 3.2 pixels. Values of median Hausdorff distance for global thresholding of original cases are in five out of six cases higher than those for the proposed method, in three cases even extremely high (above 10 pixel), indicating overestimation of the threshold on the global level. Values of median Hausdorff distance for thresholding of vesselness filtered images are mostly higher than those observed for the proposed method, ranging between 2.2 pixels and 4 pixels. As for median ASSD, values

for all methods are in almost all cases below 1.2 pixels, except for an extreme for global thresholding in the same three cases which also provided extremes for the median Hausdorff distance.

Final quantitative results of our proposed segmentation method are given in Tables 2 and 3. In Table 2 we provide results of validating the segmentation of all vessels that are critical for electroporation-based treatments of liver metastases as indicated previously in the paper. The mean hit rate for these vessels is high: 96.7% of objects that build up main vessels were detected. The mean value of median sensitivity of the detected objects is 93.7%. The mean error measured through ASSD is 1 pixel, while maximum error in specificity expressed through mean Hausdorff distance reaches 4.26 pixels.

The statistics in Table 3 includes all the vessels that were marked by the radiologist. Median sensitivity nearly equals the one of main vessels with 96.65%. Mean value of median ASSD which equals 0.92 pixel and mean value of median Hausdorff distance which equals 2.77 pixels indicate smaller level of error in specificity for smaller, more regularly shaped vessels.

Discussion

The main aim of the study described in this paper was to find a method which would successfully

TABLE 2. Results of segmentation of major hepatic vessels only from six clinical cases. Segmentation was performed by the method based on local thresholding. Results show hit rate of all objects in all slices, median sensitivity (SEN), median average symmetric surface distance and median Hausdorff distance

CASE	Number of objects	Pixel resolution [mm]	Hit rate [%]	Median SEN	Median ASSD [pix]	Median ASSD [mm]	Median Hausdorff distance [pix]	Median Hausdorff distance [mm]
1	43	0.684	92.9	98.0	1.3	0.9	4.4	3.0
2	69	0.684	98.4	96.4	1.1	0.7	3.6	2.5
3	38	0.684	100.0	100.0	1.1	0.7	4.1	2.8
4	31	1.188	96.4	85.3	0.7	0.8	2.2	2.7
5	31	1.188	92.3	84.2	1.3	1.5	8.1	9.6
6	25	1.188	100.0	98.2	0.6	0.7	3.2	3.8
OVERALL (mean)			96.7	93.7	1.0	0.9	4.3	4.1

TABLE 3. Results of segmentation of all hepatic vessels from six clinical cases. Segmentation was performed by the method based on local thresholding. Results show median sensitivity (SEN), median average symmetric surface distance and median Hausdorff distance

CASE	Number of objects	Pixel resolution [mm]	Median SEN	Median ASSD [pix]	Median ASSD [mm]	Median Hausdorff distance [pix]	Median Hausdorff distance [mm]
1	305	0.684	100.0	1.0	0.7	2.2	1.5
2	347	0.684	100.0	1.2	0.8	3.2	2.2
3	328	0.684	100.0	1.1	0.8	3.2	2.2
4	327	1.188	89.9	0.7	0.8	2.8	3.4
5	400	1.188	90.0	0.6	0.8	2.2	2.7
6	454	1.188	100.0	0.9	1.1	3.0	3.6
OVERALL (mean)			96.7	0.9	0.8	2.8	2.6

segment hepatic vessels from MRI images for the purpose of generating a patient-specific treatment plan for electroporation-based treatment like electrochemotherapy and non-thermal irreversible electroporation. The purpose for which the segmentation will be used has resulted in specific criteria the segmentation method must meet. Firstly, the segmentation method must detect all hepatic vessels that are considered critical in electroporation-based treatments of the liver, which are basically all major hepatic vessels with branches up to second order. Secondly, the method has to be robust. Thirdly, the method has to perform segmentation with minimal or no user interaction required. As for accuracy of the segmentation method, there were no limits posed prior to the beginning of the study. Having in mind that no segmentation method provides absolutely accurate results we rather aimed at finding the best method that would meet the set criteria and assess what is the maximum inaccuracy that method produces. Only after the maximum inaccuracy has been quantified we can conclude if segmenting hepatic vessels from MRI images for electroporation-based treatments is feasible or not.

The first step in finding a method that could segment hepatic vessels from MRI images while satisfying all the mentioned criteria was using the

established methods already used on CT images. Since we intended to test several methods we needed means of evaluation that would enable objective comparison of segmentation results. We decided to start with a simple phantom model of a single vessel for detailed observation of methods' behaviors and continue assessing robustness of methods on clinical data.

Our first choice of segmentation methods were the most widely used approaches of identifying vessels with vessel-enhancing filters and automatic thresholding. Regarding automatic thresholding, we have tested two different methods: thresholding based on intra-variance minimization and thresholding based on entropy maximization. Both thresholding methods were applied on both original de-biased and vesselness filtered images, thus resulting in in four different combinations. All four segmentation procedure combinations were run on both phantom data and clinical data. The results of evaluation on phantom data showed that intra-variance minimization thresholding applied on both original and vesselness filtered images of phantoms provides segmentation without errors. An entropy-maximizing thresholding applied on phantom data was not successful and showed tendency to over-estimate the optimal threshold, both for original and vesselness-filtered images.

Application of variance-minimization thresholding alone and in combination with vessel enhancement on clinical data did not provide satisfying results. Although variance-minimization thresholding on the level of the whole slice had a high hit-rate and sensitivity (as seen in Figures 8 and 9, respectively) it resulted in large oversegmentation error in half of clinical cases (seen in Figures 10 and 11). Namely, the large oversegmentation error appeared in clinical cases with larger image resolution. The reason for this is the fact that the difference between the size (expressed in number of pixels) of foreground (vessels) and the size of background (liver) is larger in images with higher resolution. Additionally, larger difference between foreground and background size also means larger difference between their variance, which was shown to cause oversegmentation of foreground objects when the intra-variance minimization thresholding method is applied.⁶⁵⁻⁶⁷ The other issue of variance-minimization thresholding applied on original images was that it detected not only vessels but also the liver border which had intensity values similar to vessels (Figure 6.C). Vessel enhancement on the other hand was not sensitive enough. The reason for such low sensitivity is primarily large slice thickness of the clinical data. With a gap of 3 mm between neighboring slices the changes in vessel forms are not smooth enough. Most cases where vessel enhancement was used so far had much smaller slice thickness, with sometimes even isotropic voxels.^{20,30,32,33,36} Also, hepatic vessels as seen in medical images, especially major vessels, do not have a shape of a perfect tube. These shape irregularities result in smaller values of vesselness for large vessels which can then not be detected by automatic thresholding.

The complementing weaknesses of vessel enhancement and thresholding on a global level resulted in a segmentation method that would combine these two approaches in a different way. The proposed segmentation method utilizes vessel enhancement thresholded with a low threshold to determine the existence of a vessel. The automatic thresholding method then performs the thresholding in a small region of interest just around the location of a vessel detected in the first step. Regarding the dimension in which each step of the proposed method was performed, we have utilized 3D information only to determine the basic vessel model. For determining the accurate vessel borders we relied on the original 2D information in order to avoid interpolation necessary to obtain isotropic voxels.

The evaluation of the proposed method on clinical data resulted in no large over-segmentations (Figures 10 and 11) with high values of hit-rate (Figure 8) and sensitivity (Figure 9) for both major vessels and all vessels together (tables 2 and 3, respectively). Value of average symmetric surface distance indicates that an error in segmentation of any vessel, major or small is mostly likely to be smaller than 1 pixel. Value of the median Hausdorff distance indicates that, if a larger segmentation error, i.e. an *outlier* appears, it is most likely to be 4.3 pixel for major vessels and 2.8 pixel in general, as seen in Tables 2 and 3, respectively.

A comparison with results of previously developed methods for segmentation of hepatic vessels from CT images was difficult. The general obstacle for such comparison is lack of a publicly available database that all methods would be tested on as well as the lack of unified, standard criteria for validation. Some attempts to standardize validation that would enable direct comparison were made through MICCAI grand challenges which were already organized for segmentation of liver and liver tumors from CT images.^{61,68} A similar grand challenge yet remains to be organized for segmentation of hepatic vessels from images of any modality. The main obstacle to performing any kind of comparison of our results was the fact that there are not many results to be compared with. We have searched the Web of Science directory for all papers on the topic of hepatic/liver vessel segmentation from CT images, along with referenced and referencing papers of matches. The search yielded only 19 matches in the past 20 years. Out of 19 papers, 17 of them were tested on clinical data while the remaining 2 were tested only on phantom data. Out of the mentioned 17 papers only 1 paper³⁹ included a detailed evaluation similar to ours in which the authors assessed the method accuracy and error in the form of average distance as we have. The results from that paper report an average distance of 0.9 mm to 4.4 mm, which is comparable to our findings. The authors also state that »the misclassified vessels do not deviate from the ground truth far away«. ³⁹ In the majority of the remaining 16 papers the evaluation was qualitative based on visual inspection of “goodness” of the segmentation.

Although no definite conclusions can be made about the validity of our method based on direct comparison with other methods, positive conclusions can be drawn with respect to the criteria set at the beginning of our research. Firstly, the method we propose is able to detect all vessels critical for electroporation-based treatments of liver with

above 93% sensitivity. The errors that are produced in segmentation of critical vessels appear in amount which is sufficiently low to enable a fast correction by an expert radiologist. Namely, manual validation by an expert radiologist is a step that should still be mandatory in the process of treatment planning and would also provide valuable feedback for improvement of the segmentation method.

Secondly, the proposed segmentation method is robust to variations in image resolution, imaging devices and protocols. We have shown that the method consistently provided results of high sensitivity when validated on images of different intra-slice resolution. Regarding the slice thickness the results could only be improved using smaller thickness while we would not suggest using images with slices thicker than 3 mm because of high complexity of hepatic vasculature. Given the fact that main method parameters (namely thresholds and parameter c that regulates response of the vesselness filter to high contrast) are automatically calculated from the image, the method is expected to perform well regardless of the imaging device. In order to be used on image series imaged with different protocols only one change should be made. Should the vessels in such case appear brighter instead of darker against the background a minus sign should be added in front of the equation for the vesselness filter.

Thirdly, the method is performed completely automatically with no user input, assuming that the liver is segmented automatically.¹⁷

Finally, the evaluation of the proposed method resulted in a quantitative estimation of a segmentation error which is most likely to appear in the worst case of segmentation – 2.8 pixels. Assuming the lowest image resolution of our test images, which was 1.188 mm per pixel, the above mentioned segmentation error would translate to 3.3 mm. For comparison, a study on registering CT with MRI images of the liver performed in 2005 reports a mean registration error of 14.0-18.9 mm,⁶⁹ while a newer study from 2010 reports a mean error of 3.3 mm.⁷⁰ If a segmentation of hepatic vessels was performed on CT images and then registered with MRI images for colorectal metastases segmentation the total error of vessel model would be even higher due to the error of segmentation on CT images itself. It is thus indeed more feasible to perform the hepatic vessel segmentation with our proposed method directly on MRI images. Still, in order to give a final decision if the proposed method of segmentation of hepatic vessels from MRI images can be used in treatment planning of liver

tumors with electroporation-based treatments an additional assessment is needed. The additional assessment would be based on introducing the estimated value of the segmentation error – 2.8 pixels – into treatment plan calculations and observe its influence on the distribution of the electric field.

Acknowledgements

This work was supported by the Slovenian Research Agency. Research was conducted in the scope of the Electroporation in Biology and Medicine, European Associated Laboratory. The first author would like to thank Uroš Mitrović for constructive discussion on image segmentation and Dr. Barbara Mali for discussion on statistical methods, both from University of Ljubljana, Faculty of Electrical Engineering. This manuscript is a result of the networking efforts of the COST Action TD1104 (<http://www.electroporation.net>).

References

- 1 Neumann E, Schaefer-Ridder M, Wang Y, Hofschneider PH. Gene transfer into mouse lymphoma cells by electroporation in high electric fields. *EMBO J* 1982; **1**: 841-5.
- 2 Kotnik T, Kramar P, Pucihar G, Miklavcic D, Tarek M. Cell membrane electroporation- Part 1: The phenomenon. *IEEE Electr Insul Mag* 2012; **28**: 14-23.
- 3 Mir LM, Orłowski S, Belehradek J, Paoletti C. Electrochemotherapy potentiation of antitumour effect of bleomycin by local electric pulses. *Eur J Cancer* 1991; **27**: 68-72.
- 4 Sersa G, Miklavcic D, Cemazar M, Rudolf Z, Pucihar G, Snoj M. Electrochemotherapy in treatment of tumours. *Eur J Surg Oncol* 2008; **34**: 232-40.
- 5 Mali B, Jarm T, Snoj M, Sersa G, Miklavcic D. Antitumor effectiveness of electrochemotherapy: a systematic review and meta-analysis. *Eur J Surg Oncol* 2013; **39**: 4-16.
- 6 Lacković I, Magjarević R, Miklavčić D. Three-dimensional finite-element analysis of joule heating in electrochemotherapy and in vivo gene electrotransfer. *IEEE Trans Dielectr Electr Insul* 2009; **16**: 1338-47.
- 7 Davalos R V., Mir LM, Rubinsky B. Tissue Ablation with Irreversible Electroporation. *Ann Biomed Eng* 2005; **33**: 223-31.
- 8 Chu KF, Dupuy DE. Thermal ablation of tumours: biological mechanisms and advances in therapy. *Nat Rev Cancer* 2014; **14**: 199-208.
- 9 Kos B, Zupanic A, Kotnik T, Snoj M, Sersa G, Miklavcic D. Robustness of treatment planning for electrochemotherapy of deep-seated tumors. *J Membr Biol* 2010; **236**: 147-53.
- 10 Miklavcic D, Beravs K, Semrov D, Cemazar M, Demsar F, Sersa G. The importance of electric field distribution for effective in vivo electroporation of tissues. *Biophys J* 1998; **74**: 2152-8.
- 11 Mali B, Miklavcic D, Campana LG, Cemazar M, Sersa G, Snoj M, et al. Tumor size and effectiveness of electrochemotherapy. *Radiol Oncol* 2013; **47**: 32-41.
- 12 Miklavcic D, Snoj M, Zupanic A, Kos B, Cemazar M, Kropivnik M, et al. Towards treatment planning and treatment of deep-seated solid tumors by electrochemotherapy. *Biomed Eng Online* 2010; **9**: 10.
- 13 Pavliha D, Kos B, Zupanič A, Marčan M, Serša G, Miklavčić D. Patient-specific treatment planning of electrochemotherapy: Procedure design and possible pitfalls. *Bioelectrochemistry* 2012; **87**: 265-73.

- 14 Kos B, Zupanic A, Kotnik T, Snoj M, Sersa G, Miklavcic D. Robustness of treatment planning for electrochemotherapy of deep-seated tumors. *J Membr Biol* 2010; **236**: 147-53.
- 15 Županič A, Čorović S, Miklavčič D. Optimization of electrode position and electric pulse amplitude in electrochemotherapy. *Radiol Oncol* 2008; **42**: 93-101.
- 16 Edhemovic I, Gadzjev EM, Breclj E, Miklavcic D, Kos B, Zupanic A, et al. Electrochemotherapy: a new technological approach in treatment of metastases in the liver. *Technol Cancer Res Treat* 2011; **10**: 475-85.
- 17 Pavliha D, Mušič MM, Serša G, Miklavčič D. Electroporation-based treatment planning for deep-seated tumors based on automatic liver segmentation of MRI images. *PLoS One* 2013; **8**: e69068.
- 18 Fraass B, Doppke K, Hunt M, Kutcher G, Starkschall G, Stern R, et al. American Association of Physicists in Medicine Radiation Therapy Committee Task Group 53: quality assurance for clinical radiotherapy treatment planning. *Med Phys* 1998; **25**: 1773-829.
- 19 Payne S, Flanagan R, Pollari M, Alhonnoro T, Bost C, O'Neill D, et al. Image-based multi-scale modelling and validation of radio-frequency ablation in liver tumours. *Philos Trans A Math Phys Eng Sci* 2011; **369**: 4233-54.
- 20 Alhonnoro T, Pollari M, Lijja M, Flanagan R, Kainz B, Muehl J, et al. Vessel Segmentation for Ablation Treatment Planning and Simulation. In: Jiang T, Navab N, Pluim JPW, et al., editors. *Medical image computing and computer-assisted intervention: MICCAI International Conference on Medical Image Computing and Computer-Assisted Intervention*. Volume 6361. Berlin, Heidelberg: Springer; 2010. p. 45-52.
- 21 Hansen PD, Rogers S, Corless CL, Swanstrom LL, Siperstien AE. Radiofrequency ablation lesions in a pig liver model. *J Surg Res* 1999; **87**: 114-21.
- 22 Sersa G, Jarm T, Kotnik T, Coer A, Podkrajsek M, Sentjurs M, et al. Vascular disrupting action of electroporation and electrochemotherapy with bleomycin in murine sarcoma. *Br J Cancer* 2008; **98**: 388-98.
- 23 Lesage D, Angelini ED, Bloch I, Funke-Lea G. A review of 3D vessel lumen segmentation techniques: models, features and extraction schemes. *Med Image Anal* 2009; **13**: 819-45.
- 24 Glombitza G, Lamade W, Demiris AM, Gopfert M, Mayer A, Bahner ML, et al. Virtual planning of liver resections: image processing, visualization and volumetric evaluation. *Int J Med Inform* 1999; **53**: 225-37.
- 25 Zahlten C, Jürgens H, Evertz CJG, Leppke R, Peitgen HO, Klose KJ. Portal vein reconstruction based on topology. *Eur J Radiol* 1995; **19**: 96-100.
- 26 Selle D, Preim B, Schenk A, Peitgen HO. Analysis of vasculature for liver surgical planning. *IEEE Trans Med Imaging* 2002; **21**: 1344-57.
- 27 Sato Y, Nakajima S, Shiraga N, Atsumi H, Yoshida S, Koller T, et al. Three-dimensional multi-scale line filter for segmentation and visualization of curvilinear structures in medical images. *Med Image Anal* 1998; **2**: 143-68.
- 28 Frangi AF, Niessen WJ, Vincken KL, Viergever MA. Multiscale vessel enhancement filtering. In: Wells WM, Colchester A, Delp S, editors. *Medical Image Computing and Computer-Assisted Intervention - MICCAI '98 (1998)*. Berlin, Heidelberg: Springer; 1998. p. 130-7.
- 29 Krissian K, Malandain G, Ayache N, Vaillant R, Troussset Y. Model-based detection of tubular structures in 3D images. *Comput Vis Image Underst* 2000; **80**: 130-71.
- 30 Conversano F, Franchini R, Demitri C, Massoptier L, Montagna F, Maffezzoli A, et al. Hepatic vessel segmentation for 3D planning of liver surgery experimental evaluation of a new fully automatic algorithm. *Acad Radiol* 2011; **18**: 461-70.
- 31 Bauer C, Pock T, Sorantin E, Bischof H, Beichel R. Segmentation of interwoven 3d tubular tree structures utilizing shape priors and graph cuts. *Med Image Anal* 2010; **14**: 172-84.
- 32 Shang Q, Clements L, Galloway RL, Chapman WC, Dawant BM. Adaptive directional region growing segmentation of the hepatic vasculature. In: Reinhardt JM, Pluim JPW, editors. *Proceedings of SPIE*. Volume 6914. SPIE; 2008. p. 69141F-10.
- 33 Beichel R, Pock T, Janko C, Zotter RB, Reitingner B, Bornik A, et al. Liver segment approximation in CT data for surgical resection planning. In: Fitzpatrick JM, Sonka M, editors. *Proceedings of SPIE*. SPIE; 2004. p. 1435-46.
- 34 Wang G, Zhang S, Li F, Gu L. A new segmentation framework based on sparse shape composition in liver surgery planning system. *Med Phys* 2013; **40**: 051913.
- 35 Soler L, Delingette H, Malandain G, Montagnat J, Ayache N, Koehl C, et al. Fully automatic anatomical, pathological, and functional segmentation from CT scans for hepatic surgery. *Comput aided Surg Off J Int Soc Comput Aided Surg* 2001; **6**: 131-42.
- 36 Pamulapati V, Wood BJ, Linguraru MG. Intra-hepatic vessel segmentation and classification in multi-phase CT using optimized graph cuts. In: Yoshida H, Sakas G, Linguraru MG, editors. *2011 IEEE International Symposium on Biomedical Imaging: From Nano to Macro*. Volume 7029. IEEE; 2011. p. 1982-5.
- 37 Esneault S, Lafon C, Dillenseger J-L. Liver vessels segmentation using a hybrid geometrical moments/graph cuts method. *IEEE Trans Biomed Eng* 2010; **57**: 276-83.
- 38 Shang Y, Deklerck R, Nyssen E, Markova A, de Mey J, Yang X, et al. Vascular active contour for vessel tree segmentation. *IEEE Trans Biomed Eng* 2011; **58**: 1023-32.
- 39 Chi Y, Liu J, Venkatesh SK, Huang S, Zhou J, Tian Q, et al. Segmentation of liver vasculature from contrast enhanced CT images using context-based voting. *IEEE Trans Biomed Eng* 2011; **58**: 2144-53.
- 40 Bipat S, van Leeuwen MS, Comans EFI, Pijl MEJ, Bossuyt PMM, Zwinderman AH, et al. Colorectal liver metastases: CT, MR imaging, and PET for diagnosis-meta-analysis. *Radiology* 2005; **237**: 123-31.
- 41 Chan VO, Das JP, Gerstenmaier JF, Geoghegan J, Gibney RG, Collins CD, et al. Diagnostic performance of MDCT, PET/CT and gadoteric acid (Primovist®)-enhanced MRI in patients with colorectal liver metastases being considered for hepatic resection: initial experience in a single centre. *Ir J Med Sci* 2012; **181**: 499-509.
- 42 Floriani I, Torri V, Rulli E, Garavaglia D, Compagnoni A, Salvolini L, et al. Performance of imaging modalities in diagnosis of liver metastases from colorectal cancer: a systematic review and meta-analysis. *J Magn Reson Imaging* 2010; **31**: 19-31.
- 43 Fowler KJ, Linehan DC, Menias CO. Colorectal liver metastases: state of the art imaging. *Ann Surg Oncol* 2013; **20**: 1185-93.
- 44 Mainenti PP, Mancini M, Mainolfi C, Camera L, Maurea S, Manchia A, et al. Detection of colo-rectal liver metastases: prospective comparison of contrast enhanced US, multidetector CT, PET/CT, and 1.5 Tesla MR with extracellular and reticulo-endothelial cell specific contrast agents. *Abdom Imaging* 2010; **35**: 511-21.
- 45 Muhi A, Ichikawa T, Motosugi U, Sou H, Nakajima H, Sano K, et al. Diagnosis of colorectal hepatic metastases: comparison of contrast-enhanced CT, contrast-enhanced US, superparamagnetic iron oxide-enhanced MRI, and gadoteric acid-enhanced MRI. *J Magn Reson Imaging* 2011; **34**: 326-35.
- 46 Kranjc M, Bajd F, Serša I, Miklavčič D. Magnetic resonance electrical impedance tomography for monitoring electric field distribution during tissue electroporation. *IEEE Trans Med Imaging* 2011; **30**: 1771-8.
- 47 Kranjc M, Bajd F, Sersa I, Woo EJ, Miklavcic D. Ex vivo and in silico feasibility study of monitoring electric field distribution in tissue during electroporation-based treatments. *PLoS One* 2012; **7**: e45737.
- 48 Pavliha D, Kos B, Marčan M, Zupanič A, Serša G, Miklavčič D. Planning of electroporation-based treatments using Web-based treatment planning software. *J Membr Biol* 2013; **246**: 833-42.
- 49 Vovk U, Pernus F, Likar B. A review of methods for correction of intensity inhomogeneity in MRI. *IEEE Trans Med Imaging* 2007; **26**: 405-21.
- 50 Zheng Y, Grossman M, Awate SP, Gee JC. Automatic correction of intensity nonuniformity from sparseness of gradient distribution in medical images. *Med Image Comput Comput Assist Interv* 2009; **12**: 852-9.
- 51 Sankur B. Survey over image thresholding techniques and quantitative performance evaluation. *J Electron Imaging* 2004; **13**: 146.
- 52 Otsu N. A Threshold Selection Method from Gray-Level Histograms. *IEEE Trans Syst Man Cybern* 1979; **9**: 62-6.
- 53 Kapur JN, Sahoo PK, Wong AKC. A new method for gray-level picture thresholding using the entropy of the histogram. *Comput Vision, Graph Image Process* 1985; **29**: 273-85.
- 54 Yaroslavsky LP. Efficient algorithm for discrete sinc interpolation. *Appl Opt* 1997; **36**: 460-3.
- 55 Van Dongen E, van Ginneken B. Automatic segmentation of pulmonary vasculature in thoracic CT scans with local thresholding and airway wall removal. In: *2010 IEEE International Symposium on Biomedical Imaging: From Nano to Macro*. IEEE; 2010. p. 668-71.

- 56 Augusto L, Braga F, Silveira C, Paula V, Fazan S. Arterial diameter of the celiac trunk and its branches. Anatomical study 1 Diâmetro arterial do tronco celiaco e seus ramos. *Estudo Anatômico* 2009; **24**: 43-7.
- 57 Olabarriaga S, Breeuwer M, Niessen W. Evaluation of Hessian-based filters to enhance the axis of coronary arteries in CT images. *Int Congr Ser* 2003; **1256**: 1191-6.
- 58 Merckx M a G, Bescós JO, Geerts L, Bosboom EMH, van de Vosse FN, Breeuwer M. Accuracy and precision of vessel area assessment: manual versus automatic lumen delineation based on full-width at half-maximum. *J Magn Reson Imaging* 2012; **36**: 1186-93.
- 59 Jiang J, Haacke EM, Dong M. Dependence of vessel area accuracy and precision as a function of MR imaging parameters and boundary detection algorithm. *J Magn Reson Imaging* 2007; **25**: 1226-34.
- 60 Virtanen JM, Komu ME, Parkkola RK. Quantitative liver iron measurement by magnetic resonance imaging: in vitro and in vivo assessment of the liver to muscle signal intensity and the R2* methods. *Magn Reson Imaging* 2008; **26**: 1175-82.
- 61 Deng X, Du G. Editorial: 3D segmentation in the clinic: A grand challenge II-liver tumor segmentation. In: *International Conference on Medical Image Computing and Computer Assisted Intervention*. 2008. p. 1-12.
- 62 Van Erkel a R, Pattynama PM. Receiver operating characteristic (ROC) analysis: basic principles and applications in radiology. *Eur J Radiol* 1998; **27**: 88-94.
- 63 Obuchowski NA. Receiver operating characteristic curves and their use in radiology. *Radiology* 2003; **229**: 3-8.
- 64 Wagner RF, Metz CE, Campbell G. Assessment of medical imaging systems and computer aids: a tutorial review. *Acad Radiol* 2007; **14**: 723-48.
- 65 Hou Z, Hu Q, Nowinski WL. On minimum variance thresholding. *Pattern Recognit Lett* 2006; **27**: 1732-43.
- 66 Medina-Carnicer R, Madrid-Cuevas FJ. Unimodal thresholding for edge detection. *Pattern Recognit* 2008; **41**: 2337-46.
- 67 Xu X, Xu S, Jin L, Song E. Characteristic analysis of Otsu threshold and its applications. *Pattern Recognit Lett* 2011; **32**: 956-61.
- 68 Heimann T, Van Ginneken B, Styner MA, Arzhaeva Y, Aurich V, Bauer C, et al. Comparison and evaluation of methods for liver segmentation from CT datasets. *IEEE Trans Med Imaging* 2009; **28**: 1251-65.
- 69 Christina Lee W-C, Tublin ME, Chapman BE. Registration of MR and CT images of the liver: comparison of voxel similarity and surface based registration algorithms. *Comput Methods Programs Biomed* 2005; **78**: 101-14.
- 70 Elhawary H, Oguro S, Tuncali K, Morrison PR, Tatli S, Shyn PB, et al. Multimodality non-rigid image registration for planning, targeting and monitoring during CT-guided percutaneous liver tumor cryoablation. *Acad Radiol* 2010; **17**: 1334-44.

Microinvasive cervical squamous cell carcinoma in Slovenia during the period 2001-2007

Helena Gutnik¹, Jasenka P. Maticic², Maja Primic Zakelj³, Margareta Strojan Flezar⁴

¹ Institute of Pathology, Faculty of Medicine, University of Ljubljana, Slovenia

² British Columbia Cancer Agency, Vancouver, Canada

³ Epidemiology and Cancer Registry, Institute of Oncology Ljubljana, Slovenia

⁴ Institute of Pathology, Faculty of Medicine, University of Ljubljana, Slovenia

Radiol Oncol 2014; 48(3): 282-288.

Received 21 November 2013

Accepted 14 February 2014

Correspondence to: Margareta Strojan Fležar, M.D., Ph.D., Institute of Pathology, Faculty of Medicine, University of Ljubljana. Korytkova 2, SI-1000 Ljubljana, Slovenia. E-mail: margareta.strojan-flezar@mf.uni-lj.si

Disclosure: No potential conflicts of interest were disclosed.

Background. Microinvasive squamous cell carcinoma (MISCC) comprises a significant portion of all cervical cancers in Slovenia. Criteria of carcinomatous invasion are well described in the literature, however histopathological assessment of MISCC is difficult, because morphological characteristics can overlap with cervical intraepithelial neoplasia grade 3 (CIN 3) and other pathological changes. The aim of our study was to evaluate the reliability of the histopathological diagnosis of MISCC in Slovenia during the period from 2001 to 2007.

Materials and methods. Data on patients with a histopathological diagnosis of cervical MISCC (FIGO stage IA) in the period of 2001 to 2007 were obtained from the Cancer Registry of Slovenia. Histological slides were obtained from the majority of pathology laboratories in Slovenia. We received 250 cases (69% of all MISCC) for the review; 30 control cases with CIN 3 and invasive squamous cell carcinoma FIGO stage IB were intermixed. The slides were coded and reviewed.

Results. Among 250 cases originally diagnosed as MISCC, there was an agreement with MISCC diagnosis in 184 (73.6%) cases (of these 179/184 (97.3%) cases were FIGO stage IA1 and 5/184 (2.7%) cases were FIGO stage IA2). Among 179 FIGO stage IA1 cases 117 (65.4%) showed only early stromal invasion.

Conclusions. The retrospective review of cases diagnosed as MISCC during the period 2001- 2007 in Slovenia showed a considerable number of overdiagnosed cases. Amongst cases with MISCC confirmed on review, there was a significant proportion with early stromal invasion (depth of invasion less than 1 mm).

Key words: cervical cancer; cervical squamous cell carcinoma; microinvasive squamous cell carcinoma; cervical intraepithelial neoplasia

Introduction

For more than 50 years, the Cancer Registry of the Republic of Slovenia has collected epidemiological data on the incidence rate of cervical cancer and cervical intraepithelial neoplasia (CIN). The incidence rate of cervical cancer was declining until the late 1980s, however it began to rise by the beginning of the 1990s and exceeded 20 new cases per 100.000 women (the highest incidence rate was 23.0/100.000 in 1997).¹⁻⁴ During the same time period, incidence of the earliest stage of cervical

squamous cell carcinoma, microinvasive (early invasive) squamous cell carcinoma (MISCC), increased and contributed substantially to overall cervical cancer incidence (Figure 1).¹⁻⁴ The incidence of MISCC was highest in the age group 20-49 years. In the time period 2004-2006 it even exceeded 40% of all cervical cancer cases in this age group (Figure 2). Of the two FIGO clinical stages of MISCC the incidence of stage IA1 (tumor invasion 3 mm or less in depth) was much higher than the incidence of stage IA2 (tumor invasion 5 mm or less in depth) (Figures 1, 2).⁵ After the

implementation of an organized national cervical cancer screening program in Slovenia in 2003 named Zgodnje Odkrivanje predRAkavih sprememb materničnega vratu (ZORA) the incidence of cervical cancer started to decline in 2004 with a concurrent rise in incidence of cervical intraepithelial neoplasia grade 3 (CIN 3).³ In the year 2007 the number of newly detected cervical cancers declined to 153 (incidence rate 14.8/100.000) and in 2008 and 2009 to 130 (incidence rate 12.6/100.000). Simultaneously the incidence rate of CIN 3 rose from 60.0/100.000 in 1997 to 115.0/100.000 in 2007.³

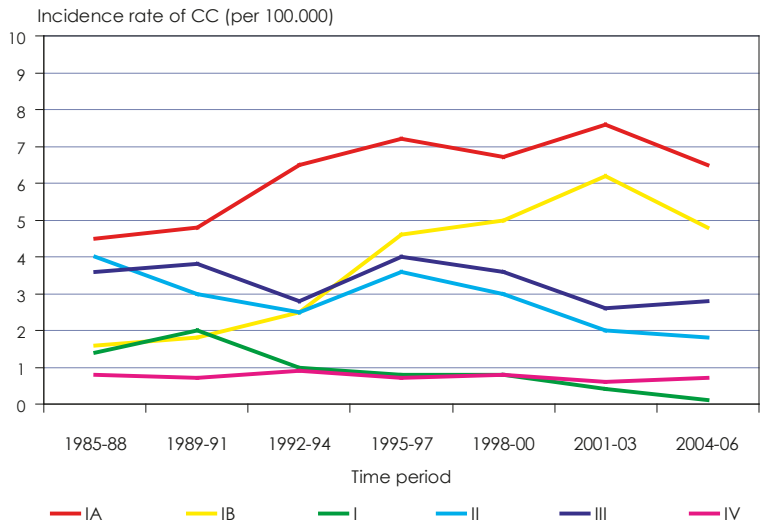
In many cervical biopsies light-microscopic evaluation of MISCC is a difficult task. It is partially the consequence of the anatomical and histological peculiarities of the cervix uteri, namely the tendency of CIN 3, from which the MISCC foci derive, to involve the cervical gland crypts.^{6,7} On the other hand histopathological changes linked to inflammation, prior biopsies, cautery artefacts and tangential sectioning of epithelium may mimic the MISCC.^{6,7} The experienced pathologist should consider all the options and carefully confirm or exclude them to avoid overdiagnosing invasive disease.⁶⁻¹⁰

The earliest form of MISCC is early stromal invasion, with the depth of invasion up to 1 mm. Early stromal invasion is encompassed in the IA1 FIGO clinical stage of cervical squamous carcinoma and was never staged as a separate category.^{5,11,12} Some authors think early stromal invasion should be considered as a separate category excluded from IA1 FIGO clinical stage because its management and prognosis is similar to that of CIN 3.^{13,14}

Some authors describe the impact of biopsy management (different sectioning) and the number of histological levels per tissue block made on the evaluation of MISCC. According to the results of two studies, MISCC was present in the first tissue level in the majority of biopsies and that suggested that the processing of many hematoxylin eosin (HE) slides per tissue block causes an unnecessary burden for the pathologist.^{15,16}

The purpose of our study was to find out whether the recorded incidence of cervical cancer in Slovenia in the period 2001-2007 was correct or overestimated resulting from difficulties implementing the histopathological criteria of MISCC and the existence of many histopathological changes that can mimic MISCC.

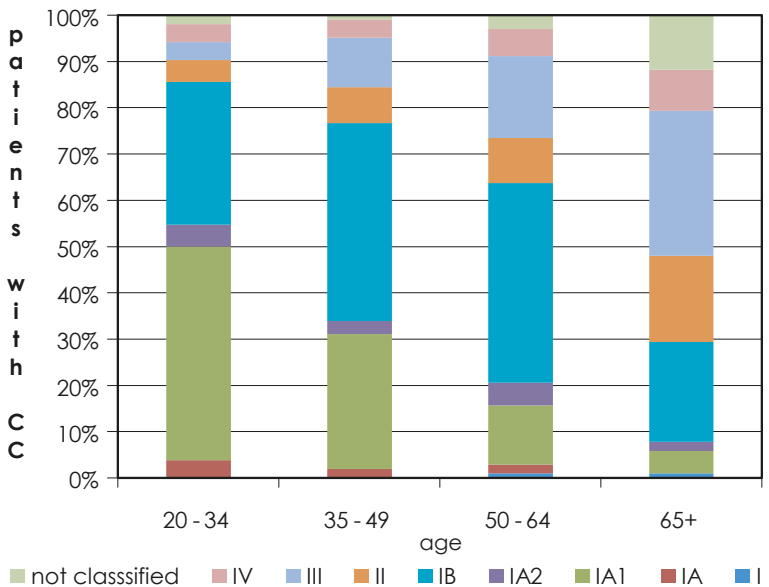
We also evaluated the presence of MISCC in the first tissue level and whether or not the number of HE slides per tissue block influenced the reliability of histopathological evaluation.



CC = cervical carcinoma; IA, IB, I, II, III, IV: clinical stages of cervical cancer according to international federation of gynecology and obstetrics (FIGO)

(Source: Report on results of the national cervical cancer screening programme ZORA (in the period 2007-2008))

FIGURE 1. Incidence rate of cervical cancer according to the clinical stage at the diagnosis (Slovenia 1985-2006).



CC = cervical carcinoma; IA, IA1, IA2, IB, II, III, IV: clinical stages of cervical carcinoma according to the International Federation of Gynecology and Obstetrics (FIGO)

(Source: Report on results of the national cervical cancer screening program ZORA (in the period 2007-2008))

FIGURE 2. Proportion of patients with cervical carcinoma by clinical stage of International Federation of Gynaecology and Obstetrics (FIGO) and by age groups (Slovenia 2004-2006).

Materials and methods

The study was approved by Slovenian national medical ethics committee (Approval No. 51/05/09). The data on microinvasive cervical squamous cell

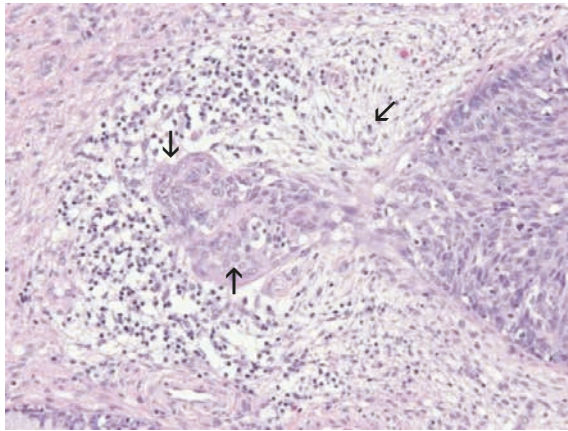


FIGURE 3. Focus of cervical microinvasive squamous cell carcinoma (left) emerging from cervical intraepithelial lesion grade 3 (right); maturation of the neoplastic epithelium (\uparrow), irregularities of the epithelial stromal interface (\downarrow) and desmoplastic reaction in the adjacent stroma (\leftarrow) are seen (hematoxylin and eosin stain; original magnification: $\times 200$).

carcinoma (FIGO stage IA1 and IA2) in the period 2001-2007 were obtained from the Cancer Registry of RS. Original histological HE stained slides of cone biopsies and hysterectomies from which the original diagnoses of MISCC were made were requested from various pathology laboratories. In the period 2001-2007 eleven laboratories reported MISCC to the Cancer Registry of RS and 363 patients were diagnosed with MISCC. We managed to obtain 285 specimens from nine laboratories representing 78.5% of patients with the diagnosis of MISCC. After checking the HE slides 35 biopsies were missing or damaged and therefore excluded. The remaining 250 biopsies (69% of patients with the diagnosis of MISCC) were suitable for light microscopic review. The original diagnoses of 250 biopsies were: 230 carcinomas FIGO stage IA1, 16 carcinomas FIGO stage IA2, and 4 MISCC without stage evaluation.

To avoid bias in review, 30 control cone biopsies were included in the study (15 with the original histopathological diagnosis of CIN 3 and 15 with the original histopathological diagnosis of cervical squamous cell carcinoma, FIGO stage IB (SCC, IB)). The control biopsies were selected from the archives of the Institute of Pathology, Faculty of Medicine Ljubljana and from Department of Pathomorphology, Division of Obstetrics and Gynecology, University Medical Centre Ljubljana. Overall the study included 280 biopsies (274 cervical cone biopsies and 6 hysterectomies). The cases were anonymized and assigned randomly chosen successive numbers from 1 to 280.

Firstly the HE slides were reviewed independently by two pathologists (pathologist A, pathologist B) experienced in the histopathological diagnosis of uterine cervical lesions. Then third pathologist (pathologist C) independently, without knowing the original diagnoses or diagnoses of pathologists A and B, reviewed selected cases including those where the first two pathologists did not find any MISCC, the biopsies where they disagreed, the biopsies where the histopathological changes were difficult to interpret but were considered suspicious for MISCC, and some randomly chosen control biopsies. The established criteria for histopathological evaluation of microinvasive cervical squamous cell carcinoma were used: focal maturation of the neoplastic epithelium with prominent nucleoli, desmoplastic response in the adjacent stroma, blurring and irregularity of the epithelial-stromal interface (Figure 3).^{6,7,10,11} The depth and width of MISCC was measured in millimeters (mm) and classified according to the FIGO classification of cervical squamous carcinoma clinical stages.⁵ Every foci of invasion were measured separately from the CIN 3 epithelial-stromal interface. When the pathologists could not confirm the diagnosis of microinvasive carcinoma, they also assessed which histopathological changes that were present in the biopsy could mimic early invasion.

The results of the review were compared to the original diagnoses and presented with the methods of descriptive statistics. The interobserver variability between the three pathologists was measured by Cohen's kappa coefficient. The diagnosis of MISCC was confirmed when two or all three pathologists agreed on diagnosis.

Because the data on the type of cone biopsy and tissue management in the histopathology laboratories were not available for all patients, we also recorded the type of cone biopsy (cold knife or large loop excision of the transformation zone (LLETZ)) and the method of tissue sectioning (parallel or radial). The average number of tissue levels per tissue block was also counted.

In all biopsies with the review assessment of MISCC we evaluated the presence of MISCC in the first level cut from the tissue block.

Results

The average age of patients with an original diagnosis of microinvasive carcinoma was 41.1 years (range 22-74 years, median 40). The average age of patients from the control group with the CIN 3 di-

TABLE 1. Results of review of 88 biopsies with original diagnosis of cervical microinvasive squamous cell carcinoma examined by three pathologists (Pathologist A, Pathologist B, Pathologist C)

CKC	B +	B -	A +	A -	B +	B -
	31	10	28	3	28	3
	4	43	13	44	7	50
0,80		0,80		0,88		

CKC = Cohen's kappa coefficient; + = diagnosis of microinvasive squamous cell carcinoma confirmed; - = diagnosis of microinvasive squamous cell carcinoma not confirmed; A = Pathologist A; B = Pathologist B; C = Pathologist C

agnosis was 35.9 years (range 24-55 years, median 40) and from the control group with the diagnosis of SCC, IB was 39.5 years (range 31-51 years, median 40). Among all 280 biopsies included in the study, 196 (70%) were cold-knife cones, 78 (28%) were LLETZ, and 6 (2%) were hysterectomy specimens. There were 269 (96%) cones sectioned in the parallel way, and 5 cones and 6 hysterectomies (4%) sectioned using the radial method. The average number of tissue levels per tissue block was 8 (range 1-40).

The results of the review by pathologists A and B were: among 250 biopsies with an original MISCC diagnosis 184 biopsies were confirmed as MISCC (31 as suspicious for MISCC). In 50 biopsies the reviewers agreed there was no MISCC. In 15 biopsies the agreement could not be reached. 1 biopsy was assessed as SCC, stage IB by both pathologists. All CIN 3 control biopsies were confirmed as CIN 3. Among SCC, FIGO stage IB control biopsies the diagnosis of SCC, FIGO stage IB was confirmed in 12 cases. However, 3 biopsies were evaluated as MISCC, 2 as FIGO stage IA1 and 1 as FIGO stage IA2. Cohen's kappa coefficient for pathologists A and B diagnostic agreement was 0.85.

Pathologist C evaluated 92 biopsies (32.8%): all 15 biopsies where pathologists A and B could not reach an agreement, 42 biopsies where pathologists A and B agreed there was no MISCC, 31 biop-

sies where pathologists A and B thought they were difficult to interpret and agreed on suspicious of MISCC diagnosis and 4 randomly chosen control biopsies. The Cohen's kappa coefficients for this group of biopsies (with the original diagnosis of MISCC), reviewed by all three pathologists were: 0,80 for pathologists A and B, 0,80 for pathologists A and C and 0,88 for pathologists B and C (Table 1). We considered the case as MISCC when two or all three pathologists agreed on this diagnosis. The 31 cases that pathologists A and B found difficult to interpret were reexamined concurrently by all three pathologists to reach a consensus diagnosis.

The final results of the three pathologists' review are shown in Table 2. Among 184 biopsies with confirmed MISCC 179 were defined as FIGO stage IA1 (117 early stromal invasion) with maximum depth of invasion of 1 mm, 62 with depth of invasion between 1 and 3 mm) and 5 biopsies were defined as FIGO stage IA2.

The major histopathological criteria of early invasion were evaluated in all 187 biopsies scored as MISCC (184 with original MISCC diagnosis, 3 with original SCC, FIGO stage IB diagnosis). Focal maturation of the neoplastic epithelium with prominent nucleoli was confirmed in all 187 biopsies. Blurring and irregularities of the epithelial-stromal interface was seen in 159 (85%) of 187 biopsies. A desmoplastic response in the adjacent stroma was

TABLE 2. Final results of review on 280 biopsies with original diagnosis of cervical microinvasive squamous cell carcinoma: 250 biopsies with the original diagnosis of cervical microinvasive squamous cell carcinoma and 30 control biopsies

	Number of biopsies	Original diagnosis	Diagnosis after the review N (%)
Control biopsies	15	CIN 3	15 (100,0) CIN 3
Control biopsies	15	SCC IB	12 (80,0) SCC IB 3 (20,0) SCC IA
Biopsies to reevaluate (with the original MISCC diagnosis)	250	MISCC	184 (73,6) SCC IA 2 (0,8) SCC IB 64 (25,6) no MISCC
All	280		280

MISCC = microinvasive squamous cell carcinoma; IA, IB = clinical stages of cervical squamous cell carcinoma according to International Federation of Gynecology and Obstetrics (FIGO) classification; CIN 3 = cervical intraepithelial lesion grade 3; SCC = squamous cell carcinoma

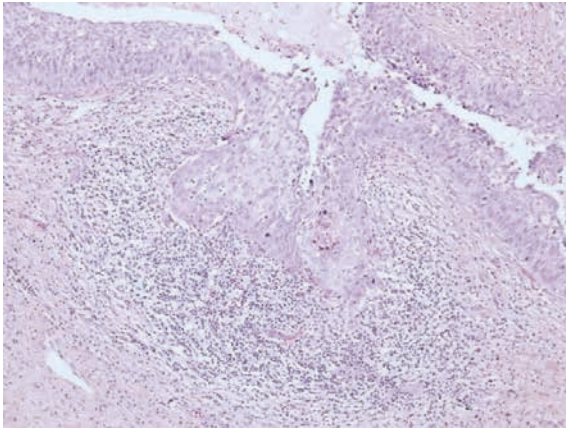


FIGURE 4. Heavy inflammatory infiltrate surrounding the focus of invasion; cell maturation and scalloped margins are present but no convincing desmoplasia. (hematoxylin and eosin stain; original magnification: x200).

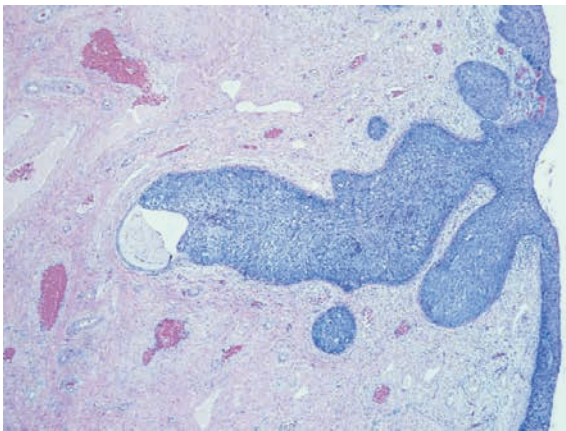


FIGURE 5. Cervical intraepithelial neoplasia grade 3 involving the cervical gland crypts (hematoxylin and eosin stain; original magnification: x40).

confirmed in 133 (71%) of 187 biopsies (in the remaining 54 biopsies a heavy mononuclear inflammatory infiltrate was surrounding invasive foci making the evaluation of desmoplastic reaction impossible) (Figure 4).

In 64 biopsies evaluated as not containing MISCC we evaluated the histopathological changes that could possibly mimic early invasion and cause false overdiagnoses of MISCC. We classified these histopathological changes into eight groups: deposits of normal squamous or CIN epithelium in the subepithelial tissue, tangentially sectioned epithelium, prior biopsy site changes, reactive epithelial changes (regeneration, pseudoepithelomatous hyperplasia), inflammatory changes with blurred epithelial-stromal interface, complex CIN 3 with

extensive gland-crypt involvement, cautery tissue artifacts, and normal squamous epithelium without evident pathological changes. The most frequent solitary histopathological change was complex CIN 3 with extensive gland crypt involvement (41 of 64 biopsies (64%)) followed by inflammatory changes and tangentially sectioned epithelium (Figure 5).

In 187 biopsies confirmed as MISCC after review (184 with an original diagnosis of MISCC, and 3 SCC, FIGO stage IB from the control group) we also evaluated the presence of MISCC in the first tissue level of the block. We found MISCC in first tissue level in 141 of 187 biopsies (75%). In the remaining 46 biopsies (25%) MISCC was present in the second or subsequent tissue levels. In 42 of 46 biopsies the absence of MISCC in the first tissue level was the consequence of a poorly prepared first cut HE slide with large areas of epithelium missing. MISCC was found in 2nd level in 5/42 cases, 3rd level in 12/42 cases, 4th level in 8/42 cases, 5th level in 5/42 cases, 6th level in 4/42 cases, 7th level in 6/42 cases, 8th and 9th level in one case each/42 cases. In only 4 of 46 biopsies no MISCC was found in suitably prepared first cut HE slide; MISCC was found in 2nd level in 2/4 cases and 3rd level in 2/4 cases.

Discussion

Cervical cancer is still a significant public health problem even in some countries with successfully implemented cytological screening programs for early detection of cervical precancerous lesions. Due to the high incidence of cervical carcinoma in Slovenia and the especially high incidence of MISCC, we tried to assess, the reliability of the histopathological diagnosis of MISCC during the period 2001-2007.¹⁻⁴

Our study exposes several problems in the diagnosis of MISCC. 25.6% of biopsies with an original diagnosis of MISCC were assessed as not containing MISCC after review. Among the biopsies assessed as MISCC after the review, 63.6% were evaluated as early stromal invasion. In the majority of biopsies the established criteria of early invasion were readily assessable with the exception of the desmoplastic reaction which could not be reliably assessed due to heavy inflammatory infiltrate in 29% of cases. In cases confirmed as MISCC, the MISCC was found in the first tissue level in only 75% of biopsies.

The rate of overdiagnosis of MISCC in our study (25.6%) is comparable to that found in large biopsy series reviews.¹⁷⁻¹⁹ The rate of overdiagnosis is

much higher than of underdiagnosis of MISCC. These results show that when in doubt pathologists are prone to overdiagnose MISCC. Overdiagnosis of MISCC not only increases cervical cancer incidence rates but also exposes women to unnecessary overtreatment and is a cause of psychological and social stresses.^{17,18,20}

We were unable to obtain epidemiologic data about the proportion of MISCC in the overall FIGO stage IA1 groups of cervical carcinoma in other countries, but according to the data of some published studies the incidence of MISCC is below the Slovenian incidence. Two separate studies reported that MISCC comprised 15% and 19% of cervical cancers.^{19,21} In our study we found out that among MISCC not only the percentage of FIGO stage IA1 is especially high (92% of original MISCC diagnoses and even 97% cases with MISCC confirmed after review) but also the early stromal invasion with invasive foci of less than 1 mm depth represented a high proportion of FIGO stage IA1 cases. To our knowledge cancer registries do not classify early stromal invasion as a separate category, although some authors think it should be excluded from MISCC because its prognosis and management are similar to those of CIN 3. In their opinion reporting early stromal invasion as invasive squamous carcinoma increases the incidence of cervical cancer and the cancer burden.^{13,14} We agree with this opinion which is supported by Slovenian epidemiological data that show that mortality from cervical cancer is low compared with its incidence rate.^{2-4,22}

Regarding the evaluation of criteria for early invasion we had no substantial difficulties in assessing focal maturation with prominent nucleoli of the neoplastic epithelium and blurring and irregularities of the epithelial-stromal interface.^{6,7,10} However a desmoplastic response in the adjacent stroma was difficult or impossible to evaluate in 29% of all biopsies reevaluated as MISCC because of the heavy mononuclear inflammatory infiltrate surrounding and sometimes invading the foci of MISCC. We found no evidence of this problem in the literature, but the difficulties in assessing this criterion are disturbing because we believe that a clearly expressed desmoplastic reaction is a valuable criterion of early invasion.

We also estimated the presence of MISCC in first tissue level per block and compared the results of data from previous studies. Pathologists from different countries examine variable number of tissue levels per blocks of cone biopsies, depending on their national societies' recommendations and

laboratory protocols. In our study we noticed that the number of tissue levels varied from 1 to 40 levels from nine different pathology laboratories we received the biopsies from. This is the consequence of the fact that in Slovenia we are only now starting to prepare standard operating procedures to manage uterine cervical biopsies whereas previously pathology laboratories would follow their own recommendations. Nevertheless, the results of previous studies showed that MISCC was present in the first tissue level in the majority of the cone biopsies; therefore larger numbers of levels have been regarded as unnecessary except when there was discordance between cytologic, colposcopic and histologic data.^{15,16} The results of our present study do not confirm these previous findings, as we found MISCC in the first tissue level in only 75% of cone biopsies with a confirmed diagnosis of MISCC. The reason for this discordance is suboptimal quality of the first tissue level (first HE slide) preparation in some laboratories. In our opinion the first levels are often not suitable for pathological evaluation because of large areas of squamous epithelium missing. In previous studies this issue was not evident as the tissue levels were presumably suitable for evaluation. This fact emphasizes the need for proper recommendations and quality assurance for pathology laboratories. According to our study 5 tissue levels would assure diagnosis in all cases if the optimal quality of the first tissue level preparation was secured.

In conclusion, our findings suggest that diagnosis of MISCC is demanding and pathologists in their routine work tend to overdiagnose the invasive disease. This leads to increased cervical cancer incidence rates and also exposes women to unnecessary overtreatment. The results of our study show the need for national recommendations and quality assurance at all levels of uterine cervical diagnostics related to national cervical screening program.

Acknowledgements

The authors thank to Dr. Malcolm Hayes and Brenda Smith for reading the manuscript and giving the valuable comments.

References

1. Primic Žakelj M, Kirar Fazarinc I, Zadnik V. Epidemiology of cervical cancer in Slovenia (in the period 1990-2003). Available at: <http://www.onko-i.si/zora/epidemiologija.html>.

2. Primic Žakelj M, Pogačnik A, Uršič Vrščaj M. Report on results of the national cervical cer screening programme ZORA (in the period 2006-2007). Ljubljana: Onkološki inštitut; 2008.
3. Primic Žakelj M, Ivanuš U, Pogačnik A, Uršič Vrščaj M. Report on results of the national cervical cancer screening programme ZORA (in the period 2007-2008). Ljubljana: Onkološki inštitut; 2009.
4. SLORA (Register raka Republike Slovenije): Podatki o incidenci RMV. Available at: <http://www.slora.si>.
5. Tavassoli FA, Devilee P. Tumors of the breast and female genital organs. World Health Organization Classification of Tumours. Lyon: IARC Sci Publ; 2003.
6. Wright TC, Ferenczy A, Kurman RJ. Carcinoma and other tumors of the cervix. In: Kurman RJ, TeLinde RW, editors. *Blaustein's Pathology of the Female Genital Tract*. 5th edition New York: Springer Verlag; 2002. p. 326-31.
7. Crum CP, Rose PG. Cervical squamous neoplasia. In: Crum CP, Lee KR, editors. *Diagnostic and obstetric pathology*. 1st edition Elsevier Inc.; 2006. p. 320-34.
8. Boyle DP, McCluggage WG. Pseudoinvasion of benign squamous epithelium following cervical biopsy: a pseudoneoplastic phenomenon mimicking invasive squamous carcinoma. *J Clin Pathol* 2011; **64**: 1093-6.
9. Nafussi A, Hughes DE. Histological features of CIN 3 and their value in predicting invasive microinvasive squamous carcinoma. *J Clin Pathol* 1994; **47**: 799-804.
10. Burghardt E, Girardi F, Lahousen M, Pickel H, Tamussino K. Microinvasive carcinoma of the uterine cervix (International Federation of Gynecology and Obstetrics Stage IA). *Cancer* 1991; **67**: 1037-45.
11. Hirschowitz L, Nucci M, Zaino RJ. Problematic issues in the staging of endometrial, cervical and vulval carcinomas. *Histopathology* 2013; **62**: 176-202.
12. Pecorelli S, Zigliani L, Odicino F. Revised FIGO staging for carcinoma of the cervix. *Int J Gynecol Obstet* 2009; **105**: 107-8.
13. Burghardt E, Ostör A, Fox H. The new FIGO definition of cervical cancer stage IA: a critique. *Gynecol Oncol* 1997; **65**: 1-5.
14. Mota F. Microinvasive squamous carcinoma of the cervix: treatment modalities. *Acta Obstet Gynecol Scand* 2003; **82**: 505-9.
15. Gutnik H, Strojjan Flezar M, Pizem J, Ellis K, Don O, Perunović B. Impact of different sectioning of excision biopsies of the cervical transformation zone for detection of invasive cervical cancer in two European centers related to national cervical screening programmes. *Int J Gynecol Cancer* 2010; **20**: 593-6.
16. Heatley MK. How many histological levels should be examined from tissue blocks originating in cone biopsy and large loop excision of the transformation zone specimens of cervix? *J Clin Pathol* 2001; **54**: 650-1.
17. Morgan PR, Anderson MC, Buckley CH, Murdoch JB, Lopes A, Duncan ID, et al. The Royal College of Obstetricians and Gynecologists micro-invasive carcinoma of cervix study: results. *Br J Obstet Gynecol* 1993; **100**: 664-8.
18. Ebeling K, Bilek K, Johannsmeyer D, Rohde E, Wagner F, Buchmann J, et al. Microinvasive stage IA cancer of the uterine cervix-results of a multicenter clinic based analysis. *Geburtshilfe Frauenheilkd* 1989; **49**: 776-81.
19. Raspagliesi F, Ditto A, Solima E, Quattrone P, Fontanelli R, Zanaboni F. Microinvasive squamous cell cervical carcinoma. *Crit Rev Oncol Hematol* 2003; **48**: 251-61.
20. Cairns M, Gray NM, Cruickshank ME. The impact of microinvasive cancer of the cervix on women during follow – up. *Int J Gynecol Cancer* 2008; **8**: 1289-93.
21. Hasumi K, Sakamoto A, Sugano H. Microinvasive carcinoma of the uterine cervix. *Cancer* 1980; **45**: 928-31.
22. Arbyn M, Raifu AO, Autier P, Ferlay J. Burden of cervical cancer in Europe: estimates for 2004. *Ann Oncol* 2007; **18**: 1708-15.

The influence of folate pathway polymorphisms on high-dose methotrexate-related toxicity and survival in children with non-Hodgkin malignant lymphoma

Nina Erculj¹, Barbara Faganel Kotnik², Marusa Debeljak³, Janez Jazbec², Vita Dolzan¹

¹ Pharmacogenetics Laboratory, Institute of Biochemistry, Faculty of Medicine, University of Ljubljana, Ljubljana, Slovenia

² Department of Hematology and Oncology, University Children's Hospital, University Medical Centre, Ljubljana, Slovenia

³ Centre for Medical Genetics, University Children's Hospital, University Medical Centre, Ljubljana, Slovenia

Radiol Oncol 2014; 48(3): 289-292.

Received: 1 September 2013

Accepted: 16 September 2013

Correspondence to: Prof. Vita Dolzan, M.D., Ph.D., Pharmacogenetics Laboratory, Institute of Biochemistry, Faculty of Medicine, University of Ljubljana, Vrazov trg 2, 1000 Ljubljana, Slovenia. Phone: +386 1 543 7670; Fax: +386 1 543 7641; E-mail: vita.dolzan@mf.uni-lj.si

Disclosure: No potential conflicts of interest were disclosed.

Background. We evaluated the influence of folate pathway polymorphisms on high-dose methotrexate (HD-MTX) related toxicity in paediatric patients with T-cell non-Hodgkin lymphoma (NHL).

Patients and methods. In total, 30 NHL patients were genotyped for selected folate pathway polymorphisms.

Results. Carriers of at least one *MTHFR* 677T allele had significantly higher MTX area under the time-concentration curve levels at third MTX cycle ($P = 0.003$). These patients were also at higher odds of leucopenia ($P = 0.006$) or thrombocytopenia ($P = 0.041$) and had higher number of different HD-MTX-related toxicity ($P = 0.035$) compared to patients with wild-type genotype.

Conclusions. Our results suggest an important role of *MTHFR* 677C>T polymorphism in the development of HD-MTX-related toxicity in children with NHL.

Key words: childhood; non-Hodgkin lymphoma; folate pathway; polymorphism; high-dose methotrexate; toxicity

Introduction

Lymphomas are the second most common group of cancers in children and adolescents in Slovenia (www.slora.si). Non-Hodgkin's lymphomas (NHLs) represent approximately 50% of these diagnoses in children and have an average 10-year incidence in Slovenia of six cases per year. NHL comprises a heterogeneous group of lymphoid neoplasms.¹ Among the three major subgroups of childhood NHL according to the World Health Organization Classification, children with lymphoblastic lymphoma of the precursor B- or T-cell types (LBL) are treated according to childhood acute lymphoblastic leukaemia (ALL) protocols², which include administration of high-dose methotrexate (HD-MTX).

MTX is folate analogue, which inhibits several enzymes of the folate pathway. The imbalance of folate homeostasis may lead to DNA synthesis arrest and could disrupt DNA and protein methylation reaction. Our previous studies showed that genetic variability in the key folate pathway enzymes, 5,10-methylenetetrahydrofolate dehydrogenase 1 (MTHFD1), 5,10-methylenetetrahydrofolate reductase (MTHFR), and thymidylate synthase (TYMS), might influence MTX pharmacokinetics and treatment outcome in children with ALL.^{3,4} Therefore, the aim of the present study was to assess the influence of polymorphisms in these genes on HD-MTX-related toxicity in children with NHL treated according to Berlin-Frankfurt-Münster (BFM) protocols.

TABLE 1. Clinical and treatment characteristics of paediatric patients with lymphoblastic T-cell non-Hodgkin lymphoma (n = 29)

Characteristic	n (%)	Mean (± SD)
Median age, years^a		11.0 (1.0-18.0)
Gender		
Male	25 (86.2)	
Female	4 (13.8)	
Treatment protocol		
BFM86	2 (6.9)	
BFM90	9 (31.0)	
BFM95	9 (31.0)	
ICBFM02	9 (31.0)	
MTX dose, mg/m²		
2000	1 (3.5)	
5000	28 (96.5)	
Any cycle with delayed MTX clearance	14 (46.7)	
C_{max}, µmol/l^b		49.9 (± 31.2)
AUC₁, µmol*h/l^c		323.3 (± 250.6)
AUC₂, µmol*h/l^c		356.8 (± 215.6)
AUC₃, µmol*h/l^d		297.7 (± 202.0)
AUC₄, µmol*h/l^e		418.4 (± 340.2)
Treatment outcome		
First remission	21 (72.4)	
Event ^f	8 (27.6)	

AUC = area under the time-concentration curve after first (1), second (2), third (3), and fourth (4) application; BFM = Berlin-Frankfurt-Münster; C_{max} = maximal MTX plasma concentration; ICBFM = intercontinental Berlin-Frankfurt-Münster; MTX = methotrexate; SD = standard deviation

^a Age is presented as median (range); ^b Data missing for 2 (6.9%) patients; ^c Data missing for 8 (27.6%) patients; ^d Data missing for 11 (37.9%) patients; ^e Data missing for 10 (34.5%) patients; ^f Event was defined as disease relapse at any site, death from any cause, or the occurrence of second malignant neoplasm

TABLE 2. Prevalence of high-dose methotrexate-related toxicities in the group of paediatric patients with lymphoblastic T-cell non-Hodgkin lymphoma (n = 27)

Toxicity	Number of patients	(%)
anaemia grade ≥ 2	5	(17.2)
leucopenia grade ≥ 2	6	(20.7)
thrombocytopenia grade ≥ 2	7	(24.1)
hepatotoxicity grade ≥ 1 ^b	16	(55.2)
renal toxicity	1	(3.5)
gastrointestinal toxicity	2	(6.9)
mucositis grade ≥ 1	8	(27.6)

^bData on hepatotoxicity missing for 4 (13.8%) patients

Patients and methods

The cohort consisted of all the patients with primary NHL aged ≤ 18 years at the time of diagnosis who were diagnosed and treated between the years 1993 and 2009 at the Department of Hematology and Oncology, University Children's Hospital, Ljubljana, Slovenia. Only patients with lymphoblastic T-cell NHL treated according to the BFM protocols³ who received HD-MTX during consolidation phase were included into the study group. Toxicity evaluation and HD-MTX pharmacokinetics data collection and analysis were described previously.⁴ All the subjects and/or their parents or legal guardians gave their written informed consent to participate in the study. The study was approved by the Slovenian Ethics Committee for Research in Medicine and was carried out according to the Declaration of Helsinki.

Genomic DNA was isolated from archived bone marrow slides using QIAamp DNA Mini kit (Qiagen).⁵ *MTHFD1* 1958G>A (rs2236225), *MTHFR* 677C>T (rs1801133), and 1298A>C (rs1801131) were determined by TaqMan SNP genotyping method (Applied Biosystems, Foster City, CA, USA). *TYMS* 2R>3R (rs34743033) and 3RG>3RC (rs2853542) polymorphisms were genotyped as previously described.⁴

For each polymorphism, deviation of genotype frequency distribution from those expected under Hardy-Weinberg equilibrium (HWE) was assessed using standard chi-square test. To test the difference between two groups the Student's t-test was used in case of normally distributed data and the nonparametric correlations were used for non-normally distributed data. Associations of investigated polymorphisms with HD-MTX-related toxicity were examined using logistic regression models.⁴ The level of significance was set to 0.050. All statistical analyses were carried out by SPSS for Windows, version 19.0 (Statistical Package for the Social Sciences, Chicago, IL).

Results

Patients

Among the entire cohort of 76 children with NHL, 29 patients with lymphoblastic T-cell NHL were included into study group as they were treated according to BFM protocols. For one patient, no treatment-related data were available. In total, patients received 110 cycles of HD-MTX. Clinical and treat-

TABLE 3. The influence of *MTHFD1*, *MTHFR*, and *TYMS* polymorphisms on high-dose methotrexate-related toxicity in pediatric patients with non-Hodgkin lymphoma (n = 28)

Polymorphism	Genotype	Number (%)	Anaemia grade $\geq 2a$		Leucopenia grade ≥ 2		Thrombocytopenia grade ≥ 2		Hepatotoxicity grade $\geq 1b$		Mucositis grade ≥ 1	
			OR (95% CI)	P	OR (95% CI)	P	OR (95% CI)	P	OR (95% CI)	P	OR (95% CI)	P
<i>MTHFD1</i> 1958G>A	GG	11 (37.9)	Reference		Reference		Reference		Reference		Reference	
	GA	16 (55.2)	0.94 (0.13-6.78)	0.923	3.75 (0.37-37.95)	0.263	1.67 (0.26-10.79)	0.592	0.51 (0.08-3.49)	0.496	2.18 (0.35-13.76)	0.406
	AA	2 (6.9)										
<i>MTHFR</i> 677C>T	CC	16 (55.2)	Reference		Reference		Reference		Reference		Reference	
	CT	11 (37.9)	5.33 (0.51-56.24)	0.164	1.86 (1.12-3.07)	0.006^c	11.14 (1.11-112.01)	0.041	0.13 (0.01-1.34)	0.087	1.11 (0.21-5.80)	0.901
	TT	2 (6.9)										
<i>MTHFR</i> 1298A>C	AA	12 (41.4)	Reference		Reference		Reference		Reference		Reference	
	AC	15 (51.7)	1.13 (0.15-8.21)	0.908	0.25 (0.04-1.71)	0.158	0.17 (0.03-1.14)	0.069	0.96 (0.16-5.80)	0.968	1.21 (0.22-6.61)	0.824
	CC	2 (6.9)										
<i>TYMS</i> 2R>3R	2R/2R	7 (24.1)	Reference		Reference		Reference		Reference		Reference	
	2R/3R	12 (41.4)	1.60 (0.15-17.41)	0.700	2.00 (0.19-20.90)	0.563	0.33 (0.05-2.13)	0.246	1.20 (0.16-8.80)	0.858	0.44 (0.07-2.71)	0.379
	3R/3R	10 (34.5)										
<i>TYMS</i> 2R>3RC/ 3RC^d	Low	14 (48.3)	Reference		Reference		Reference		Reference		Reference	
	High	13 (46.8)	0.82 (0.11-5.99)	0.815	3.00 (0.44-20.44)	0.262	0.36 (0.06-2.34)	0.284	0.50 (0.08-3.08)	0.455	0.36 (0.06-2.34)	0.284

CI = confidence interval; OR = odds ratio

TYMS low expression genotypes: 2RG/2RG, 2RG/3RC, and 3RC/3RC. *TYMS* high expression genotypes: 2RG/3RG, 3RC/3RG, and 3RG/3RG.

ORs, 95% CIs, and *P* values were calculated by univariable logistic regression and the dominant genetic model was used. Bold characters indicate statistically significant results

^a Data on anaemia missing for 1 patients (3.9%); ^b Data on hepatotoxicity missing for 4 patients (13.8%); ^c *P*-value was calculated using Fisher's exact test; ^d Genotyping data missing for 2 patients (6.7%)

ment characteristics of the study group are summarized in Table 1.

HD-MTX-related toxicity was observed in 25 (86.2%) patients and the number of different toxicities in individual patients ranged from one to five. Prevalence of HD-MTX-related toxicities is shown in Table 2. Frequencies of all investigated polymorphisms were in HWE and were consistent with published data for Slovenian healthy young individuals⁶ and paediatric patients with ALL.⁴

There were no influences of investigated polymorphisms on *C*_{max}; however, the mean AUC levels at third HD-MTX cycle were significantly higher in carriers of at least one *MTHFR* 677T allele compared to patients with wild-type genotype (mean AUC3 \pm standard deviation: 163.7 \pm 108.0 $\mu\text{mol}\cdot\text{h}/\text{l}$ versus 431.7 \pm 186.1 $\mu\text{mol}\cdot\text{h}/\text{l}$, *P* = 0.003). AUC levels also correlated with the number of different HD-MTX-related toxicities in individual patients (AUC1: τ = 0.423, *P* = 0.015 and AUC3: τ = 0.586, *P* = 0.001). The influence of investigated polymorphisms on HD-MTX-related toxicity is presented in Table 3. *MTHFD1* 1958G>A, *MTHFR* 1298A>C, and *TYMS* polymorphisms were not associated with any of investigated toxicities. In contrast, carriers of *MTHFR* 677T allele had significantly increased odds of leucopenia grade ≥ 2 (OR = 1.86; 95% CI = 1.12–3.07; *P* = 0.006) and thrombocytopenia grade ≥ 2 (OR = 11.14; 95% CI = 1.11–112.01; *P* = 0.041).

The association of thrombocytopenia grade ≥ 2 (OR = 39.42; 95% CI = 2.11–734.94; *P* = 0.014) remained significant in multivariable model adjusted for patients' age. In addition, the number of polymorphic *MTHFR* 677T alleles positively correlated with number of different HD-MTX-related toxicities in individual patients (τ = 0.442, *P* = 0.010). We did not observe any associations between *MTHFR* haplotypes and HD-MTX-related toxicity (data not shown).

Discussion

The present study investigated the role of several folate pathway polymorphisms in development of HD-MTX-related toxicity and survival in a group of paediatric patients with lymphoblastic T-cell NHL treated according to BFM protocols.

We did not observe any association of *MTHFD1* or *TYMS* polymorphisms with HD-MTX-related toxicity. In contrast to these results, our previous study showed an influence of *TYMS* 2R>3R polymorphism on different haematotoxicities, as well as an influence of *MTHFD1* 1958G>A polymorphism on hepatotoxicity grade ≥ 2 in paediatric patients with ALL.⁴ The association between *MTHFD1* 1958G>A polymorphism and hepatotoxicity grade ≥ 2 could not be assessed in the present

study due to the low frequency of hepatotoxicity grade ≥ 2 . Moreover, the lack of association between *TYMS* polymorphisms and treatment outcomes in our study might be due to the low frequency of wild-type 2R/2R genotype and a small study population, leading to insufficient statistical power to detect significant associations.

In concordance with our previous studies, investigating HD-MTX pharmacokinetics³ and HD-MTX-related toxicity in children with ALL⁴, we observed significantly higher AUC levels in carriers of at least one *MTHFR* 677T allele compared to patients with wild-type genotype. Similar to our findings, other studies also reported the influence of *MTHFR* 677T allele on higher MTX plasma levels.^{7,8} In addition, we observed significantly increased odds of leucopenia and thrombocytopenia, as well as higher number of different HD-MTX-related toxicities in carriers of at least one *MTHFR* 677T allele compared to patients with wild-type genotype. Although these findings do not support our results obtained in a group of paediatric patients with ALL⁴, it must be noted that compared to ALL patients, patients with NHL were predominantly male, older at the time of diagnosis, and received higher doses of MTX. A few studies that investigated the influence of *MTHFR* polymorphisms on HD-MTX-related toxicity in patients with NHL reported conflicting results.^{3,7,9} However, most of these studies included heterogeneous groups of patients, regarding the type of hematologic malignancy and treatment protocols.

We are aware that one of the limitations of our study is the small sample size; however, it was population-based and included a homogenous group of paediatric patients with lymphoblastic T-cell NHL treated according to BFM protocols in Slovenia over the past 17 years. Therefore, the chances of reporting and detection biases due to random sampling were minimized.

In conclusion, our study suggests that *MTHFR* 677C>T polymorphism might modulate MTX pharmacokinetics, and hence influence HD-MTX-related toxicity in patients with lymphoblastic T-cell NHL treated according to BFM protocols.

Acknowledgement

This work was financially supported by the Slovenian Research Agency (ARRS Grants No. P1-0170 and P3-0343).

References

- Gregoric B, Zadnik V, Jezersek Novakovic B. The diffuse large B-cell lymphoma – where do we stand now in everyday clinical practice. *Radiol Oncol* 2012; **46**: 153-9.
- Reiter A, Schrappe M, Ludwig WD, Tiemann M, Parwaresch R, Zimmermann M, et al. Intensive ALL-type therapy without local radiotherapy provides a 90% event-free survival for children with T-cell lymphoblastic lymphoma: a BFM group report. *Blood* 2000; **95**: 416-21.
- Faganel Kotnik B, Grabnar I, Bohanec Grabar P, Dolzan V, Jazbec J. Association of genetic polymorphism in the folate metabolic pathway with methotrexate pharmacokinetics and toxicity in childhood acute lymphoblastic leukaemia and malignant lymphoma. *Eur J Clin Pharmacol* 2011; **67**: 993-1006.
- Erculj N, Kotnik BF, Debeljak M, Jazbec J, Dolzan V. Influence of folate pathway polymorphisms on high-dose methotrexate-related toxicity and survival in childhood acute lymphoblastic leukemia. *Leuk Lymphoma* 2012; **53**: 1096-104.
- Jazbec J, Kitanovski L, Aplenc R, Debeljak M, Dolzan V. No evidence of association of methylenetetrahydrofolate reductase polymorphism with occurrence of second neoplasms after treatment of childhood leukemia. *Leuk Lymphoma* 2005; **46**: 893-7.
- Petra BG, Janez J, Vita D. Gene-gene interactions in the folate metabolic pathway influence the risk for acute lymphoblastic leukemia in children. *Leuk Lymphoma* 2007; **48**: 786-92.
- Imanishi H, Okamura N, Yagi M, Noro Y, Moriya Y, Nakamura T, et al. Genetic polymorphisms associated with adverse events and elimination of methotrexate in childhood acute lymphoblastic leukemia and malignant lymphoma. *J Hum Genet* 2007; **52**: 166-71.
- Kantar M, Kosova B, Cetingul N, Gumus S, Toroslu E, Zafer N, et al. Methylenetetrahydrofolate reductase C677T and A1298C gene polymorphisms and therapy-related toxicity in children treated for acute lymphoblastic leukemia and non-Hodgkin lymphoma. *Leuk Lymphoma* 2009; **50**: 912-7.
- Seidemann K, Book M, Zimmermann M, Meyer U, Welte K, Stanulla M, et al. *MTHFR* 677 (C->T) polymorphism is not relevant for prognosis or therapy-associated toxicity in pediatric NHL: results from 484 patients of multicenter trial NHL-BFM 95. *Ann Hematol* 2006; **85**: 291-300.

MRI-assisted cervix cancer brachytherapy pre-planning, based on application in paracervical anaesthesia: final report

Primoz Petric^{1,2}, Robert Hudej², Omar Hanuna², Primoz Marolt², Noora Mohammed A A Al-Hammadi¹, Mohamed P. Riyas¹, Barbara Segedin²

¹ Department of Radiation Oncology, National Center for Cancer Care and Research, Doha, Qatar

² Department of Radiotherapy, Institute of Oncology Ljubljana, Ljubljana, Slovenia

Radiol Oncol 2014; 48(3): 293-300.

Received 13 December 2013

Accepted 14 January 2014

Correspondence to: Barbara Šegedin, M.D., Department of Radiotherapy, Institute of Oncology Ljubljana, Ljubljana, Slovenia. Phone +386 1 5879 206; Fax: +386 1 5879 400; E-mail: bsegedin@onko-i.si

Disclosure: Publication of this study was supported by Nucletron™, an Elekta company.

Background. Optimal applicator insertion is a precondition for the success of cervix cancer brachytherapy (BT). We aimed to assess feasibility and efficacy of MRI-assisted pre-planning, based on applicator insertion in para-cervical anaesthesia (PCA).

Patients and methods. Five days prior to BT, the pre-planning procedure was performed in 18 cervix cancer patients: tandem-ring applicator was inserted under PCA, pelvic MRI obtained and applicator removed. Procedure tolerability was assessed. High risk clinical target volume (HR CTV) and organs at risk were delineated on the pre-planning MRI, virtual needles placed at optimal positions, and dose planning performed. At BT, insertion was carried out in subarachnoidal anaesthesia according to pre-planned geometry. Pre-planned and actual treatment parameters were compared.

Results. Pre-planning procedure was well tolerated. Median difference between the pre-planned and actual needle insertion depth and position were 2 (0–10) mm and 4 (0–30) degrees, respectively. The differences between the pre-planned and actual geometric and dosimetric parameters were statistically non-significant. All actual needles were positioned inside the HR CTV and outside the organs at risk (OAR).

Conclusions. Our pre-planning approach is well tolerated and effective. Pre-planned geometry and dose distribution can be reproduced at BT.

Key words: cervix cancer; MRI; pre-planning; image-guided brachytherapy

Introduction

MRI is the recommended modality for image guided adaptive brachytherapy (IGABT) of cervix cancer.¹⁻⁹ MRI enables an accurate and reproducible delineation of the target volume and organs at risk (OAR). Individualized application techniques, treatment planning systems and remote afterloaders permit adaptation of the dose distribution to the delineated volumes and evaluation of dose volume histogram (DVH) parameters. This approach has been reflected in encouraging dosimetric and clinical results.¹⁰⁻¹⁸ Combined intracavitary (IC) and in-

terstitial (IS) application techniques, using modified IC applicators are beneficial in cases of unfavourable pelvic topography and/or large tumours.^{10,11,19-21} At our institution, MRI-assisted IGABT, based on the GEC ESTRO recommendations, has been used since 2006.²²⁻²⁴ In our practice, 3D conformal external beam radiotherapy (EBRT: 45–50.4 Gy in 1.8 Gy daily fractions) +/- concurrent chemotherapy (weekly 40 mg/m² of cisplatin) is followed by two weekly applications of MRI-assisted pulsed dose rate IGABT, prescribing a nominal dose of 18.5 Gy in 25 hourly pulses per insertion to the high risk clinical target volume (HR CTV).^{17,18,25}



FIGURE 1. Para-cervical injection of anaesthetic prior to the pre-planning insertion of the intracavitary applicator.

Accurate applicator insertion with optimal geometric distribution of eventual IS channels is a precondition for the tight control and fine-tuning of the dose distribution. The inadequacies of a sub-optimal application cannot always be compensated by treatment plan optimization. Applicator insertion geometry is typically based on clinical and MRI findings at diagnosis and clinical findings at IGABT.^{1,22} Planning MRI is performed only after the insertion, limiting the ability for corrections in case of suboptimal implantation. In such cases, the inadequacies from the first procedure should be taken into account during eventual subsequent insertion(s), improving the cumulative dosimetric outcome.

Attempting to increase the likelihood of optimal implant geometry already at the first application, we developed an MRI-assisted pre-planning protocol, based on applicator insertion in paracervical anaesthesia (PCA). Our preliminary results on the efficacy of this technique were published recently.²⁵ We report on the final results of our study here. Our primary objective was to quantify the geometric and dosimetric variation between the pre-planned and actual application and to assess feasibility of the pre-planning approach. Our secondary objective was to quantify the dosimetric benefit of the MR IGABT when compared with conventional point A-based treatment planning.

Patients and methods

The study protocol was approved by the institutional and national ethics committees, multidisciplinary tumour board and the cost analysis office of the Institute of Oncology Ljubljana.

Patients and tumours

Twenty consecutive patients with histologically verified inoperable cervix cancer, treated with curative intent, were enrolled after signing an informed consent. One patient was excluded from analysis due to non-compliance to the study protocol. In the second patient, pre-planning and inclusion in the dosimetric analysis was precluded by vasovagal syncope during PCA injection. Eighteen patients were eligible for the dosimetric analysis.

Pre-planning applicator insertion in paracervical anaesthesia

Preplanning insertion was performed in sterile conditions immediately after or in the last week of EBRT. On the morning of the insertion, a laxative suppository and an anxiolytic were applied and one hour intravenous analgesic/antiemetic infusion of tramadol, metamizole and metoclopramide was administered. With the patient in lithotomy position, 10% lidocaine spray was applied topically on the vaginal mucosa and 3 mL of 2% lidocaine injected bilaterally in the paracervical region to achieve PCA (Figure 1). After 5 minutes, the anterior lip of the portio was grabbed with a tenaculum and cervical canal dilated. Following dilatation, a plastic tandem & ring applicator (©2005–2009 Varian Medical Systems, Inc., Palo Alto, USA) was inserted and vaginal packing performed. During the procedure, pain was reported by the patient, using the visual analogue scale (VAS) from 0 (no pain) to 10 (most intense pain). Peak pain score was recorded. In case of persistent pain of > 2 on VAS, additional 2 mL of 2% lidocaine was injected paracervically. In case of pain of 4 on VAS, the procedure was terminated. Patient's vital functions were monitored and anaesthesiologist was available on call. Procedure time, from placing the patient into the lithotomy position to the applicator removal was recorded.

Pre-planning MRI and applicator removal

Pre-planning MRI was performed after applicator insertion at a 1.5 Tesla scanner (Siemens Magnetom

Avanto, ©2006 Siemens AG, Erlangen, Germany), using a pelvic surface phased-array coil. 2D T2w fast spin echo images (slice thickness 3 mm, interslice gap 0.9 mm, in-plane pixel size 0.6×0.6 mm, field of view 20×20 cm, matrix size 288×320 , echo time 98 ms, repetition time 5700 ms, flip angle 150° , acquisition time 3 minutes), were obtained in para-transverse (perpendicular to cervical canal) plane. In addition, a 3D T2 weighted sequence with high sampling efficiency was performed (176 slices, isotropic voxel size of 1 mm, field of view 40×40 cm, matrix size 384×386 , echo time 131 ms, repetition time 1500 ms, flip angle 150 degrees, acquisition time 7 minutes). Both data sets were transferred to the treatment planning system (Brachyvision, version 8.5, Copyright ©1996-2008 Varian Medical Systems Inc., Palo Alto, USA) and co-registered, using shared DICOM coordinates. Registration was corrected manually when indicated. From the 3D data-set, para-transverse, para-coronal and parasagittal reconstructions were resampled within the treatment planning system to match the slice thickness and acquisition planes of the 2D images.²⁶ The applicator was removed after imaging and the patient discharged.

Contouring and creation of pre-plan

HR CTV and the OAR (bladder, rectum and sigmoid colon) were delineated and the applicator reconstructed. The preplanning process started by using the standard IC loading pattern. A nominal dose of 18.5 Gy in 25 hourly pulses was specified at point A. For treatment plan optimization and reporting, biologically equivalent doses (EQD2; linear-quadratic model; $\alpha/\beta = 10$ Gy for the tumour and 3 Gy for the OAR; repair half-time = 1.5 hours), were used. After evaluating the dose distribution and DVH parameters, the standard IC pre-plan was modified, aiming to meet our dose constraints for the OAR (D2cc - minimal EQD2 to the most exposed 2cm^3 of the rectum, sigmoid colon and bladder below 12.5 Gy, 12.5 Gy and 15 Gy, respectively). When HR CTV was adequately covered following this modifications ($D_{90} >$ prescribed dose, $V_{100} > 90\text{--}95\%$), no further action was taken and the preplan was considered optimized. When indicated, virtual interstitial channels were placed at optimal radial angles and optimal insertion depths in the parametria to improve the HR CTV coverage and/or OAR avoidance (Figure 2). The degrees of freedom, offered by our modified IC applicator, in which the ring serves as a template for guidance of parametrial needles, were respected.^{11,12,25} The pre-

planned radial angles of insertion positions and insertion depths were recorded (Figure 2). Virtual needles were loaded in the treatment planning system, keeping the source dwell-times below 20% of the tandem dwell-times and aiming to achieve an optimized pre-plan (adequate HR CTV coverage, while respecting the OAR dose constraints). The DVH parameters for the HR CTV (V_{100} , D_{100} , D_{90}) and OAR (D_{2cc}) of the standard and optimized pre-plan were recorded.

Actual BT application, imaging and treatment planning

One week after the preplanning, first actual BT application was performed in subarachnoidal anaesthesia. In addition to the IC tandem-ring applicator, IS needles were inserted through the modified ring, taking the preplanned geometry (needle insertion positions and depths) into account. T2 weighted FSE MR images in para-transverse, para-coronal and para-sagittal orientation were obtained in addition to the 3D isotropic MRI with high sampling efficiency. Contouring, applicator reconstruction and treatment planning was carried out. The actual radial angles of needle insertion positions and depths were recorded and compared with the preplanned values (Figure 2). The Standard and optimized actual treatment plans were created and the respective DVH parameters for the HR CTV and OAR compared. The optimization index (OIN) was defined as the ratio between the D_{90} to the HR CTV and the D_{2cc} to the most irradiated OAR. The OINs of the standard and optimized plans were compared. Second BT application was not the subject of this study.

Statistical analysis

The non-parametric Wilcoxon signed-rank test for matched pairs was used to compare the treatment plan parameters. The p-value of 0.05 was used as the limit of statistical significance. Statistical program SPSS was used for statistical analysis.

Results

The patient who developed syncope following PCA injection recovered spontaneously, rapidly and without complications. However, the pre-planning procedure was terminated and the patient was ineligible for dosimetric analysis. FIGO stage distribution of the included patients was as follows: IB1:

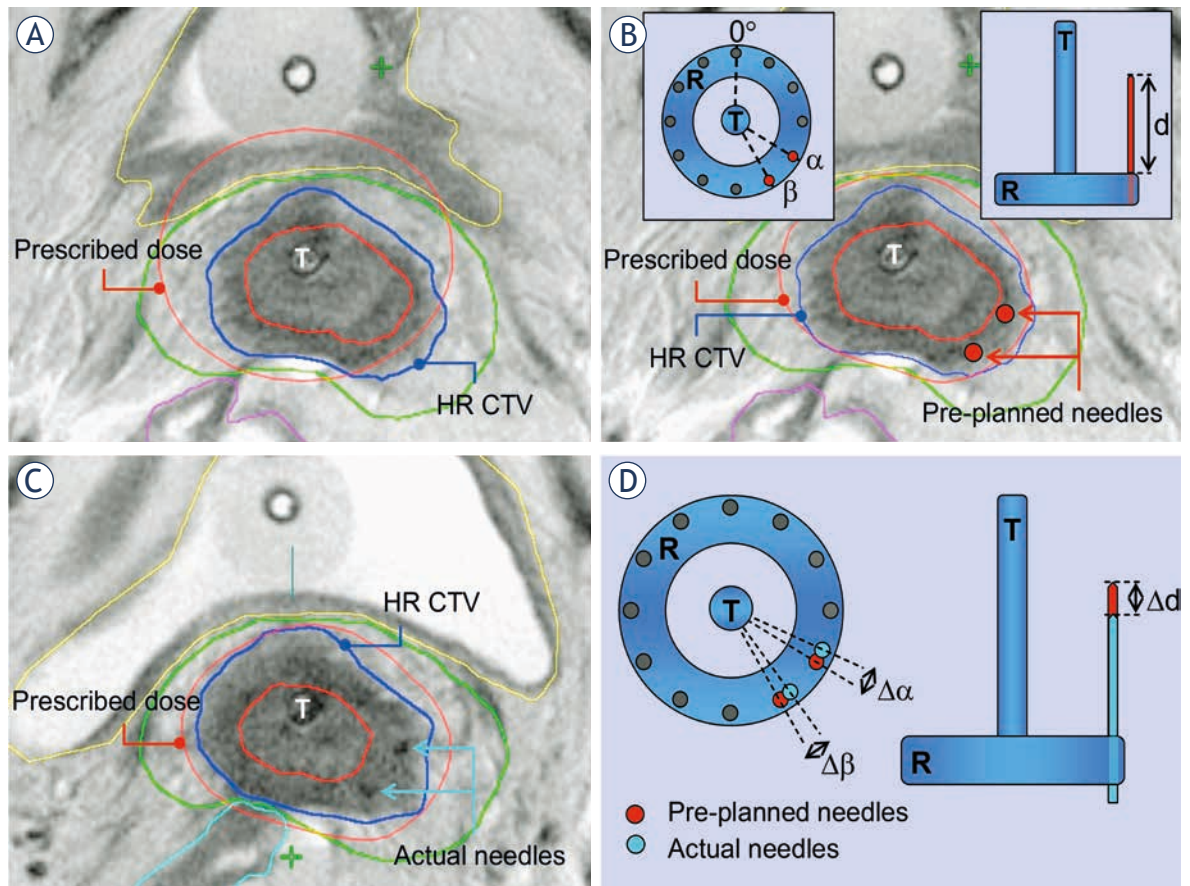


FIGURE 2. T2-weighted post-insertion pelvic MRI in para-transverse (perpendicular to cervical canal) orientation at pre-planning (A, B) and actual (C) brachytherapy. Principal steps of the pre-planning process are outlined. (A) Pre-planning MRI, obtained after insertion of the intracavitary tandem/ring applicator in para-cervical anaesthesia. Prescribed isodose of a standard intracavitary treatment plan with dose prescription at point A is shown. There is suboptimal coverage of the high risk clinical target volume (HR CTV) with the prescribed isodose at the left posterolateral aspect in this slice. In addition, the prescribed isodose extends to the bladder, exceeding our departmental dose constraints for this organ. Reducing the tandem dwell-weight in order to spare the posterior bladder wall would further compromise the coverage of the left part of the HR CTV due to unfavourable topography between the applicator and the patho-anatomical structures. (B) Virtual optimized intracavitary/interstitial pre-plan. After reducing the tandem dwell weight, two virtual interstitial needles (red circles) were placed at optimal positions within the target volume, respecting the degrees of freedom, offered by the ring cap template (Figure insert). Treatment plan optimization, utilizing needle dwell positions in addition to the intracavitary component, resulted in a pre-plan with a conformal dose distribution. The prescribed isodose conformally encompasses the HR CTV while the dose constraints for the bladder and other organs are respected. Radial angle of needle insertion position is defined on para-transverse MRI for a given ring diameter as the angle between the antero-posterior patient axis and the line, connecting the centre of the tandem and the needle. (C) Planning MRI, acquired at time of actual brachytherapy, following insertion of a combined intracavitary/interstitial applicator. In addition to the tandem/ring applicator, two interstitial needles were inserted through the ring template, aiming at an accurate reproduction of the pre-planned insertion angles and depths. Actual needle insertion angles and depths were recorded. Treatment plan optimization resulted in an actual dose distribution, comparable to the pre-planned situation. (D) Schematic representation of assessment of the geometric deviations between the pre-planned and actual implant. For each needle, the difference between the pre-planned and actual radial angle of needle insertion and depth was calculated.

2, IIB: 13, IIIB: 2 and IVA: 1 patient. The median HR CTV size was 26 cm³ (range: 15.1 – 68.3 cm³).

Subjective pain sensation during the pre-planning insertion in PCA was reported by all 18 patients included in the dosimetric study. Eight (44.5%) patients reported a peak VAS score of 0 (no pain); 6 (33.5%) a peak VAS score of 1; and 4 (22%) patients a peak VAS score of 3. The median dura-

tion of the pre-planning procedure was 69 minutes (range 55 to 90 minutes).

At first BT application, a total of 55 IS needles were inserted in 18 patients (median: 3.2 needles per patient; range: 0–9) through the ring template, respecting the pre-planned specifications. The differences between the pre-planned and actual geometric radial angle of insertion and insertion depth

TABLE 1. Needle geometry and DVH parameters of the pre-planned and actual optimized treatment plans and the individual differences between them. Biologically equivalent doses are given (linear quadratic model, $\alpha/\beta=10$ Gy for the HR CTV and 3 Gy for the organs at risk, half time of sublethal damage repair = 1.5 h). The differences between the pre-planned and actual geometric and dosimetric parameters were statistically non-significant. HR CTV = High Risk Clinical Target Volume

	Pre-planned median (range)	Actual median (range)	Difference median (range)
Needle geometry			
Depth (mm)	23 (10 – 49)	23 (7 – 47)	2 (0 – 10)
Radial angle (°)	150 (30 – 330)	145 (30-334)	4 (0-30)
HR CTV			
D90 (Gy)	23.4 (20.0 – 27.1)	23.4 (20.1 – 30.7)	1.0 (0.0 – 3.6)
D100 (Gy)	13.2 (7.1 – 17.8)	14.9 (8.6 – 18.3)	1.9 (0.2 – 5.8)
V100 (%)	96.2 (90.0 – 99.8)	97.9 (90.0 – 100)	1.4 (0.1 – 9.2)
Organs at risk			
D2cc bladder (Gy)	13.5 (9.1 – 16.6)	12.9 (7.4 – 15.9)	0.7 (0.0 – 7.3)
D2cc rectum (Gy)	9.5 (4.9 – 15.8)	8.1 (4.2 – 11.8)	1.4 (0.3 – 11.5)
D2cc sigmoid (Gy)	10.1 (4.6 – 13.4)	9.2 (3.0 – 12.8)	1.2 (0.0 – 5.5)

were statistically non-significant (Table 1). All actual needles were positioned inside the HR CTV and outside the OAR. The differences between the pre-planned and actual optimized DVH parameter values were not significant (Table 1).

All patients benefited from 3D MRI-guided treatment plan optimization (Table 2, Figure 3). In standard point A-based plans, the dose constraints for the D2cc to the most irradiated OAR and the D90 to the HR CTV were met in none of the 18 patients. In optimized treatment plans, both constraints were met in 16 (89%) cases. The OIN was above 1.0 in 8 (44%) and 18 (100%) patients for the standard and optimized plans, respectively. Median OIN was significantly higher for the optimized (1.3; range: 1.0–1.8), when compared with standard plans (1.0; range: 0.7–1.9) (Table 2).

Discussion

Several reports have demonstrated favourable results of cervix cancer IGABT when compared to conventional x-ray based method.^{13-18,26} In our experience, one of the most challenging aspects of IGABT remains the decision on the optimal geometry of insertion of the applicators, which is a precondition for treatment success. The possibility to compensate for geometric inadequacies of the insertion by treatment plan optimization is limited. While there is paucity of published reports on the actual gynaecological BT pre-planning, several ap-

TABLE 2. DVH parameter values for the high risk clinical target volume (HR CTV) and the most exposed organ at risk. OIN = optimization index (D90 for the HR CTV / D2cc of the OAR max).

	Standard plan [median (range)]	Optimized plan [median (range)]
HR CTV		
D90 (Gy)	27.9 (15.9 – 47.0)	23.4 (20.1 – 30.7)
D100 (Gy)	15.0 (7.2 – 25.7)	14.9 (8.6 – 18.3)
V100 (%)	99.0 (77.3 – 100.0)	97.9 (90.0 – 100)
OAR_{max}		
D2cc (Gy)	19.0 (8.2 – 34.4)	12.7 (9.0 – 15.9)
OIN		
	1.0 (0.7 – 1.9)	1.3 (1.0 – 1.8)

proaches to image guidance have been suggested to increase the chance of optimal implant geometry.^{25,27}

US-guidance has proven helpful in achieving good position of the intrauterine tandem and is a promising method in interstitial gynaecological BT.²⁸⁻³³ However; adaptations of US devices and development of an US-based target concept are required before this approach can be fully exploited in practice. Currently, MRI remains the gold standard imaging modality for cervix cancer IGABT. Recommendations on different aspects of its implementation, including a target volume concept, were published.^{22-24,34} Accordingly, various methods of MRI guided applicator insertion

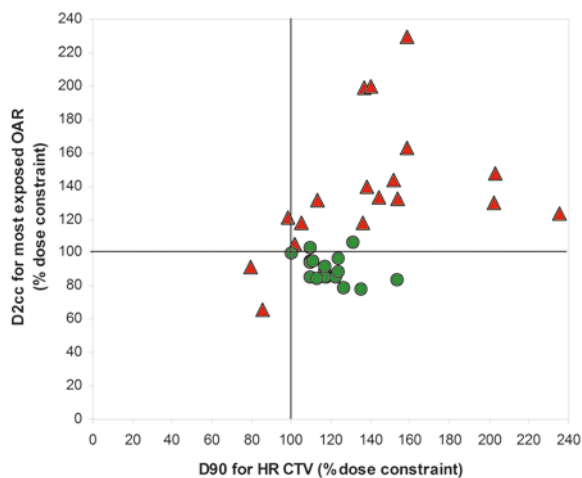


FIGURE 3. D2cc to the organ at risk (OAR) receiving the highest dose and D90 to the high risk clinical target volume (HR CTV) in standard (red triangles) and optimized (green circles) plans for all patients. The doses are expressed in percentage of respective dose constraints. The lower right quadrant includes the patients in whom both the OAR and the HR CTV dose constraints were respected.

have been proposed. One approach, which is utilized at author's institutions in selected cases, consists of temporal interruptions of the application in order to acquire MRI for verification and off-line guidance. This, however, results in a considerable prolongation of the application time. Specialized MRI devices have been developed to allow for real-time imaging of the insertion and enable guidance in BT of different tumour sites.³⁵⁻³⁹ In one study, intra-operative MRI-guided needle insertion for BT of vaginal recurrence in endometrial cancer demonstrated high accuracy of needle placement and limited toxicity.³⁵ However, access to MRI in the operating theatre is a pre-requisite for this approach, limiting it to a few specialized centres. Alternatively, an additional MRI before BT application may identify the extent of residual disease and enable to plan an optimal insertion. Translation of pre-insertion MRI findings to the post-insertion situation is hindered by topographical changes in the pelvis, induced by the applicator insertion at BT. Ideally; the pre-planning MRI should therefore be obtained with the IC applicator in place. Due to its risks and infrastructural requirements, the need for general or spinal anaesthesia at pre-planning insertion is an important limitation to such an approach.²⁷ The technique described in our study mitigates this limitation by using PCA for pain control.

PCA is used for cervical dilatation in various obstetric and gynaecological procedures.

Nevertheless, the data on its effectiveness and safety are conflicting. A recent review concluded that PCA is ineffective in achieving pain control for women undergoing uterine interventions.⁴⁰ However, in this review; various procedures including suction termination of pregnancy and bimanual removal of placenta were assessed. Therefore, its negative conclusion may not be applicable to cervical dilatation at BT. To our knowledge, there are no studies examining the role of PCA in the field of BT. A recent meta-analysis, comparing effectiveness of various local anaesthetic techniques used during outpatient hysteroscopy (which may be more comparable to uterine insertion of BT applicator), concluded that PCA is the best method of pain control in this setting.⁴¹ In our study, 14 (78%) patients reported a peak VAS score of 0 or 1 during the pre-planning procedure. Our favourable results are in line with conclusions of the meta-analysis. In our protocol, mild sedation was instituted prior to the procedure and local anaesthetic applied topically to ameliorate pain during PCA injection, manipulation with specula and vaginal gauze packing. In addition, intravenous infusion of analgesics was given to reduce pain due to vaginal packing and applicator removal. We can assume that these additional measures had an important effect on the overall favourable level of pain control in our study.

With exception of one case of syncope after PCA injection (resolving spontaneously without consequences, but leading to procedure termination and exclusion from dosimetric analysis), we observed no adverse events of the pre-planning procedure. About 20% of women undergoing outpatient dilatation of cervical canal are reported to experience vasovagal reactions.⁴² It has to be noted that similar symptoms might arise from intravasation of the local anaesthetic. Meta-analysis of the studies on PCA in hysteroscopy failed to conclude on potential harms of the PCA, since most of the analysed studies did not explicitly report on the adverse events.⁴² According to our experience, IC applicator insertion under PCA can be regarded a safe procedure. This pain control technique may therefore represent a strategy to improve patient care in centres where general or spinal anaesthesia is not readily accessible. Moreover, PCA-based BT application has been used with success at our institution in patients with medical contraindications for anaesthesia, not only in cervical, but also in endometrial cancer, where co-morbidity often poses significant challenge to the medical team. It has to be noted, however, that we only assessed its

effectiveness in insertion of the IC applicator, not the IS needles.

In our study, an excellent reproduction of the pre-planned implant geometry was achieved at first actual BT application, resulting in clinically and statistically non-significant dosimetric differences between the pre-plan and actual BT plan (Table 1). At actual BT, the dose constraints for the HR CTV could be respected in all cases, while they were only slightly violated for the OAR in 2 cases (2% and 6% above the constraint for the sigmoid colon and bladder, respectively) (Figure 3). As far as the benefit from pre-planning is concerned, our cohort could be divided into 2 groups of patients. In 4 (22%) patients (median HR CTV: 20 cm³, range: 15.1 – 26.1 cm³), the IS needles were not used. In these cases, the DVH constraints could be met by adapting the standard IC plan and the dosimetric benefit of pre-planning was small. In the remaining 14 patients (median HR CTV: 28.8 cm³, range: 17.0 – 68.3 cm³), the IS needles were used in addition to the IC applicator and the dosimetric benefit of pre-planning was demonstrated. To summarize, the pre-planning procedure, as described here, may be advantageous in cases with bad tumour response to EBRT and/or where unfavourable topography of residual pathological tissues at time of BT can be expected. In small and/or well responding tumours pre-planning was not beneficial.

Limitations of our pre-planning approach include the need for an additional MRI study, staff requirements and administration of additional medications. Therefore, it may be limited to centres with high resources. However, according to our experience, the pre-planning reduced the time needed for the actual BT application and improved the operator confidence and patient compliance during the procedure. In addition, the need for iterative imaging and implant corrections or even removing the applicator due to a potentially sub-optimal geometry could be avoided in all cases. By omitting multi-planar MRI and employing 3D MRI for pre-planning, total image acquisition time was shortened for approximately 50%, when compared to our standard MRI study at time of actual BT.⁴³ In fact, due to the possibility to achieve an optimal implant already at the first application, the described procedure may serve as a basis for accomplishment of BT in a reduced number of optimized insertions, reducing the total MRI-time and costs. The clinical impact of favourable dosimetric results of IGABT in our patient population remains to be quantified and compared with our retrospective series on conventional 2D BT.⁴⁴

Conclusions

MRI-assisted cervix cancer BT pre-planning, based on applicator insertion in PCA is well tolerated, safe and fast. In cases with bad tumour response to EBRT and/or unfavourable target volume topography at time of BT it enables determination of an optimal distribution of the interstitial applicator channels. At actual BT implantation, an excellent reproduction of the pre-planned insertion geometry and DVH outcome can be achieved. MR assisted IGABT improves dosimetric outcome when compared with conventional dose prescription methods. PCA may be an effective method of pain control in a setting with limited resources and in patients with medical contraindications for general or spinal anaesthesia, requiring cervico-uterine BT.

Acknowledgments

The authors thank Mark R. Vogel, MA, and David J. Howell, PhD, San Francisco, CA, for their contributions to the writing and editing of the manuscript.

References

- Haie-Meder C, Pötter R, Van Limbergen E, Briot E, De Brabandere M, Dimopoulos J, et al. Recommendations from Gynaecological (GYN) GEC-ESTRO Working Group (I): concepts and terms in 3D image based 3D treatment planning in cervix cancer brachytherapy with emphasis on MRI assessment of GTV and CTV. *Radiother Oncol* 2005; **74**: 235-45.
- Dimopoulos JCA, Schard G, Berger D, Lang S, Goldner G, Helbich T, et al. Systematic evaluation of MRI findings in different stages of treatment of cervical cancer: potential of MRI on delineation of target patho-anatomical structures and organs at risk. *Int J Radiat Oncol Biol Phys* 2006; **64**: 1380-8.
- Boss EA, Barentsz JO, Massuger LF, Boonstra H. The role of MRI imaging in invasive cervical carcinoma. *Eur Radiol* 2000; **10**: 256-70.
- Subak LL, Hricak H, Powell CB, Azizi L, Stern JL. Cervical carcinoma: computed tomography and magnetic resonance imaging for preoperative staging. *Obstet Gynecol* 1995; **86**:3-50.
- Mitchell DG, Snyder B, Coakley F, Reinhold C, Thomas G, Amendola M, et al. Early invasive cervical cancer: tumor delineation by magnetic resonance imaging, computed tomography, and clinical examination, verified by pathologic results, in the ACRIN 6651/GOG 183 Intergroup Study. *J Clin Oncol* 2006; **24**: 5687-94.
- Oszarlak O, Tjalma W, Scheppens E, Corthouts B, Op de Beeck B, Van Marck E, et al. The correlation of preoperative CT, MR imaging, and clinical staging (FIGO) with histopathology findings in primary cervical carcinoma. *Eur Radiol* 2003; **13**: 338-45.
- Hricak H, Gatsonsis C, Coakley FV, Snyder B, Reinhold C, Schwartz LH, et al. Early invasive cervical cancer: CT and MR imaging in preoperative evaluation – ACRIN/GOG comparative study of diagnostic performance and interobserver variability. *Radiology* 2007; **245**: 491-8.
- Jung DC, Ju W, Choi HJ, Kang S, Park S, Yoo CW, et al. The validity of tumour diameter assessed by magnetic resonance imaging and gross specimen with regard to tumour volume in cervical cancer patients. *Eur J Cancer* 2008; **44**: 1524-8.

9. Bipat S, Glas AS, van der Velden J, Zwinderman AH, Bossuyt PM, Stoker J. Computed tomography and magnetic resonance imaging in staging of uterine cervical carcinoma: a systemic review. *Gynecol Oncol* 2003; **91**: 59-66.
10. Dimopoulos JCA, Schirl G, Baldinger A, Helbich TH, Pötter R. MRI assessment of cervical cancer for adaptive radiotherapy. *Strahlenther Onkol* 2009; **185**: 282-7.
11. Kiristis C, Lang S, Dimopoulos J, Berger D, Georg D, Pötter R. The Vienna applicator for combined intracavitary and interstitial brachytherapy of cervical cancer: design, application, treatment planning, and dosimetric results. *Int J Radiat Oncol Biol Phys* 2006; **65**: 624-30.
12. Dimopoulos JCA, Kiristis C, Petric P, Georg P, Lang S, Berger D, et al. The Vienna applicator for combined intracavitary and interstitial brachytherapy of cervical cancer: clinical feasibility and preliminary results. *Int J Radiat Oncol Biol Phys* 2006; **66**: 83-90.
13. Pötter R, Dimopoulos J, Georg P, Lang S, Waldhäusl C, Wachter-Gerstner N, et al. Clinical impact of MRI assisted dose volume adaptation and dose escalation in brachytherapy of locally advanced cervix cancer. *Radiother Oncol* 2007; **83**: 148-55.
14. Haie-Meder C. MRI-based brachytherapy (BT) in the treatment of cervical cancer: experience of the Institute Gustave-Roussy. *Radiother Oncol* 2007; **83**(Suppl 1): S11-12.
15. Lindegaard JC, Tandercup K, Nielsen SK, Haack S, Gelineck J. MRI-guided 3D optimization significantly improves DVH parameters of pulsed-dose-rate brachytherapy in locally advanced cervical cancer. *Int J Radiat Oncol Biol Phys* 2008; **71**: 756-64.
16. De Brabandere M, Mousa AG, Nulens A, Swinnen A, Van Limbergen E. Potential of dose optimization in MRI-based PDR brachytherapy of cervix carcinoma. *Radiother Oncol* 2008; **88**: 217-26.
17. Petrič, P, Hudej R, Šegedin B, Zobec Logar HB. MRI assisted treatment planning improves the DVH parameters in cervix cancer brachytherapy. *Radiother Oncol* 2011; **99**: 264-265.
18. Hudej R, Petric P, Burger J. Standard versus 3D optimized MRI-based planning for uterine cervix cancer brachyradiotherapy-the Ljubljana experience. In: Jarm T, Kramar P, Županič A, editors. International Federation for Medical and Biological Engineering proceedings. 11th Mediterranean Conference on Medical and Biological Engineering and Computing 2007, 26-30 June, 2007, Ljubljana, Slovenia. New York: Springer; 2007(16). p. 875-8.
19. Jürnenliemk-Schulz IM, Tersteeg RJ, Roesink JM, Bijmolt S, Nomden CN, Moerland MA, et al. MRI-guided treatment-planning optimisation in intracavitary or combined intracavitary/interstitial PDR brachytherapy using tandem ovoid applicators in locally advanced cervical cancer. *Radiother Oncol* 2009; **93**: 322-30.
20. Petrič P, Hudej R, Rogelj P, Lindegaard J, Tanderup K, Kirisits C, et al. Frequency-distribution mapping of HR CTV in cervix cancer: possibilities and limitations of existent and prototype applicators. *Radiother Oncol* 2010; **96**: 70.
21. Kuipers T, Hoekstra CJ, van Riet A, Mak AC, Vonk EJ, Elders LH. HDR brachytherapy applied to cervical carcinoma with moderate lateral expansion: modified principles of treatment. *Radiother Oncol* 2001; **58**: 25-30.
22. Pötter R, Haie-Meder C, Van Limbergen E, Barillot I, De Brabandere M, Dimopoulos J, et al. Recommendations from gynaecological (GYN) GEC-ESTRO Working Group: (II): concepts and terms of 3D imaging, radiation physics, radiobiology, and 3D dose volume parameters. *Radiother Oncol* 2006; **78**: 67-77.
23. Hellebust TP, Kirisits C, Berger D, Pérez-Calatayud J, De Brabandere M, De Leeuw A, et al. Recommendations from Gynaecological (GYN) GEC-ESTRO Working Group: Considerations and pitfalls in commissioning and applicator reconstruction in 3D image-based treatment planning of cervix cancer brachytherapy. *Radiother Oncol* 2010; **96**: 153-60.
24. Dimopoulos JC, Petrow P, Tanderup K, Petric P, Berger D, Kirisits C, et al. Recommendations from Gynaecological (GYN) GEC-ESTRO Working Group (IV): Basic principles and parameters for MRI imaging within the frame of image based adaptive cervix cancer brachytherapy. *Radiother Oncol* 2012; **103**: 113-22.
25. Petric P, Hudej R, Music M. MRI assisted cervix cancer brachytherapy pre-planning, based on insertion of the applicator in para-cervical anaesthesia: preliminary results of a prospective study. *J Contemp Brachyther* 2009; **1**: 163-9.
26. Gerbaulet A, Pötter R, Haie-Meder C. Cervix cancer. In: Gerbaulet A, Pötter R, Mazon JJ, Meertens H, Van Limbergen E, eds. *The GEC ESTRO Handbook of Brachytherapy*. Brussels: European Society of Therapeutic Radiology and Oncology; 2002. p. 301-63.
27. Fokdal L, Tanderup K, Hokland SB, Røhl L, Pedersen EM, Nielsen SK, et al. Clinical feasibility of combined intracavitary/interstitial brachytherapy in locally advanced cervical cancer employing MRI with a tandem/ring applicator in situ and virtual preplanning of the interstitial component. *Radiother Oncol* 2013; **107**: 63-8.
28. Granai CO, Allee P, Doherty F, Madoc-Jones H, Curry SL. Ultrasound used for assessing the in situ position of intrauterine tandems. *Gynecol Oncol* 1984; **18**: 334-8.
29. Sahinler I, Cepni I, Colpan D, Cepni K, Koksul S, Koca A, et al. Tandem application with transvaginal ultrasound guidance. *Int J Radiat Oncol Biol Phys* 2004; **59**: 190-6.
30. Mayr NA, Montebello JF, Sorosky JJ, Daugherty JS, Nguyen DL, Mardirossian G, et al. Brachytherapy management of the retroverted uterus using ultrasound-guided implant applicator placement. *Brachytherapy* 2005; **4**: 24-9.
31. Davidson MT, Yuen J, D'Souza D, Radwan JS, Hammond JA, Batchelar DL. Optimization of high-dose-rate cervix brachytherapy applicator placement: the benefits of intraoperative ultrasound guidance. *Brachytherapy* 2008; **7**: 248-53.
32. Stock RG, Chan K, Terk M, Dewyngaert JK, Stone NN, Dottino P. A new technique for performing Syed-Neblett template interstitial implants for gynecologic malignancies using transrectal-ultrasound guidance. *Int J Radiat Oncol Biol Phys* 1997; **37**: 819-25.
33. Weitmann HD, Knocke TH, Waldhäusl C, Pötter R. Ultrasound-guided interstitial Brachytherapy in the treatment of advanced vaginal recurrences from cervical and endometrial carcinoma. *Strahlenther Onkol* 2006; **182**: 86-95.
34. Petric P, Pötter R, Van Limbergen E, Haie Meder C. Adaptive contouring of the target volume and organs at risk. In: Viswanathan AN, editor. *Gynecologic radiation therapy: novel approaches to image-guidance and management*. Heidelberg: Springer cop.; 2011. p. 99-118.
35. Viswanathan AN, Cormack R, Holloway CL, Tanaka C, O'Farrell D, Devlin PM, et al. Magnetic resonance-guided interstitial therapy for vaginal recurrence of endometrial cancer. *Int J Radiat Oncol Biol Phys* 2006; **66**: 91-9.
36. D'Amico AV, Cormack R, Tempny CM, Kumar S, Topulos G, Kooy HM, et al. Real-time magnetic resonance image-guided interstitial brachytherapy in the treatment of select patients with clinically localized prostate cancer. *Int J Radiat Oncol Biol Phys* 1998; **42**: 507-15.
37. Menard C, Susil RC, Choyke P, Gustafson GS, Kammerer W, Ning H, et al. MRI-guided HDR prostate brachytherapy in standard 1.5T scanner. *Int J Radiat Oncol Biol Phys* 2004; **59**: 1414-23.
38. Albert M, Tempny CM, Schultz D, Chen MH, Cormack RA, Kumar S, et al. Late genitourinary and gastrointestinal toxicity after magnetic resonance image-guided prostate brachytherapy with or without neoadjuvant external beam radiation therapy. *Cancer* 2003; **98**: 949-54.
39. Kettenbach J, Pokrajac B, Schamp S, Fellner C, Schmid R, Gustorff B, et al. MRI-assisted brachytherapy of nonresectable liver metastases. Preliminary technical and clinical experiences. *Radiologe* 2001; **41**: 56-63.
40. Tangsirawatthana T, Sangkomkham US, Lumbiganon P, Loopaiboon M. Paracervical local anaesthesia for cervical dilatation and uterine intervention. Cochrane Database of Systematic Reviews 2013, Issue 9. Art. No.: CD005056. DOI: 10.1002/14651858.CD005056.
41. Cooper NA, Khan KS, Clark TJ. Local anaesthesia for pain control during outpatient hysteroscopy: systematic review and meta-analysis. *Br Med J* 2010; **340**: c1130.
42. Finikiotis G. Side-effects and complications of outpatient hysteroscopy. *Aust N Z J Obstet Gynaecol* 1993; **33**: 61-2.
43. Petric P, Hudej R, Rogelj P, Blas M, Segedin B, Logar HB, et al. Comparison of 3D MRI with high sampling efficiency and 2D multiplanar MRI for contouring in cervix cancer brachytherapy. *Radiol Oncol* 2012; **46**: 242-51.
44. Zobec Logar HL, Segedin B, Hudej R, Petric P. Definitive radiotherapy for uterine cervix cancer: long term results for patients treated in the period from 1998 till 2002 at the Institute of Oncology Ljubljana. *Radiol Oncol* 2013; **47**: 280-8.

Olfaction and gustation abilities after a total laryngectomy

Gordana Mumovic¹ and Irena Hocevar-Boltezar²

¹ University Hospital for Ear, Nose and Throat Diseases, Novi Sad, Serbia

² Department of Otorhinolaryngology and Cervicofacial Surgery, University Medical Centre, Ljubljana, Slovenia

Radiol Oncol 2014; 48(3): 301-306.

Received: 22 June 2013
Accepted: 13 August 2013

Correspondence to: Prof. Irena Hocevar-Boltežar M.D., Ph.D., Department of Otorhinolaryngology and Cervicofacial Surgery, University Medical Centre, Zaloška 2, 1000 Ljubljana, Slovenia. Phone: +386 41 958336; Fax: +386 1 5224815; E-mail: boltezar.irena@gmail.com

Disclosure: No potential conflicts of interest were disclosed.

Background. A laryngectomy affects many of a patient's functions. Besides speech and respiratory-tract problems, olfaction and gustation problems can also have an influence on the quality of life. The aim of this study was to find out how often various nasal problems and decreased gustation appear after a laryngectomy.

Patients and methods. One hundred and five laryngectomized patients (9 women, 96 men, aged 45-88 years), treated in two tertiary centers, were included in the study. They completed a questionnaire about various nasal problems, olfactory and gustatory capabilities, possible allergies and irritants in their environment, and the impact of the nasal and gustation problems on their quality of life.

Results. Olfaction was impaired in 51.4%, and was even not possible in 30.5%, of patients. Decreased gustation abilities were reported in 26.7%, and dysgeusia in 11.4%, of patients. Almost 21% of patients were bothered by an impaired gustatory ability and 50.5% of patients were affected by their loss of olfaction. Frequent nasal discharge was reported in 20%, frequent sneezing in 58.1%, and nasal itching in 33.3% of the laryngectomized patients. There were no correlations between the age and the olfaction and gustation abilities and between the allergy and the nasal symptoms, whereas the correlation between olfaction and gustation appeared significant ($p=0.025$).

Conclusions. Various nasal and gustatory problems were reported in more than 80% of laryngectomized patients. The olfaction and gustation abilities are connected and have a substantial impact on the quality of life. Like in the case of speech, the rehabilitation of olfaction is also necessary in all laryngectomized patients and must take place soon after the completion of the treatment.

Key words: laryngectomy; olfaction; gustation; questionnaire; quality of life

Introduction

Laryngectomy is a surgical procedure that is usually reserved for patients with advanced-stage laryngeal or hypopharyngeal carcinoma. It is used when organ-preservation treatment programs are not possible or for the salvage of failure after a non-surgical treatment.¹ The procedure can cure the patient, but it can also affect many of his/her functions. Respiration and speech are altered forever; swallowing needs to be re-learned; smell and taste are attenuated; lifting heavy objects, straining and coughing are compromised. Therefore, there are numerous potential problems (emotional, psycho-

logical, physical, economic, social, and communicative) that can affect the quality of a patient's life.²⁻⁴

There are a large number of papers on speech and respiratory rehabilitation after a laryngectomy. However, laryngectomized patients have already reported that they do not get enough information about the potential problems with their ability to smell and taste and the consequent changes with respect to eating after the surgical treatment.⁵ However, in the past two decades, olfaction and gustation problems in laryngectomees have begun to receive more attention.

After a laryngectomy, the nose and mouth are disconnected from the lower respiratory tract,

which results in a loss of smell. According to a systematic review of the literature dealing with the functions of smell and taste after a laryngectomy, there is a consensus that the inability to make air flow through the nose to reach the olfactory epithelium is the main reason for the deterioration of these functions.⁶ In addition, some authors reported changes in the nasal mucosa and olfactory system that can also affect the ability to smell in laryngectomized patients. Various degrees of neuroepithelial degeneration and decreased proportion of mucus-producing cells were described.^{7,8} Other authors reported atrophic nasal mucosa, but normal olfactory mucosa, in the majority of laryngectomized patients.⁹

In a canine model, the olfactory mucosa showed involution after the simulation of a laryngectomy. The changes were supposed to be caused not only by the cessation of the air flow through the olfactory groove, but also by a nonfunctioning connection between the vagal laryngeal innervation and the olfactory cortex.¹⁰

Veyseller *et al.* performed magnetic resonance imaging in laryngectomees and in subjects with a normal olfactory function, with smaller olfactory bulb volumes found in the former group. However, it is not completely clear whether the lack of sensorial stimulation from the olfactory neuroepithelium in laryngectomized patients and reduced smelling abilities are the only reasons for the decreased size of the olfactory bulb.¹¹

In the past two decades there were an increasing number of studies reporting on olfaction and gustation problems after a laryngectomy. Hyposmia or anosmia was reported to be experienced by 35–78% of patients.^{12–15} Gustation was found to be less disturbed after a laryngectomy than odor perception, *i.e.*, in 15% of patients after a laryngectomy.¹² An interaction between olfaction and gustation was also detected^{12,13}, but only a few studies report on other nasal problems. *e.g.*, a frequent nasal discharge.¹²

The aim of this study was to find out how often various nasal problems and decreased gustation appear in laryngectomized patients; how these problems influence the quality of their lives; and what are the risk factors for the various affected functions.

Patients and methods

One hundred and five patients who underwent a laryngectomy for advanced laryngeal or hypopharyngeal cancer in two tertiary centers

(University Hospital for Ear, Nose and Throat Diseases, Novi Sad, Serbia and Department of Otorhinolaryngology and Cervicofacial Surgery, University Medical Centre, Ljubljana, Slovenia) more than 6 months previously were included in the study. Sixty-two patients received postoperative or up-front radiotherapy (with the laryngectomy being a salvage procedure). The other patients were treated only surgically. There were 9 women and 96 men, aged 45–88 years (mean 61.86 years, standard deviation 9.45 years). They all completed an anonymous questionnaire about their olfactory and gustatory capabilities. They stated whether they had received radiation therapy or not in the course of the treatment. The patients were asked about various nasal problems (decreased olfaction, nasal discharge, sneezing, and nasal itching) and decreased gustation. They were asked about known allergic diseases before or after the laryngectomy (asthma, allergic rhinitis, allergic dermatitis) and about their living and working environments. They also estimated how much the nasal and gustation problems disturbed them and influenced the quality of their lives. The questionnaire was created for the purpose of the study. The data on the time interval between the laryngectomy and the inclusion of the individual patient in the study, and the details about the radiation therapy given to the patients were not collected.

Analyses were performed using the statistical package SPSS 19.0 (SPSS Corporation, USA). Descriptive analysis and 2-sided t-test, χ^2 -test, Fisher exact test were used and the strength of the correlations between the different parameters were calculated using a Spearman rank correlation. The significance level was set at 0.05.

Results

The results of the questionnaire about the various nasal symptoms, gustation problems, and factors causing nasal problems are presented in Table 1. There were answers missing in the questionnaires of some patients.

Thirty-seven (35.2%) patients declared that their decreased olfaction abilities bother them and 16 (15.2%) patients stated extreme inconvenience due to a decreased ability to smell. Nineteen (18.1%) patients stated that their decreased or altered ability to taste bothers them and three (2.9%) patients were very affected by it. Four (3.8%) patients declared that their social life was affected because of their nasal discharge.

TABLE 1. Nasal symptoms, allergic diseases (asthma, allergic rhinitis, allergic dermatitis), olfaction and gustation abilities in laryngectomized patients (N = 105)

Nasal or gustation problem		No. of patients (%)
Nasal discharge	Never	24 (22.8%)
	Sometimes	56 (53.3%)
	Often	21 (19%)
	The same as before the laryngectomy	2 (1.9%)
Nasal discharge	Not present	24 (22.9%)
	Watery	66 (62.9%)
	Mucous	14 (13.3%)
Often sneezing	No	44 (41.9%)
	Yes	61 (58.1%)
Nasal itching	No	70 (66.7%)
	Sometimes	32 (30.5%)
	Often	2 (1.9%)
Allergy	No	89 (84.8%)
	Yes	16 (15.2%)
Olfaction ability	The same as before the laryngectomy	19 (18.1%)
	Decreased	54 (51.4%)
	Completely absent	32 (30.5%)
Gustation ability	The same as before the laryngectomy	65 (61.9%)
	Decreased	28 (26.7%)
	Altered	12 (11.4%)

A decreased or altered gustation ability appeared significantly more often in the patients with decreased olfaction abilities (37 out of 86, 43%) than in the group with the normal ability to smell (3 out of 19, 15.8%) ($p = 0.035$). Among 40 patients with decreased or altered gustation abilities, there were 37 (92.5%) patients with a decreased or absent olfaction ability. A significant correlation was found between the olfaction and gestation abilities ($R_s = 0.222$, $p = 0.025$). There were no significant associations between the age and olfaction abilities ($R_s = 0.090$, $p = 0.532$) and between the age and gustation abilities ($R_s = -0.098$, $p = 0.511$).

Sixty-nine (65.7%) patients stopped working after their laryngectomy and retired. The others did not confirm the possibility of irritants at their living or working place (12, 11.4%) or did not answer the question about possible irritants in their environment (24, 22.8%). Therefore, no analysis with regard to the microclimate in their environment influencing nasal problems was possible.

Among those with known allergic diseases (asthma, allergic rhinitis, allergic dermatitis) there were significantly more patients with nasal discharge compared to the group without allergy (87.5% vs. 71.9%, $p = 0.035$). No other significant

differences were detected between these two groups (Table 2).

Discussion

The results of our study showed that the olfaction and gustatory functions were reduced in a substantial proportion of laryngectomized patients; this affected the quality of their lives. The results also revealed that other nasal problems (nasal discharge, sneezing) were common after a laryngectomy.

In the present study, more than 50% of patients reported a decreased quality of life because of the loss of an ability to smell and/or taste after the laryngectomy. Specifically, among 105 laryngectomized subjects, olfaction was impaired in 51.4% and was even not possible in 30.5% of patients. Decreased gustation abilities were reported in 26.7%, and dysgeusia in 11.4%, of patients. Almost 21% of patients were bothered by an impaired gustatory ability and 50.5% of patients were affected by their loss of olfaction.

Some authors have reported similar results. Caldas *et al.* detected fewer patients with olfaction and gustatory problems after a laryngectomy in

TABLE 2. Nasal symptoms and gustation problems in the laryngectomized patients with and without known allergic diseases (N = 105)

Nasal or gustation problem	Patients with known allergic diseases N = 16	Patients without known allergic diseases N = 89	p
Nasal discharge	14 (87.5%)	64 (71.9%)	0.035
Frequent nasal discharge	4 (25%)	17 (19.1%)	0.482
Frequent sneezing	10 (62.5%)	49 (55.1%)	0.641
Nasal itching	8 (50%)	26 (29.2%)	0.138
Decreased olfaction ability	14 (87.5%)	71 (79.8%)	0.732
Handicap because of loss of olfaction ability	8 (50%)	46 (51.7%)	1.000
Decreased or altered gustation ability	4 (25%)	35 (39.3%)	0.270
Handicap because of loss of gestation ability	2 (12.5%)	24 (26.9%)	0.753

their study than were discovered in ours. In their group of 63 laryngectomized patients, 52% of the patients reported hyposmia, while 15% reported dysgeusia. There was a significant correlation between hyposmia and dysgeusia, as was found in our study as well. All the patients with taste problems from Caldas's study also had a reduced ability to smell.⁶ In our study, 37 out of 40 patients with dysgeusia had a decreased or absent olfaction ability. A significant correlation between hyposmia and dysgeusia was also found in several other studies.^{12,13}

Smelling can be orthonasal or retronasal. In the first case the odorants come in the nasal cavity and olfactory epithelium through the nostrils. In the latter case the olfactory area is reached from the mouth through the nasopharynx and choanae.¹⁶ While orthonasal stimuli are strongly associated with sniffing and the airflow through the nostrils, retronasal stimuli are also related to the intake of food.¹⁷ Chewing induces an air stream into the oral cavity by which the olfactory organ can be stimulated backwards.¹⁸ Most of the taste sensation depends upon retronasal olfaction.¹⁹ This can be the reason for fewer gustatory than olfactory problems in our laryngectomized patients.

Smelling and gustation abilities can decrease with advancing age, although no significant correlation between the age and the olfaction abilities was found in the present study.

Other nasal problems in our laryngectomized patients were also identified. A nasal discharge was reported to appear occasionally in 53%, and frequently in 20%, of the included patients. Four patients declared that their social life was affected because of their nasal discharge. Nasal discharge in laryngectomized patients has already been re-

ported in several studies.^{12,20,21} Sesterhenn *et al.* studied the incidence of sinunasal disease in laryngectomized patients. They stated that sinunasal diseases appear in patients after laryngectomy less frequently than before surgery. In addition, they report on an increased nasal discharge that is not related to common colds, acute or chronic sinusitis.²⁰ The reason for the increased mucous production in laryngectomized patients could be the increase of goblet cells, which starts in the second week after the laryngectomy.²² Deniz *et al.* also report on a hypersecretory phase in an early period after the laryngectomy.²³ On the other hand, some authors report on decreased mucus production during the first 12 post-operative months.⁸ In our study we included only those patients who had a laryngectomy at least 6 months before the start of the survey. For this reason, we suppose that the problems with nasal discharge persisted for more than just during the early postlaryngectomy period in our patients. However, because the data on the length of time after the laryngectomy were not included in the anonymous questionnaire we were not able to confirm our hypothesis.

The patients from our study complained about other nasal problems as well, e.g., frequent sneezing in 58.1%, and nasal itching in 33.3%, of cases. As the causes of nasal discharge, sneezing and nasal itching can be allergies or irritants, we tried to determine their importance on the incidence of these symptoms. Unfortunately, about two-thirds of the included patients were retired after the laryngectomy and the others could not assess the presence of irritant substances in their environment. Therefore, the analysis of the impact of irritants in the living or working place on some nasal symptoms could not be performed.

Allergies and some allergic diseases were reported by 16 of the patients. The presence of nasal discharge was the only significant characteristic of the allergic patients in comparison to the others without allergy. There were no significant differences with regard to frequent nasal discharge, type of nasal discharge, sneezing or nasal itching. We concluded that allergy did not significantly influence the nasal symptoms in our patients. The nasal problems can thus be related to the laryngectomy. A possible explanation could be a longer nasal mucociliary clearance time in the laryngectomized patients, which has already been described in some studies²², and consequently the persistence of various irritating air-born particles on nasal mucosa in laryngectomized patients.

It was also reported that gustation can change after radiation therapy of the head and neck cancer. A loss of gustation abilities was most pronounced 2 months after the completed radiation therapy and recovered gradually and not always completely during the first year after the treatment.²⁴ In a Japanese study including 118 patients irradiated in the head and neck region, a loss of taste was found when the anterior part of the tongue was included in the radiation field.²⁵ The main cause of diminished gustation abilities resulting from the radiation therapy is probably the disappearance of taste buds on the tongue.²⁶ In our study the questionnaire was anonymous and therefore the data on radiation-therapy details were not known. Thus we cannot exclude the possibility that some of the gustation problems were the consequence of the radiation therapy and not related only to the laryngectomy and the loss of smelling abilities.

Sinkiewicz *et al.* reported that the loss of olfaction abilities was related to the time after the laryngectomy.²⁷ As the data on time between the laryngectomy and the entry of every patient into the study were not collected, it was impossible to analyse the time dependence of the occurrence of the impairment of gustation, olfaction and other nasal problems.

A deficiency of the study was also the use of a not-yet-validated tool. The questionnaire was designed for the study with the purpose of including all possible nasal and gustation problems in the laryngectomized patients, their impact on the quality of the patients' lives and to exclude other possible reasons for the studied problems. In order to increase the impact of the study, the questionnaire should be validated on a larger group of patients and healthy controls, and compared to a validated tool for the assessment of quality of life.

In conclusion, we can say that nasal and gustatory problems are not rare among laryngectomized patients. They are connected and have a substantial impact on the quality of the patients' lives. Therefore, as in the case of speech, the rehabilitation of olfaction is necessary in all laryngectomized patients and must take place soon after the treatment is completed.

References

1. Silver CE, Beitler JJ, Shaha AR, Rinaldo A, Ferlito A. Current trends in initial management of laryngeal cancer: the declining use of open surgery. *Eur Arch Otorhinolaryngol* 2009; **266**: 1333-52.
2. Casper JK, Colton RH. *Clinical manual for laryngectomy and head and neck cancer rehabilitation*. San Diego, California: Singular Publishing Group, INC.; 1993. p. 55-78.
3. Hočevár Boltežar I, Šmid L, Žargi M, Župevc A, Fajdiga I, Fischinger J, et al. Factors influencing rehabilitation in patients with head and neck cancer. *Radiol Oncol* 2000; **34**: 289-94.
4. Hočevár Boltežar I, Žargi M. Communication after laryngectomy. *Radiol Oncol* 2001; **35**: 249-54.
5. Lennie TA, Christman SK, Jadack RA. Educational needs and altered eating habits following a total laryngectomy. *Oncol Nurs Forum* 2001; **28**: 667-74.
6. Caldas AS, Facundes VL, Melo TM, Dourado Filho MG, Pinheiro Júnior PF, Silva HJ. Modifications and evaluation of smell and taste functions in total laryngectomy: systematic review. *J Soc Bras Fonoaudiol* 2011; **23**: 82-8.
7. Miani C, Ortolani F, Bracale AM, Petrelli L, Staffieri A, Marchini M. Olfactory mucosa histological findings in laryngectomees. *Eur Arch Otorhinolaryngol* 2003; **260**: 529-35.
8. Fisher EW, Lund VJ, Rutman A. The human nasal mucosa after deprivation of airflow: a study of laryngectomy patients. *Rhinology* 1992; **30**: 5-10.
9. Fujii M, Fukazawa K, Hatta C, Yasuno H, Sakagami M. Olfactory acuity after total laryngectomy. *Chem Senses* 2002; **27**: 117-21.
10. Netzer A, Golz A, Goldenberg D, Silberman M, Joachims HZ. Hyposmia following laryngectomy: experimental model. *J Otolaryngol* 2002; **31**: 9-12.
11. Veyseller B, Aksoy F, Yildirim YS, Bayraktar FG, Gurbuz D, Savas Y, et al. Reduced olfactory bulb volume in total laryngectomy patients: a magnetic resonance imaging study. *Rhinology* 2011; **49**: 112-6.
12. Ackerstaff AH, Hilgers FJ, Aaronson NK, Balm AJ. Communication, functional disorders and lifestyle changes after total laryngectomy. *Clin Otolaryngol Allied Sci* 1994; **19**: 295-300.
13. van Dam FS, Hilgers FJ, Emsbroek G, Tuow FI, van As CJ, de Jong N. Deterioration of olfaction and gustation as a consequence of total laryngectomy. *Laryngoscope* 1999; **109**: 1150-5.
14. Risberg-Berlin B, Ylitalo R, Finizia C. Screening and rehabilitation of olfaction after total laryngectomy in Swedish patients: results from the intervention study using Nasal Airflow-Inducing Maneuver. *Arch Otolaryngol Head Neck Surg* 2006; **132**: 301-6.
15. Morales-Puebla JM, Morales-Puebla AF, Jiménez-Antolín JA, Muñoz-Platón E, Padilla-Parrado M, Chacón-Martínez J. Olfactory rehabilitation after total laryngectomy. *Acta Otorrinolaringol Esp* 2010; **61**: 128-34.
16. Leon EA, Catalanotto FA, Werning JW. Retronasal and orthonasal olfactory ability after laryngectomy. *Arch Otolaryngol Head Neck Surg* 2007; **133**: 32-6.
17. Rozin P. "Taste-smell" confusions and the duality of the olfactory sense. *Percept Psychophys* 1982; **31**: 397-401.
18. Burdach KJ, Doty RL. The effects of mouth movements, swallowing, and spitting on retronasal odor perception. *Physiol Behav* 1987; **47**: 353-6.
19. Henkin RI, Smith FR. Hyposmia in acute viral hepatitis. *Lancet* 1971; **1** (7704): 823-6.

20. Sesterhenn AM, Fiedler G, Müller HH, Wiegand S, Folz BJ, Werner JA. Incidence of sinonasal disease in laryngectomized patients. *ORL J Otorhinolaryngol Relat Spec* 2008; **70**: 185-8.
21. Magardino TM, Suskind-Liu D, Kroger H, Mirza N. Ipratropium bromide nasal spray for treatment of rhinorrhea in the laryngectomized patient: a pilot study. *Am J Rhinol* 2001; **15**: 203-6.
22. Hellin Mesequer D, Merino Gálvez E, Garcia Ortega F, Rosique Arias M. The mucociliary function and the morphology of the nasal mucous membrane in laryngectomees compared with normal subjects. *An Otorrinolaringol Ibero Am* 1996; **23**: 81-90.
23. Deniz M, Uslu C, Ogedik EA, Akduman D, Gursan SQ. Nasal mucociliary clearance in total laryngectomized patients. *Eur Arch Otorhinolaryngol* 2006; **263**: 1099-104.
24. Maes A, Huygh I, Weltens C, Vandeveldel G, Delaere P, Evers G, et al. De Gustibus: time scale of loss and recovery of tastes caused by radiotherapy. *Radiother Oncol* 2002; **63**: 195-201.
25. Yamashita H, Nakagawa K, Tago M, Nakamura N, Shiraishi K, Eda M, et al. Taste dysfunction in patients receiving radiotherapy. *Head Neck* 2006; **28**: 508-16.
26. Yamashita H, Nakagawa K, Nakamura N, Abe K, Asakage T, Ohmoto M, et al. Relation between acute and late irradiation impairment of four basic tastes and irradiated tongue volume in patients with head-and-neck cancer. *Int J Radiat Oncol Biol Phys* 2006; **66**: 1422-9.
27. Sinkiewicz A, Winiarski P, Mackiewicz H, Owczarzak H, Janicka-Beutch L, Betlejewski S. Estimation of smell sense rehabilitation in patients after total laryngectomy. *Otolaryngol Pol* 2006; **60**: 33-6.

Circulating serum sVCAM-1 concentration in advanced ovarian cancer patients: correlation with concentration in ascites

Marina Jakimovska¹, Katarina Cerne², Ivan Verdenik¹, Borut Kopal¹

¹ Department of Obstetrics and Gynaecology University Medical Centre, Ljubljana, Slovenia

² Department of Pharmacology and Experimental Toxicology, Faculty of Medicine, University of Ljubljana, Ljubljana, Slovenia

Radiol Oncol 2014; 48(3): 307-313.

Received 25 June 2013

Accepted 30 August 2013

Correspondence to: Borut Kopal, M.D., Department of Obstetrics and Gynaecology University Medical Centre, Štajmarjeva 3, SI-1000 Ljubljana, Slovenia. E-mail: borut.kopal1@siol.net

Disclosure: No potential conflicts of interest were disclosed.

Background. Vascular cell adhesion molecule-1 (VCAM-1) is associated with ovarian cancer progression but the origin of its soluble form (sVCAM-1) in serum is not well investigated. The purpose of this study was to elucidate whether the concentration of sVCAM-1 in serum correlates with the concentration in ascites, that represents local tumour environment, and with systemic inflammation, various clinicopathological characteristics, and patient outcome.

Patients and methods. Thirty-six patients with advanced ovarian cancer were included in the study. Serum for sVCAM-1 analysis was obtained prior to surgery. Ascites samples were collected at the beginning of the operation. Clinical data were collected from patients' medical records. sVCAM-1 in samples was analysed by flow cytometric bead-based assay. The mean follow-up period was 11 months (range 0-23) from the time of surgery.

Results. Serum sVCAM-1 concentrations are positively correlated to ascites sVCAM-1 concentrations. There was a weakly positive correlation of serum sVCAM-1 with tumour size and no correlation with inflammatory tumour markers, FIGO stage or grade. Higher concentrations of sVCAM-1 were associated with poor disease outcome (death from ovarian cancer) in almost all cases before chemotherapy was started.

Conclusions. This is the first study demonstrating that serum concentrations of sVCAM-1 in advanced ovarian cancer patients correlate with sVCAM-1 concentrations in ascites, thus expressing the biologic potential of malignant disease to metastasis, rather than systemic inflammation. Higher serum and ascites sVCAM-1 concentrations might have predictive potential for different biologic behaviour.

Key words: sVCAM-1; ovarian cancer; flow cytometry

Introduction

Ovarian cancer (OC) is relatively asymptomatic in the early stages; over 70% of all OC cases are diagnosed at advanced stages, with extensive seeding of the peritoneal cavity by tumour cells associated with ascites.^{1,2} Many promising biomarkers have been studied in serum and plasma of OC patients in order to provide early diagnosis and disease monitoring, but only carbohydrate antigen 125 (CA125) is approved in clinical use, and human epididymis protein 4 (HE4) that has

been approved only as aid for monitoring patients.³⁻⁸ CA125 and HE4 are far from ideal, since both have limitations in their specificity and sensitivity.⁷ An excellent body fluid for discovering potentially more specific biomarkers is the local tumour environment represented by ascites, due to the presence of tumour cells and soluble proteins, reflecting the secretome of the tumour environment.^{4,9-11} It has been proposed that ascites is crucial for OC progression by favouring the dissemination of OC cells, which are detached from the primary tumour, within the peritoneal cavity.

TABLE 1. Clinical characteristics of the patients and laboratory data

Variables	Data
No. of patients	36
Age, years	
Mean	59.9 ± 12.1
Range	28-83
Vital status for the follow up period of 11,2 monthsn (%)	
Dead	5 (13.9 %)
Alive	31 (86.1 %)
FIGOstage, n (%)	
III	26 (72.2 %)
IV	10 (27 %)
Grade of differentiation, n (%)	
3	19 (52.8 %)
2	11 (30.5 %)
1	5 (13.9 %)
NA	1 (2.8 %)
Hystological type	
serous carcinoma	29 (80.5 %)
endometrioid carcinoma	3 (8.3 %)
mixed type and clear cell	4 (11.1 %)
Tumour size, cm	14.2 ± 6.8
WBC, x10 ⁶ /l	9.28 ± 4.7
CRP, mg/l	55.1 ± 56.2
Serum sVCAM-1, ng/ml	1639.3 ± 537.2
Ascites sVCAM-1, ng/ml	817.9 ± 287.7
Ratio ascites/serum, range	0.51 ± 0.15 (0.30 – 0.97)

FIGO = International Federation of Gynecology and Obstetrics; NA = not available; CRP = C-reactive protein; WBC = white blood cells; sVCAM-1 = soluble Vascular Cell Adhesion Molecule-1

Transcoelomic dissemination is the most common manner of OC spread.^{12,13}

A large proportion of soluble proteins in the acellular fraction of ascites have been found to be related to the processes of adhesion and cell movement.¹⁴ The disseminated OC cells preferentially adhere to the mesothelium, a layer of mesothelial cells that lines the peritoneum and surrounds the serosal surface of organs in the abdominal cavity. Vascular cell adhesion molecule-1 (VCAM-1), expressed in activated mesothelial cells, has been identified as an important mediator for adhesion of OC cells to and invasion through the mesothelium.¹⁵ Although the membrane-bound form is diffi-

cult to measure *in vivo*, the soluble form of VCAM-1 (sVCAM-1) can be detected in ascites. However, its concentration in ascites of OC patients has not previously been measured.

sVCAM-1 was analysed in the serum of OC patients, and an association with tumour presence was reported.¹⁶⁻¹⁸ Interpretation of detected levels of sVCAM-1 in serum in terms of its importance as a biomarker is hindered by lack of knowledge as to what factors determine the steady-state levels of this adhesion molecule in serum. Since VCAM-1 is involved in inflammatory reaction and systemic inflammatory response in cancer patients is a common phenomenon, there is a need to elucidate whether detected concentrations of sVCAM-1 in serum are truly cancer-specific.¹⁹

The aim of this study was to elucidate whether concentrations of serum sVCAM-1 detected in OC patients correlate with sVCAM-1 concentrations in the local tumour environment represented by ascites, thus expressing the biologic processes of malignant disease. To evaluate whether serum concentrations of sVCAM-1 are related to systemic inflammation, we investigated the relationship between concentrations of sVCAM-1 and markers of inflammation (C-reactive protein (CRP) and total white blood cells (WBC)). Additionally, we examined the relationship of sVCAM-1 concentrations to various clinicopathologic variables, as well as to patient outcome.

Patients and methods

Patients

Thirty-six patients with stage III and IV primary ovarian cancer, operated in two years period of time (from 2011 to 2012) at the Department of Gynecology, University Medical Centre Ljubljana, were included in the study. Staging of the disease was according to the International Federation of Gynecology and Obstetrics (FIGO) classification for staging ovarian cancer. CRP value, WBC count, data on tumour histological type, grade and primary tumour size were collected from patients documentation. Prior to analysis, all patients received detailed oral and written information about the research and procedures, and they signed informed consent for analysis of their blood and ascites for the purposes of the research. The trial was approved by the National Medical Ethics Committee of Republic of Slovenia with number of approval 82/01/11 and was in agreement with the Helsinki Declaration.

Collection and storage of samples

Venous blood samples were obtained prior to surgery while the patients were hospitalized for pre-operative preparation. Four ml of peripheral blood were collected into a vacutainer, without anticoagulant or other additives. Serum was separated by centrifugation at $2000 \times g$ for 15 minutes at 4°C . Blood for full blood count and CRP was obtained at the same time as for sVCAM-1 analysis. At the beginning of the operation, immediately after entry to the abdominal cavity, twenty ml of ascites were aspirated into a sterile syringe and immediately transferred into a conical tube, which was kept on ice until centrifugation at $1000 \times g$ for 10 min at 4°C within 30 minutes. Sera and supernatant of ascites were stored in aliquots at -80°C . No more than 2 freeze-thaw cycles were allowed for any sample.

Analysis of sVCAM-1 with flow cytometric bead-based assay

Concentrations of sVCAM-1 in samples were measured using a FlowCytomix Simplex Kit (eBioscience, Vienna). The kit consists of fluorescent microspheres (diameter: $4 \mu\text{m}$, emission wavelength at 700 nm) coated with specific antibodies raised against sVCAM-1. It also contains a biotin-conjugated second antibody and streptavidine-phycoerythrin emitting at 575 nm . Samples were run on a Cell Lab Quanta™ SC-MPL (Beckman Coulter). Samples were acquired by the Cell Lab Quanta™ SC-MPL software (Beckman Coulter) and analysed using Flowcytomix™ Pro 3.0 software (eBioscience). Electronic volume *vs.* side scatter gating was employed to exclude any sample particles other than $4 \mu\text{m}$ microspheres. A seven point standard curve ranging from 2.74 to 2000 ng/ml was obtained by serial dilution of the reconstituted lyophilized standard. The lower limit of detection was 0.9 ng/ml.

Statistical analysis

Data are presented as mean \pm SD. The normality of distribution was tested with the Kolmogorov-Smirnov test. Pearson's correlation coefficient was used to calculate the strength of the relationship between normally distributed variables. Since data for tumour size was non-normally distributed, Spearman's correlation coefficient was used to calculate the strength of the relationship between serum sVCAM-1 and tumour size. An independent samples t-test, and Pearson's chi-square test were

used to compare variables between patients that died before the start or during the adjuvant chemotherapy and those who finished complete treatment and are still living. A p of <0.05 was considered significant. Statistical analysis was performed using software statistical package SPSS, version 19 (IBM Statistics, USA).

Results

The clinical characteristics of the investigated patients are summarized in Table 1.

The data were approximately normally distributed for all variables included in the analysis, except for tumour size.

The mean concentration of sVCAM-1 in ascites was significantly lower (two fold) than that in serum (Table 1). A significant positive correlation between sVCAM-1 concentrations in serum and ascites was observed ($r = 0.733$, $p < 0.001$) (Figure 1).

Thirty-four (90%) patients had elevated CRP levels. The mean CRP value was $59.8 \pm 56.6 \text{ mg/l}$. Thirteen (36%) patients had elevated WBC levels. The mean WBC count was $13.3 \pm 5.8 \times 10^6 / \text{L}$. There was no correlation between serum sVCAM-1 concentration and each of CRP and WBC levels (Figure 1).

When sVCAM-1 concentrations were compared with standard clinicopathologic variables, only serum sVCAM-1 concentrations were weakly correlated to tumour size by the Spearman test ($r = 0.347$; $p = 0.038$). Concentrations of sVCAM-1 in neither ascites nor serum were correlated with FIGO stage or tumour grade (data not shown).

During the mean follow-up period of 11 months (range 0-23) from the time of surgery, 5 (14%) patients died from ovarian cancer, 4 out of 5 before chemotherapy was started. We therefore evaluated the association of VCAM-1 concentrations in serum and ascites with patient outcome. In view of the small number of patients included and the short period of follow-up, only univariate analysis was performed. Our intention was to obtain preliminary data on whether sVCAM-1 has potential as a prognostic factor and, if so, to evaluate it in the future. Higher concentrations of sVCAM-1 in serum and ascites turned out to be associated with poor outcome, since there was a significant difference in sVCAM-1 serum concentration between the 31 patients who are still living and the 5 who did not survive; $1557.4 \pm 470 \text{ ng/ml}$ versus $2147.2 \pm 702.8 \text{ ng/ml}$ ($p = 0.02$) (Table 2). The same is also true for sVCAM-1 concentrations in ascites: 776.2

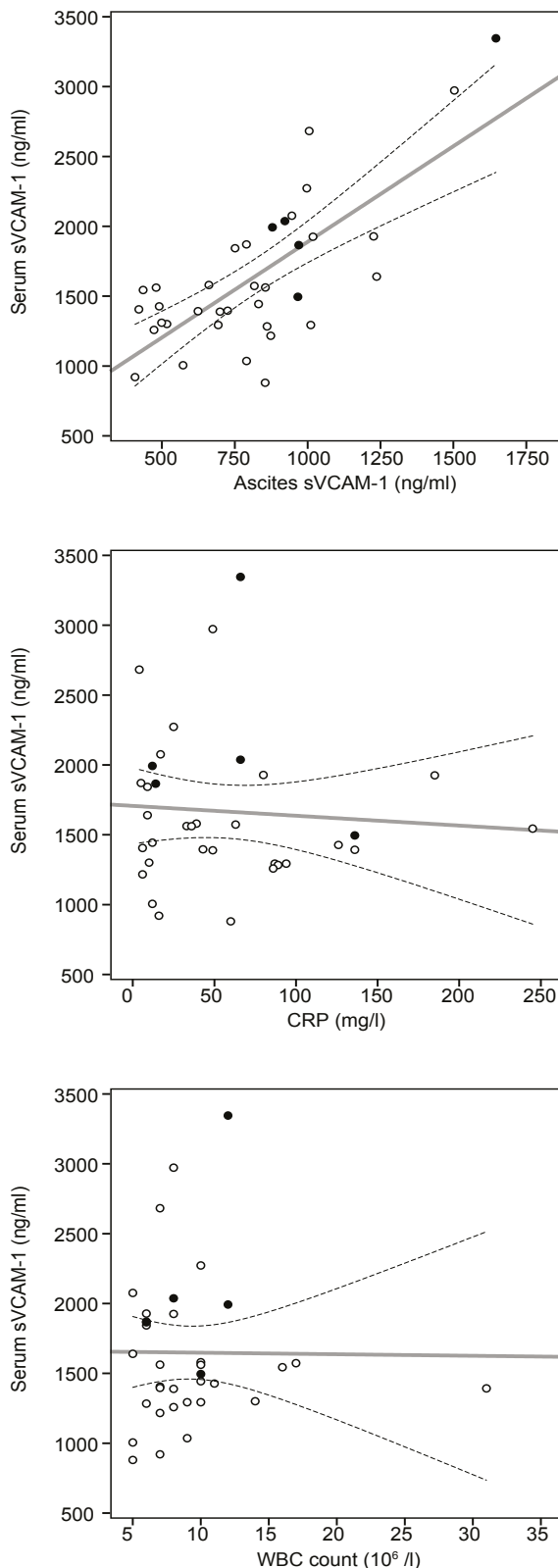


FIGURE 1. Correlation between serum sVCAM-1 concentrations and sVCAM-1 concentrations in ascites, C-reactive protein (CRP) level and white blood cell (WBC) count. Dashed lines represent 95% confidence intervals for the regression line. Black dots represent patients who died from ovarian cancer.

± 264.4 ng/ml for those who are still living versus 1076.5 ± 320.4 ng/ml for those who died ($p = 0.028$). Contrary to our expectation, none of the other variables included in the univariate analysis (age, tumour size, tumour grade, FIGO stage) were correlated with patient outcome (Table 2).

Discussion

Blood assay for detecting tumour biomarkers is an important non-invasive method for establishing cancer diagnosis, patient prognosis and treatment outcome.²⁰ One promising candidate for an OC biomarker, as demonstrated by a recent study, is the sialoglycoprotein VCAM-1.¹⁷⁻²¹ Its soluble form sVCAM-1 has been detected in serum but its origin is not well investigated. We therefore performed a study that might elucidate the relationship of sVCAM-1 in two different environments: ascites as the local environment, to which VCAM-1 is shed, and serum, where other influences that determine the steady-state levels of sVCAM-1, could be expected (*e.g.*, systemic inflammation). The concentration of sVCAM-1 in ascites of OC patients has not been measured yet. Additionally, we examined the relationship of sVCAM-1 concentrations to various clinicopathologic variables, as well as to patient outcome. The major new findings in our study are as follows: (1) the sVCAM-1 concentration in ascites is approximately half of that in serum; (2) ascites is an important source of sVCAM-1 in systemic circulation, since serum sVCAM-1 concentrations are positively correlated to ascites sVCAM-1 concentrations; (3) serum sVCAM-1 concentrations are not correlated to CRP and WBC levels, so elevated serum sVCAM-1 levels are probably not the result of systemic inflammation; (4) serum sVCAM-1 but not ascites concentrations are weakly correlated to tumour size, which might suggest that sVCAM-1 originating from the primary tumour can at least partly reach serum directly and not through ascites; (5) higher concentrations of sVCAM-1 are associated with patient death from OC in a short period after surgery, in almost all cases (4 out of 5) before chemotherapy was started. This might indicate a relation of sVCAM-1 to an aggressive form of the disease.

The detected sVCAM-1 concentration in ascites reflects its production in the local tumour environment. The cellular fraction of ascites consists mainly of OC cells, lymphocytes and mesothelial cells.¹² The expression of a membrane-bound form of VCAM-1 in OC patients' peritoneal biopsies

and ascites has been shown in activated mesothelial cells, monocytes/macrophages, and rarely in T cells.¹⁵⁻²² We therefore assume that the main cellular sources of sVCAM-1 in ascites are probably mesothelial cells and monocytes/macrophages. VCAM-1 expressed in activated mesothelial cells has been identified as an important mediator of adhesion of OC cells to and invasion through the mesothelium.¹⁵ An increased concentration of sVCAM-1 in ascites could therefore indicate a biologic potential of disease progression to highly invasive tumours, growing under the mesothelium, which is associated with a poor prognosis.¹⁵ Whereas the mechanism that regulates VCAM-1 expression in mesothelial cells in OC patients is unknown, a known inducer of VCAM-1 expression, tumour necrosis factor α (TNF- α), is expressed by OC cells, macrophages, and is found in ascites.^{23,24} Increased production of sVCAM-1 in ascites could also be due to enhanced proteolytic cleavage from the cell surface. VCAM-1 shedding from the cell surface *in vitro* can be mediated by two distinct metalloprotease activities: a constitutive VCAM-1 sheddase that is active under normal conditions, and inducible protease identified as a tumour necrosis factor- α -converting enzyme (TACE or ADAM 17).²⁵ The significance of VCAM-1 shedding *in vivo* is not yet known, but at least two roles are possible. First, cleavage of VCAM-1 may play a role in regulation of its adhesive function by rapidly decreasing its levels at the cell surface. A second potential role is that cleavage near the transmembrane region leads to the release of intact sVCAM-1, which may remain functionally active.²⁵

Using Pearson correlation test, we were able to confirm a positive correlation between ascites and serum sVCAM-1 concentrations. This result reflects the important contribution of sVCAM-1 from ascites to increasing the concentration of sVCAM-1 in serum, which is possibly because of the direct access of ascites from the peritoneum to circulation. Ascites carrying soluble proteins can enter the subperitoneal lymphatic lacunae and the lymphatic fluid finally drains into the left subclavian vein.²⁶ The concentration of sVCAM-1 in ascites is approximately half of the concentration in serum, assuming that all of the sVCAM-1 from ascites reached the blood. Other sources of sVCAM-1 in serum should therefore be considered. The existence of high basal levels of sVCAM-1 in serum of healthy people suggests a likely physiological role.²⁷ Another source might be systemic inflammation, as an inherent component in cancer patients.¹⁹ Inflammatory cytokines markedly

TABLE 2. Univariate analysis of OC prognostic factors for cancer-specific survival

Variables	Dead (n=5)	Alive (n=31)	p*
Continuous			
Age, years	69.0 \pm 8.6	58.5 \pm 12.1	0.072
Serum sVCAM-1, ng/ml	2147.2 \pm 702.8	1557.5 \pm 470.1	0.02
Ascites sVCAM-1, ng/ml	1076.5 \pm 320.4	776.2 \pm 264.4	0.028
Tumour size, cm	18.0 \pm 9.3	13.3 \pm 6.1	0.145
Categorical Tumour grade, n			
	(n=4)	(n=31)	0.588
1	0	5	
2	1	10	
3	3	16	
FIGO stage, n			
	(n=5)	(n=31)	0.511
III	3	23	
IV	2	8	

FIGO = International Federation of Gynecology and Obstetrics; sVCAM-1 = soluble Vascular Cell Adhesion Molecule-1; * Independent t test for continuous variables and chi-square test for categorical ones.

induce VCAM-1 expression in endothelial cells. Endothelial VCAM-1 functions by regulating leukocyte attachment and extravasation at sites of inflammation, a process that is similar to invasion of OC cells through the mesothelium.²⁸ Inflammatory markers (CRP and WBC) were elevated in our population, providing confirmatory evidence of a connection between the inflammation process and carcinogenesis.^{19,29,30} The results of our study showed no correlation between sVCAM-1 and inflammatory markers, so an influence of systemic inflammation on increased sVCAM-1 can be excluded.

Among standard clinicopathologic characteristics, only tumour size was weakly correlated with sVCAM-1 in serum. Tumour size was not in correlation with sVCAM-1 concentration in ascites, indicating that sVCAM-1 originating from the primary tumour, could at least partly reach serum directly. sVCAM-1 could exit from the primary tumour through new micro vessels functionally connected to the peripheral blood circulation. Without angiogenesis, tumour expansion cannot proceed beyond 1-2 mm, and invading blood vessels occupy 1.5% of the tumour volume.³¹ We speculate that the origin of sVCAM-1 might be perivascular cells in developing vessels. VCAM-1 expressed in perivascular cells and integrin $\alpha 4\beta 1$ in endothelial cells mediate adhesion between these two types of cells, an event that is required for the survival of proliferating endothelial and perivascular cells and, therefore, for neovascularization. VCAM-1 is

expressed only by proliferating and not by quiescent perivascular cells.³² The growth of peritoneal metastasis has also been reported to be dependent on neovasculature.^{31,33} An explanation of the weak correlation between tumour size and serum sVCAM-1 concentration in our study might be that only the size of the primary tumour was included in the comparison and not the extent of peritoneal metastasis. A direct measurement of the degree of neoangiogenesis by a technique such as microvessel density would yield a more conclusive result.

Serum and ascites sVCAM-1 concentrations were not in correlation with other clinicopathologic variables, such as FIGO stage (III versus IV), grade of differentiation and histological tumour type. Huang *et al.* also found no correlation between VCAM-1 and FIGO stage in OC patients in their study but they examined the expression of VCAM-1 in ovarian cancer tissue samples and not in human fluids.²¹ A possible explanation could be that sVCAM-1 in the two fluids does not reflect the stabilized spread of the disease defined by stage but by the biologic potential of ovarian cancer to metastasis. In support of this hypothesis, we found that patients with more aggressive disease, who did not survive, had significantly higher levels of sVCAM-1 in both serum and ascites, although we are aware that the number of cases in our sample is not sufficient to confirm the predictive potential of sVCAM-1 for different biologic behaviour. More extensive research should be done to prove this assumption. However, one recently published study showed that VCAM-1 overexpression in OC cells was an independent predictor of overall survival in 251 OC patients, thereby providing support for our result.²¹ VCAM-1 in this study was localized in the cytoplasm of tumour and stromal cells and not on the cell surface. How the intracellular form of VCAM-1 is related to sVCAM-1 in body fluids is as yet unknown. A limitation of our study was the small number of patients included, which prevented reliable analysis of subgroups, especially in the case of histological tumour type.

In conclusion, the present study demonstrates that serum concentrations of sVCAM-1 in advanced stage OC patients correlate with sVCAM-1 concentrations in ascites, that represents tumour local environment, and not with systemic inflammation, thus expressing the biologic potential of malignant disease to metastasis. Another important practical implication is that higher serum and ascites sVCAM-1 concentrations are correlated with worse patient outcome, which supports the predictive potential of sVCAM-1 for different bio-

logic behaviour of OC, which needs to be proven in more extensive research.

Acknowledgements

This work was supported by research grants from the University Medical Centre Ljubljana (Project Number: 20110224) and the Slovenian Research Agency (P3-067).

References

- Lengyel E. Ovarian cancer development and metastasis. *Am J Pathol* 2010; **177**: 1053-64.
- Rauh-Hain JA, Krivak TC, Del Carmen MG, Olawaiye AB. Ovarian cancer screening and early detection in the general population. *Rev Obstet Gynecol* 2011; **4**: 15-21.
- Nguyen L, Cardenas-Goicoechea SJ, Gordon P, Curtin C, Momeni M, Chuang L, et al. Biomarkers for early detection of ovarian cancer. *Womens Health (Lond Engl)* 2013; **9**: 171-85; quiz 186-177.
- Amon LM, Law W, Fitzgibbon MP, Gross JA, O'Briant K, Peterson A, et al. Integrative proteomic analysis of serum and peritoneal fluids helps identify proteins that are up-regulated in serum of women with ovarian cancer. *PLoS One* 2010; **5**: e11137.
- Kuk C, Kulasingam V, Gunawardana CG, Smith CR, Batruch I, Diamandis EP. Mining the ovarian cancer ascites proteome for potential ovarian cancer biomarkers. *Mol Cell Proteomics* 2009; **8**: 661-9.
- Drapkin R, von Horsten HH, Lin Y, Mok SC, Crum CP, Welch WR, et al. Human epididymis protein 4 (HE4) is a secreted glycoprotein that is overexpressed by serous and endometrioid ovarian carcinomas. *Cancer Res* 2005; **65**: 2162-9.
- Anton C, Carvalho FM, Oliveira EI, Maciel GA, Baracat EC, Carvalho JP. A comparison of CA125, HE4, risk ovarian malignancy algorithm (ROMA), and risk malignancy index (RMI) for the classification of ovarian masses. *Clinics (Sao Paulo)* 2012; **67**: 437-41.
- Daniel W, Chan RCB, Ie-Ming Shih, Lori J, Sokoll, and György Sölétormos. Use of tumor markers in testicular, prostate, colorectal, breast, and ovarian cancers. *Laboratory Medicine Practice Guidelines* 2009; **6**: 51-9.
- Good DM, Thongboonkerd V, Novak J, Bascands JL, Schanstra JP, Coon JJ, et al. Body fluid proteomics for biomarker discovery: lessons from the past hold the key to success in the future. *J Proteome Res* 2007; **6**: 4549-55.
- Berchuck A, Carney M. Human ovarian cancer of the surface epithelium. *Biochem Pharmacol* 1997; **54**: 541-4.
- Verheul HM, Hoekman K, Jorna AS, Smit EF, Pinedo HM. Targeting vascular endothelial growth factor blockade: ascites and pleural effusion formation. *Oncologist* 2000; **5** (Suppl1): 45-50.
- Puiffe ML, Le Page C, Filali-Mouhim A, Zietarska M, Ouellet V, Tonin PN, et al. Characterization of ovarian cancer ascites on cell invasion, proliferation, spheroid formation, and gene expression in an in vitro model of epithelial ovarian cancer. *Neoplasia* 2007; **9**: 820-9.
- Mantur M, Snarska J, Koper O, Dzieciol J, Plonski A, Lemancewicz D. Serum sICAM, sVCAM and sE-selectin levels in colorectal cancer patients. *Folia Histochem Cytobiol* 2009; **47**: 621-5.
- Faca VM, Hanash SM. In-depth proteomics to define the cell surface and secretome of ovarian cancer cells and processes of protein shedding. *Cancer Res* 2009; **69**: 728-30.
- Slack-Davis JK, Atkins KA, Harrer C, Hershey ED, Conaway M. Vascular cell adhesion molecule-1 is a regulator of ovarian cancer peritoneal metastasis. *Cancer Res* 2009; **69**: 1469-76.

16. Banks RE, Gearing AJ, Hemingway IK, Norfolk DR, Perren TJ, Selby PJ. Circulating intercellular adhesion molecule-1 (ICAM-1), E-selectin and vascular cell adhesion molecule-1 (VCAM-1) in human malignancies. *Br J Cancer* 1993; **68**: 122-4.
17. Yurkovetsky Z, Skates S, Lomakin A, Nolen B, Pulsipher T, Modugno F, et al. Development of a multimarker assay for early detection of ovarian cancer. *J Clin Oncol* 2010; **28**: 2159-66.
18. Nolen B, Marrangoni A, Velikokhatnaya L, Prosser D, Winans M, Gorelik E, et al. A serum based analysis of ovarian epithelial tumorigenesis. *Gynecol Oncol* 2009; **112**: 47-54.
19. Kowalewska M, Nowak R, Chechlinska M. Implications of cancer-associated systemic inflammation for biomarker studies. *Biochim Biophys Acta* 2010; **1806**: 163-71.
20. Bhatt AN, Mathur R, Farooque A, Verma A, Dwarakanath BS. Cancer biomarkers - current perspectives. *Indian J Med Res* 2010; **132**: 129-49.
21. Huang J, Zhang J, Li H, Lu Z, Shan W, Mercado-Urbe I, et al. VCAM1 expression correlated with tumorigenesis and poor prognosis in high grade serous ovarian cancer. *Am J Transl Res* 2013; **5**: 336-46.
22. Wang X, Deavers M, Patenia R, Bassett RL, Jr., Mueller P, Ma Q, et al. Monocyte/macrophage and T-cell infiltrates in peritoneum of patients with ovarian cancer or benign pelvic disease. *J Transl Med* 2006; **4**: 30.
23. Szlosarek PW, Grimshaw MJ, Kulbe H, Wilson JL, Wilbanks GD, Burke F, et al. Expression and regulation of tumor necrosis factor alpha in normal and malignant ovarian epithelium. *Mol Cancer Ther* 2006; **5**: 382-90.
24. Moradi MM, Carson LF, Weinberg B, Haney AF, Twigg LB, Ramakrishnan S. Serum and ascitic fluid levels of interleukin-1, interleukin-6, and tumor necrosis factor-alpha in patients with ovarian epithelial cancer. *Cancer* 1993; **72**: 2433-40.
25. Garton KJ, Gough PJ, Philalay J, Wille PT, Blobel CP, Whitehead RH, et al. Stimulated shedding of vascular cell adhesion molecule 1 (VCAM-1) is mediated by tumor necrosis factor-alpha-converting enzyme (ADAM 17). *J Biol Chem* 2003; **278**: 37459-64.
26. Abu-Hijleh MF, Habbal OA, Moqattash ST. The role of the diaphragm in lymphatic absorption from the peritoneal cavity. *J Anat* 1995; **186**: 453-67.
27. Levesque JP, Takamatsu Y, Nilsson SK, Haylock DN, Simmons PJ. Vascular cell adhesion molecule-1 (CD106) is cleaved by neutrophil proteases in the bone marrow following hematopoietic progenitor cell mobilization by granulocyte colony-stimulating factor. *Blood* 2001; **98**: 1289-97.
28. van Buul JD, Hordijk PL. Signaling in leukocyte transendothelial migration. *Arterioscler Thromb Vasc Biol* 2004; **24**: 824-33.
29. Oikonomopoulou K, Brinc D, Kyriacou K, Diamandis EP. Infection and cancer: reevaluation of the hygiene hypothesis. *Clin Cancer Res* 2013; **19**: 2834-41.
30. Mantovani A, Allavena P, Sica A, Balkwill F. Cancer-related inflammation. *Nature* 2008; **454**: 436-44.
31. Bamberger ES, Perrett CW. Angiogenesis in epithelial ovarian cancer. *Mol Pathol* 2002; **55**: 348-59.
32. Garmy-Susini B, Jin H, Zhu Y, Sung RJ, Hwang R, Varner J. Integrin alpha4beta1-VCAM-1-mediated adhesion between endothelial and mural cells is required for blood vessel maturation. *J Clin Invest* 2005; **115**: 1542-51.
33. Yamamoto S, Konishi I, Mandai M, Kuroda H, Komatsu T, Nanbu K, et al. Expression of vascular endothelial growth factor (VEGF) in epithelial ovarian neoplasms: correlation with clinicopathology and patient survival, and analysis of serum VEGF levels. *Br J Cancer* 1997; **76**: 1221-7.

Post-mastectomy radiotherapy benefits subgroups of breast cancer patients with T1-2 tumor and 1-3 axillary lymph node(s) metastasis

Yu-Li Su¹, Shan-Hsuan Li^{1,2}, Yen-Yang Chen¹, Hui-Chun Chen³, Yen Tang⁴, Cheng-Hua Huang¹, Fong-Fu Chou^{2,5}, Shih-Chung Wu⁵, Kun-Ming Rau^{1,2,6}

¹ Division of Hematology-Oncology, Department of Internal Medicine, Kaohsiung Chang Gung Memorial Hospital, Kaohsiung, Taiwan

² Chang Gung University, College of Medicine, Taoyuan, Taiwan

³ Department of Radiation Oncology, Kaohsiung Chang Gung Memorial Hospital, Kaohsiung, Taiwan

⁴ Division of Hematology-Oncology, Department of Internal Medicine, E-Da Hospital, Kaohsiung, Taiwan

⁵ Department of General Surgery, Kaohsiung Chang Gung Memorial Hospital, Kaohsiung, Taiwan

⁶ Cancer Center, Kaohsiung Chang Gung Memorial Hospital, Kaohsiung, Taiwan

Radiol Oncol 2014; 48(3): 314-322.

Received 26 July 2013

Accepted 20 October 2013

Correspondence to: Kun-Ming Rau, M.D., Division of Hematology-Oncology, Department of Internal Medicine, Kaohsiung Chang Gung Memorial Hospital and Chang Gung University, College of Medicine, Taiwan, No.123, Dapi Rd., Niasong Dist., Kaohsiung City 833, Taiwan (R.O.C.). Phone: +886-7-7317123 ext. 8303; Fax: +886-7-7322402; E-mail: kmrau58@adm.cgmh.org.tw

Disclosure: No potential conflicts of interest were disclosed.

Background. To determine the role of postmastectomy radiotherapy (PMRT) in breast cancer patients with T1-2 and N1 disease.

Patients and methods. A total of 207 postmastectomy women were enrolled. The 5-year Kaplan-Meier estimates of locoregional recurrence rate (LRR), distant recurrence rate (DRR) and overall survival (OS) were analyzed by different tumor characteristics. Multivariate analyses were performed using Cox proportional hazards modeling.

Results. With median follow-up 59.5 months, the 5-year LRR, DRR and OS were 9.1%, 20.3% and 84.4%, respectively. On univariate analysis, age < 40 years old ($p = 0.003$) and Her-2/neu over-expression ($p = 0.016$) were associated with higher LRR, whereas presence of LVI significantly predicted higher DRR ($p = 0.026$). Negative estrogen status ($p = 0.033$), Her-2/neu overexpression ($p = 0.001$) and LVI ($p = 0.01$) were significantly correlated with worse OS. PMRT didn't prove to reduce 5-year LRR ($p = 0.107$), as well as 5-year OS ($p = 0.918$). In subgroup analysis, PMRT showed significant benefits of improvement LRR and OS in patients with positive LVI.

Conclusions. For patients with T1-2 and N1 stage breast cancer, PMRT can decrease locoregional recurrence and increase overall survival only in patients with lymphovascular invasion.

Key words: breast cancer; postmastectomy radiotherapy; overall survival; locoregional recurrence; lymphovascular invasion

Introduction

Treating breast cancer patients often requires a multidisciplinary approach. The standard treatment is resection of primary breast tumor with axillary lymph nodes dissection, and adjuvant

therapies such as chemotherapy, hormonal therapy or post-mastectomy radiotherapy (PMRT) should be done guided by clinicopathologic factors. Adjuvant radiotherapy is indicated for patients who undergo breast-conserving surgery (BCS). For patients who received total mastec-

tomy, there are also many studies demonstrated that PMRT reduced locoregional recurrence (LR) as well as improved disease free survival (DFS) and overall survival (OS).¹⁻⁷ Although results from the Early Breast Cancer Trialists' Cooperative Group (EBCTCG) showed that benefits of PMRT were emerged in all patients with positive lymph nodes (LN)⁸, the guideline of American Society of Clinical Oncology recommends adjuvant radiotherapy is only suggested for patients who received BCS or total mastectomy with T3 or more than three (N2) positive axillary LN.⁹ In St. Gallen Consensus Conference 2011, routine PMRT was clearly endorsed for patients with more than 3 involved nodes (88% yes, 5% no), but was reduced for patients with 1-3 affected nodes (18% yes, 71% no), unless if young patients (< 45 years of age; 51% yes, 42% no) or presented with extensive vascular invasion (57% yes, 26% no).¹⁰ Even in the guideline of National Comprehensive Cancer Network (NCCN), PMRT is still not routinely suggested for 1-3 positive LN patients. Therefore, for patients with T1-2 tumors and 1-3 positive LN, there is much of controversy whether PMRT has significant survival benefit, especially the side effects from radiation always happen during or after the course of radiotherapy.

There are existing evidences proved that PMRT and adjuvant chemotherapy significantly improve locoregional DFS in N1 breast cancer patients.^{1-4,11,12} The Danish 82b & 82c and British Columbia trials showed survival benefits from PMRT in both patients with 1-3 versus 4 or more positive LN.¹⁻⁴ On the contrast, McArdle *et al.* presented that a significant advantage in cancer specific survival afforded by PMRT was seen only in patients with ≥ 4 positive nodes.¹² The discrepancy may be partly because suboptimal dissection of axillary LN in the Danish Trials (median, 7 nodes), compared with other similar series (median, 15 nodes)¹³⁻¹⁶, and it resulted in higher locoregional failure rate in the subgroup (1-3 LN without PMRT) of the Danish Trials (30%) compared with others (15%).¹³⁻¹⁶ The recent analysis, selecting patients from the Danish study with 8 or more nodes removed concluded that the 15-year absolute magnitude of survival benefit was 9% in patients with either 1-3 or 4 or more positive LN.¹⁷

Several retrospective series tried to determine predictive and risk factors of recurrence among this subgroup. Age < 45 years old, more than 25% positive node ratio, medial tumor location, estrogen receptor (ER) negative status and lymphovascular invasion (LVI) all are independently signifi-

cant factors of LR.¹⁸⁻²⁰ Multidisciplinary therapy, including PMRT, should be considered to apply in this subgroup for optimal local control and possible survival benefit. Subsequent studies need to identify the risk factors of LR, in order to clarify actual benefits from PMRT in different subgroups.

The aim of our study is to find the predictive markers of the indication of PMRT in patients with T1-2 and 1-3 positive LN. In addition, for patients with known risk factors, we also examined the differences of LRR and OS whether PMRT was performed or not.

Patients and methods

Patients

With the permission from institutional review board, we retrospectively reviewed medical records of patients who were pathologically diagnosed with T1-T2 and N1 staged invasive breast cancer at the Kaohsiung Chang Gung Memorial Hospital between Jan. 2000 and Dec. 2006. A total of 207 patients received modified radical mastectomy (MRM) or simple mastectomy, with or without PMRT were included consecutively.

The basic characteristics of patients included age, histopathology, size of primary tumor (T1 or T2), numbers of removed and involved LN, LVI, ER, Her-2/neu status and types of systemic therapy. The location and timing of recurrence, together with date of death, were recorded to define locoregional recurrence (LR), distant recurrence (DR) and OS. LR was defined as recurrent tumors at residual breast, previous operation area, ipsilateral chest wall and clinical or radiographic proved lymphadenopathy over regional lymphatics (ipsilateral axillary, supraclavicular, internal mammary LN).

Treatments

All patients underwent mastectomy with axillary LN dissection. External-beam irradiation was delivered with a total dose of 45-50.4 Gy in 25-28 fractions, and a subsequent 10-14 Gy boost to tumor bed if pathologically positive or close base margin (< 2mm). The fields of irradiation included tumor bed, chest wall, axillary and supraclavicular nodes. The internal mammary nodes were irradiated only if tumor located in medial side.

Adjuvant chemotherapy was chosen by clinicians in view of the characteristics of patients and tumors. The most commonly used regimens were anthracycline-based regimen and cyclophospha-

TABLE 1. Clinicopathologic characteristics of patient, tumor and treatment

Characteristics	Radiotherapy	No Radiotherapy	p value
No. of patients	81	126	
Age			
Median (years)	50.75	50.43	0.83
< 40	9	20	
≥ 40	72	106	
Histology			
Invasive ductal carcinoma	71	112	0.83
Others	10	14	
Tumor size (T)			
T1	26	48	0.46
T2	55	78	
No. of positive lymph nodes			
1	41	56	0.46
2	21	43	
3	19	27	
Percentage of positive lymph nodes			
< 25%	65	112	0.11
≥ 25%	16	14	
Estrogen receptor status			
Positive	55	82	0.65
Negative	25	43	
Unknown	1	1	
Her-2/neu status			
Over-expressed	19	24	0.72
Not over-expressed	56	84	
Unknown	6	18	
Lymphovascular invasion			
Presence	46	59	0.41
Absence	21	36	
Unknown	14	31	
Adjuvant chemotherapy			
Yes	76	112	0.33
No	5	14	
Adjuvant hormone therapy			
Yes	56	90	0.91
No	24	35	
Unknown	1	1	

PMRT = postmastectomy radiotherapy

mid/methotrexate/5-fluorouracil (CMF). Patients with positive ER status would take at least 5-year of adjuvant endocrine therapy unless known contraindication or intolerance.

Statistical analysis

To compare the clinicopathologic characteristics of tumors and patients between two study cohorts, we used Chi-square and Fisher's exact test for categorical variables. The 5-year estimates of LRR, DRR and OS were computed by Kaplan-Meier methods and log-rank tests to determine statistic significance. Cox proportional hazard modeling was used for multivariate analysis of LRR, DRR and OS. Factors such as age (< 40 or ≥ 40), histopathologic types (invasive ductal carcinoma or others), primary tumor size, percentage of positive LN (< 25% or ≥ 25%), ER and Her-2/neu status and adjuvant chemotherapy or PMRT were all included as parameters. P value < 0.05 was considered as statistic significance, and all tests were two-tailed. All analyses were performed by PASW software version 18.1 (IBM & SPSS Inc., Somers, NY, USA).

Results

Patients and treatment characteristics

The clinicopathologic characteristics of study cohort were shown as Table 1. A total of 207 breast cancer patients who were pathologically diagnosed with T1-2 tumors and N1 status were enrolled. The median follow-up was 59.5 months, and mean age at diagnosis was 50.6 years. All patients received modified radical mastectomy or simple total mastectomy with axillary LN dissection. Of these patients, 35.7% (N = 74) and 64.3% (N = 133) patients were with T1 and T2 tumors, respectively. The percentage of ER positive and Her-2/neu overexpression were 66.2% and 20.5%. The mean number of removed LN was 15.4 (range, 2-38). Eighty-one patients (39%) received PMRT, which was decided by clinicians or combined conference. Adjuvant systemic therapies, including chemotherapy and hormone therapy were administered in 90.8% and 70.5% of the patients, respectively, and 67.1% of patients received both treatments. There were 8 of 207 patients (3.8%) who did not receive any adjuvant chemotherapy, endocrine therapy, or irradiation. For Her-2/neu overexpression patients, none of them received adjuvant trastuzumab-based treatment.

TABLE 2. Five-year Kaplan-Meier analysis of locoregional recurrence rate, distant recurrence rate and overall survival by basic characteristics of patients and tumors

Characteristic	No. of patients	LRR		DRR		OS	
		%	P	%	P	%	P
Age (y)			0.003*		0.18		0.69
< 40	29	22±9.0%		30.3±9.7%		79.6±8.3%	
≥ 40	178	7±2.2%		17.7±3.1%		85.2±2.9%	
Pathology			0.50		0.52		0.78
Invasive ductal carcinoma	183	9.6±2.5%		18.4±3.2%		84.8±2.9%	
Others	24	5.9±5.7%		26.2±9.3%		81.3±8.6%	
T stage			0.64		0.23		0.27
T1	74	7.7±3.3%		14.0±4.3%		92.4±3.3%	
T2	133	10.1±3.1%		23.8±4.2%		80.2±3.8%	
Numbers of positive LN			0.34		0.22		0.87
1	97	4.7±2.3%		14.3±3.9%		84.8±3.9%	
2	64	15.4±5.4%		22.4±5.5%		85.7±4.7%	
3	46	10.3±4.9%		31.4±8.4%		81.5±6.4%	
% of Positive nodes			0.24		0.77		0.63
< 25%	177	7.7±2.2%		21.1±3.4%		83.1±3.1%	
≥ 25%	30	18.5±8.8%		15.3±7.1%		91.7±5.7%	
ER status			0.25		0.08		0.033*
Negative	68	11.0±4.3%		18.8±6.4%		76.8±5.5%	
Positive	137	8.2±2.6%		15.2±3.2%		87.9±3.1%	
Unknown	2						
Her-2/neu			0.016*		0.59		0.001*
Negative	140	6.2±2.3%		18.8±3.6%		89.2±2.9%	
Positive	43	19.4±6.7%		24.7±7.5%		71.9±7.3%	
Unknown	24						
LVI			0.62		0.026*		0.01*
Negative	57	6.1±3.4%		3.9±2.7%		96.4±2.5%	
Positive	105	9.7±3.3%		21.1±4.4%		82.7±4.0%	
Unknown	45						
Adjuvant Chemotherapy			0.94		0.16		0.29
No	19	6.2±6.1%		38.1±14.1%		68.9±13.1%	
Yes	188	9.2±2.4%		18.7±3.1%		85.8±2.7%	
PMRT			0.11		0.94		0.92
No	126	11.8±3.2%		20.3±3.9%		83.8±3.5%	
Yes	81	4.7±2.7%		22.9±6.3%		85.6±4.4%	

LRR = locoregional recurrence rate; DRR = distant recurrence rate; OS = overall survival; ER = estrogen receptor; LVI = lymphovascular invasion;

*p < 0.05

Risk factors for locoregional recurrence, distant recurrence and overall survival

Overall, 16 patients (7.7%) experienced locoregional recurrence: 12 patients recurred on ipsilateral chest wall, two in axillary LN, and the other two

patients recurred in supraclavicular LN. The median interval between surgery and locoregional recurrence was 27.9 months (5 to 82 months). Forty of 207 patients (19.3%) developed distant metastasis. Bone, liver and lung metastasis accounted for the

most common metastatic sites. Thirty-four patients (16.4%) died during the follow-up.

The relationship between the 5-year LRR, DRR, OS and clinicopathologic characteristics are shown in Table 2. On univariate analysis, young patients ($p = 0.003$), defined as age less than 40 years, and Her2/neu over-expression ($p = 0.016$) were significantly related to higher LRR. Presence of LVI was related to higher DRR ($p = 0.026$). PMRT demonstrated a non-significant, marginal trend of reducing 5-year LRR (from 11.8% to 4.7%, $p = 0.1$). There were several significant factors correlated with worse 5-year OS, including negativity of ER status ($p = 0.033$), over-expression of Her-2/neu ($p = 0.001$) and presence of LVI ($p = 0.01$). PMRT did not show significance in affecting 5-year OS ($p = 0.918$).

On multivariate analysis, shown in Table 3, young age patients (HR, 6.53, 95% CI, 1.82-23.38; $p = 0.004$) and Her-2/neu over-expression (HR, 6.6; 95% CI, 1.79-24.28; $p = 0.005$) were still associated with higher LRR. Adjuvant chemotherapy, positivity of ER status and LVI showed a non-significant trend of lower incidence of DR. Her-2/neu over-expression (HR, 4.01, 95% CI, 1.64-9.84; $p = 0.002$) and presence of LVI (HR, 4.99; 95% CI, 1.16-21.55; $p = 0.031$) were associated with inferior OS significantly.

Subgroup analysis of LRR and OS in patients treated with or without PMRT

We consequently examined the effect of PMRT on LRR and OS in subgroups. PMRT reduced LR significantly in patients with >25% positive LN ($p = 0.033$) and in presence of LVI ($p = 0.049$). Positive LVI was also a predictive marker of better OS if adding PMRT to T1-2 and N1 breast cancer patients ($p = 0.047$). Although young age and Her2/neu overexpression were independent risk factors of LR, PMRT did not improve LR in such high-risk patients. These results were shown as Table 4.

Discussion

Curing patients is the paramount goal of treating early breast cancers. Improvement of local-regional control often translates into better survival, not only in eradicating residual local malignant cells but also in reducing distant metastasis.^{21,22} The EBCTCG study had analyzed more than 42,000 patients, which showed 19% reduction of 5-year LR risks with PMRT would also reduce 5% risk of 15-year breast cancer mortality.⁸ Although a validated merit of PMRT was confirmed, delayed com-

plications from irradiation including secondary malignancy, cardiac toxicity, lymphedema, skin fibrosis and so on, should be taken into consideration.⁴¹ Thus, to avoid unnecessary irradiation, it is reasonable to choose patients with high risk of LR to apply PMRT, also to find subgroups of patients who can get benefits from PMRT.

Several predictive markers of LR have been widely discussed. Patients with larger tumor, advanced nodal status, presence of extracapsular extension, positive of LVI, high grade, involvement of the skin, nipple or pectoral fascia, and close or positive resection margins all had been reported to associate with higher risks of recurrence.^{14,22-24} Therefore, the current consensus by the American Society of Clinical Oncology and other guidelines recommend patients with T3-4 or N2 should receive adjuvant chemotherapy and PMRT definitely if no contraindication.⁹ On the contrast, for patients with T1-2 tumors and 1-3 positive LNs, there are getting more and more debates about whether adjuvant PMRT is needed. The reason of such chaos is because of different intrinsic characteristics of different breast cancers. If we do the Oncotype DX[®] or MammaPrint[®] test, we also can see not every patient with positive LN needs adjuvant chemotherapy. But for patients with T1-2 and N1 breast cancer who received total mastectomy, there are still no definite predictive markers for PMRT.

With a retrospective analysis of 8,106 patients enrolled in 13 randomized trials, the 10-year cumulative incidence > 15% for chest wall recurrence in patients with 1-3 positive nodes were age < 40, peritumoral vessel invasion or 0-7 uninvolved nodes. In this study, all patients were PMRT naïve. One of the conclusions proved in patients with 1-3 positive nodes, chest wall PMRT should be considered in patients aged < 40 years, with 0-7 uninvolved nodes or with vascular invasion.²⁵ Hunt *et al.* also reported that young age was a risk factor of local recurrence in T1-2 and N0 patients.²⁶ In our analysis, the LRR of T1-2 and N1 breast cancer was only 7.7%. Age less than 40 was one of the risk factors of LR, which was compatible with previous reports. Although PMRT did not improve LRR in young age group in our study, small case number might be the major reason of statistic insignificance.

Her-2/neu overexpression, a well-known predictive marker in distant metastasis, is seldom allocated to risk factors of local recurrence from literature review. Currently almost all patients in this group will receive trastuzumab-based adjuvant chemotherapy, which can decrease the chance of distant recurrence but not clearly beneficial on local recur-

TABLE 3. Multivariate analysis of locoregional recurrence, distant recurrence and overall survival

Variable	LRR		DRR		OS	
	P	HR (95% CI)	P	HR (95% CI)	P	HR (95% CI)
Age (≥ 40 vs. < 40)	0.004*	0.15 (0.04-0.55)	NS		NS	
% Positive nodes ($>25\%$ vs. $\leq 25\%$)	NS (0.064)	3.87 (0.92-16.23)	NS		NS	
ER status (Positive vs. negative)	NS		NS (0.061)	0.45 (0.19-1.04)	NS	
Her-2/neu (Positive vs. negative)	0.005*	6.6 (1.8-24.28)	NS		0.002*	4.01 (1.63-9.84)
LVI (Positive vs. negative)	NS		NS (0.056)	2.92 (0.97-8.76)	0.031*	4.99 (1.16-21.55)
Adjuvant chemotherapy (Yes vs. no)	NS		NS (0.067)	0.36 (0.12-1.08)	NS	
PMRT (Yes vs. no)	NS (0.30)		NS (0.92)		NS (0.23)	

LRR = locoregional recurrence rate; DRR = distant recurrence rate; NS = Non-significant; OS = overall survival; ER = estrogen receptor; LVI = lymphovascular invasion; HR = hazard ratio; CI = confidence interval, PMRT=Postmastectomy radiotherapy;

* p < 0.05

rence. Albert *et al.* retrospectively reviewed 911 T1a-bN0 breast cancer patients who had received definite treatment including surgery and adjuvant chemotherapy. The 8-year LRR were greater in the patients with Her-2/neu-positive (17.5% vs. 3.9%, $p = 0.009$) tumors.²⁷ In our study, there were 43 Her-2/neu overexpression patients, and none of them received adjuvant trastuzumab therapy. The reason for lack of adjuvant trastuzumab is that during the period of study enrollment (January 2000 to December 2006), the concept of adjuvant trastuzumab had not been built up. Our study corroborated Her-2/neu-positive tumor was associated with higher LR, however, PMRT failed to add benefits in locoregional control. The reason of radioresistance was supported by preclinical studies; in addition, adding anti-Her-2/neu monoclonal antibody can reverse resistance to irradiation.^{28,29}

Another risk factor of LR in Karlsson's study was 0-7 uninvolved LN. Fewer uninvolved LN might be associated with inadequate surgical sampling or pathological examination. Similar result was reported by Duraker *et al.*, who reported fewer removed LN was associated with worse survival.³⁰ An indirect method to evaluate the adequacy of removed LN is the ratio of positive LN of all removed LN.³⁰⁻³³ In our analysis, we also found that PMRT can significantly reduce LR in T1-2, N1 breast cancers with ratio > 0.25 of positive LN. We believe ratio 0.25 can be used as an indicator for PMRT, but it is only suitable for patients who received axillary LN dissection. Besides, there is accumulating

data to suggest PMRT, with the coverage of level I-II lymph node areas, can lower the rate of axillary recurrences in patients with positive sentinel LN without LN dissection. This makes PMRT even more important and deservedly.³⁴

Lymphovascular invasion has been confirmed as an independent poor prognostic factor in patients with invasive breast cancer.^{35,36} The prognostic role of LVI was reported independent of menopausal and LN status, tumor size, tumor grade, or adjuvant treatments. Breast cancers with LVI are candidates for more intensive adjuvant therapies.²⁰ Trovo *et al.* analyzed 150 stages I-II breast cancer patients treated with radical mastectomy without adjuvant irradiation. They found statistically significant factors associated with increased risk of LR were premenopausal status ($p = 0.004$), ER negative ($p = 0.02$), grade 3 ($p = 0.02$), and LVI ($p = 0.001$). They assumed PMRT might be beneficial in patients within these subsets.³⁷ In our analysis, we found the presence of LVI significantly related to DR ($p = 0.026$), which also translated to worse OS ($p = 0.01$). Although LVI did not directly related to LR in our report, PMRT could reduce LR in the presence of LVI ($p = 0.049$), just as Trovo *et al.* supposed.

The major debate of PMRT has been focused on whether it should be applied to all T1-2 and N1 breast cancer patients, regardless stratification of high risks. In contrast to DBCG and British Columbia trials, a Japanese study found that PMRT did not offer better locoregional control and OS in patients with 1-3 positive LN who received

TABLE 4. Analysis of clinical benefits on local regional recurrence and overall survival from PMRT

Characteristic (case numbers)	PMRT	LRR		OS	
		%	p	%	p
Age (y)					
< 40 (29)	No	25	0.6	75	0.37
	Yes	11.1		88.9	
≥ 40 (178)	No	7.5	0.16	84	0.64
	Yes	2.8		84.7	
Pathology					
Invasive ductal carcinoma (183)	No	10.7	0.14	82.1	0.83
	Yes	4.2		85.9	
Others (24)	No	7.1	0.46	85.7	0.4
	Yes	0		80	
T stage					
T1 (74)	No	10.4	0.088	85.4	0.28
	Yes	0		92.3	
T2 (133)	No	10.3	0.42	80.8	0.83
	Yes	5.5		81.8	
Numbers of positive LN					
1 (97)	No	7.1	0.42	85.7	0.77
	Yes	2.4		85.4	
2 (63)	No	11.6	0.82	81.4	0.8
	Yes	9.5		85.7	
3 (46)	No	14.8	0.085	77.8	0.67
	Yes	0		84.2	
% of positive nodes					
< 25% (177)	No	8	0.46	82.1	0.8
	Yes	4.4		86.2	
≥ 25% (30)	No	28.6	0.033*	85.7	0.37
	Yes	0		81.3	
ER status					
Negative (68)	No	14	0.24	74.4	0.97
	Yes	4		76	
Positive (137)	No	8.5	0.27	86.6	0.96
	Yes	3.6		89.1	
Her-2/neu status					
Negative (140)	No	7.1	0.43	89.3	0.48
	Yes	3.6		87.5	
Positive (43)	No	25	0.1	58.3	0.45
	Yes	5.3		78.9	
LVI status					
Negative (57)	No	5.6	0.53	97.2	0.24
	Yes	9.5		90.5	
Positive (105)	No	11.9	0.049*	72.9	0.047*
	Yes	2.2		89.1	

LRR = locoregional recurrence rate; OS = overall survival; ER = estrogen receptor; LVI = lymphovascular invasion; PMRT=Postmastectomy radiotherapy;

*p < 0.05

systemic therapy and adequate dissection.³⁸ The recent published study by Yang *et al.* who analyzed 544 T1-2 N1 breast cancer patients with or without PMRT has shown significant reduction of LR and improvement of OS in ER negative and LVI positive patients.³⁹ Kyndi *et al.* had analyzed 1,000 of the 3,083 patients in the DBCG 82b & c stratified by ER, PgR and Her-2/neu status. In contrast to Yang's result, PMRT did not have a survival benefit in ER negative cohort.⁴⁰ Our study examined the effects of PMRT on 207 cases of T1-2, N1 breast cancer patients who received total mastectomy. Although PMRT didn't influence results of LR and OS in general cohort and may not be routinely applied to be a part of adjuvant treatments, in patients with known risks such as >25% positive LN and LVI present, PMRT certainly reduced locoregional recurrence. Moreover, PMRT significantly improved 5-year OS in LVI positive patients. It makes sense to offer PMRT in selected patients.

Our report possesses several limitations. Firstly, a 5-year observation period is not long enough to precisely predict survival outcome. Secondly, the retrospective nature and small sample size of study have limited statistic power. Due to lack of prospective studies up to now, several large phase III randomized trials are ongoing to solve this issue. The MA 25 study is designed to enroll stage II patients with 1-3 positive nodes treated with radiotherapy versus observation only after mastectomy and adjuvant chemotherapy (NCT00005983). The other trial, SUPREMO study, has been activated recently in order to compare overall survival between PMRT and observation in patients with pT1-2N1 or pT2N0 with histological grade III or LVI positive tumors (NCT00966888). We hope the results will end to long-standing debate.

In conclusion, our work confirmed previous studies that risk factors, including negativity of ER, Her2/neu over-expression, young age and presence of LVI correlated with poor survival outcome and higher locoregional recurrence. In patients with T1-2 and N1 breast cancer, although PMRT by itself is of limited value in establishing locoregional control and OS, it should still be considered in high-risk patients such as with lymphovascular invasion, which will bring on better locoregional control and longer survival.

Acknowledgments

The authors thank all patients who participated in this study, and the team of breast cancer working

group at cancer center. This work was supported by Chang Gung Memorial Hospital [CMRPG870691].

References

- Ragaz J, Olivetto IA, Spinelli JJ, Phillips N, Jackson SM, Wilson KS, et al. Locoregional radiation therapy in patients with high-risk breast cancer receiving adjuvant chemotherapy: 20-year results of the British Columbia randomized trial. *J Natl Cancer Inst* 2005; **97**: 116-26.
- Overgaard M, Jensen MB, Overgaard J, Hansen PS, Rose C, Andersson M, et al. Postoperative radiotherapy in high-risk postmenopausal breast-cancer patients given adjuvant tamoxifen: Danish Breast Cancer Cooperative Group DBCG 82c randomised trial. *Lancet* 1999; **353**: 1641-8.
- Ragaz J, Jackson SM, Le N, Plenderleith IH, Spinelli JJ, Basco VE, et al. Adjuvant radiotherapy and chemotherapy in node-positive premenopausal women with breast cancer. *N Engl J Med* 1997; **337**: 956-62.
- Overgaard M, Hansen PS, Overgaard J, Rose C, Andersson M, Bach F, et al. Postoperative radiotherapy in high-risk premenopausal women with breast cancer who receive adjuvant chemotherapy. Danish Breast Cancer Cooperative Group 82b Trial. *N Engl J Med* 1997; **337**: 949-55.
- Gebski V, Lagleva M, Keech A, Simes J, Langlands AO. Survival effects of post-mastectomy adjuvant radiation therapy using biologically equivalent doses: a clinical perspective. *J Natl Cancer Inst* 2006; **98**: 26-38.
- Van de Steene J, Vinh-Hung V, Cutuli B, Storme G. Adjuvant radiotherapy for breast cancer: effects of longer follow-up. *Radiother Oncol* 2004; **72**: 35-43.
- Whelan TJ, Julian J, Wright J, Jadad AR, Levine ML. Does locoregional radiation therapy improve survival in breast cancer? A meta-analysis. *J Clin Oncol* 2000; **18**: 1220-9.
- Clarke M, Collins R, Darby S, Davies C, Elphinstone P, Evans E, et al. Effects of radiotherapy and of differences in the extent of surgery for early breast cancer on local recurrence and 15-year survival: an overview of the randomised trials. *Lancet* 2005; **366**: 2087-106.
- Recht A, Edge SB, Solin LJ, Robinson DS, Estabrook A, Fine RE, et al. Postmastectomy radiotherapy: clinical practice guidelines of the American Society of Clinical Oncology. *J Clin Oncol* 2001; **19**: 1539-69.
- Gnant M, Harbeck N, Thomssen C. St. Gallen 2011: Summary of the consensus discussion. *Breast Care* 2011; **6**: 136-41.
- Vélez-García E, Carpenter JT, Moore M, Vogel CL, Marcial V, Ketcham A, et al. Postsurgical adjuvant chemotherapy with or without radiotherapy in women with breast cancer and positive axillary nodes: a South-Eastern Cancer Study Group (SEG) Trial. *Eur J Cancer* 1992; **28**: 1833-7.
- McArdle CS, Crawford D, Dykes EH, Calman KC, Hole D, Russell AR, et al. Adjuvant radiotherapy and chemotherapy in breast cancer. *Br J Surg* 1986; **73**: 264-6.
- Taghian A, Jeong J-H, Mamounas E, Anderson S, Bryant J, Deutsch M, et al. Patterns of locoregional failure in patients with operable breast cancer treated by mastectomy and adjuvant chemotherapy with or without tamoxifen and without radiotherapy: results from five National surgical adjuvant breast and bowel project randomized clinical trials. *J Clin Oncol* 2004; **22**: 4247-54.
- Wallgren A, Bonetti M, Gelber RD, Goldhirsch A, Castiglione-Gertsch M, Holmberg SB, et al. Risk factors for locoregional recurrence among breast cancer patients: results from International Breast Cancer Study Group Trials I through VII. *J Clin Oncol* 2003; **21**: 1205-13.
- Katz A, Strom EA, Buchholz TA, Thames HD, Smith CD, Jhingran A, et al. Locoregional recurrence patterns after mastectomy and doxorubicin-based chemotherapy: implications for postoperative irradiation. *J Clin Oncol* 2000; **18**: 2817-27.
- Recht A, Gray R, Davidson NE, Fowble BL, Solin LJ, Cummings FJ, et al. Locoregional failure 10 years after mastectomy and adjuvant chemotherapy with or without tamoxifen without irradiation: experience of the Eastern Cooperative Oncology Group. *J Clin Oncol* 1999; **17**: 1689-700.
- Overgaard M, Nielsen HM, Overgaard J. Is the benefit of postmastectomy irradiation limited to patients with four or more positive nodes, as recommended in international consensus reports? A subgroup analysis of the DBCG 82 b&c randomized trials. *Radiother Oncol* 2007; **82**: 247-53.

18. Truong PT, Lesperance M, Culhaci A, Kader HA, Speers CH, Olivotto IA. Patient subsets with T1-T2, node-negative breast cancer at high locoregional recurrence risk after mastectomy. *Int J Radiat Oncol Biol Phys* 2005; **62**: 175-82.
19. Truong PT, Berthelet E, Lee J, Kader HA, Olivotto IA. The prognostic significance of the percentage of positive/dissected axillary lymph nodes in breast cancer recurrence and survival in patients with one to three positive axillary lymph nodes. *Cancer* 2005; **103**: 2006-14.
20. Lauria R, Perrone F, Carlomagno C, De Laurentiis M, Morabito A, Gallo C, et al. The prognostic value of lymphatic and blood vessel invasion in operable breast cancer. *Cancer* 1995; **76**: 1772-8.
21. Yildirim E, Berberoglu U. Local recurrence in breast carcinoma patients with T(1-2) and 1-3 positive nodes: indications for radiotherapy. *Eur J Surg Oncol* 2007; **33**: 28-32.
22. Cheng JC-H, Chen CM, Liu MC, Tsou MH, Yang PS, Jian JJ-M, et al. Locoregional failure of postmastectomy patients with 1-3 positive axillary lymph nodes without adjuvant radiotherapy. *Int J Radiat Oncol Biol Phys* 2002; **52**: 980-8.
23. Katz A, Strom EA, Buchholz TA, Theriault R, Singletary SE, McNeese MD. The influence of pathologic tumor characteristics on locoregional recurrence rates following mastectomy. *Int J Radiat Oncol Biol Phys* 2001; **50**: 735-42.
24. Jager JJ, Volovics L, Schouten LJ, de Jong JM, Hupperets PS, von Meyenfeldt MF, et al. Loco-regional recurrences after mastectomy in breast cancer: prognostic factors and implications for postoperative irradiation. *Radiother Oncol* 1999; **50**: 267-75.
25. Karlsson P, Cole BF, Chua BH, Price KN, Lindtner J, Collins JP, et al. Patterns and risk factors for locoregional failures after mastectomy for breast cancer: an International Breast Cancer Study Group report. *Ann Oncol* 2012; **23**: 2852-8.
26. Hunt KK, Ballman KV, McCall LM, Boughey JC, Mittendorf EA, Cox CE, et al. Factors associated with local-regional recurrence after a negative sentinel node dissection. *Ann Surg* 2012; **256**: 428-36.
27. Albert JM, Gonzalez-Angulo AM, Guray M, Sahin A, Strom EA, Tereffe W, et al. Estrogen/progesterone receptor negativity and HER2 positivity predict locoregional recurrence in patients with T1a,bN0 breast cancer. *Int J Radiat Oncol Biol Phys* 2010; **77**: 1296-302.
28. Pietras RJ, Poen JC, Gallardo D, Wongvipat PN, Lee HJ, Slamon DJ. Monoclonal antibody to HER-2/neureceptor modulates repair of radiation-induced DNA damage and enhances radiosensitivity of human breast cancer cells overexpressing this oncogene. *Cancer Res* 1999; **59**: 1347-55.
29. Pirolo KF, Tong YA, Villegas Z, Chen Y, Chang EH. Oncogene-transformed NIH 3T3 cells display radiation resistance levels indicative of a signal transduction pathway leading to the radiation-resistant phenotype. *Radiat Res* 1993; **135**: 234-43.
30. Duraker N, Demir D, Bati B, Yilmaz BD, Bati Y, Caynak ZC, et al. Survival benefit of post-mastectomy radiotherapy in breast carcinoma patients with T1-2 tumor and 1-3 axillary lymph node(s) metastasis. *Jpn J Clin Oncol* 2012; **42**: 601-8.
31. Song YJ, Shin SH, Cho JS, Park MH, Yoon JH, Jegal YJ. The Role of Lymphovascular invasion as a prognostic factor in patients with lymph node-positive operable invasive breast cancer. *J Breast Cancer* 2011; **14**: 198-203.
32. Duraker N, Bati B, Demir D, Caynak ZC. Prognostic significance of the number of removed and metastatic lymph nodes and lymph node ratio in breast carcinoma patients with 1-3 axillary lymph node(s) metastasis. *Oncology* 2011; **2011**: 1-10.
33. Truong PT, Olivotto IA, Kader HA, Panades M, Speers CH, Berthelet E. Selecting breast cancer patients with T1-T2 tumors and one to three positive axillary nodes at high postmastectomy locoregional recurrence risk for adjuvant radiotherapy. *Int J Radiat Oncol Biol Phys* 2005; **61**: 1337-47.
34. Nitsche M, Hermann R. Axillary irradiation as an imperative alternative to axillary dissection in clinically lymph node-negative but sentinel node-positive breast cancer patients? *Breast Care* 2011; **6**: 353-8.
35. Woo CS, Silberman H, Nakamura SK, Ye W, Sposto R, Colburn W, et al. Lymph node status combined with lymphovascular invasion creates a more powerful tool for predicting outcome in patients with invasive breast cancer. *Am J Surg* 2002; **184**: 337-40.
36. McCready DR, Chapman JA, Hanna WM, Kahn HJ, Murray D, Fish EB, et al. Factors affecting distant disease-free survival for primary invasive breast cancer: use of a log-normal survival model. *Ann Surg Oncol* 2000; **7**: 416-26.
37. Trovo M, Durofil E, Polesel J, Roncadin M, Perin T, Mileto M, et al. Locoregional failure in early-stage breast cancer patients treated with radical mastectomy and adjuvant systemic therapy: Which patients benefit from postmastectomy irradiation? *Int J Radiat Oncol Biol Phys* 2012; **83**: e153-e157.
38. Nagao T, Kinoshita T, Tamura N, Hojo T, Morota M, Kagami Y. Locoregional recurrence risk factors in breast cancer patients with positive axillary lymph nodes and the impact of postmastectomy radiotherapy. *Int J Clin Oncol* 2013; **18**: 54-61.
39. Yang PS, Chen CM, Liu MC, Jian JM, Horng CF, Liu MJ, et al. Radiotherapy can decrease locoregional recurrence and increase survival in mastectomy patients with T1 to T2 breast cancer and one to three positive nodes with negative estrogen receptor and positive lymphovascular invasion status. *Int J Radiat Oncol Biol Phys* 2010; **77**: 516-22.
40. Kyndi M, Sørensen FB, Knudsen H, Overgaard M, Nielsen HM, Overgaard J, et al. Estrogen receptor, progesterone receptor, HER-2, and response to postmastectomy radiotherapy in high-risk breast cancer: the Danish Breast Cancer Cooperative Group. *J Clin Oncol* 2008; **26**: 1419-26.
41. Rucigaj TP, Leskovec NK, Zunter VT. Lymphedema following cancer therapy in Slovenia: a frequently overlooked condition? *Radiol Oncol* 2010; **44**: 244-8.

MRI to delineate the gross tumor volume of nasopharyngeal cancers: which sequences and planes should be used?

Aron Popovtzer¹, Mohannad Ibrahim², Daniel Tatro¹, Felix Y. Feng¹, Randall K. Ten Haken¹, Avraham Eisbruch¹

¹ Department of Radiation Oncology, University of Michigan, Ann Arbor, USA

² Department of Radiology, University of Michigan, Ann Arbor, USA

Radiol Oncol 2014; 48(3): 323-330.

Received: 2 December 2013

Accepted: 2 March 2014

Correspondence to: Avraham Eisbruch, M.D., Department of Radiation Oncology, 1500 E Med Ctr Dr, Ann Arbor MI 48109, USA.
E-mail: eisbruch@umich.edu

Disclosure: No potential conflicts of interest were disclosed.

Background. Magnetic resonance imaging (MRI) has been found to be better than computed tomography for defining the extent of primary gross tumor volume (GTV) in advanced nasopharyngeal cancer. It is routinely applied for target delineation in planning radiotherapy. However, the specific MRI sequences/planes that should be used are unknown.

Methods. Twelve patients with nasopharyngeal cancer underwent primary GTV evaluation with gadolinium-enhanced axial T1 weighted image (T1) and T2 weighted image (T2), coronal T1, and sagittal T1 sequences. Each sequence was registered with the planning computed tomography scans. Planning target volumes (PTVs) were derived by uniform expansions of the GTVs. The volumes encompassed by the various sequences/planes, and the volumes common to all sequences/planes, were compared quantitatively and anatomically to the volume delineated by the commonly used axial T1-based dataset.

Results. Addition of the axial T2 sequence increased the axial T1-based GTV by 12% on average ($p = 0.004$), and composite evaluations that included the coronal T1 and sagittal T1 planes increased the axial T1-based GTVs by 30% on average ($p = 0.003$). The axial T1-based PTVs were increased by 20% by the additional sequences ($p = 0.04$). Each sequence/plane added unique volume extensions. The GTVs common to all the T1 planes accounted for 38% of the total volumes of all the T1 planes. Anatomically, addition of the coronal and sagittal-based GTVs extended the axial T1-based GTV caudally and cranially, notably to the base of the skull.

Conclusions. Adding MRI planes and sequences to the traditional axial T1 sequence yields significant quantitative and anatomically important extensions of the GTVs and PTVs. For accurate target delineation in nasopharyngeal cancer, we recommend that GTVs be outlined in all MRI sequences/planes and registered with the planning computed tomography scans.

Key words: gross tumor volume; MRI; nasopharyngeal cancer; radiotherapy

Introduction

The introduction of intensity modulated radiation therapy (IMRT) has led to improvements in the treatment of nasopharyngeal cancer (NPC).¹⁻³ Traditionally, the treatment of all gross tumor was secured through large lateral opposed radiation fields that included the base of the skull and

adjacent tissues, with wide margins.⁴ By contrast, highly conformal techniques produce sharp dose fall-off gradients, sparing noninvolved tissues. Therefore, precise knowledge of the boundaries of the gross tumor volume (GTV) is crucial for defining the high-risk clinical target volume (CTV), and treatment must be carefully planned by imaging.

For evaluating tumor extent in advanced paranasal sinus cancer and NPC, magnetic resonance imaging (MRI) has been found to be better than computed tomography (CT).⁵⁻¹³ It more accurately demonstrates base-of-skull involvement, intracranial extension, involvement of the prevertebral fascia, and subtle marrow space infiltration.^{6,7,9} Some studies have suggested that in patients with NPC and cranial nerve involvement, the more accurate contouring associated with MRI translates into a survival advantage.⁸ Accordingly, many radiologists rely on MRI scans for determination of target volumes for purposes of radiotherapy.¹⁴⁻¹⁹

However, the optimal MRI dataset (imaging sequences) that should be used for planning radiotherapy has not been established. For tumor staging, studies emphasize the importance of axial T1-weighted images acquired with fat suppression, both with and without gadolinium contrast, in addition to T2-weighted images and the use of coronal and sagittal acquisition planes.⁸ Although some authors found that the coronal imaging planes added important information regarding the cranial extent of tumors^{7,19}, others reported that enhanced and nonenhanced T1 sequences were sufficient.²⁰

This issue is particularly important in modern treatment planning which increasingly supports some form of interactive or automated image registration. Many studies describing techniques in clinical series of IMRT for NPC, as well as the recent NPC protocol of the Radiation Therapy Oncology Group²⁰, recommended the registration and fusion of the MRI image with the planning CT scan whenever possible. However, they did not detail the MRI dataset used.^{1,14,15,21} Although Emami *et al.*⁶, in a comparative study of MRI and CT-based GTV delineation, used all MRI sequences, other studies that provided any specifics about the MRI methods applied for GTV delineation and fusion with the planning CT typically used axial T1-weighted images alone.²²

The aim of the present study was to determine if radiotherapy planning may be based solely on MRI axial T1 imaging or if information from all available MRI datasets is required for accurate target delineation.

Patients and methods

Patients and setting

The study group consisted of 12 patients treated for NPC in 2003-2007. The study was approved

by the institutional review board (IRB). The planning CT scans and pre-therapy MRI images were collected for analysis. The disease was categorized pathologically according to the classification of the World Health Organization (WHO) as type 3 in 9 patients, type 2 in 2 patients, and type 1 in 1 patient. Staging of the primary tumor was done according to published guidelines²³: 9 patients had stage T4 tumor, 1 had T3, and 2 had T2.

Procedure

The original CT treatment-planning scans were obtained at 3-mm slice thickness, and Intravenous contrast was injected in all cases. Patients were immobilized, scanned, and treated in the supine position, with the aid of a thermoplastic mask. CT-based sagittal, coronal, and oblique reconstruction images were made with the in-house radiation planning system. MRI was performed with a 1.5 Tesla GE Magnet scanner (Milwaukee, WI) using the regular head coil. The procedure was performed in the supine position, but neither a mask nor external markers were used. The imaging protocol was designed to obtain maximum information within a 1-1.5 h total scan time. T2-weighted sequences (TR/TE/excitations: 2000-2500 ms / 80-90 ms / 3) and T1-weighted sequences (TR/TE/excitations: 500-600 ms / 10-30 ms / 2-4) were acquired by standard spin-echo technique. Acquisition parameters of the axial and sagittal images were as follows: slice thickness 4 mm, slice gap 1 mm, field of view 20 cm with an image matrix of 256 x 256; parameters of the coronal images were slice thickness 3 mm, slice gap 0.5 mm, field of view 20 cm with an image matrix of 256 x 256. Four MRI datasets were studied: T2-weighted images in the axial plane without fat suppression (T2-AX, n = 12); gadolinium-enhanced T1-weighted images in the axial plane with (n = 10) and without (n = 2) fat suppression (T1-AX); gadolinium-enhanced T1-weighted images in the coronal plane (COR, n = 12); and unenhanced T1-weighted images in the sagittal plane (SAG, n = 11).

In order to minimize inter-observer differences, the GTVs of the primary tumors were defined on each of the 4 MRI datasets by consensus of a neuroradiologist and two head and neck radiation oncologists. To assess the reproducibility of the consensus-based contour delineation, the GTVs on all 4 datasets of 3 patients were redrawn by the same team 3 months after the first contouring session, without review or presentation of the original contours. The magnitude of change in GTV size and the overlapping volumes between contouring

sessions were noted and averaged. The percentage difference in GTV was defined according to the formula, $(GTV1-GTV2)/(GTV1+GTV2)/2 \times 100$, where GTV1 is the GTV outlined in the first session and GTV2 is the volume outlined in the second session, using the same MRI dataset.

Image registration

The CT data served as the basis for registration of the MRI data. Registration of each dataset was achieved in each case using a mutual information rigid translation algorithm.²⁴ Final registration was accomplished by simultaneously superimposing the intersection of the brain surface with the axial CT slices, with the reconstructed sagittal and coronal CT images as contours. The MRI brain surface was interactively translated and rotated through a series of 3-D MRI dataset coordinate transformations until satisfactory visual agreement between the MRI surface and the CT images was obtained. Particular attention was addressed to the fixed bony landmarks in the region: vertebral bodies of C1 and C2, hard palate, lateral and medial pterygoid plates, and the clinoid processes. In this manner, the GTV outlined on each MRI study was fused to the CT dataset for comparison of extension and overlap, both qualitatively (in terms of anatomical extent) and quantitatively (in terms of physical volume, after computation of encompassing and overlapping volumes).

Composite GTVs

Composite GTVs were formed by spatially adding the individual GTVs obtained by each MRI sequence and the physical volume (in cubic centimeters) of each composite structure. First, the COR and SAG datasets were assessed to determine if they added information to the traditional axial T1 image primarily, if they revealed potential GTV extensions attributable to differences in the imaging plane. The value of each composite GTV obtained from each MRI sequence was calculated. Second, two or more GTVs were combined, and the total volume (totV) and the common volume (comV), defined as volumes overlapping all sequences, were calculated. Three conditions were tested: T1-AX and T1-COR; T1-AX, T1-COR and T1-SAG; T1-AX and T2-AX). The T1-based volumes (standard) were compared to the additional volumes defined by the union of the COR and/or SAG datasets to the totV. Thereafter, the axial T2 datasets were compared to the axial T1 datasets to investigate

TABLE 1. Volume Percentage differences between the initial GTVs and the re-drawn GTVs for 3 cases for all sequences (average difference across all planes/sequences = 1.5%)

	% Diff. GTV SIZES			
	Sag (%)	T1 (%)	Cor (%)	T2 (%)
PATIENT 1	4.1	1.9	-0.5	-3.6
PATIENT 2	-0.4	9.5	-4.3	-4.3
PATIENT 3	-8.2	15.4	0.1	8.3
Sequence Avg.	-1.5	8.9	-1.6	0.1

differences obtained in GTVs due to the different pulse sequences. A uniform 5-mm expansion of the GTVs was made to yield the corresponding CTVs, and an additional uniform 4-mm expansion was made to yield the PTVs of the primary tumors.

Anatomical assessment was performed by visual inspection of the axial and the reconstructed sagittal and coronal CT planes in each case, together with the different fused MRI-based GTVs. Any extension in any direction of more than 1 cm beyond the axial T1-based GTV borders, in which the volume would not be covered by the PTV, or similar underestimation, was considered potentially clinically significant.

GTVs outlined using different MRI sequences in the same patients were quantitatively compared by two-tailed paired t-tests. Statistical significance was set at $p < 0.05$.

Results

Reproducibility

The reproducibility of the GTV delineation was examined in each MRI sequence/plane in 3 patients. There was an average change of 1.5% between the re-drawn GTVs (GTV2s) and the initial drawings (GTV1s) (Table 1). Examination of the anatomical overlap between the GTV1s and GTV2s showed that the envelope (union) of GTV1 and GTV2 averaged 10% larger than the GTV1 (Table 2), and the overlap (intersection) of GTV1 and GTV2 averaged 90% of the GTV1. These results were considered to indicate satisfactory reproducibility.^{25,26}

GTV and PTV statistics

A summary of the GTV statistics for the T1 imaging planes is presented in Table 2 and Figures 1 and 2. In all cases, the T1-AX GTVs were larger than the

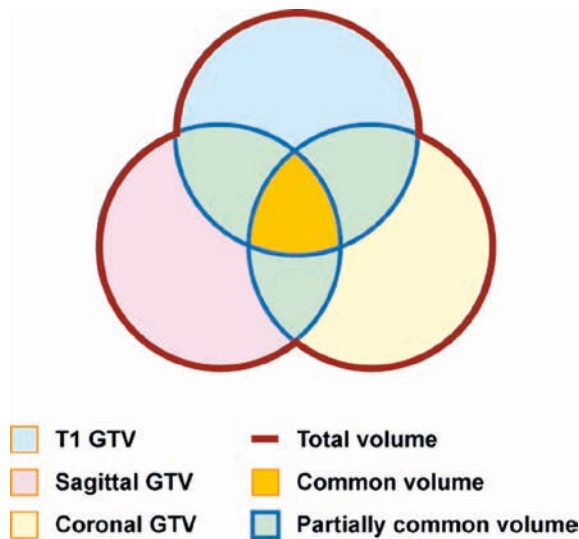


FIGURE 1. Differences among MRI sequences/planes. (A) Comparisons of gross tumor volume (GTVs) delineated by axial T1, axial T1+T2, and total axial T1+ sagittal + coronal T1 images for each patient. (B) Comparisons of total volume and axial T1-defined GTVs for each patient.

GTVs of the other sequences/planes, and the addition of both the COR and SAG studies yielded an extension of the GTV beyond that defined by the T1-AX dataset alone (Figure 1). On average, addition of the COR GTVs increased the T1-AX GTVs by 21% (SD = 18) ($p = 0.005$). Further addition of the SAG GTVs increased this combined volume by 10% (SD = 6) of the original T1-AX volume ($p = 0.003$), for an average combined increase of 30% over the original T1-AX volume. On average, 38%

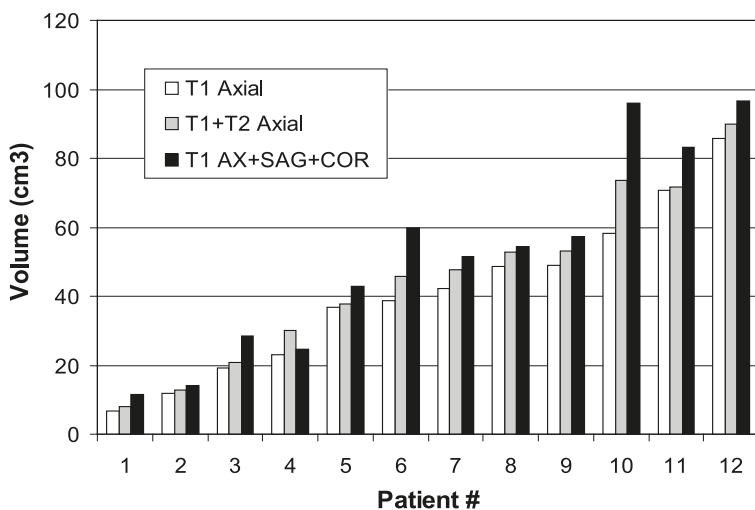


FIGURE 2. Comparisons of adding axial T2-defined GTVs to axial T1-defined gross tumor volume (GTVs) for each patient.

of the extended GTV volumes were common to all T1 sequences (Table 2).

A summary of the GTV statistics for the addition of T2-AX images to the T1-AX images is presented in Table 3 and Figure 2. On average, the GTVs derived from the T2-AX images increased the T1-AX GTVs by 12% (SD = 9) ($p = 0.004$).

A summary of the PTV statistics for all patients and all T1 imaging planes is presented in Table 4. As the PTVs were geometric expansions of the GTVs, the results were similar, but the percentage changes were smaller. On average, the addition of the COR PTVs increased the T1-AX PTVs by 14% (SD = 13) ($p = 0.002$), and the further addition of the SAG PTVs increased the combined volumes by 6% (SD = 4) ($p = 0.04$). On average, 50% (SD = 10) of the extended PTV volumes were common to both AX sequences and the COR and SAG sequences.

Volume increase relative to T stage

There was no substantial difference between advanced and early local tumors in the increase in GTVs with the addition of various MRI sequences to the T1-AX sequence. In the 10 patients with T3-4 disease, the addition of SAG and COR-based volumes extended the T1-AX-based volumes by an average of 27% (SD = 20). The addition of T2-AX-based GTVs extended the T1-based GTVs by 12% (SD = 9.8). In the 2 patients with T2a disease, the addition of the Cor- and SAG-based GTVs increased the T1-AX-based GTVs by 20% and 48%, and the addition of the T2-AX-based GTVs increased the T1-AX-based GTVs, by 18% and 8%.

Anatomical assessments

Table 5 shows the findings of the anatomical assessments of the extensions/ underestimations of the GTVs delineated by various MRI sequences or by T1-AX sequences alone. Representative cases are illustrated in Figures 3A-D. Addition of the COR-based images to the T1-AX sequences led to an extension of the caudal border of the GTV in 3 cases (Figure 3B) and of the cranial border in 2 cases; however, the COR images underestimated the posterior or anterior extent in 4 cases and the medial extent in 1 case (Table 5). Addition of the SAG images led to an extension of the superior and inferior borders of the GTVs in 2 cases (Figures 3A, 3C). Addition of the T2-AX images generally led to nonspecific extensions (in terms of direction) into soft tissue regions which were more subtly visualized than on the T1-AX images.

TABLE 2. GTVs derived from different T1 imaging planes

	Axial T1 (cm3)	COR T1 (cm3)	SAG T1 (cm3)	Total T1 (A+C+S) (cm3)	Total T1 (% of AX)	Common T1 (A&C&S) (cm3)	Common T1 (% of Total)
Mean	40.9	34.7	30.4	51.7	130.1%	21.2	38.3%
Range	7-86	6-76	6-60	12-97	107-170	3-47	18-55
STD	23.6	21.6	19.7	29.3	22.5%	14.0	10.9%

TABLE 3. GTVs derived from different T1 and T2 Axial imaging planes

	Axial T1 (cm3)	Axial T2 (cm3)	Total (T1+T2) (cm3)	Total (T1+T2) (% of T1 AX)	Common (T1&T2) (cm3)	Common (T1&T2) (% of Total)
Mean	40.9	32.7	45.3	112.3%	28.3	62.6%
Range	7-86	7-63	8-90	101-130	6-57	51-71
STD	23.6	21.6	25.1	9.1%	15.8	6.7%

TABLE 4. PTVs derived from different T1 imaging planes

	Axial T1 (cm3)	COR T1 (cm3)	SAG T1 (cm3)	Total T1 (A+C+S) (cm3)	Total T1 (% of AX)	Common T1 (A&C&S) (cm3)	Common T1 (% of Total)
Mean	136.0	117.5	103.6	160.9	120.1%	81.4	50.0%
Range	43-234	44-221	38-191	71-280	106-149	28-139	37-68
STD	57.7	52.6	49.4	68.9	16.7%	38.1	10.0%

There were 3 cases in which volumes based on different sequences and planes were almost identical qualitatively (Table 5, Figure 3D). In these cases, the comV:totV ratio was between 42% and 48%, and the addition of the COR and SAG images extended the T1-AX-based volume by 12–16%.

Anatomically, the superior extensions of the COR- and SAG-based GTVs led to the identification of cavernous sinus, brain, and clivus involvements in which subtle involvement was not appreciated on axial MRI (Figures 3A, 3C). Drawing the GTVs in the COR and SAG planes also aided in extending the targets caudally into muscles that were not included in the T1-AX-based GTVs (Figures 3B, 3C).

Discussion

In the radiology literature, there is a consensus regarding the necessity of performing MRI for staging nasopharyngeal tumors, and several authors have examined the benefits of different MRI

sequences in this setting.^{6,7,27} However, unlike the diagnostic radiologist who uses MRI to assess the extent of the gross tumor for staging purposes, the radiation oncologist requires an accurate definition of the edges of the radiological abnormalities in order to define the GTV in 3 dimensions as reliably as possible. To the best of our knowledge, the present study is the first to assess in detail the utility of various MRI sequences/planes in defining the GTVs of NPC. The results show that when the GTV data from the axial T2 sequence and coronal and sagittal planes were added to the gadolinium-enhanced axial T1 sequence, the size and extent of the GTVs increased significantly. It has been proven that there is a correlation between volume of tumor and outcome²⁸, and therefore the changes might have been large enough to have clinical importance as well. Notably, the main changes were in the caudal and cranial direction, including cavernous sinus involvement which was occasionally missed when the axial dataset was used alone. We suggest that as we do not know which dataset represents the “true” extent of the GTVs,

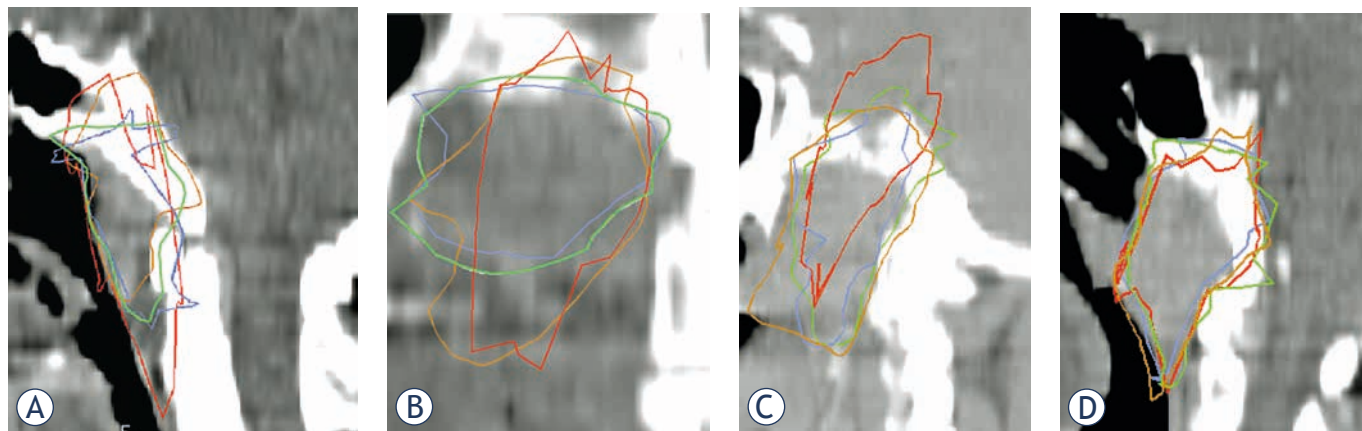


FIGURE 3. Gross tumor volume (GTVs) based on different MRI sequences fused into sagittal (A, C, D) or coronal (B) CT images. Brown = sagittal-based GTV; blue = axial T2-based GTV; red = coronal-based GTV; and green = axial T1-based GTV.

defining a composite GTV that encompasses the targets outlined using all datasets is the safest approach to defining the target for highly conformal radiotherapy of NPC. Our study suggests that if only axial images are available, the GTVs may be underestimated. Adding coronal and sagittal MRI images is expected to substantially improve target delineation. It is reasonable to continue the current study by analyzing the impact of MRI on radiation volume assessment when tumor delineation is performed in all three planes with the use of T1 sequence and fat suppression after administration of contrast. This will be the subject of future study.

These findings support previous diagnostic radiology studies, such as those of Chung *et al.*⁷ and Sakata *et al.*¹⁹, which suggested that coronal imaging plays a unique role in detecting cranial, base of skull, and clivus tumor extension. However, they disagree with the study of Lau *et al.*²⁰ which suggested that coronal, sagittal and axial T2-weighted images do not have an impact on tumor staging and are therefore redundant. We found that sagittal plane-based GTVs significantly increased the volume obtained by the coronal and axial-plane MRI, whereas Vogl *et al.*²⁷ stated that for staging purposes, the sagittal views had little impact and could be omitted. Furthermore, although Ng *et al.*⁹ suggested that for smaller tumors, relying only on axial T1 images is sufficient for staging purposes, our findings suggest that the addition of the coronal and sagittal views has a similarly important impact on GTV estimation in both early-stage and locally advanced tumors.

Previous studies of GTV measurements in head and neck cancers, including NPC, suggested prom-

TABLE 5. Anatomical GTV extents based on various MRI sequences compared with the axial T1-based GTVs

Direction of Extension	Coronal MRI	Sagittal MRI
Cranial	2+	2+
Caudal	3+	2+ & 2-
Medial	1-	2-
Lateral		3-
Posterior	3-	
Anterior	1-	

+ = No. of patients where the GTV border extended beyond the T1 axial GTV;

- = No. of patients where the GTV border underestimated compared to the T1 axial GTV (By at least 1 cm in each direction)

inent interobserver differences and smaller though still considerable intraobserver differences.^{25,26} To limit this problem in our study, the GTV was derived by consensus among several observers. The reproducibility of GTV delineation by the consensus members, as tested in our study, was reasonable, and the differences noted in the reproducibility test were substantially smaller than the differences in the GTVs that were related to the different MRI datasets.

This study was limited by the need to register MRI and CT scans made at different head and neck positions. The tight head and neck coil used for the clinical MRI scans did not accommodate the immobilization system used for the planning CT. The registration of MRI-based GTVs with the planning CTs using landmarks in the skull and base of the skull was previously found to be highly reliable for brain tumors and for tumors residing near the base

of the skull, and this technique has been used clinically in our department for many years. However, the caudal-most extension of the tumors, beyond the base of the skull, may have not been well registered, potentially leading to an error in our volumetric calculations. Nevertheless, the most important message of our study is that different MRI sequences may produce different extensions of the GTV cranially, toward the cavernous sinus and related anatomical structures, which may not be appreciated using the axial T1 sequence alone.

The ability to register non-axial MRI images into the axial planning CT dataset, as performed in this study, is available in the in-house treatment planning system used at our institution. Some commercial planning systems do not have this capability, although in many cases, manufacturers have come out with new versions that do (Bruce Curran, PhD, personal communication). Our results suggest that this capability should be used for multi-sequence delineation of GTVs of tumors near the base of the skull.

PTVs were obtained in this study by uniform expansions of the GTVs. As expected, there was a lesser difference between the axial T1 and multiple MRI sequences for PTVs than GTVs. We speculate that as PTV margins are tightened by daily localization and correction of the set-up uncertainties^{29,30}, the benefits of multi-sequence MRI for PTVs will be close to the ones found for GTVs.

In conclusion, using MRI for defining the primary NPC GTV, fusion of GTVs delineated on axial T1 sequences with coronal and sagittal images as well as with T2 sequences significantly changes the sizes and extents of the GTVs calculated on the basis of gadolinium-enhanced T1 axial images alone. These differences may have a major impact on GTV definition in some cases. Our results suggest that incorporating all MRI datasets in GTV delineation should be routine clinical practice in highly conformal radiation therapy.

Acknowledgement

This study was supported in part by NIH grant PO1 CA59827 and the Newman Family Foundation.

References

- Kam MK, Leung SF, Zee B, Chau RM, Suen JJ, Mo F, et al. Prospective randomized study of intensity-modulated radiotherapy on salivary gland function in early-stage nasopharyngeal carcinoma patients. *J Clin Oncol* 2007; **25**: 4873-9.
- Pow EH, Kwong DL, McMillan AS, Wong MC, Sham JS, Leung LH, et al. Xerostomia and quality of life after intensity modulated radiotherapy vs conventional radiotherapy for early stage nasopharyngeal carcinoma: Initial report on a randomized controlled trial. *Int J Radiat Oncol Biol Phys* 2006; **66**: 981-91.
- Sultanem K, Shu HK, Xia P, Akazawa C, Quivey JM, Verhey LJ, et al. Three-dimensional intensity-modulated radiotherapy in the treatment of nasopharyngeal carcinoma: the University of California-San Francisco experience. *Int J Radiat Oncol Biol Phys* 2000; **48**: 711-22.
- Al-Sarraf M, LeBlanc M, Giri PG, Fu KK, Cooper J, Vuong T, et al. Chemoradiotherapy versus radiotherapy in patients with advanced nasopharyngeal cancer: phase III randomized intergroup study 0099. *J Clin Oncol* 1998; **16**: 1310-7.
- Rasch C, Eisbruch A, Remeijer P. Irradiation of paranasal sinus tumors: a delineation and dose comparison study. *Int J Radiat Oncol Biol Phys* 2002; **52**: 120-7.
- Emami B, Sethi A, Petruzzelli GJ. Influence of MRI on target volume delineation and IMRT planning in nasopharyngeal carcinoma. *Int J Radiat Oncol Biol Phys* 2003; **57**: 481-8.
- Chung NN, Ting LL, Hsu WC, Lui LT, Wang PM. Impact of magnetic resonance imaging versus CT on nasopharyngeal carcinoma: primary tumor target delineation for radiotherapy. *Head Neck* 2004; **26**: 241-6.
- Chang JT, Lin CY, Chen TM, Kang CJ, Ng SH, Chen IH, et al. Nasopharyngeal carcinoma with cranial nerve palsy: the importance of MRI for radiotherapy. *Int J Radiat Oncol Biol Phys* 2005; **63**: 1354-60.
- Ng SH, Chang TC, Ko SF, Yen PS, Wan YL, Tang LM, et al. Nasopharyngeal carcinoma: MRI and CT assessment. *Neuroradiology* 1997; **39**: 741-6.
- Chen L, Liu LZ, Mao YP, Tang LL, Sun Y, Chen Y, et al. Grading of MRI-detected skull-base invasion in nasopharyngeal carcinoma and its prognostic value. *Head Neck* 2011; **33**: 1309-13.
- Liang SB, Sun Y, Liu LZ, Chen Y, Chen L, Mao YP, et al. Extension of local disease in nasopharyngeal carcinoma detected by magnetic resonance imaging: improvement of clinical target volume delineation. *Int J Radiat Oncol Biol Phys* 2009; **75**: 742-50.
- Liu L, Liang S, Li L, Mao Y, Tang L, Tian L, et al. Prognostic impact of magnetic resonance imaging-detected cranial nerve involvement in nasopharyngeal carcinoma. *Cancer* 2009; **115**: 1995-2003.
- Abdel Razek AAK, King A. MRI and CT of nasopharyngeal carcinoma. *AJR Am J Roentgenol* 2012; **198**: 11-8.
- Lee N, Xia P, Quivey JM, Sultanem K, Poon I, Akazawa C, et al. Intensity-modulated radiotherapy in the treatment of nasopharyngeal carcinoma: an update of the UCSF experience. *Int J Radiat Oncol Biol Phys* 2002; **53**: 12-22.
- Wolden SL, Chen WC, Pfister DG, Kraus DH, Berry SL, Zelefsky MJ. Intensity-modulated radiation therapy (IMRT) for nasopharynx cancer: update of the Memorial Sloan-Kettering experience. *Int J Radiat Oncol Biol Phys* 2006; **64**: 57-62.
- Chong Z. Improved local control with intensity modulated radiation therapy in patients with nasopharyngeal carcinoma. *Int J Radiat Oncol Biol Phys* 2004; **60**: 317.
- Bucci M, Xia P, Lee N, Fishbein N, Kramer A, Weinberg V, et al. Intensity modulated radiation therapy for carcinoma of the nasopharynx: an update of the UCSF experience. *Int J Radiat Oncol Biol Phys* 2004; **60**: 317-8.
- Kam MK, Teo PM, Chau RM, Cheung KY, Choi PH, Kwan WH, et al. Treatment of nasopharyngeal carcinoma with intensity-modulated radiotherapy: the Hong Kong experience. *Int J Radiat Oncol Biol Phys* 2004; **60**: 1440-50.
- Sakata K, Hareyama M, Tamakawa M. Prognostic factors of nasopharynx tumors investigated by MR imaging and the value of MR imaging in the newly published TNM staging. *Int J Radiat Oncol Biol Phys* 1999; **43**: 273-8.
- Lau KY, Kan WK, Sze WM, Lee AW, Chan JK, Yau TK, et al. Magnetic resonance for T-staging of nasopharyngeal carcinoma: the most informative pair of sequences. *Jpn J Clin Oncol* 2004; **34**: 171-5.
- Radiation Therapy Oncology Group. *RTOG protocol information*. Available from: <http://www.rtog.org/ClinicalTrials/ProtocolTable/StudyDetails.aspx?action>. Accessed on 2 December, 2013.
- Fowler A, Forstner D, Lin P, Cuganeasean R, Clark J. Multimodality imaging in the radiation treatment planning for a case of carcinoma of the nasopharynx. *Acta Oncol* 2008; **47**: 1459-60.

23. American Joint Committee on Cancer. *AJCC staging manual*. 6th edition. New York, Berlin, Heidelberg: Springer; 2002.
24. Kessler ML. Image registration and data fusion in radiation therapy. *Br J Radiol* 2006; **79**: S99-108.
25. Hermans R, Feron M, Bellon E, Dupont P, Van den Bogaert W, Baert AL. Laryngeal tumor volume measurements determined with CT: a study on intra- and interobserver variability. *Int J Radiat Oncol Biol Phys* 1998; **40**: 553-7.
26. Chang CC, Chen MK, Wu HK, Liu MT. Nasopharyngeal carcinoma volume measurements determined with computed tomography: study of intraobserver and interobserver variability. *J Otolaryngol* 2002; **31**: 361-5.
27. Vogl T, Dresel S, Bilaniuk LT, Grevers G, Kang K. Tumors of nasopharynx and adjacent areas: MR imaging with Gd-DTPA. *AJNR Am J Neuroradiol* 1990; **11**: 187-94.
28. Lee CC, Huang TT, Lee MS, Hsiao SH, Lin HY, Su YC, et al. Clinical application of tumor volume in advanced nasopharyngeal carcinoma to predict outcome. *Radiat Oncol* 2010; **5**: 20.
29. Lam KL, Balter JM, Haken RKT. Effect of daily localization and correction on the setup uncertainty. *Phys Med Biol* 2007; **52**: 6575-87.
30. Li H, Zhu XR, Zhang L, Dong L, Tung S, Ahamad A, et al. Comparison of 2D radiographic images and 3D cone beam computed tomography for positioning head and neck radiotherapy patients. *Int J Rad Oncol Biol Phys* 2008; **71**: 916-25.

Radiol Oncol 2014; 48(3): 219-227.
doi:10.2478/raon-2013-0067

Vloga pozitronske emisijske računalniške tomografije s fluorodeoksiglukozo za vrednotenje odgovora na zdravljenje s tirozin kinaznimi zaviralci pri bolnikih s primarnim metastatskim rakom ledvic

Caldarella C, Muoio B, Isgrò MA, Porfiri E, Treglia G, Giovanella L

Izhodišča. Pozitronsko emisijsko tomografijo – računalniško tomografijo (PET-CT) s fluorodeoksiglukozo (FDG) vedno bolj uporabljamo pri vrednotenju bolnikov z napredovalim rakom ledvic. Najpogosteje z njo opredelimo stadij bolezni. Namen članka je sistematično pregledati uporabnost PET-CT s FDG za oceno odgovora na zdravljenje s tirozin kinaznimi zaviralci pri bolnikih z napredovalim rakom ledvic.

Materiali in metode. Sistematično smo pregledali raziskovalno literaturo, ki opisuje vlogo PET-CT s FDG pri ocenjevanju odgovora na zdravljenje s tirozin kinaznimi zaviralci pri bolnikih z napredovalim rakom ledvic.

Rezultati. Našli smo sedem raziskav o vlogi PET-CT s FDG pri oceni odgovora na zdravljenje s tirozin kinaznimi zaviralci (sunitinib in sorafenib) pri bolnikih z napredovalim rakom ledvic. Na voljo je bilo celotno besedilo, ki smo ga analizirali, da bi ugotovili napovedno vlogo te morfološko funkcionalne metode slikanja na izid bolezni.

Zaključki. Vloga PET-CT s FDG za oceno odgovora na tirozin kinazne zaviralce pri metastatskem rakom ledvic do danes še ni natančno opredeljena, delno tudi zaradi heterogenosti narejenih raziskav. Vendar pa PET-CT razkriva morebitno vlogo pri izboru bolnikov za zdravljenje s tirozin kinaznimi zaviralci. Uporaba PET-CT s kontrastom je obetavna za večdimenzionalno vrednotenje odziva na zdravljenje teh bolnikov.

Radiol Oncol 2014; 48(3): 228-234.
doi:10.2478/raon-2013-0075

Naključno kopičenje 18-F fluoroholina (FCH) v področju glave in vratu pri bolnikih z rakom prostate

Hodolič M, Huchet V, Balogova S, Michaud L, Kerrou K, Nataf V, Cimitan M, Fettich J, Talbot JN

Izhodišča. Pozitronska emisijska tomografija z računalniško tomografijo (PET/CT) z 18-F fluoroholinom (FCH) je postala rutinska preiskava pri bolnikih z rakom prostate. Mesta patološko zvišanega kopičenja radioindikatorja v področju glave in vratu smo pri bolnikih z rakom prostate ocenjevali kot incidentalome (naključno odkrite tumorje), razen če smo dokazali zasevke v okostju.

Rezultati. Pri osmih bolnikih je naključno zvišano kopičenje predstavljalo benigni tumor. Končna diagnoza je bila adenom hipofize v 3 primerih, meningeom v 2, adenom obščitnice v 2 in lokalizirano avtonomno tkivo ščitnice (hiperfunkcijski adenom) pri 1 bolniku. Diagnozo smo potrdili s histološkim pregledom pri 4 bolnikih, z magnetnoresonančnim slikanjem (MRI) pri 4 ter z dodatno ultrazvočno preiskavo, scintigrafijo z 99m-Tc sestaMIBI in biokemičnimi preiskavami pri 1 bolniku.

Zaključki. V nam znani literaturi kopičenje FCH še ni bilo dokumentirano pri bolnikih z adenomom obščitnice in adenomom hipofize. Predlagamo, da bi PET/CT preiskava s FCH lahko postala indicirana pri bolnikih, kjer je tovrsten tumor že znan (n.pr. adenom obščitnice), pri sumu na ostanek ali recidiv adenoma hipofize in za načrtovanje operacije ali obsevanja meningeomov. Pri teh potencialnih indikacijah so potrebne primerjave z drugimi radioindikatorji PET-a oziroma v primeru hiperparatiriodizma primerjava z 99m-Tc sestaMIBI.

Radiol Oncol 2014; 48(3): 235-242.
doi:10.2478/raon-2014-0005

Klinični in radiološki znaki izvenskeletnega miksoidnega hondrosarkoma. Znaki bolezni ob diagnozi, lokalnih ponovitvah in zasevanju

Kapoor N, Shinagare AB, Jagannathan JP, Shah SH, Krajewski KM, Hornick JL, Ramaiya NH

Izhodišča. Namen raziskave je bil oceniti klinične in radiološke znake izvenskeletnega miksoidnega hondrosarkoma vključno z začetnimi znaki bolezni, ob ponovitvi in ob zasevanju bolezni.

Bolniki in metode. V raziskavi smo retrospektivno analizirali radiološke slike 13 bolnikov s patološko potrjenim izvenskeletnim miksoidnim hondrosarkomom, ki smo ga odkrili med avgustom 1995 in decembrom 2011. V skupini so bile tri ženske in deset moških, povprečne starosti 54 let (29–73). Slikovni material sta neodvisno ocenjevala dva radiologa. O vrednotila sta mesto, velikost in radiološke značilnosti primarnega tumorja, prisotnost ponovitve bolezni in lokacijo zasevkov.

Rezultati. Med 13 bolniki so trije umrli v času poteka klinične raziskave. 9 bolnikov je imelo tumor na spodnjih okončinah, povprečne velikosti 9,3 cm (3,3–18). Na T2 obteženih slikah, pridobljenih z magnetno resonanco (MRI) so bili primarni tumorji hiperintenzivni in podobne intenzitete kot mišice na T1 obteženih slikah. 3 bolniki so imeli lokalno ponovitev bolezni in 12 jih je imelo oddaljene zasevke, najpogosteje v pljuča. Tumorska gostota (denziteteta) na preiskavah računalniške tomografije (CT) s kontrastnim sredstvom je bila med 8,2 in 82,9 HE. Fluorodeoksiglukoza pozitronsko emisijsko tomografijo (FDG-PET) s CT-jem smo naredili pri 3 bolnikih. Eden ni imel znakov kopičenja FDG, ostala dva pa sta imela metastatsko obliko bolezni z vrednostjo standardnega prevzema izotopa (SUV) 2,8 in 7,4. Bolnik z večjim kopičenjem FDG je imel bolj solidno obliko tumorja in krajše preživetje.

Zaključki. Izvenskeletni miksoidni hondrosarkom je redek tumor. V raziskavi smo ga najpogosteje odkrili na spodnjih okončinah, pogosto je zaseval v pljuča. Večja gostota tumorja pri preiskavah CT in MRI ter večje privzemanje FDG pri preiskavi PET-CT sta lahko povezana z bolj agresivno obliko bolezni.

Radiol Oncol 2014; 48(3): 243-246.
doi:10.2478/raon-2013-0034

Osteoblastni kostni zasevki pri ledvičnem raku

Salapura V, Zupan I, Šeruga B, Gašljević G, Kavčič P

Izhodišča. Ledvični rak predstavlja le 2-3% vseh rakastih obolenj. Zaradi neznačilnih simptomov bolezni mnogokrat ugotovimo šele v napredovalem stadiju. Razširjeni rak ledvice pogosto zaseva v kosti, zasevki so praviloma zelo destruktivni, dobro prekrvljeni in povsem osteolitični.

Prizak primera. V prispevku predstavljamo primer 71 let starega bolnika z razširjenim ledvičnim rakom in številnimi osteoblastnimi zasevki v kosteh. Hkrati predstavljamo kratek pregled literature, kjer poročajo o osteoblastnih zasevkih ledvičnega raka. Vodilni klinični simptom pri našem bolniku je bila prsna bolečina, ki se je stopnjevala ob gibanju. S slikovno diagnostiko smo ugotovili pretežno osteoblastne kostne zasevke v vretcih prsne in ledvene hrbtenice, v črevnici, rebrih, nadlaktnici in ključnici. Sprva je bil izvor zasevkov neznan, kasneje pa smo pri bolniku ugotovili majhen tumor v desni ledvici. Mikroskopska ocena tkiva po odprti biosiji je pokazala velikocelični karcinom ledvice s sarkomatoidno diferenciacijo.

Zaključki. Zaradi svoje redkosti ledvični rak ni vključen v primarno diferencialno diagnozo pri bolnikih z osteoblastnimi zasevki. Primeri, kot je naš, kažejo, da bi bilo ledvični rak smiselno uvrstiti med možne diagnoze pri bolnikih, kjer nismo našli sprememb, ki bi odkrivala druge primarne tumorje.

Radiol Oncol 2014; 48(3): 247-256.
doi:10.2478/raon-2014-0025

Učinki različnih doz sevanja na preoblikovanje skeletne mišice

Hardee JP, Puppa MJ, Fix DK, Gao S, Hetzler KL, Bateman TA, Carson JA

Izhodišča. Namen študije je bil določiti učinek dveh klinično ustreznih doz na preoblikovanje mišjih skeletnih mišic.

Materiali in metode. Spremembe v morfologiji mišic in regulatornih signalnih poteh smo preučili na mišici tibialis anterior in gastrocnemius po obsevanju z dozami, ki so se razlikovale glede na popolno biološko učinkovito dozo (BED). Miši C57Bl/6 ženskega spola so bile naključno razporejene v kontrolno, neobsevano skupino, ki je prejela 4 frakcijske doze po 4 Gy (4 x 4 Gy; BED 37 Gy), in skupino, ki je prejela 16 Gy v enkratni dozi (16 Gy; BED 100 Gy). Miši smo žrtvovali 2 tedna po začetku prvega obsevanja.

Rezultati. Skupna količina proteinov in ribonukleinske kisline v mišici se je zmanjšala po obsevanju s 16 Gy, ne pa po obsevanju s 4 x 4 Gy. Pri obeh skupinah se je povečalo število miofibril s centralno postavljenim jedrom, kar kaže na mišično regeneracijo. Samo pri skupini, ki je bila obsevana s 16 Gy, se je povečala prostornina zunajceličnega matriksa. Na drugi strani pa je prišlo do povečanega izražanja 4-hidroksinonenala samo pri skupini obsevani s 4 x 4 Gy. Medtem ko se je pri obeh skupinah zmanjšala presečna površina IIB miofibril, se je presečna površina miofibril IIA zmanjšala samo pri skupini obsevani s 16 Gy. Obsevanje s 16 Gy je tudi povečalo pojavljanje manjših premerov miofibril obeh tipov, IIA in IIB, obsevanje s 4 x 4 Gy pa samo pri tipu IIB. Obe terapiji sta zmanjšali pogostost in presečno površino fibril z zmanjšano sukcinat dehidrogenazno aktivnostjo. Samo pri skupini obsevani s 16 Gy je bil zmanjšan tudi premer teh fibril. Signalne poti vpletene v proteinsko pretvorbo in oksidativni metabolizem niso bile spremenjene pri nobeni terapiji.

Zaključki. Dobljeni rezultati kažejo na to, da uporabljeni dozi sevanja različno učinkujeta na mišično preoblikovanje in da so ti učinki povezani s tipom mišičnih fibril in oksidativnim metabolizmom.

Radiol Oncol 2014; 48(3): 257-266.
doi:10.2478/raon-2014-0014

Ugotavljanje možnih plazemskih bioloških označevalcev pri glioblastomu z uporabo proteomske tehnike mikromrež s protitelesi

Zupančič K, Blejec A, Herman A, Veber M, Verbovšek U, Koršič M, Knežević M, Rozman P, Lah Turnšek T, Gruden K, Motaln H

Izhodišča. Glioblastoma multiforme (GBM) je možganski tumor z zelo visoko stopnjo smrtnosti, saj je srednje preživetje bolnikov z GBM le 47 tednov. Preživetje bolnikov z GBM bi lahko izboljšali z novimi diagnostičnimi in napovednimi biološkimi označevalci v krvi bolnikov, pa tudi z biološkimi označevalci, ki napovedujejo odziv na zdravljenje. Oboji bi olajšali diagnozo, izbiro primerne terapije in sledenje bolezni. Cilj raziskave je bil določiti vpliv GBM na količino prisotnih proteinov v krvi bolnikov v primerjavi z zdravimi prostovoljci.

Bolniki in metode. Uporabili smo komercialno dostopne mikromreže, ki so vključevale 656 različnih protiteles, z njimi smo analizirali vzorce krvne plazme 17 zdravih prostovoljcev ter 17 bolnikov z GBM.

Rezultati. Identificirali smo 11 plazemskih proteinov, katerih nivo je bil statistično značilno spremenjen pri bolnikih z GBM. Funkcija teh proteinov je bila opisana v treh signalnih poteh: T-celični signalizaciji in imunskem odzivu; celični adheziji in migraciji; nadzoru celičnega cikla in apoptozi. Ta set ugotovljenih proteinov zato predstavlja potencialne kandidate diagnostičnih bioloških označevalcev za GBM. Nadalje smo ugotovili tudi 16 plazemskih proteinov, ki so bili statistično značilno povezani s preživetjem GBM bolnikov. Gvanin nukleotid vezni protein alfa (GNAO1), katerega nivo je bil statistično značilno spremenjen v plazmi bolnikov z GBM, je bil edini ugotovljen tudi v omenjenem setu proteinov, ki so sovpadali s preživetjem GBM bolnikov.

Zaključki. Menimo, da so mikromreže s protitelesi uporabne za presejevalno testiranje plazemskih vzorcev in ugotavljanje potencialnih kandidatnih tumorskih bioloških označevalcev v manjših laboratorijskih poskusih. Za prenos tako dobljenih rezultatov v klinično uporabo pa je slednje potrebno najprej ovrednotiti v neodvisnih raziskavah na večjem naboru bolnikov z GBM.

Radiol Oncol 2014; 48(3): 267-281.

doi:10.2478/raon-2014-0022

Razgradnja jetrnih žil na magnetnoresonančnih slikah za načrtovanje terapij, ki temeljijo na elektroporaciji

Marčan M, Pavliha D, Marolt Mušič M, Fučkan I, Magjarević R, Miklavčič D

Izhodišča. Elektroporacija zagotavlja povečanje prepustnosti celične membrane zaradi izpostavitve celic električnemu polju. Za zagotovitev pokritja celotnega tumorja z dovolj visokim električnim poljem lahko uporabimo numerični model, ki ga zgradimo na osnovi razgrajenih medicinskih slik. Za namene rekonstrukcije jetrnih žil iz magnetnoresonančnih slik smo poiskali optimalno metodo razgradnje, ki bi zadoščala vnaprej zastavljenim kriterijem: identifikaciji glavnih jetrnih žil, robustnosti in z najmanjšim naporom uporabnika.

Materiali in metode. Preizkusili smo različne metode razgradnje slik, temelječih na filtriranju, ki ojačuje žilne strukture, na upragovljanju, ter na njihovi kombinaciji v obliki lokalnega upragovljanja. Preizkušene metode smo ovrednotili na fantomih in kliničnih podatkih.

Rezultati. Metoda upragovljanja, ki temelji na minimizaciji variance, daje manjše napake kot metoda, ki temelji na maksimizaciji entropije. Najboljše rezultate smo dosegli z izvajanjem lokalnega upragovljanja na izvornih slikah, na katerih smo odpravili nehomogenost intenzitete. Rezultati so bili najboljši v območjih interesa, ki smo jih pred tem določili s filtrom, ki ojačuje žilne strukture. Pri vrednotenju na kliničnih primerih smo s predlagano optimalno metodo dosegli povprečno občutljivost 93,68 %, povprečno simetrično površinsko razdaljo 0,89 mm in Hausdorffovo razdaljo 4,04 mm.

Zaključki. Predlagana metoda za razgradnjo jetrnih žil na magnetnoresonančnih slikah, ki temelji na lokalnem upragovljanju, izpolnjuje vse v začetku zastavljene kriterije. Ti so nujni za uporabo metode razgradnje v načrtovanju zdravljenja z metodami, ki temeljijo na elektroporaciji. Metoda razgrajuje glavne žile, daje rezultate z dosledno točnostjo in deluje popolnoma avtomatično. Ali je dosežena točnost sprejemljiva za modele načrtovanja zdravljenja ali ne, pa je potrebno še potrditi z numeričnim modeliranjem vpliva napake razgradnje na porazdelitev električnega polja.

Radiol Oncol 2014; 48(3): 282-288.

doi:10.2478/raon-2014-0010

Mikroinvazivni ploščatocelični karcinom materničnega vratu v Sloveniji v obdobju od 2001 do 2007

Gutnik H, Matišič JP, Primic Žakelj M, Strojman Fležar M

Izhodišča. Mikroinvazivni ploščatocelični karcinom predstavlja znaten delež v incidenci rak materničnega vratu v Sloveniji. Čeprav so merila karcinomske invazije v literaturi dobro opisana, je histopatološko ocenjevanje mikroinvazivnega ploščatoceličnega karcinoma zahtevno, saj se morfološke spremembe lahko prekrivajo s cervikalno intraepitelijsko neoplazijo 3. stopnje (CIN 3) in drugimi patološkimi spremembami. Namen raziskave je bil ugotoviti zanesljivost svetlobnomikroskopske histopatološke ocene mikroinvazivnega ploščatoceličnega karcinoma v Sloveniji v obdobju 2001–2007.

Materiali in metode. Iz Registra raka Republike Slovenije smo dobili podatke o bolnicah s histopatološko diagnozo mikroinvazivni ploščatocelični karcinom materničnega vratu (stadija Mednarodne zveze za ginekologijo in porodništvo [FIGO] IA) za obdobje 2001–2007. Iz večine laboratorijev za patologijo v Sloveniji smo dobili histološke preparate biopsijskih vzorcev materničnega vratu. Prejeli smo 250 vzorcev (69 % vseh mikroinvazivnih ploščatoceličnih karcinomov v obdobju 2001–2007) primernih za ponovni pregled; dodali smo 30 kontrolnih vzorcev s CIN 3 in ploščatoceličnim karcinomom, stadija FIGO IB. Preparata smo anonimizirali in znova pregledali.

Rezultati. Od 250 primerov s primarno diagnozo mikroinvazivni ploščatocelični karcinom jih je bilo 184 (73,6 %) znova ocenjenih kot mikroinvazivni ploščatocelični karcinom (179/184 [97,3 %] stadij FIGO IA1 in 5/184 [2,7 %] stadij FIGO IA2). Med 179 primeri s stadijem FIGO IA1 je bilo 117 primerov z zgodnjo stromalno invazijo.

Zaključki. Ponovni pregled primerov mikroinvazivnega ploščatoceličnega karcinoma materničnega vratu v Sloveniji v obdobju 2001–2007 je pokazal znaten delež preocenjenih vzorcev in tudi velik delež primerov z zgodnjo stromalno invazijo (globina invazije do 1 mm) v ustrezno ocenjenih mikroinvazivnih ploščatoceličnih karcinomih.

Radiol Oncol 2014; 48(3): I-VII.

Radiol Oncol 2014; 48(3): 289-292.
doi:10.2478/raon-2013-0076

Vpliv polimorfizmov folatne poti na pojav neželenih učinkov metotreksata v visokih odmerkih in preživetje pri otrocih z ne-Hodgkinovim limfomom

Erčulj N, Faganel Kotnik B, Debeljak M, Jazbec J, Dolžan V

Izhodišča. V raziskavi smo želeli opredeliti vpliv polimorfizmov folatne poti na pojav neželenih učinkov metotreksata v visokih odmerkih pri pediatričnih bolnikih z ne-Hodgkinovim limfomom.

Bolniki in metode. Pri 30 bolnikih z ne-Hodgkinovim limfomom, zdravljenimi z metotreksatom v visokih odmerkih, smo določili izbrane polimorfizme folatne poti.

Rezultati. Nosilci alela *MTHFR* 677T so imeli značilno večjo površino pod časovno-koncentracijsko krivuljo metotreksata. Ti bolniki so imeli tudi povečano tveganje za levkopenijo ($P = 0,006$) in trombocitopenijo ($P = 0,028$) ter večje število različnih neželenih učinkov povezanih z metotreksatom v visokih odmerkih ($P = 0,006$) v primerjavi z bolniki z normalnim genotipom.

Zaključki. Rezultati nakazujejo pomembno vlogo polimorfizma *MTHFR* 677C>T na pojav neželenih učinkov metotreksata v visokih odmerkih pri pediatričnih bolnikih z ne-Hodgkinovim limfomom.

Radiol Oncol 2014; 48(3): 293-300.
doi:10.2478/raon-2014-0009

Vnaprejšnje načrtovanje brahiterapije raka materničnega vratu v para-cervikalni anesteziji na podlagi magnetnoresonančnega slikanja. Končno poročilo

Petrič P, Hudej R, Hanuna O, Marolt P, Al-Hammadi NMAA, Riyas MP, Šegedin B

Izhodišča. Ustrezna vstavitve aplikatorja je predpogoj za uspešno izvedbo brahiterapije raka materničnega vratu. Namen naše raziskave je bil opredeliti učinkovitost vnaprejšnjega načrtovanja brahiterapije na podlagi vstavitve aplikatorja v paracervikalni anesteziji (PCA) in magnetnoresonančnega slikanja.

Bolniki in metode. 18 bolnicam z rakom materničnega vratu smo 5 dni pred brahiterapijo vstavili intrakavitarni aplikator (obroček in sonda) v PCA, opravili magnetnoresonančno slikanje medenice in aplikator odstranili. Na magnetnoresonančne slike smo vrisali visoko rizični tarčni volumen (*high risk clinical target volume* – HR CTV) in rizične organe, vstavili virtualne igle na optimalne položaje in opravili dozno planiranje. Brahiterapijo smo izvedli v subarahnoidni anesteziji, upoštevaje vnaprej načrtovano geometrijo.

Rezultati. Postopek vnaprejšnjega načrtovanja so bolnice dobro prenašale. Srednja razlika med vnaprej načrtovano in dejansko globino oz. kotom vstavitve je bila 2 (0-10) mm oz. 4 (0-30) stopinj. Vse igle smo vstavili znotraj HR CTV in izven rizičnih organov.

Zaključki. Opisani postopek omogoča dobro reprodukcijo vnaprej načrtovane optimalne geometrije implantacije in dozno porazdelitve ob brahiterapiji raka materničnega vratu.

Radiol Oncol 2014; 48(3): 301-306.
doi:10.2478/raon-2013-0070

Sposobnosti voha in okušanja po laringektomiji

Mumović G, Hočvar-Boltežar I

Izhodišča. Laringektomija vpliva na številne bolnikove funkcije. Poleg izgube glasnega govora in težav z dihalnim traktom vplivajo na kakovost bolnikovega življenja tudi težave z vohom in sposobnostjo okušanja. Namen raziskave je bil ugotoviti, kako pogoste so nosne težave in slabše sposobnosti okušanja po odstranitvi grla.

Metode. V raziskavo smo vključili 105 laringektomiranih bolnikov (9 žensk, 96 moških, starih od 45 do 88 let), ki smo jih zdravili v dveh terciarnih centrih. Bolniki so izpolnili vprašalnik o različnih nosnih težavah in sposobnosti okušanja, možnih alergijah in dražečih snoveh v njihovem okolju ter ocenili vpliv težav z nosom in okušanjem na kakovost njihovega življenja.

Rezultati. Slabši voh je navedlo 51,4 % bolnikov, 30,5 % pa jih sploh ni vohalo. Slabšo sposobnost okušanja je navedlo 26,7 % bolnikov, pri 11,4 % je bilo okušanje spremenjeno. Skoraj 21 % bolnikov je bilo prizadetih zaradi slabše sposobnosti okušanja in 50,5 % bolnikov zaradi izgube sposobnosti vohanja. Pri 20 % bolnikov se je pojavljal pogost izcedek iz nosu, 58,1 % bolnikov je pogosto kihalo in 33,3 % bolnikov je navedlo srbenje nosu. Povezav med starostjo ter vohom in sposobnostjo okušanja nismo ugotovili, prav tako ne med alergijo in nosnimi simptomi. Ugotovili pa smo pomembno soodvisnost med sposobnostjo okušanja in vohanja ($p = 0,025$).

Zaključki. Različne težave z nosom in okušanjem so se pojavljale pri več kot 80 % laringektomiranih bolnikov. Sposobnosti vohanja in okušanja sta povezani in bistveno vplivata na kakovost bolnikovega življenja. Enako kot rehabilitacija govora je po laringektomiji nujna tudi rehabilitacija voha. Pomembno je, da jo pričnemo čim prej po zaključenem zdravljenju.

Radiol Oncol 2014; 48(3): 307-313.
doi:10.2478/raon-2013-0066

Koncentracija v krvi krožeče sVCAM-1 pri bolnicah z napredovalim rakom jajčnikov: korelacija s koncentracijo v ascitesu

Jakimovska M, Černe K, Verdenik I, Kobal B

Izhodišča. Žilna adhezijska molekula-1 (VCAM-1) je vpletena v napredovanje raka jajčnikov, vendar izvor njene topne oblike (sVCAM-1) v serumu ni dobro raziskan. Namen raziskave je bil ugotoviti, ali je koncentracija sVCAM-1 v serumu povezana s koncentracijo v ascitesu, ki predstavlja lokalno tumorsko okolje, ter ali je povezana z različnimi kliničnopatološkimi značilnostmi, sistemskim vnetjem in kliničnim izhodom bolnic.

Bolnice in metode. V raziskavo smo vključili 36 bolnic z napredovalim rakom jajčnikov. Serum za analizo sVCAM-1 smo odvzeli pred operacijo, vzorce ascitesa pa na začetku operacije. Klinične podatke smo zbrali iz medicinske dokumentacije bolnic. sVCAM-1 v vzorcih smo analizirali s pretočno citometrijo na osnovi fluorescentnih kroglic. Povprečni čas spremljanja bolnic po operaciji je bil 11 mesecev (interval 0-23).

Rezultati. Med koncentracijo sVCAM-1 v serumu in v ascitesu smo ugotovili pozitivno povezavo. Koncentracija serumskega sVCAM-1 je bila šibko povezana z velikostjo tumorja, medtem ko z vnetnimi označevalci, FIGO stadijem in stopnjo diferenciacije tumorja ni bila povezana. Pri bolnicah, ki so umrle v skoraj vseh primerih še pred kemoterapijo, smo ugotovili višje koncentracije sVCAM-1.

Zaključki. To je prva raziskava, ki je pokazala, da je koncentracija serumskega sVCAM-1 pri bolnicah z napredovalim rakom jajčnikov povezana s koncentracijo sVCAM-1 v ascitesu, ki predstavlja lokalno tumorsko okolje. Koncentracija sVCAM-1 v serumu tako izraža potencial maligne bolezni za zasevanje in ni odsev sistemskega vnetja. Visoke koncentracije sVCAM-1 v serumu in ascitesu imajo lahko napovedno vrednost za biološko vedenje raka jajčnikov.

Radiol Oncol 2014; 48(3): 314-322.

doi:10.2478/raon-2013-0085

Radioterapija po mastektomiji koristi podskupinam bolnic z rakom dojke, ki so imele tumorje T1-2 in 1-3 zasevke v pazdušnih bezgavkah

Su YL, Li SH, Chen YY, Chen HC, Tang Y, Huang CH, Chou FF, Wu SC, Rau KM

Izhodišča. Namen raziskave je bil določiti vlogo radioterapije po mastektomiji pri bolnicah z rakom dojke, ki so imele tumorje T1-2 in bezgavke N1.

Bolnice in metode. V raziskavo smo vključili 207 bolnic. Glede na različne lastnosti tumorjev smo analizirali 5-letno oceno po Kaplan-Meierju za lokalno ponovitev bolezni, oddaljeno ponovitev bolezni in celokupno preživetje. Multivariatno analizo smo naredili po Coxovem modelu sorazmernih tveganj.

Rezultati. Srednji čas spremljanja bolnic je bil 59,5 mesecev; 5-letna lokalna ponovitev bolezni je bila 9,1 %, oddaljena ponovitev bolezni 20,3 % in celokupno preživetje 84,4 %. Univariatna analiza je pokazala, da sta starost < 40 let ($p = 0,003$) in povečano izražanje Her2/neu ($p = 0,016$) povezana z bolj pogosto lokalno ponovitvijo bolezni, medtem ko je prisotnost limfno-vaskularne invazije značilno napovedovala bolj pogosto oddaljeno ponovitev bolezni ($p = 0,026$). S slabšim celokupnim preživetjem so bili značilno povezani negativni estrogenski status ($p = 0,033$), povečano izražanje Her-2/neu ($p = 0,001$) in prisotnost limfno-vaskularne invazije ($p = 0,01$). Radioterapija po mastektomiji ni zmanjšala pogostnosti 5-letne lokalne ponovitve bolezni ($p = 0,107$) ali podaljšala 5-letnega celokupnega preživetja ($p = 0,918$). Nasprotno pa je analiza posameznih podskupin bolnic pokazala, da je radioterapija po mastektomiji značilno zmanjšala pogostnosti 5-letne lokalne ponovitve bolezni in podaljšala 5-letno celokupno preživetje pri bolnicah s tumorsko limfno-vaskularno invazijo.

Zaključki. Pri bolnicah z rakom dojke lahko radioterapija po mastektomiji zmanjša pogostnost lokoregionalne ponovitve bolezni in poveča celokupno preživetje samo pri tistih bolnicah s tumorji T1-2 in bezgavkami N1, kjer ugotovimo tumorsko limfno-vaskularno invazijo.

Radiol Oncol 2014; 48(3): 323-330.

doi:10.2478/raon-2014-0013

MR za označevanje tumorskega volumna (GTV) pri raku nosnega žrela. Katere ravnine in sekvence bi morali uporabiti

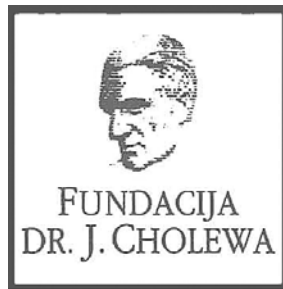
Popovtzer A, Ibrahim M, Tatro D, Feng FY, Ten Haken RK, Eisbruch A

Izhodišča. Pri napredovalem raku nosnega žrela slikanje z magnetno resonanco (MR) izboljša opredelitev obsega primarnega tumorskega volumna (GTV). Zato MR rutinsko uporabljamo za opredeljevanje tarče pri načrtovanju radioterapije. Niso pa znane specifične ravnine in sekvence, ki jih naj bi uporabljali.

Metode. Pri 12 bolnikih z rakom nosnega žrela smo naredili oceno primarnega GTV z gadolinijem obarvanim aksialnim slikanjem T1 in T2, koronarnimi sekvencami T1 ter sagitalnimi sekvencami T1. Vsako sekvenco smo registrirali z računalniškimi tomografskimi posnetki za načrtovanje radioterapije. Planirni tarčni volumen (PTV) smo ustvarili z uniformnim povečanjem GTV. Kvantitativno in anatomsko smo primerjali volumne, ki so vključevali različne ravnine in sekvence, pa tudi volumne, ki so bili skupni vsem ravninam in sekvencam, z volumni označenimi s pomočjo običajno uporabljenih aksialnih slik T1.

Rezultati. Dodatek aksialne sekvence T2 je povečal GTV, označen na aksialnih posnetkih T1 v povprečju za 12 % ($p = 0,004$). Skupne ocene, ki so vključevale koronarne ravnine T1 in sagitalne ravnine T1, pa so povečale aksialni GTV T1 v povprečju za 30 % ($p = 0,003$). Aksialni PTV T1 se je z dodatnimi sekvencami povečal za 20 % ($p = 0,04$). Vsaka ravnina in sekvenca je prispevala originalna povečanja volumna. GTV, ki so bili skupni vsem ravninam T1, so prispevali 38 % skupnih volumnov vseh ravnin T1. Anatomsko je dodatek koronarnih in sagitalnih GTV povečal aksialni GTV T1 v kaudalni in kranialni smeri, vse do baze lobanje.

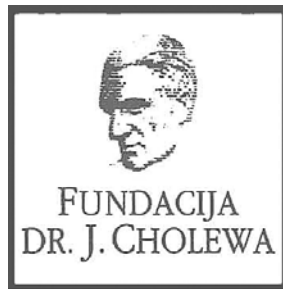
Zaključki. Dodatek MR ravnin in sekvenc k tradicionalni aksialni sekvenci T1 prispeva k statistično pomembnim kvantitativnim in anatomsko pomembnim povečanjem GTV in PTV. Za natančno označevanje tarče pri raku nosnega žrela priporočamo, da je GTV označen na vseh MR ravninah in sekvencah ter registriran skupaj z računalniškimi tomografskimi posnetki za načrtovanje radioterapije.



FUNDACIJA "DOCENT DR. J. CHOLEWA"
JE NEPROFITNO, NEINSTITUCIONALNO IN NESTRANKARSKO
ZDRUŽENJE POSAMEZNIKOV, USTANOV IN ORGANIZACIJ, KI ŽELIJO
MATERIALNO SPODBUJATI IN POGLABLJATI RAZISKOVALNO
DEJAVNOST V ONKOLOGIJI.

DUNAJSKA 106
1000 LJUBLJANA

ŽR: 02033-0017879431



Activity of "Dr. J. Cholewa" Foundation for Cancer Research and Education - a report for the second quarter of 2014

The Dr. J. Cholewa Foundation for Cancer Research and Education is a non-profit, non-political and non-government organisation that unites medical professionals, medical institutions and other individuals and organisations in their support of cancer research, education, treatment and prevention. It provides financial support for all qualified individuals and organisations interested in problems associated with cancer, resulting in a number of successful initiatives, publications and projects.

The symposium to honour the 20th anniversary of the Dr. J. Cholewa Foundation for Cancer Research and Education took place on December 13th, 2013, in Ljubljana, Slovenia, and was considered a success by organizers and participants alike. Preliminary discussions are being held to organise a similar Symposium in 2014 and to establish enough support to organise such symposia on a regular basis in the future.

The Foundation continues to provide regular financial support to "Radiology and Oncology", an international scientific journal that is edited, published and also printed in Ljubljana, Slovenia. "Radiology and Oncology" publishes scientific research articles, reviews, case reports, short reports and letters to the editor about research and studies in experimental and clinical oncology, supportive therapy, experimental and clinical research in radiology, radiophysics, prevention and early diagnostics of different types of cancer. It is an open access journal available in pdf format and with an important Science Citation Index Impact factor. All the abstracts in "Radiology and Oncology" are translated in Slovenian and the journal can thus provide sufficient scientific information from various fields of high quality cancer research to interested lay public in Slovenia.

The Dr. J. Cholewa Foundation for Cancer Research and Education is evaluating ways to intensify financial and other means of support to all in Slovenia interested in the fight against cancer. Efforts to help to organise scientific and other meetings of specific interest in different fields of cancer research and education are thus perhaps the first step in expanding Foundation's activities in the future.

Tomaž Benulič, MD
Viljem Kovač, MD, PhD
Andrej Plesničar, MD, MSc
Borut Štabuc, MD, PhD

TANTUM VERDE®



Lajšanje bolečine in oteklina pri vnetju v ustni votlini in žrelu, ki nastanejo zaradi okužb in stanja po operaciji in kot posledica radioterapije (t.i. radiomukozitis).



Imetnik dovoljenja za promet
CSC Pharma d.o.o.
Jana Husa 1a
1000 Ljubljana



www.tantum-verde.si

Tantum Verde 1,5 mg/ml oralno pršilo, raztopina

Kakovostna in količinska sestava

1 ml raztopine vsebuje 1,5 mg benzidaminijevega klorida, kar ustreza 1,34 mg benzidamina. V enem razpršku je 0,17 ml raztopine. En razpršek vsebuje 0,255 mg benzidaminijevega klorida, kar ustreza 0,2278 mg benzidamina. En razpršek vsebuje 13,6 mg 96 odstotnega etanola, kar ustreza 12,728 mg 100 odstotnega etanola, in 0,17 mg metilparahidroksibenzoata (E218).

Terapevtske indikacije

Samozdravljenje: lajšanje bolečine in oteklina pri vnetju v ustni votlini in žrelu, ki so lahko posledica okužb in stanja po operaciji. Po nasvetu in navodilu zdravnika: lajšanje bolečine in oteklina v ustni votlini in žrelu, ki so posledica radiomukozitisa.

Odmerjanje in način uporabe

Uporaba 2- do 6-krat na dan (vsake 1,5 do 3 ure). Odrasli: 4 do 8 razprškov 2- do 6-krat na dan. Otroci od 6 do 12 let: 4 razprški 2- do 6-krat na dan. Otroci, mlajši od 6 let: 1 razpršek na 4 kg telesne mase; do največ 4 razprške 2 do 6-krat na dan.

Kontraindikacije

Znana preobčutljivost za zdravilno učinkovino ali katerikoli pomožni snov.

Posebna opozorila in previdnostni ukrepi

Pri manjšini bolnikov lahko resne bolezni povzročijo ustne/žrelne ulceracije. Če se simptomi v treh dneh ne izboljšajo, se mora bolnik posvetovati z zdravnikom ali zobozdravnikom, kot je primerno. Zdravilo vsebuje aspartam (E951) (vir fenilalanina), ki je lahko škodljiv za bolnike s fenilketonurijo. Zdravilo vsebuje izomalt (E953) (sinonim: izomaltitol (E953)). Bolniki z redko dedno intoleranco za fruktozo ne smejo jemati tega zdravila. Uporaba benzidamina ni priporočljiva za bolnike s preobčutljivostjo za salicilno kislino ali druga nesteroidna protivnetna zdravila. Pri bolnikih, ki imajo ali so imeli bronhialno astmo, lahko pride do bronhospazma. Pri takih bolnikih je potrebna previdnost.

Medsebojno delovanje z drugimi zdravili in druge oblike interakcij

Pri ljudeh raziskav o interakcijah niso opravljali.

Nosečnost in dojenje

Tantum Verde z okusom mentola 3 mg pastile se med nosečnostjo in dojenjem ne smejo uporabljati.

Vpliv na sposobnost vožnje in upravljanja s stroji

Uporaba benzidamina lokalno v priporočenem odmerku ne vpliva na sposobnost vožnje in upravljanja s stroji.

Neželene učinki

Bolezni prebavil Redki: pekoč občutek v ustih, suha usta.

Bolezni imunskega sistema Redki: preobčutljivostna reakcija.

Bolezni dihal, prsnega koša in mediastinalnega prostora Zelo redki: laringospazem.

Bolezni kože in podkožja Občasni: fotosenzitivnost. Zelo redki: angioedem.

Rok uporabnosti

4 leta. Zdravila ne smejo uporabljati po datumu izteka roka uporabnosti, ki je naveden na ovojnini. Posebna navodila za shranjevanje Za shranjevanje pastil niso potrebna posebna navodila. Platenko z raztopino shranjujte v zunanji ovojnini za zagotovitev zaščite pred svetlobo. Shranjujte pri temperaturi do 25°C. Shranjujte v originalni ovojnini in nedosegljivo otrokom.

XGEVA®: PRVI IN EDINI ZAVIRALEC LIGANDA RANK, KI PREPREČUJE ZAPLETE KOSTNIH ZASEVKOV

SUPERIORNO PREPREČEVANJE.¹ TARČNO DELOVANJE.¹ SUBKUTANO INJICIRANJE.¹

- Zdravilo XGEVA® je indicirano za preprečevanje zapletov kostnih zasevkov pri odraslih s kostnimi zasevki solidnih tumorjev.
- Priporočen odmerek zdravila XGEVA® je 120 mg v enkratni subkutani injekciji, enkrat na 4 tedne.¹

XGEVA®
(denosumab)
NATANČEN. MOČAN. DOKAZAN.

XGEVA® 120 mg raztopina za injiciranje (denosumab) – SKRAJŠAN POVZETEK GLAVNIH ZNAČILNOSTI ZDRAVILA

Samo za strokovno javnost. Pred predpisovanjem si preberite celoten povzetek glavnih značilnosti zdravila.

▼ Za to zdravilo se izvaja dodatno spremljanje varnosti. Poročati je potrebno o vseh domnevnih neželenih učinkih zdravila.

SESTAVA ZDRAVILA: Ena viala vsebuje 120 mg denosumaba v 1,7 ml raztopine (70 mg/ml). Pomožne snovi s prepoznavnim delovanjem: 1,7 ml raztopine vsebuje 78 mg sorbitola (E420). **TERAPEVTSKE**

INDIKACIJE: Preprečevanje skeletnih dogodkov (patoloških zlomov, obsevanja kosti, kompresije hrbtenjače ali operacije kosti) pri odraslih s kostnimi metastazami solidnih tumorjev. **ODMERJANJE IN NAČIN**

UPORABE: Priporočeni odmerek zdravila XGEVA® je 120 mg enkrat na 4 tedne v enkratni subkutani injekciji v stegno, trebuh ali nadlaket. Vsi bolniki morajo prejemati dodatek vsaj 500 mg kalcija in 400 i.e.

vitamina D dnevno, razen če ima bolnik hiperkalcemijo. **Bolniki z okvaro ledvic:** Prilagoditev odmerka ni potrebna. Izkušnje pri bolnikih na dializi ali s hudo okvaro ledvic (očistek kreatinina < 30 ml/min) so omejene. **Bolniki z okvaro jeter:** Varnost in učinkovitost denosumaba nista raziskani. **Starejši bolniki (stari ≥ 65 let):** Prilagoditev odmerka ni potrebna. **Pediatrični bolniki:** Uporaba zdravila XGEVA® ni priporočljiva

za pediatrične bolnike (stare < 18 let), ker njegovi učinkovitost in varnost pri teh bolnikih nista dokazani. Za subkutano uporabo. Zdravilo XGEVA® mora aplicirati zdravstveni delavec. **KONTRAINDIKACIJE:**

Preobčutljivost na zdravilno učinkovino ali katero koli pomožno snov. Huda, nezdravljena hipokalcemija. **POSEBNA OPOZORILA IN PREVIDNOSTNI UKREPI:** Vsi bolniki morajo prejemati dodatek kalcija in

vitamina D, razen če ima bolnik hiperkalcemijo. Obstoječo hipokalcemijo je treba odpraviti še pred začetkom zdravljenja z zdravilom XGEVA®. Hipokalcemija se lahko pojavi kadarkoli med zdravljenjem z

zdravilom XGEVA®. Najpogosteje se pojavi v prvih 6 mesecih zdravljenja. Bolniki s hudo okvaro ledvic (očistek kreatinina < 30 ml/min) ali na dializi imajo večje tveganje za pojav hipokalcemije, tem bolnikom je

priporočljivo kontrolirati koncentracijo kalcija. Če se med prejetjem zdravila XGEVA® pojavi hipokalcemija, je lahko potrebno dodatno dodajanje kalcija. Bolniki z aktivnimi zobnimi boleznimi ali boleznimi

čeljustnice morajo pred zdravljenjem z zdravilom XGEVA® opraviti zobozdravstveni pregled, vključno z ustreznimi preventivnimi zobozdravstvenimi ukrepi. Med zdravljenjem se morajo bolniki izogniti

invazivnim zobozdravstvenim posegom, če je to mogoče, ter skrbeti za dobro ustno higieno. Bolnike, pri katerih med zdravljenjem z zdravilom XGEVA® obstaja sum na osteonekrozo čeljustnice ali se jim ta

razvije, mora zdraviti zobozdravnik ali ustni kirurg. Pri takšnih bolnikih lahko obsežna zobna operacija za zdravljenje osteonekroze čeljustnice stanje še poslabša. Preden zdravnik predpiše zdravilo XGEVA®

bolniku z neugodnimi dejavniki tveganja za osteonekrozo čeljustnice in če se med zdravljenjem z zdravilom XGEVA® pojavi osteonekroza čeljustnice, je treba narediti individualno oceno koristi in tveganja.

Atipični zlomi stegenice se lahko pojavijo že ob majhni poškodbi ali celo brez poškodbe, in sicer v subtrohanternem in diafiznem predelu stegenice. Za te dogodke so značilni specifični radiografski izvidi.

O njih so poročali tudi pri bolnikih z določenimi sočasnimi bolezenskimi stanji (npr. s pomanjkanjem vitamina D, revmatoidnim artritisom, hipofosfatazijo) in med uporabo določenih zdravil (npr. difosfonatov,

glukokortikoidov, zaviralcev protonске črpalke). Ti dogodki so se pojavili tudi brez antiresorpcijskega zdravljenja. Podobni zlomi, opisani v zvezi z difosfonati, so pogosto obojestranski, zato je treba pri

bolnikih, ki se zdravijo z denosumabom in so imeli zlom srednjega dela stegenice, opraviti tudi pregled druge stegenice. Pri bolnikih, pri katerih obstaja sum na atipičen zlom stegenice, je treba razmisliti

o prenehanju uporabe zdravila XGEVA® ob vrednotenju bolnika glede na individualno oceno koristi in tveganja. Bolnikom je treba naročiti, da morajo med zdravljenjem z zdravilom XGEVA® zdravniku poročati o

novi ali nenavadni bolečini v stegnu, kolku ali dimljah. Bolnike s takšnimi simptomi je treba preiskati glede nepopolnega zloma stegenice. Bolniki, zdravljeni z zdravilom XGEVA®, sočasno ne smejo prejemati

drugih zdravil, ki vsebujejo denosumab (za indikacije pri osteoporozii), in difosfonatov. Bolniki z redko prirojeno motnjo intolerance za fruktozo ne smejo uporabljati zdravila XGEVA®. **INTERAKCIJE:** Študij

medsebojnega delovanja niso izvedli. V kliničnih preskušanih sočasna kemoterapija in/ali hormonsko zdravljenje ali predhodna intravenska izpostavljenost difosfonatom niso klinično pomembno spremenili

najmanjše koncentracije denosumaba v serumu in farmakodinamike denosumaba (N-telopeptid v urinu, prilagojen na kreatinin, uNTx/Cr). **POVZETEK NEŽELENIH UČINKOV:** Zelo pogosti (≥ 1/10): dispneja,

driska. Pogosti (≥ 1/100 do < 1/10): hipokalcemija, hipofosfatemija, ekstrakcija zoba, hiperhidroza, osteonekroza čeljustnice. Redki (≥ 1/10.000 do < 1/1.000): preobčutljivost na zdravilo, anafilaktična reakcija,

atipični zlom stegenice. **FARMACEVTSKI PODATKI:** Shranjujte v hladilniku (2 °C - 8 °C). Ne zamrzujte. **NAČIN IN REŽIM PREDPISOVANJA TER IZDAJE ZDRAVILA:** Predpisovanje in izdaja zdravila je le na

recept s posebnim režimom – ZZ. **IMETNIK DOVOLJENJA ZA PROMET:** Amgen Europe B.V., Minervum 7061, NL-4817 ZK Breda, Nizozemska. **Dodatna pojasnila lahko dobite v lokalni pisarni:** Amgen zdravila

d.o.o., Šmartinska 140, SI-1000 Ljubljana. **DATUM ZADNJE REVIZIJE BESEDILA:** 24. oktober 2013. **DATUM PRIPRAVE INFORMACIJE:** Julij 2014. Podrobne informacije o zdravilu so objavljene na spletni strani

Evropske agencije za zdravila <http://www.ema.europa.eu/>.

Literatura: 1. Povzetek glavnih značilnosti zdravila XGEVA® (denosumab), Amgen 2013.

AMGEN®

SKRAJŠAN POVZETEK GLAVNIH ZNAČILNOSTI ZDRAVILA

Samo za strokovno javnost.

Ime zdravila: Tarceva 25 mg/100 mg/150 mg filmsko obložene tablete

Kakovostna in količinska sestava: Ena filmsko obložena tableta vsebuje 25 mg, 100 mg ali 150 mg erlotiniba (v obliki erlotinibijevga klorida).

Terapevtske indikacije: Nedrobnocelični rak pljuč: Zdravilo Tarceva je indicirano za prvo linijo zdravljenja bolnikov z lokalno napredovalim ali metastatskim nedrobnoceličnim rakom pljuč z EGFR-aktivirajočimi mutacijami. Zdravilo Tarceva je indicirano tudi za samostojno vzdrževalno zdravljenje bolnikov z lokalno napredovalim ali metastatskim nedrobnoceličnim rakom pljuč s stabilno boleznijo po 4 ciklih standardne kemoterapije na osnovi platine v prvi liniji zdravljenja. Zdravilo Tarceva je indicirano tudi za zdravljenje bolnikov z lokalno napredovalim ali metastatskim nedrobnoceličnim rakom pljuč po neuspehu vsaj ene predhodne kemoterapije. Pri predpisovanju zdravila Tarceva je treba upoštevati dejavnike, povezane s podaljšanim preživetjem. Koristnega vpliva na podaljšanje preživetja ali drugih klinično pomembnih učinkov zdravljenja niso dokazali pri bolnikih z EGFR-negativnimi tumorji (glede na rezultat imunohistokemije). Rak trebušne slinavke: Zdravilo Tarceva je v kombinaciji z gemcitabinom indicirano za zdravljenje bolnikov z metastatskim rakom trebušne slinavke. Pri predpisovanju zdravila Tarceva je treba upoštevati dejavnike, povezane s podaljšanim preživetjem. Koristnega vpliva na podaljšanje preživetja niso dokazali za bolnike z lokalno napredovalo boleznijo.

Odmernost in način uporabe: Zdravljenje z zdravilom Tarceva mora nadzorovati zdravnik z izkušnjami pri zdravljenju raka. Pri bolnikih z lokalno napredovalim ali metastatskim nedrobnoceličnim rakom pljuč, ki še niso prejeli kemoterapije, je treba testiranje za določanje mutacij EGFR opraviti pred začetkom zdravljenja z zdravilom Tarceva. Zdravilo Tarceva vzamemo najmanj eno uro pred zaužitjem hrane ali dve uri po tem. Kadar je potreben odmerek prilagoditi, ga je treba zmanjševati v korakih po 50 mg. Pri sočasnem jemanju substratov in modulatorjev CYP3A4 bo morda potrebna prilagoditev odmerka. Pri dajanju zdravila Tarceva bolnikom z jetrno okvaro je potrebna previdnost. Če se pojavijo hudi neželeni učinki, pride v poštev zmanjšanje odmerka ali prekinitev zdravljenja z zdravilom Tarceva. Uporaba zdravila Tarceva pri bolnikih s hudo jetrno ali ledvično okvaro ter pri otrocih ni priporočljiva. Bolnikom kadilcem je treba svetovati, naj prenehajo kaditi, saj so plazemske koncentracije erlotiniba pri kadilcih manjše kot pri nekadilcih. Nedrobnocelični rak pljuč: Priporočeni dnevni odmerek zdravila Tarceva je 150 mg. Rak trebušne slinavke: Priporočeni dnevni odmerek zdravila Tarceva je 100 mg, v kombinaciji z gemcitabinom. Pri bolnikih, pri katerih se kožni izpuščaji v prvih 4 do 8 tednih zdravljenja ne pojavijo, je treba ponovno pretehtati nadaljnje zdravljenje z zdravilom Tarceva.

Kontraindikacije: Preobčutljivost na erlotinib ali katero koli pomožno snov.

Posebna opozorila in previdnostni ukrepi: Pri določanju bolnikovega statusa mutacij EGFR je pomembno izbrati dobro validirano in robustno metodologijo, da se izognemo lažno negativnim ali lažno pozitivnim rezultatom. *Kadilci:* Bolnikom, ki kadijo, je treba svetovati, naj prenehajo kaditi, saj so plazemske koncentracije erlotiniba pri kadilcih zmanjšane v primerjavi s plazemskimi koncentracijami pri nekadilcih. Verjetno je, da je velikost zmanjšanja klinično pomembna. *Intersticijska bolezen pljuč:* Pri bolnikih, pri katerih se akutno pojavijo novi in/ali poslabšajo nepojasnjeni pljučni simptomi, kot so dispneja, kašelj in vročina, je treba zdravljenje z zdravilom Tarceva prekiniti, dokler ni znana diagnoza. Bolnike, ki se sočasno zdravijo z erlotinibom in gemcitabinom, je treba skrbno spremljati zaradi možnosti pojava toksičnosti, podobni intersticijski boleznini pljuč. Če je ugotovljena intersticijska bolezen pljuč, zdravilo Tarceva ukinemo in uvedemo ustrezno zdravljenje. *Driska, dehidracija, neravnovesje elektrolitov in ledvična odpoved:* Pri približno polovici bolnikov, ki so se zdravili z zdravilom Tarceva, se je pojavila driska (vključno z zelo redkimi primeri, ki so se končali s smrtnim izidom). Zmerno do hudo drisko zdravimo z loperamidom. V nekaterih primerih bo morda potrebno zmanjšanje odmerka. V primeru hude ali dolgotrajne driske, navzee, anoreksije ali bruhanja, povezanih z dehidracijo, je treba zdravljenje z zdravilom Tarceva prekiniti in dehidracijo ustrezno zdraviti. O hipokalemiji in ledvični odpovedi so poročali redko. Posebno pri bolnikih z dejavniki tveganja (zlasti sočasnim jemanjem kemoterapevtikov in drugih zdravil, simptomi ali boleznimi ali drugimi dejavniki, vključno z visoko starostjo) moramo, če je driska huda ali dolgotrajna oziroma vodi v dehidracijo, zdravljenje z zdravilom Tarceva prekiniti in bolnikom zagotoviti intenzivno intravensko rehidracijo. Dodatno je treba pri bolnikih s prisotnim tveganjem za razvoj dehidracije spremljati ledvično delovanje in serumske elektrolite, vključno s kalijem. *Hepatitis, jetrna odpoved:* Pri uporabi zdravila Tarceva so poročali o redkih primerih jetrne odpovedi (vključno s smrtnimi). K njenemu nastanku je lahko pripomogla predhodno obstoječa jetrna bolezen ali sočasno jemanje hepatotoksičnih zdravil. Pri teh bolnikih je treba zato premisliti o rednem spremljanju jetrnega delovanja. Dajanje zdravila Tarceva je treba prekiniti, če so spremembe jetrnega delovanja hude. *Perforacije v prebavilih:* Bolniki, ki prejemajo zdravilo Tarceva, imajo večje tveganje za razvoj perforacij v prebavilih, ki so jih opazili občasno (vključno z nekaterimi primeri, ki so se končali s smrtnim izidom). Pri bolnikih, ki sočasno prejemajo zdravila, ki zavirajo angiogenezo, kortikosteroide, nesteroidna protivnetna zdravila (NSAID) in/ali kemoterapijo na osnovi taksanov, ali so v preteklosti imeli peptični ulkus ali divertikularno bolezen, je tveganje večje. Če pride od tega, je treba zdravljenje z zdravilom Tarceva dokončno ukiniti. *Kožne bolezni, pri katerih so prisotni mehurji in luščenje kože:* Poročali so o primerih kožnih bolezni z mehurji in luščenjem kože, vključno z zelo redkimi primeri, ki so nakazovali na Stevens-Johnsonov sindrom/toksično epidermalno nekrozo in so bili v nekaterih primerih smrtni. Zdravljenje z zdravilom Tarceva je treba prekiniti ali ukiniti, če se pri bolniku pojavijo hude oblike mehurjev ali luščenja kože. Pri bolnikih s kožnimi boleznimi z mehurji in luščenjem kože je treba preveriti prisotnost okužbe kože in jih zdraviti v skladu z lokalnimi smernicami. *Očesne bolezni:* Bolniki, pri katerih se pojavijo znaki in simptomi, ki nakazujejo na keratitis in so lahko akutni ali se poslabšujejo: vnetje očesa, solzenje, občutljivost na svetlobo, zamegljen vid, bolečine v očesu in/ali rdeče oči, se morajo ta

koj obrniti na specialista oftalmologije. V primeru, da je diagnoza ulcerativnega keratitisa potrjena, je treba zdravljenje z zdravilom Tarceva prekiniti ali ukiniti. V primeru, da se postavi diagnoza keratitisa, je treba skrbno razmisliti o koristih in tveganjih nadaljnjega zdravljenja. Zdravilo Tarceva je pri bolnikih, ki so v preteklosti imeli keratitis, ulcerativni keratitis ali zelo suhe oči, uporabljati previdno. Uporaba kontaktnih leč je prav tako dejavnik tveganja za keratitis in ulceracijo. Med uporabo zdravila Tarceva so zelo redko poročali o primerih perforacije ali ulceracije roženice. *Medsebojno delovanje z drugimi zdravili:* Močni induktorji CYP3A4 lahko zmanjšajo učinkovitost erlotiniba, močni zaviralci CYP3A4 pa lahko povečajo toksičnost. Sočasno zdravljenje s temi zdravili se je treba izogibati. Tablete vsebujejo laktozo in jih ne smemo dajati bolnikom z redkimi ddnimi stanji: intoleranco za galaktozo, laponsko obliko zmanjšane aktivnosti laktaze ali malabsorpcijo glukoze/galaktoze.

Medsebojno delovanje z drugimi zdravili in druge oblike interakcij: Erlotinib se pri ljudeh presnavlja v jetrih z jetrnimi citokromi, primarno s CYP3A4 in v manjši meri s CYP1A2. Presnova erlotiniba zunaj jeter poteka s CYP3A4 v črevesju, CYP1A1 v pljučih in CYP1B1 v tumorskih tkivih. Z zdravilnimi učinkovinami, ki se presnavljajo s temi encimi, jih zavirajo ali pa so njihovi induktorji, lahko pride do interakcij. Erlotinib je srednje močan zaviralec CYP3A4 in CYP2C8, kot tudi močan zaviralec glukuronidacije z UGT1A1 *in vitro*. Pri kombinaciji ciprofloksacina ali močnega zaviralca CYP1A2 (npr. fluvoksamina) z erlotinibom je potrebna previdnost. V primeru pojava neželenih učinkov, povezanih z erlotinibom, lahko odmerek erlotiniba zmanjšamo. Predhodno ali sočasno zdravljenje z zdravilom Tarceva ni spremenilo očistka prototipov substratov CYP3A4, midazolama in eritromicina. Inhibicija glukuronidacije lahko povzroči interakcije z zdravili, ki so substrati UGT1A1 in se izločajo samo po tej poti. Močni zaviralci aktivnosti CYP3A4 zmanjšajo presnovo erlotiniba in zvečajo koncentracije erlotiniba v plazmi. Pri sočasnem jemanju erlotiniba in močnih zaviralcev CYP3A4 je zato potrebna previdnost. Če je treba, odmerek erlotiniba zmanjšamo, še posebno pri pojavu toksičnosti. Močni spodbujevalci aktivnosti CYP3A4 zvečajo presnovo erlotiniba in pomembno zmanjšajo plazemske koncentracije erlotiniba. Sočasno dajanje zdravila Tarceva in induktorjev CYP3A4 se je treba izogibati. Pri bolnikih, ki potrebujejo sočasno zdravljenje z zdravilom Tarceva in močnim induktorjem CYP3A4, je treba premisliti o povečanju odmerka do 300 mg ob skrbnem spremljanju njihove varnosti. Zmanjšana izpostavljenost se lahko pojavi tudi z drugimi induktorji, kot so fenitoin, karbamazepin, barbiturati ali šentjanževka. Če te zdravilne učinkovine kombiniramo z erlotinibom, je potrebna previdnost. Kadar je mogoče, je treba razmisliti o drugih načinih zdravljenja, ki ne vključujejo močnega spodbujanja aktivnosti CYP3A4. Bolnikom, ki jemljejo *kumarinske antikoagulanse*, je treba redno kontrolirati protrombinski čas ali INR. Sočasno zdravljenje z zdravilom Tarceva in *statinom* lahko poveča tveganje za miopatijo, povzročeno s statini, vključno z rhabdomiolizo; to so opazili redko. Sočasna uporaba zaviralcev *P-glikoproteina*, kot sta ciklosporin in verapamil, lahko vodi v spremenjeno porazdelitev in/ali spremenjeno izločanje erlotiniba. Za erlotinib je značilno zmanjšanje topnosti pri pH nad 5. *Zdravila, ki spremenijo pH v zgornjem delu prebavil*, lahko spremenijo topnost erlotiniba in posledično njegovo biološko uporabnost. Učinka antacidov na absorpcijo erlotiniba niso proučevali, vendar je ta halca zmanjšana, kar vodi v nižje plazemske koncentracije. Kombinaciji erlotiniba in zaviralca protenske črpalke se je treba izogibati. Če menimo, da je uporaba antacidov med zdravljenjem z zdravilom Tarceva potrebna, jih je treba jemati najmanj 4 ure pred ali 2 uri po dnevnem odmerku zdravila Tarceva. Če razmišljamo o uporabi ranitidina, moramo zdravili jemati ločeno: zdravilo Tarceva je treba vzeti najmanj 2 uri pred ali 10 ur po odmerku ranitidina. V študiji faze Ib ni bilo pomembnih učinkov *gemcitabina* na farmakokinetiko erlotiniba, prav tako ni bilo pomembnih učinkov erlotiniba na farmakokinetiko *gemcitabina*. Erlotinib poveča koncentracijo platine. Pomembnih učinkov *karboplatina* ali paklitaksela na farmakokinetiko erlotiniba ni bilo. *Kepecitabin* lahko poveča koncentracijo erlotiniba. Pomembnih učinkov erlotiniba na farmakokinetiko *kepecitabina* ni bilo. Zaradi mehanizma delovanja lahko od zaviralcev *proteasomov*, vključno z bortezomibom, pričakujemo, da vplivajo na učinek zaviralcev EGFR, vključno z erlotinibom.

Neželeni učinki: *Zelo pogosti neželeni učinki* so kožni izpuščaji in driska, kot tudi utrujenost, anoreksija, dispneja, kašelj, okužba, navzea, bruhanje, stomatitis, bolečina v trebuhu, pruritus, suha koža, suhi keratokonjunktivitis, konjunktivitis, zmanjšanje telesne mase, depresija, glavobol, nevropatija, dispepsija, flatulenca, alopecija, okorelost, pireskija, nenormalnosti testov jetrne funkcije. *Pogosti neželeni učinki* so krvavitve v prebavilih, epistaksa, resna intersticijska bolezen pljuč, keratitis, paronihija, folikulitis, akne/akneiformni dermatitis, fisure na koži in ledvična insuficienca. *Občasno* so poročali o perforacijah v prebavilih, hirzutizmu, spremembah obrvi, krhkih nohtih, odstopanju nohtov od kože, blagih reakcijah na koži (npr. hiperpigmentaciji), spremembah trepalnic, nefritisu in proteinuriji. *Redko* pa so poročali o jetrni odpovedi in sindromu palmarno-planarne eritrodisezestije. *Zelo redko* so poročali o Stevens-Johnsonovem sindromu/toksični epidermalni nekrozi ter o ulceracijah in perforacijah roženice.

Režim izdaje zdravila: H/Rp.

Imetnik dovoljenja za promet: Roche Registration Limited, 6 Falcon Way, Shire Park, Welwyn Garden City, AL7 1TW, Velika Britanija.

Verzija: 2.0/13

Informacija pripravljena: julij 2014

DODATNE INFORMACIJE SO NA VOLJO PRI:

Roche farmacevtska družba d.o.o., Vodovodna cesta 109, 1000 Ljubljana.

Povzetek glavnih značilnosti zdravila je dosegljiv na

www.roche.si ali www.onkologija.si.

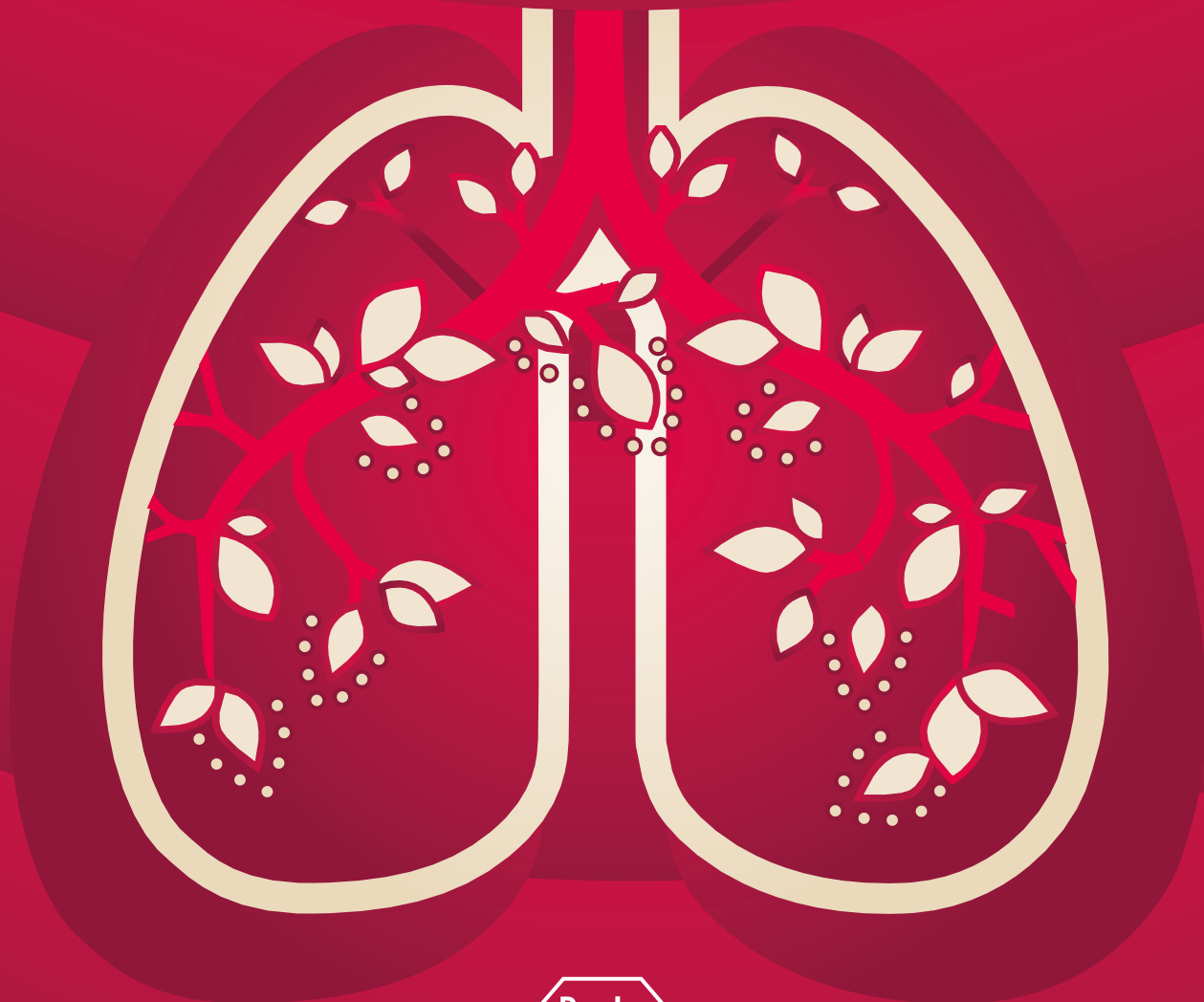


ČAS ZA ŽIVLJENJE.

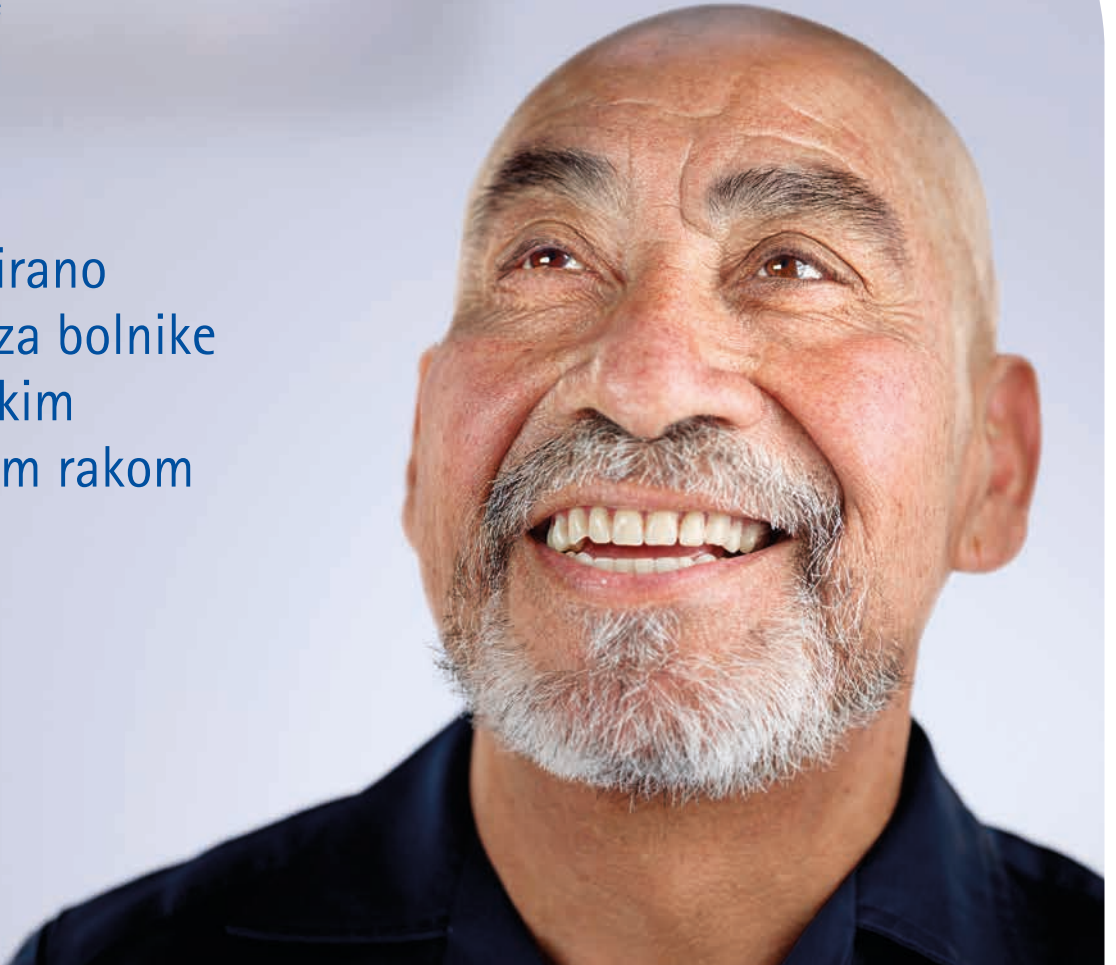
DOKAZANO PODALJŠA PREŽIVETJE PRI BOLNIKI¹:

- z lokalno napredovalim ali metastatskim nedrobnoceličnim rakom pljuč¹
- z metastatskim rakom trebušne slinavke¹

¹ Povzetek glavnih značilnosti zdravila Tarceva® 18.12.2013.



Individualizirano zdravljenje za bolnike z metastatskim kolorektalnim rakom



Merck Serono Onkologija | Ključ je v kombinaciji

Erbitux 5 mg/ml raztopina za infundiranje

Skrajšan povzetek glavnih značilnosti zdravila

Sestava: En ml raztopine za infundiranje vsebuje 5 mg cetuksimaba in pomožne snovi. Cetuksimab je himerno monoklonsko IgG₁ protitelo. **Terapevtske indikacije:** Zdravilo Erbitux je indicirano za zdravljenje bolnikov z metastatskim kolorektalnim rakom z ekspresijo receptorjev EGFR in nemutiranim tipom RAS v kombinaciji s kemoterapijo na osnovi irinotekana, kot primarno zdravljenje v kombinaciji s FOLFOX in kot samostojno zdravilo pri bolnikih, pri katerih zdravljenje z oksaliplatinom in zdravljenje na osnovi irinotekana ni bilo uspešno in pri bolnikih, ki ne prenašajo irinotekana. Zdravilo Erbitux je indicirano za zdravljenje bolnikov z rakom skvamoznih celic glave in vratu v kombinaciji z radioterapijo za lokalno napredovalo bolezen in v kombinaciji s kemoterapijo na osnovi platine za ponavljajočo se in/ali metastatsko bolezen. **Odmerjanje in način uporabe:** Zdravilo Erbitux pri vseh indikacijah infundirajte enkrat na teden. Pred prvo infuzijo mora bolnik prejeti premedikacijo z antihistaminikom in kortikosteroidom najmanj 1 uro pred uporabo cetuksimaba. Začetni odmerek je 400 mg cetuksimaba na m² telesne površine. Vsi naslednji tedenski odmerki so vsak po 250 mg/m². **Kontraindikacije:** Zdravilo Erbitux je kontraindicirano pri bolnikih z znano hudo preobčutljivostno reakcijo (3. ali 4. stopnje) na cetuksimab. Kombinacija zdravila Erbitux s kemoterapijo, ki vsebuje oksaliplatin, je kontraindicirana pri bolnikih z metastatskim kolorektalnim rakom z mutiranim tipom RAS ali kadar status RAS ni znan. **Posebna opozorila in previdnostni ukrepi:** Pojav hude reakcije, povezane z infundiranjem, zahteva takojšnjo in stalno ukinitve terapije s cetuksimabom. Če pri bolniku nastopi blaga ali zmerne reakcija, povezana z infundiranjem, lahko zmanjšate hitrost infundiranja. Priporočljivo je, da ostane hitrost infundiranja na nižji vrednosti tudi pri vseh naslednjih infuzijah. Če se pri bolniku pojavi kožna reakcija, ki je ne more prenašati, ali huda kožna reakcija (≥ 3. stopnje po kriterijih CTCAE), morate prekiniti terapijo s cetuksimabom. Z zdravljenjem smete nadaljevati le, če se je reakcija izboljšala do 2. stopnje. Če ugotovite intersticijsko bolezen pljuč, morate zdravljenje s cetuksimabom prekiniti, in bolnika ustrezno zdraviti. Zaradi možnosti pojava znižanja nivoja elektrolitov v serumu se pred in periodično med zdravljenjem s cetuksimabom priporoča določanje koncentracije elektrolitov v serumu. Pri bolnikih, ki prejemajo cetuksimab v kombinaciji s kemoterapijo na osnovi platine, obstaja večje

veganje za pojav hude nevtropenije. Takšne bolnike je potrebno skrbno nadzorovati. Pri predpisovanju cetuksimaba je treba upoštevati kardiovaskularno stanje in indeks zmogljivosti bolnika in sočasno dajanje kardiotoksičnih učinkovin kot so fluoropirimidini. Če je diagnoza ulcerativnega keratitisa potrjena, je treba zdravljenje s cetuksimabom prekiniti ali ukiniti. Cetuksimab je treba uporabljati previdno pri bolnikih z anamnezo keratitisa, ulcerativnega keratitisa ali zelo suhih oči. Cetuksimaba ne uporabljajte za zdravljenje bolnikov s kolorektalnim rakom, če imajo tumorje z mutacijo RAS ali pri katerih je tumorski status RAS neznan. **Interakcije:** Pri kombinaciji s fluoropirimidini se je v primerjavi z uporabo fluoropirimidinov, kot monoterapije, povečala pogostnost srčne ishemije, vključno z miokardnim infarktom in kongestivno srčno odpovedjo ter pogostnost sindroma dlani in stopal. V kombinaciji s kemoterapijo na osnovi platine se lahko poveča pogostnost hude levkopenije ali hude nevtropenije. V kombinaciji s kapecitabinom in oksaliplatinom (XELOX) se lahko poveča pogostnost hude driske. **Neželeni učinki:** Zelo pogosti (≥ 1/10): hipomagnezija, povečanje ravnih jetrnih encimov, kožne reakcije, blage ali zmerne reakcije povezane z infundiranjem, mukozitis, v nekaterih primerih resen. Pogosti (≥ 1/100 do < 1/10): dehidracija, hipokalcemija, anoreksija, glavobol, konjunktivitis, driska, navzeja, bruhanje, hude reakcije povezane z infundiranjem, utrujenost. **Posebna navodila za shranjevanje:** Shranjujte v hladilniku (2 °C - 8 °C). **Pakiranje:** 1 viala z 20 ml ali 100 ml raztopine. **Način in režim izdaje:** Izdaja zdravila je le na recept-H. **Imetnik dovoljenja za promet:** Merck KGaA, 64271 Darmstadt, Nemčija.

Datum zadnje revizije besedila: december 2013.

Pred predpisovanjem zdravila natančno preberite celoten Povzetek glavnih značilnosti zdravila.

Samo za strokovno javnost.

Podrobnejše informacije so na voljo pri predstavniku imetnika dovoljenja za promet z zdravilom:
Merck d.o.o., Ameriška ulica 8, 1000 Ljubljana, tel.: 01 560 3810, faks: 01 560 3830, el. pošta: info@merck.si
www.merckserono.net
www.Erbitux-international.com

Za bolnike z napredovalim neploščatoceličnim* NSCLC

OMOGOČI PREŽIVETJE.



OHRANJA BOLEZEN
POD NADZOROM.

ALIMTA®
pemetreksed

*Žlezni, velikocelični rak pljuč in druge histologije.
NSCLC - Nedrobnoocelični rak pljuč

SKRAJŠAN POVZETEK GLAVNIH ZNAČILNOSTI ZDRAVILA

Ime zdravila ALIMTA 100 mg prašek za raztopino za infundiranje in ALIMTA 500 mg prašek za koncentrat za raztopino za infundiranje **Kakovostna in količinska sestava** ALIMTA 100 mg: vsaka viala vsebuje 100 mg pemetrekseda (v obliki dinatrijevega pemetrekseda). Po pripravi vsebuje vsaka viala 25 mg/ml pemetrekseda. Pomozne snovi: Vsaka viala vsebuje približno 11 mg natrija, manitol, klorovodikova kislina, natrijev hidroksid. ALIMTA 500 mg: vsaka viala vsebuje 500 mg pemetrekseda (v obliki dinatrijevega pemetrekseda). Po pripravi vsebuje vsaka viala 25 mg/ml pemetrekseda. Pomozne snovi: Vsaka viala vsebuje približno 54 mg natrija, manitol, klorovodikova kislina, natrijev hidroksid. **Terapevtske indikacije:** ALIMTA je v kombinaciji s cisplatinom indicirana za zdravljenje bolnikov z neresekabilnim malignim plevralnim mezoteliomom, ki jih še nismo zdravili s kemoterapijo. ALIMTA je v kombinaciji s cisplatinom indicirana kot zdravljenje prvega izbora za bolnike z lokalno napredovalim ali metastatskim nedrobnooceličnim rakom pljuč, ki nima pretežno ploščatocelične histologije. ALIMTA je indicirana kot monoterapija za zdravljenje drugega izbora bolnikov z lokalno napredovalim ali metastatskega nedrobnooceličnega pljučnega karcinoma, ki nima pretežno ploščatocelične histologije pri bolnikih, pri katerih bolezen ni napredovala neposredno po kemoterapiji na osnovi platine. ALIMTA je indicirana kot monoterapija za uporabo kemoterapije za zdravljenje raka ALIMTA v kombinaciji s cisplatinom: Priporočeni odmerek cisplatina je 75 mg/m² TP, infundiran v dveh urah približno 30 minut po zaključku infuzije pemetrekseda prvi dan vsakega 21-dnevnega ciklusa. Bolniki morajo prejeti zadostno antiemetično zdravljenje, pred in/ali po prejemanju cisplatina jih moramo tudi ustrezno hidrirati. ALIMTA kot samostojno zdravljenje: Priporočeni odmerek ALIMTE je 500 mg/m² TP, dan kot intravenska infuzija v 10 minutah prvi dan vsakega 21-dnevnega ciklusa. **Režim premedikacije:** Da zmanjšamo incidenco in resnost kožnih reakcij, dajemo kortikosteroid dan pred dajanjem pemetrekseda, na dan dajanja pemetrekseda in naslednji dan. Kortikosteroid naj ustreza 4 mg doksametazona, danega peroralno dvakrat dnevno. Za zmanjšanje toksičnosti morajo bolniki dnevno jemati tudi peroralno folno kislino ali multivitaminski pripravek, ki jo vsebuje (350 do 1000 mikrogramov). V sedmih dneh pred prvim odmerkom pemetrekseda morajo vzeti vsaj pet odmerkov folne kisline, odmerjanje pa morajo nadaljevati ves čas zdravljenja in še 21 dni po zadnjem odmerku pemetrekseda. Bolniki morajo prejeti tudi intamuskularno injekcijo vitamina B12 (1000 mikrogramov) v tednu pred prvim odmerkom pemetrekseda in enkrat vsake tri cikluse zatem. Kasnejše injekcije vitamina B12 lahko dajemo isti dan kot pemetreksed. **Kontraindikacije:** Preobčutljivost za zdravilo učinkovino ali katerokoli pomožno snov. Dojenje. Sočasno cepljenje proti rumeni mrzlici. **Posebna opozorila in previdnostni ukrepi:** Pemetreksed lahko zavre delovanje kostnega mozga, kar se kaže kot neutropenija, trombocitopenija in anemija (ali pancitopenija). Mielosupresija običajno predstavlja toksičnost za omejitve odmerka. Pri bolnikih, ki pred zdravljenjem niso prejeli kortikosteroidov, so poročali o kožnih reakcijah. Uporaba pemetrekseda pri bolnikih z očistkom kreatinina < 45 ml/min ne priporočamo. Bolniki z blagim do zmernim popuščanjem delovanja ledvic naj se izogibajo jemanju NSAID-ov z dolgi razpolovni časi izločanja vsaj 5 dni pred dajanjem pemetrekseda, na dan dajanja in še vsaj 2 dni po dajanju pemetrekseda. Poročali so o resnih ledvičnih primerih, vključno z akutno ledvično odpovedjo, s pemetreksedom samim ali v povezavi z drugimi kemoterapevtiki. Pri bolnikih s klinično pomembno taksico tretjega prostora moramo razmisliti o drenaži izliva pred dajanjem pemetrekseda. Kot posledico toksičnosti pemetrekseda v kombinaciji s cisplatinom za prebavila so opažali hudo dehidracijo, zato moramo bolnike pred prejemanjem terapije in/ali po njej ustrezno hidrirati, prejeti zadostno antiemetično zdravljenje. Občasno so v kliničnih študijah pemetrekseda, običajno ob sočasnem dajanju z drugo citotoksično učinkovino, poročali o resnih srčnožilnih dogodkih, vključno z miokardnim infarktom in možganskožilnimi dogodki. Odsvetujemo uporabo živih oslabljenih cepiv. Spolno zrelim moškim odsvetujemo zaploditev otroka v času zdravljenja in še 6 mesecev zatem. Priporočamo ukrepe proti zanositvi ali vzdržnosti. Zaradi možnosti, da zdravljenje s pemetreksedom povzroči trajno neplodnost, naj se moški pred začetkom zdravljenja posvetujejo o shranjevanju semen. Ženske v rodni dobi morajo v času zdravljenja s pemetreksedom uporabljati učinkovito kontracepcijo. Poročali so o primerih radijskega pljučnice pri bolnikih, ki so jih zdravili z radiacijo pred, med ali po zdravljenju s pemetreksedom. Poročali so o radijskem izpuščaju pri bolnikih, ki so se zdravili z radioterapijo pred tedni ali leti. **Mesečno delovanje z drugimi zdravili in druge oblike interakcij:** Sočasno dajanje nefrotoksičnih zdravil (denimo, aminoglikozidov, diuretikov zanke, spojin platine, ciklosporina) lahko potencialno povzroči zakasneli odtsek pemetrekseda. Sočasno dajanje snovi, ki se tudi izločajo s tubulno sekrecijo (denimo, probenecid, penicilin), lahko potencialno povzroči zakasneli odtsek pemetrekseda. Pri bolnikih z normalnim delovanjem ledvic lahko visoki odmerki nesteroidnih protivnetnih zdravil (NSAID-ov, denimo, ibuprofen) in aceticilicilne kisline v visoki odmerkih zmanjšajo eliminacijo pemetrekseda in tako lahko povečajo pojavnost neželenih učinkov pemetrekseda. Pri bolnikih z blagim do zmernim popuščanjem delovanja ledvic se moramo izogibati sočasnemu dajanju pemetrekseda z NSAID-om (denimo, ibuprofen) ali aceticilicilne kisline v visoki odmerkih 2 dni pred dajanjem pemetrekseda, na dan dajanja in še 2 dni po dajanju pemetrekseda. Sočasno dajanje NSAID-ov z daljšimi razpolovni časi s pemetreksedom se moramo izogibati vsaj 5 dni pred dajanjem pemetrekseda, na dan dajanja in še vsaj 2 dni po dajanju pemetrekseda. Velika različnost med posamezniki v koagulacijskem statusu v času bolezni ter možnost mesečnega delovanja med peroralnimi antikoagulacijskimi učinkovinami ter kemoterapijo proti raku zahtevata povečano pogostost spremljanja INR. **Kontraindicirana sočasna uporaba:** Zelo pogosti: znižani trombociti, tveganje za smrtno generalizirano bolezen po cepljenju. **Odsvetovana sočasna uporaba:** Ziva avlajevna cepiva (razen proti rumeni mrzlici); tveganje za sistemsko, potencialno smrtno bolezen. **Neželeni učinki:** Klinične študije malignega plevralnega mezotelioma Zelo pogosti: znižani nevtrofilci/granulociti, znižani hemoglobin, znižani trombociti, nevropatija-senzorna, diareja, bruhanje, stomatitis/faringitis, slabost, anoreksija, zaprtje, izpuščaj, alopecija, povišan kreatinin, znižan odtsek kreatinina, utrujenost. **Pogosti:** dehidracija, motnje okusa, konjunktivitis, dispneja. **Klinične študije nedrobnooceličnega pljučnega karcinoma - ALIMTA monoterapija, zdravljenje 2. izbora:** Zelo pogosti: znižani nevtrofilci/granulociti, znižani levkociti, znižan hemoglobin, diareja, bruhanje, stomatitis/faringitis, slabost, anoreksija, izpuščaj/luščenje, utrujenost. **Pogosti:** znižani trombociti, zaprtje, povišanje SGPT (ALT), povišanje SGOT (AST), srbenje, alopecija, povišana telesna temperatura. **Klinične študije nedrobnooceličnega pljučnega karcinoma - ALIMTA v kombinaciji s cisplatinom, zdravljenje 1. izbora:** Zelo pogosti: znižani hemoglobin, znižani levkociti, znižani trombociti, slabost, anoreksija, zaprtje, stomatitis/faringitis, diareja brez kolostomije, alopecija, izpuščaj/luščenje, povišan kreatinin, utrujenost. **Pogosti:** nevropatija-senzorna, motnje okusa, dispneja/zgaga. **Klinične študije nedrobnooceličnega pljučnega karcinoma - ALIMTA monoterapija, vzdrževalno in nadaljevalno zdravljenje:** Zelo pogosti: znižan hemoglobin, slabost, anoreksija, utrujenost. **Pogosti:** znižani levkociti, znižani nevtrofilci, nevropatija-senzorna, bruhanje, mukozitis/stomatitis, povišanje ALT (SGPT), povišanje AST (SGOT), izpuščaj/luščenje, bolečina. Občasno so v kliničnih študijah pemetrekseda poročali o primerih resnih srčnožilnih in možganskožilnih dogodkov, vključno z miokardnim infarktom, angino pectoris, cerebrovaskularnim insultom in prehodnimi ishemičnimi atakami; primerih kolitisa ter o primerih intersticijske pljučnice z respiratorno insuficienco, primerih edema, o ezofagusni/radijskem ezofagitisu in o primerih sepse. Redkeje pa o primerih potencialno resnega hepatitisa in pancitopenije. Po uvedbi zdravila na trg so poročali o primerih akutne odpovedi ledvic s pemetreksedom samim ali v povezavi z drugimi kemoterapevtiki, primerih radijske pljučnice pri bolnikih, ki so jih zdravili z radiacijo pred, med ali po njihovem zdravljenju s pemetreksedom, primerih radijskega izpuščaja pri bolnikih, ki so se v preteklosti zdravili z radioterapijo, o primerih periferne ishemije, ki je večšah vodila v nekrozo okončin, redkih primerih buloznih stanj, kot sta Stevens-Johnsonov sindrom in toksična epidermalna nekroliza, ki so bila v nekaterih primerih usodna in o redkih primerih hemolitične anemije. Poročali so o redkih primerih anafilaktičnega šoka. **Imetnik dovoljenja za promet** Eli Lilly Nederland BV, Grootslag 1 S, NL 3991 RA, Houten, Nizozemska. Datum zadnje revizije besedila 12.11.2012. **Način izdaje zdravila:** H. SAMO ZA STROKOVNO JAVNOST.

Podrobnejše informacije o zdravilu Alimta, so dostopne na spletni strani Evropske agencije za zdravila EMA <http://www.ema.europa.eu> in na lokalnem predstavništvu.

SIJALM00067

Eli Lilly Farmaceutvska družba, d.o.o.
Brncičeva 41G, 1231 Ljubljana - Črnuče, Slovenija
Telefon: +386 (0)1 5800 010
Faks: +386 (0)1 5691 705

Lilly

Kakovost • Izbira • Zadovoljstvo

T H E

*Natrelle*TM

C O L L E C T I O N

Prsni vsadki in ekspanderji tkiv



*I*ndividualne ženske
*I*ndividualen izbor

 **ALLERGAN**

DISTRIBUCIJA IN PRODAJA:
SANOLABOR, d.d.,
Leskoškova 4, 1000 Ljubljana, Slovenija
Tel: +386 (0)1 585-42-11
Fax: +386 (0)1 585-42-98
www.sanolabor.si

 **Sanolabor**

PROMOCIJA, MARKETING IN STROKOVNA PODPORA:
EWOPHARMA d.o.o., Cesta 24. junija 23, 1000 Ljubljana, Slovenija
Jurij Pivka, vodja poslovne enote -Medicinska estetika
Tel: +386 (0) 59 084 845, mobilnik: +386 (0) 51 326 058
Fax: +386 (0) 59 084 849

Vsaka dan šteje

za bolnike z napredovalim karcinomom ledvičnih celic



28. september

15. december

30. april

2. avgust

Jesenski festival

Zimske počitnice

Družinsko srečanje

Začetek kuharskega tečaja

BISTVENI PODATKI IZ POVZETKA GLAVNIH ZNAČILNOSTI ZDRAVILA

SUTENT 12,5 mg, 25 mg, 37,5 mg, 50 mg trde kapsule

Sestava in oblika zdravila: Ena kapsula vsebuje 12,5 mg, 25 mg, 37,5 mg ali 50 mg sunitiniba (v obliki sunitinibijevega malata). **Indikacije:** Zdravljenje neizrežljivega in/ali metastatskega malignega gastrointestinalnega stromalnega tumorja (GIST) pri odraslih, če zdravljenje z imatinibom zaradi odpornosti ali neprenašanja ni bilo uspešno. Zdravljenje napredovalega/metastatskega karcinoma ledvičnih celic (MRCC) pri odraslih. Zdravljenje neizrežljivih ali metastatskih, dobro diferenciranih neuroendokrinih tumorjev trebušne slinavke (pNET), kadar gre za napredovanje bolezni pri odraslih (izkušnje z zdravilom Sutent kot zdravilom prve izbire so omejene). **Odmerjanje in način uporabe:** Terapijo mora uvesti zdravnik, ki ima izkušnje z uporabo zdravil za zdravljenje rakavih bolezni. **GIST in MRCC:** Priporočeni odmerek je 50 mg peroralno enkrat na dan, 4 tedne zapored; temu sledi 2-tedenski premor (Shema 4/2), tako da celotni cikel traja 6 tednov. **pNET:** Priporočeni odmerek je 37,5 mg peroralno enkrat na dan, brez načrtovanega premora. **Prilaganje odmerka:** Odmerek je mogoče prilagajati v povečanih po 12,5 mg, upoštevaje individualno varnost in prenašanje. Pri GIST in MRCC dnevni odmerek ne sme preseči 75 mg in ne sme biti manjši od 25 mg; pri pNET je največji odmerek 50 mg na dan, z možnimi prekinitvami zdravljenja. Pri sočasni uporabi z močnimi zaviralci ali induktorji CYP3A4 je treba odmerek ustrezno prilagoditi. **Pediatrična populacija:** Uporaba sunitiniba ni priporočljiva. **Starejši bolniki (≥ 65 let):** Med starejšimi in mlajšimi bolniki niso opazili pomembnih razlik v varnosti in učinkovitosti. **Okvara jeter:** Pri bolnikih z jetrno okvaro razreda A in B po Child-Pughu prilagoditev odmerka ni potrebna; pri bolnikih z okvaro razreda C sunitinib ni bil preizkušen, zato njegova uporaba ni priporočljiva. **Okvara ledvic:** Prilaganje začetnega odmerka ni potrebno, nadaljnje prilaganje odmerka naj temelji na varnosti in prenašanju pri posameznem bolniku. **Način uporabe:** Zdravilo Sutent se uporablja peroralno, bolnik ga lahko vzame s hrano ali brez nje. Če pozabi vzeti odmerek, ne sme dobiti dodatnega, temveč naj vzame običajni predpisani odmerek naslednji dan. **Kontraindikacije:** Preobčutljivost na zdravilno učinkovino ali katerokoli pomožno snov. **Posebna opozorila in previdnostni ukrepi:** **Bolezni kože in tkiv:** obarvanje kože, gangrenozna pioderma (običajno izgine po prekinitvi zdravljenja), hude kožne reakcije (multiformni eritem (EM), Stevens-Johnsonov sindrom (SJS) in toksična epidermalna nekroliza (TEN)). Če so prisotni znaki EM, SJS ali TEN, je treba zdravljenje prekiniti. **Krvavitve v prebavilih, dihalih, sečilih, možganih;** najpogostejše epistaksa; krvavitve tumorja, včasih s smrtnim izidom. Pri bolnikih, ki se sočasno zdravijo z antikoagulantmi, se lahko redno spremlja celotna krvna slika (trombociti), koagulacijski faktorji (PT / INR) in opravi telesni pregled. **Bolezni prebavil:** poleg diareje, navzee/bruhanja, bolečine v trebuhu, dispesije, stomatitisa/bolečine v ustih in ezofagitisa tudi hudi zapleti (včasih s smrtnim izidom), vključno s gastrointestinalno perforacijo. **Hipertenzija:** pri bolnikih s hudo hipertenzijo, ki je ni mogoče urediti z zdravili, je priporočljivo začasno prenehanje zdravljenja. **Hematološke bolezni:** zmanjšanje števila nevtrofilcev, trombocitov, anemija. **Bolezni srca in ožilja:** srčno-žilni dogodki, vključno s srčnim popuščanjem, kardiomiopatijo in motnjami v delovanju miokarda, v nekaterih primerih s smrtnim izidom. Sunitinib povečuje tveganje za pojav kardiomiopatije. **Podaljšanje intervala QT:** previdna uporaba pri bolnikih z znano anamnezo podaljšanja intervala QT, tistih, ki jemljejo antiaritmike, in tistih z relevantno, že obstoječo srčno boleznijo, bradikardijo ali elektrolitskimi motnjami. **Venski in arterijski tromboembolični dogodki:** arterijski včasih s smrtnim izidom. **Dogodki na dihalih:** dispneja, plevralni izliv, pljučna embolija

ali pljučni edem; redki primeri s smrtnim izidom. **Moteno delovanje ščitnice:** bolnike je treba med zdravljenjem rutinsko spremljati glede delovanja ščitnice vsake 3 mesece. **Pankreatitis,** tudi resni primeri s smrtnim izidom. **Hepatotoksičnost,** nekateri primeri s smrtnim izidom. **Holecistitis,** vključno z akalkuloznim in emfizemskim holecistitisom. **Delovanje ledvic:** primeri zmanjšane delovanja ledvic, odpovedi ledvic in/ali akutne odpovedi ledvic, v nekaterih primerih s smrtnim izidom. **Fistula:** če nastane fistula, je treba zdravljenje s sunitinibom prekiniti. **Oteženo celjenje ran:** pri bolnikih, pri katerih naj bi bil opravljen večji kirurški poseg, je priporočljiva začasna prekinitev zdravljenja s sunitinibom. **Osteonekroza čeljustnic:** pri sočasnem ali zaporednem dajanju zdravila Sutent in intravenskih bisfosfonatov je potrebna previdnost; invazivni zobozdravstveni posegi predstavljajo dodatni dejavnik tveganja. **Preobčutljivost/angioedem. Motnje okušanja. Konvulzije:** obstajajo poročila, nekatera s smrtnim izidom, o preiskovanih s konvulzijami in radiološkimi znaki sindroma reverzibilne posteriorne levkoencefalopatije. **Sindrom lize tumorja,** v nekaterih primerih s smrtnim izidom. **Okužbe:** hude okužbe z ali brez nevtropenije (okužbe dihal, sečil, kože in sepsa), vključno z nekaterimi s smrtnim izidom; redki primeri nekrotizirajočega fasciitisa, vključno s prizadetostjo presredka, ki so bili včasih smrtni. **Medsebojno delovanje z drugimi zdravili:** (Študije so izvedli le pri odraslih.) Zdravila, ki lahko zvečajo koncentracijo sunitiniba v plazmi (ketokonazol, ritonavir, itrakonazol, eritromicin, klaritromicin ali sok grenivke). Zdravila, ki lahko zmanjšajo koncentracijo sunitiniba v plazmi (deksametazon, fenitoin, karbamazepin, rifampin, fenobarbital, *Hypericum perforatum* oz. šentjanževka). **Plodnost, nosečnost in dojenje:** Zdravila Sutent ne smemo uporabljati med nosečnostjo in tudi ne pri ženskah, ki ne uporabljajo ustrezne kontracepcije, razen če možna korist odtehta možno tveganje za plod. Ženske v rodni dobi naj med zdravljenjem z zdravilom Sutent ne zanosi. Ženske, ki jemljejo zdravilo Sutent, ne smejo dojeti. Neklinični izsledki kažejo, da lahko zdravljenje s sunitinibom poslabša plodnost samcev in samic. **Vpliv na sposobnost vožnje in upravljanja s stroji:** Sutent lahko povzroči omotico. **Neželeni učinki:** Najbolj resni neželeni učinki (nekateri s smrtnim izidom) so: odpoved ledvic, srčno popuščanje, pljučna embolija, gastrointestinalna perforacija in krvavitve (npr. v dihalih, prebavilih, tumorju, sečilih in možganih). Najpogostejši neželeni učinki (ki so se pojavili pri vsaj 20 % bolnikov v registracijskih preskušanjih) so: zmanjšana apetit, motnje okušanja, hipertenzija, utrujenost, prebavne motnje (npr. driska, slabost, stomatitis, dispesija in bruhanje), sprememba barve kože in sindrom palmarno-plantarne eritrosidestezije. Med najbolj pogostimi neželenimi učinki so hematološke motnje (nevtropenija, trombocitopenija in anemija). Ostali zelo pogosti (≥ 1/10) neželeni učinki so: virusne okužbe, hipotiroidizem, nespečnost, omotica, glavobol, dispneja, epistaksa, ustno-žrelna bolečina, kašelj, bolečina v trebuhu, glosodinija, bolečine v ustih, zaprtje, flatulenca, suha usta, gastroezofagealna refluksna bolezen, motnje pigmentacije, izpuščaj, eritem, alopecija, spremembe barve las, suha koža, bolečine v udih, mialgija, artralgija, mišično-skeletna bolečina, mišični krči, bolečine v hrbtu, bolečina v prsnem košu, vnetje sluznice, edem, piroksija, mrzlica, zmanjšana iztisni delež, zmanjšanje telesne mase. **Način in režim izdaje:** Predpisovanje in zdaj zdravila je le na recept, zdravilo pa se uporablja samo v bolnišnicah. Izjemoma se lahko uporablja pri nadaljevanju zdravljenja na domu ob odpustu iz bolnišnice in nadaljnem zdravljenju. **Imetnik dovoljenja za promet:** Pfizer Limited, Ramsgate Road, Sandwich, Kent, CT13 9NJ, Velika Britanija. **Datum zadnje revizije besedila:** 23. 1. 2014 **Pred predpisovanjem se seznanite s celotnim povzetkom glavnih značilnosti zdravila.**

